Acknowledgements

This study is the master thesis related to the five-year master program in Biotechnology (MBIOT5) at the Norwegian University of Science and Technology (NTNU). The laboratory work was conducted at the Vilhelm Magnus Laboratory for Neurosurgical Research under the Institute of Surgical Research at Oslo University Hospital, Rikshospitalet from August 2018 to June 2019.

Firstly, I would like to thank my co-supervisor Cecilie Jonsgar Sandberg for invaluable teaching and guidance during my work, and my main supervisor Per Bruheim for help with practical issues. I must also thank Menaka Sathemugathevan for patient and thorough introduction to the cell culture methods, Emiliy Palermo for guidance in safe lab-work, and Zanina Grieg for help with Western blot analyses. I would also like to thank Marit Brynjulfsen for always providing help with whatever minor or major issues, and engaging in discussions around the methods used. I must also thank Einar Osland Vik-Mo for keeping me reminded of the clinical aspects of glioblastoma multiforme and for allowing me to get insight into the treatment, and group leader Iver Langmoen for welcoming me to do my thesis in this group. The group as a whole has allowed me to grow and develop a mind of a scientist, and they have been a major support during my work. I would also express great gratitude to Tom Ole Seljordslia (likeperson. Hjernesvulstforeningen) for sharing experiences with receiving glioblastoma diagnosis. Lastly, I must thank my family and friends for keeping me encouraged, and especially my friends in Trondheim for supporting me in moving to another city, so that I could study something I find very fascinating.

Elise Solli, Oslo, July 2019

Abstract

Glioblastoma multiforme (GBM) is one of the most devastating cancers with a mean survival time following diagnosis of only 14 months, even when standard treatment is given. Thus, there is a pressing need for novel therapeutic approaches to treat this cancer. Targeting the tumor sub-populations of cancer stem cells (CSCs), and pathways important for viability in these cells, have been proposed as a promising approach to treat this cancer. The Wnt-pathway, believed to regulate central characteristics of CSCs, has shown to be highly dysregulated in GBM, and could thus serve as a potent therapeutic target.

The aim of this study was to functionally validate knock-down of the Wnt-pathway receptor, Frizzled (Fzd7), using CRISPR/Cas9 technology, by first establishing protocol conditions for knock-down and viability assays targeting a functional control gene (SGK1) in one patient-derived primary GSC culture. Knock-down assays included evaluation of knock-down effect at the level of DNA, mRNA and protein. Second, the established protocol conditions were applied to explore CRISPR/Cas9-mediated knock-down of Fzd7 in four patient-derived primary GSC cultures. The study was done by lentiviral introduction of Cas9 and sgRNAs targeting the coding region of the gene of interest, followed by evaluation of CRISPR/Cas9 activity at DNA level by T7 endonuclease assay, at mRNA level by RT qPCR, at protein level by Western blot, and at viability by XTT assay.

It was found that CRISPR/Cas9-mediated knock-down of SGK1 partly validated the functionality of the CRISPR/Cas9 system by indicating successful and specific indel induction and decreased viability, though showcasing sub-optimal indel inductions and a potential uncertainty regarding protein knock-out from one of the sgRNAs. Further CRISPR/Cas9-mediated knock-down of FZD7 in four patient-derived GSC cultures unexpectedly showed increased viability in all cell cultures. This could be due to redundancy effects between Fzd7 and other proteins, or unaccounted for DNA damage responses. Knock-down of FZD7 also showcased sub-optimal DNA indel inductions and variations in Fzd7 gene and protein expression between the different tumors. Only one of four GSC cultures showcased both decreased mRNA and protein levels, as is desired following CRISPR/Cas9 activity. Responses on mRNA and protein level highlighted difficulties in predicting effects of cell regulation, and tumor heterogeneity in responses to CRISPR/Cas9-mediated Fzd7 knock-down. Further understanding of the Wnt-pathway and other central pathways for cancer stem cell viability, and exploration of specific molecular targets should be done in order to identify and validate functional targets for GBM treatment. Additionally, further understanding of CRIPSR/Cas9 effects in GSCs and optimization of CRISPR/Cas9 protocols and designs, should also be done in order to increase CRISPR/Cas9-mediated knock-down effects.

Sammendrag

Glioblastoma multiforme (GBM) er en svært alvorlig type kreft, men en median overlevelsestid på kun 14 måndeder etter at diagnose er satt, selv om standard behandling igangsettes. Derfor er det et stort behov for nye terapeutiske tilnærminger for behandling av dennekreftformen. Å rette behandlingen mot en tumor sub-populasjon av kreftstamceller, og signalveier sentrale for levedyktighet i disse cellene, har blitt fremlagt som en lovende tilnærming ved behandling av denne typen kreft. Wnt-signalveien, trolig involvert i regulering av sentrale funksjoner i kreftstamceller, har vist seg å være svært dysregulert i GBM, og kan dermed være et mulig terapeutisk mål.

Formålet med denne studien var å funksjonelt validere knock-down av Frizzled-7 (Fzd7), en Wnt-signalvei reseptor, ved bruk av CRISPR/Cas9 teknologi. Først skulle protokoll for knock-down etableres ved å slå ut av et funksjonelt kontroll gen, serum-glucocorticoid regulated kinase 1 (SGK1) i en pasient-derivert glioblastom-stamcelle kultur. Deretter skulle den etablerte protokollen brukes til å utforske effekten av FZD7 knock-down ved bruk av CRISPR/Cas9 i fire pasient-deriverte glioblastomstamcelle kulturer. Studien ble gjennomført ved lentiviral introduksjon av Cas9 og sgRNAer, rettet mot kodete regioner i det gitte genet, etterfulgt av evaluering av CRISPR/Cas9 activitet på DNA nivå ved T7 endonuclease assay, på mRNA nivå ved RT qPCR, på protein nivå ved Western blot, og på viabilitet og funksjonelt ved XTT viabilitet test.

Det ble funnet at CRISPR/Cas9 knock-down av SGK1 delvis validerte funksjonaliteten av CRISPR/Cas9 systemet ved å vise suksessful og spesifikk indusjon av indels og nedgang i viabiltet, samtidig som å sub-optimal indusering av indels samt en potensiell usikkerhet i protein knock-out fra et av sgRNAene. Videre viste CRIPSR/Cas9 knock-down av FZD7 i fire pasient-deriverte glioblastomstamcelle kulturer en uventet økning i viabilitet i alle cellekulturer. Dette kan skyldes kompensasjonsmekanismer mellom Fzd7 og andre proteiner, eller uforutsette DNA-skade responser. Knock-down av FZD7 viste også sub-optimal indusering av indels og variasjoner i FZD7 gen- og protein ekspresjon mellom de ulike kulturene. Bare en av fire kulturer viste både redusert mRNA og protein utrykk, som er ønsket etter CRIPSR/Cas9 aktivitet. Responsene på mRNA og protein nivå fremhevet vanskeligheter i å forutsti effekter av celle regulering, og tumor heterogenitet i respons etter CRIPSR/Cas9 knock-down av FZD7. Dypere forståelse av Wnt-signalveien og andre sentral signalveier for viabilitet i kreftstamceller, og utforskning av spesifikke molekylære målgener eller proteiner burde gjennomføres for å identifisere og validere funksjonelle mål i GBM behandling. I tillegg, dypere forståelse av CRIPSR/Cas9 effekter i glioblatomstamceller og optimalisering av CRIPSR/Cas9 protokoller og design, burde også gjøres for å øke CRISPR/Cas9 knock-down effekt.

Abbreviations

ATM	Ataxia–telangiectasia mutated
Cas9	CRISPR associated protein 9
CRISPR	Clustered regularly interspaced short palindromic repeats
crRNA	CRISPR RNA
DMEM	Dulbecco's modified eagle medium
DSB	Double-stranded break
EGF	Epidermal growth factor
FBS	Fetal bovine serum
FGF	Fibroblast growth factor
FZD7	Frizzled-7
GBM	Glioblastoma multiforme
GSC	Glioblastoma stem cells
hCMV	Human cytomegalovirus intermediate early promoter
LOH	Loss of heterogenity
MOI	Multiplicity of infection
NHEJ	Non-homologous end joining
NMD	Nonsense mediated decay
NSC	Neural stem cell
PAM	Protospacer adjacent motif
PBS	Phosphate buffered saline
Pen/Strep	Penicillin/Streptomycin
PI-domain	PAM-interacting domain
PTC	Premature termination codon
RIN	RNA integrity number
SGK1	Serum and glucocorticoid-regulated kinase 1
sgRNA	Single guide RNA
shRNA	Short hairpin RNA
TBS	Tris-buffered saline
tracrRNA	Trans-activating crRNA
VEGFR	Vascular endothelial growth factor receptor

Contents

Acknowledgements i

Abstract ii

Sammendrag iii

Abbreviations iv

1 Introduction 1
- 1.1 Motivation . . . 1
- 1.2 Glioblastoma multiforme . . . 2
  - 1.2.1 Classification and clinical relevance . . . 2
  - 1.2.2 Epidemology . . . 3
  - 1.2.3 Present treatment . . . 3
- 1.3 Cancer stem-cell hypothesis and cellular origin . . . 4
- 1.4 Glioblastoma targeted therapies . . . 6
  - 1.4.1 Our approach to identify new molecular targets . . . 6
  - 1.4.2 Serum and glucocorticoid-regulated kinase 1 . . . 6
  - 1.4.3 The Wnt-pathway and Frizzled-7 . . . 7
- 1.5 CRISPR/Cas9 . . . 9
  - 1.5.1 Bacterial CRISPR-system . . . 10
  - 1.5.2 Adaption for directed gene-editing in mammalian cells . . . 13
- 1.6 Aims of the study . . . 17

2 Materials and methods 18
- 2.1 Tumor biopsies and acquisition of primary cell cultures . . . 18
- 2.2 Culture maintenance and cell passage . . . 18
- 2.3 Optimization studies and establishment of protocol conditions . . . 19
- 2.4 Gene knock-down by CRISPR/Cas9 . . . 19
  - 2.4.1 Seeding of cells . . . 19
  - 2.4.2 The Cas9 and sgRNA constructs . . . 19
  - 2.4.3 Transduction . . . 20
- 2.5 Evaluation of genomic alterations . . . 21
  - 2.5.1 Isolation of genomic DNA . . . 22
  - 2.5.2 PCR amplification . . . 22
  - 2.5.3 T7 endonuclease mismatch detection . . . 23
- 2.6 Evaluation of gene expression . . . 23
  - 2.6.1 Isolation of RNA and cDNA conversion . . . 23
  - 2.6.2 Quantitative reverse transcriptase PCR . . . 24
- 2.7 Evaluation of protein expression . . . 25
  - 2.7.1 Isolation of proteins . . . 25
  - 2.7.2 Western blot . . . 25
- 2.8 Evaluation of viability . . . 27
  - 2.8.1 XTT-assay . . . 27
- 2.9 Statistical analysis . . . 28

3 Results **29**
3.1 Preliminary optimization . . . 29
3.1.1 Optimal multiplicity of infection for transductions . . . 29
3.1.2 Optimal seeding cell density for proliferation assay . . . 29
3.1.3 Time point for spectrophotometer read in proliferation assay . . . 29
3.1.4 Validation of specific and correct PCR primer-binding . . . 30
3.1.5 Cas9 introduction . . . 31
3.2 SGK1 knock-down and protocol optimization . . . 31
3.2.1 SGK1 knock-down and at DNA level by T7 endonuclease mismatch detection assay . 31
3.2.2 SGK1 knock-down at mRNA level by RT qPCR . . . 32
3.2.3 SGK1 knock-down at protein level by Western blot . . . 33
3.2.4 SGK1 knock-down at viability by XTT-assay . . . 34
3.2.5 Protocol optimization . . . 35
3.3 FZD7 knock-down . . . 36
3.3.1 Transduction efficiencies . . . 36
3.3.2 FZD7 knock-down at DNA level by T7 endonuclease mismatch detection assay . . . 36
3.3.3 FZD7 knock-down at mRNA level by RT qPCR . . . 37
3.3.4 FZD7 knock-down at protein level by Western blot . . . 38
3.3.5 FZD7 knock-down at viability by XTT-assay . . . 39
3.4 Validation of statistical assumptions . . . 40

4 Discussion **42**
4.1 Increased viability following FZD7 knock-down . . . 42
4.2 Heterogeneity in SGK1 knock-outs . . . 43
4.3 CRISPR/Cas9 knock-down efficiency . . . 43
4.3.1 T7 assay insensitivity to small indels and CRISPR/Cas9 system efficiency in disrupting both gene alleles . . . 43
4.3.2 Potential strand preference and general Cas9/sgRNA considerations . . . 44

5 Future studies **46**

6 Conclusion **47**

Bibliography **48**

Appendices **69**

Introduction

1.1 Motivation

Each year about four hundred Norwegians are diagnosed with glioblastoma multiforme (GBM) (Kreftregisteret). GBM is the most aggressive stage of malignant gliomas, a cancer in the brain glial cells, and is one of the most fatal types of cancers. About half of the diagnosed patients can not expect to live longer than one year following diagnosis and only around 10% live longer than five years, even when given standard treatment. Without treatment, survival is expected to be less than one year following initial diagnosis.

Figure 1.1 shows magnetic resonance (MR) images of four patients with GBM, treated at Oslo University Hospital. The images show large tumor masses infiltrating the brain parenchyma, and such tumors will have substantial effects on patient life. Hjernesvultsforeningen, a group under the Norwegian Cancer Society (Kreftforeningen), offers guidelines on how to relate to all different aspects concerning a GBM diagnosis. These guidelines give insight into patient experiences with GBM, and also serves as an important reminder of reality at the "bedside" and how it is so different from the "bench". Guidelines include informing the people around you about how they can be of help. Colleagues and others not in the immediate family can find it difficult to know how- and if they can be of any help; plan everything regarding funeral, inheritance, finances and other practical issues early on. This will reduce stress and give time to focus on what you want to; do things that makes you gain a sense of control and achievement. Many patients will have to go out of working life and become more dependent on others, which could be a massive upheaval; dependents often need more support than they give impression of, especially after death has occurred; and live life like before, but in a smaller scale.

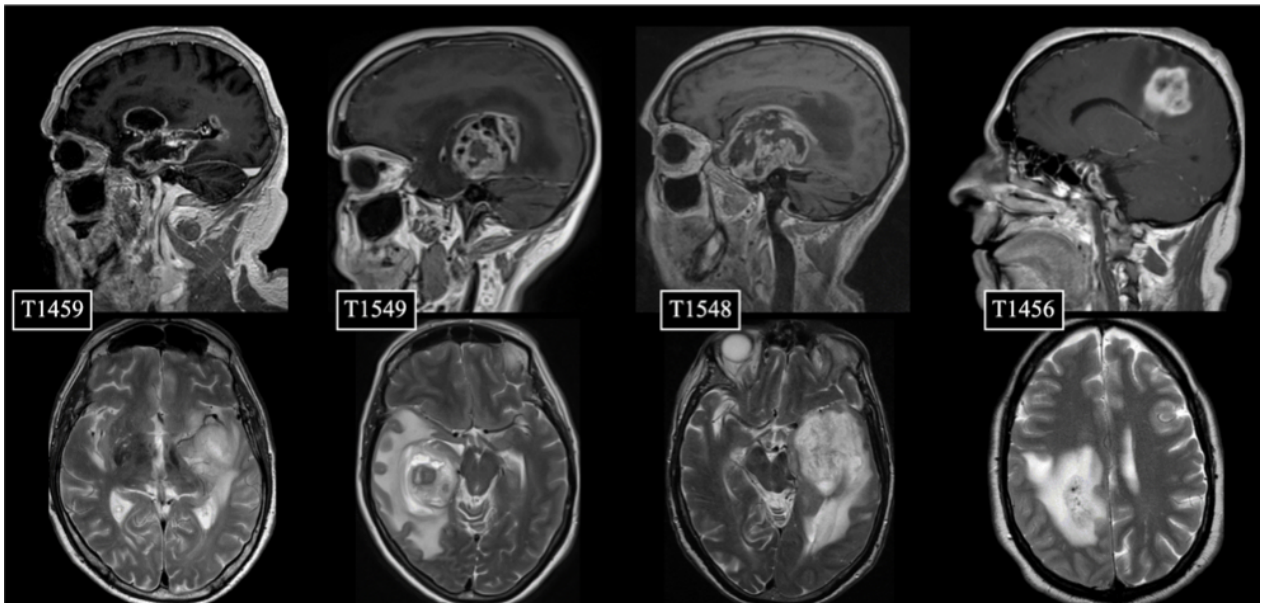

Figure 1.1: Magnetic resonance (MR) imaging of four patients with GBM diagnosis, showing sagittal and horizontal sections of the brain and head. Source: [1].

1.2 Glioblastoma multiforme

1.2.1 Classification and clinical relevance

A system for classification of brain tumors was developed by the World Health Organization (WHO) in 1978 based on previous work from 1926 [2]. The classification discriminated between different types of brain tumors based on histological features, and included a grading characterization of malignant gliomas from I-IV, where grade I and II are referred to as astrocytomas, grade III as anaplastic or diffuse astrocytomas, and grade IV as GBM (Figure 1.2). With an increasing amount of available gene expression data, the classification was updated in 2016, directed towards differences in gene expressions between the different types of brain tumors [3]. The 2016 classification focuses on two genetic alternations that have shown to have a particular impact on prognosis and effectiveness of treatment; a mutation in the enzyme isocitrate dehydrogenase (IDH) and a co-deletion on chromosome 19 and 1 (1p/19q) (Figure 1.3).

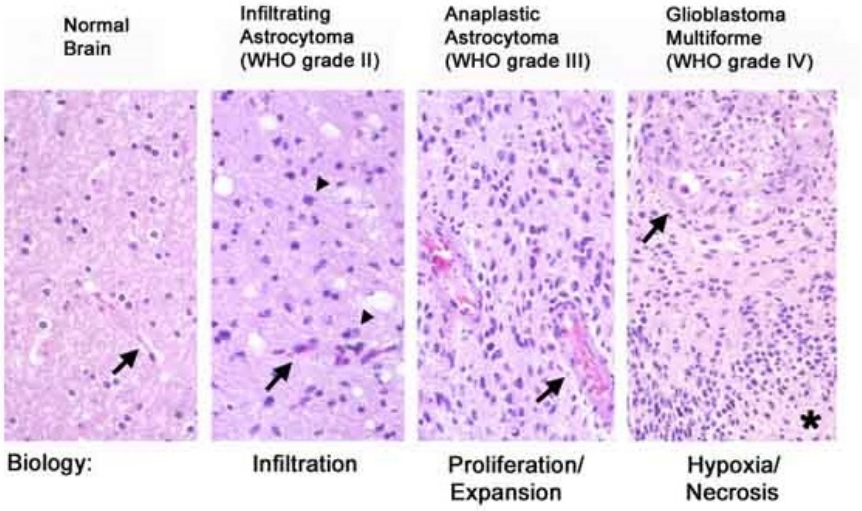

Figure 1.2: Histological features of malignant astrocytoma, illustrating aspects associated with the different WHO defined tumor grades. Grade II, infiltrating astrocytomas, are characterized by tumor cells invading the brain parenchyma (arrowheads), but the vascular innervation is similar as in normal brain (arrow). As the astrocytoma cells proliferate, and the vasculature becomes more dilated, grade III anaplastic astrocytoma develops. When necrotic areas (asterisk) and microvascular hyperplasia (increased size of newly formed vasculature supplying the tumor), are seen, grade IV GBM has developed. Histological slides are stained with hemotoxylin and eosin. Source (with alterations): [4]

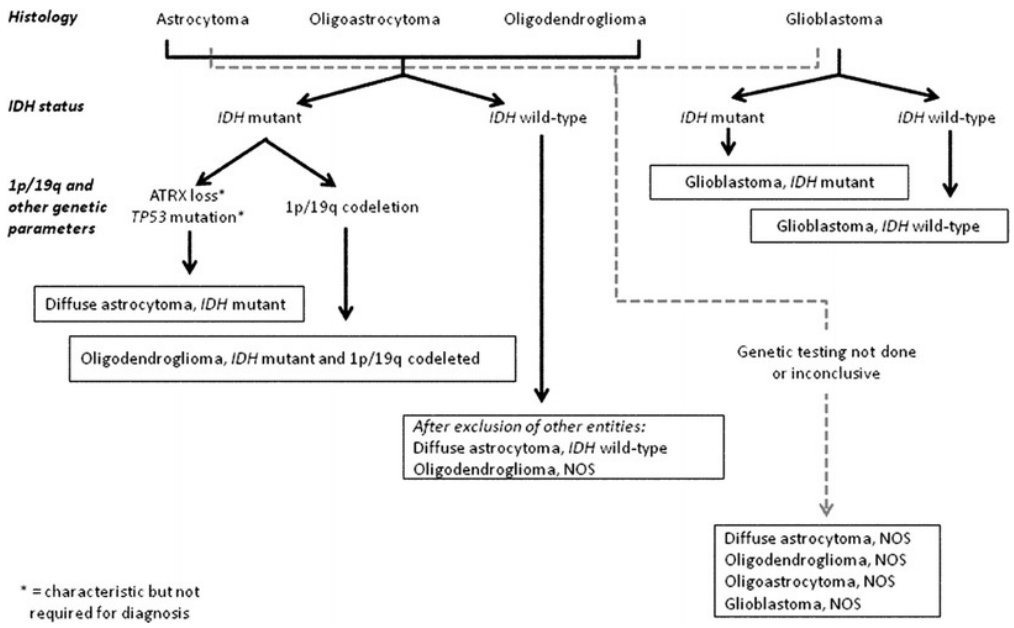

Figure 1.3: Summary of the 2016 brain tumor classification. Histological features and mutation in the gene of IDH and a co-deletion on chromosome 19 and 1 (1p/19q), forms the basis of the classification. Loss of ATRX gene and TP53 mutation also guides classification of diffuse astrocytomas. Oligodendrogliomas develop from the oligodendrocytes, another type of glial cell. NOS= not otherwise specified. Source: [5]

The IDH mutation occurs in one of two IDH isoforms, namely IDH-1 or IDH-2, and a mutant IDH-1/IDH-2 causes a irreversible cellular reaction, transforming α-ketoglutarate, a key metabolite in several cellular processes, to the oncogenic metabolite D-2-hydroxyglutarate (D2HG) [6]. The co-deletion on chromosome 19 and 1 is a loss of heterozygosity (LOH) event where one allele in a genomic locus is lost. [7] This will lead to a homozygote phenotype, and is believed to be the result of either an unbalanced translocation event, where one chromosomal arm is lost, or a balanced translocation, wher chromosomal arms have been exchanged between chromosomes but later deleted [8, 9]. Cancer-related genes have been localized to the chromosomal arms of 1p and 19q, such as the GBM-related tumor suppressor SLC17A7 on 19q [10]. In addition, mutations in the TERT gene promoter and the ARTX gene will also likely become attractive in classifying brain tumors [11, 12]. Both these mutations cause lengthening of telomeres, thus increasing cancer cell viability.

1.2.2 Epidemology

GBM is a highly devastating cancer with median survival time of 14 months following diagnosis, despite surgery, radiation and chemotherapy treatment [13, 14, 15]. The incidence rates varies between 0,59 to 3,69 per 100 000 people worldwide, and is significantly higher in descendants from Western countries than in those originating from Asia, Africa and the Middle East [16, 17, 18, 19]. The incidence of GBM also increases with age, with median age of diagnosis ranging from 75-84 years. Higher risk of developing glioma has been associated with exposure to prior ionizing radiation, e.g. in relation to treatment of head and neck cancers [20], single-nucleotide polymorphisms (SNPs) near the genes CDKN2B, RTEL1 and TERT [21, 22, 23, 24, 25, 26, 27], and a few rare inherited genetic illnesses, including neurofibromatosis 1 and 2, retinoblastoma and Li-Fraumeni syndrome, [28]. Lower risk has been associated with higher levels of serum immunoglobulin E (IgE), a mediator of allergic responses [29], and use of anti-inflammatory medications [30, 31, 32].

1.2.3 Present treatment

Standard treatment of GBM includes surgical resection with adjuvant chemotherapy and radiotherapeutic treatment [33, 34], with the goal of abolishing the tumor and facilitating DNA damage-induced cancer cell apoptosis.

Radiation therapy has the goal of generating DNA-damage induced apoptosis in cancer cells by ionizing radiation [35]. Ionizing radiation creates hydroxyl radicals, either from oxidation of water or from earlier

formed reactive oxygen species (ROS), both which have DNA damaging effects [36]. Standard radiation regiment consists of a total dose of 60 gray (Gy) gamma-radiation over a period of six weeks (2 Gy 5 times a week) [37]. This fractionation of radiation aids in preserving normal cells during radiation exposure [35]. As cancer cells proliferate more rapidly than normal cells, they also create less time for DNA damage repair before DNA replication occurs. By giving radiation in fractions, the normal cells will have time for DNA repair before a new round of treatment is initiated. The chemotherapeutic agent most frequently used is Temozolomide (TMZ), a DNA-alkylating agent that causes breakage of DNA double strands by methylating distinct purine bases in the DNA; O6-guanine, N7-guanine and N3-adenine [38, 39]. O6-guanine alkylations are the most stable and genotoxic, but these alterations can be repaired by an active O6-methylguanine-DNA methyltransferase (MGMT). Methylation status of the MGMT promoter thus impacts treatment efficiencies in GBM, as an active MGMT promoter could confer resistance to DNA damage caused by TMZ. Following this, MGMT promoter silencing has been associated with longer survival in GBM patients [40, 41]. If the O6-guanine methylation is left unrepaired by MGMT, the guanine will mispair with thymine (O6MeG:C→O6MeG:T). Later, this mismatch can be recognized by the DNA mismatch repair (MMR) system, which selectively recognizes and excises only the mispaired thymine, leaving the methylated guanine intact. The sustained methylated guanine results in futile repeating thymine re-mismatches and re-excisions, and DNA single-strand breakage, that causes replication fork arrest and later G2/M phase halt and cancer cell apoptosis.

Despite chemotherapy and radiation treatment, only 9,8% of patients survive longer than five years following diagnosis [42]. The causes of this treatment resistance is complex, and can be caused by great variations in gene expression both intra- and intertumorally, resulting in varying phenotypic profiles that makes it difficult to target and effectively erradicate all cells [43, 44, 45, 46]. The tumor also suffers from heterogeneous and dysfunctional vascularization [47], where fast growth, production of pro-angiogenic factors and changes in the microvasculature organization during tumor growth causes formation of dysfunctional and leaky blood vessels [48, 49, 50]. This causes varying degree of chemotherapy delivery to the different parts of the tumor. Additionally, GBM is characterized by diffuse and aggressive tumor growth, indicating that these cells migrate very effectively through the brain parenchyma [51, 52]. Such tumor migration makes it difficult to completely resect the tumor during surgical innervation. Lastly, the blood-brain barrier (BBB) posses an obstacle in treating GBM, as the BBB is a highly selective barrier, intended to protect the brain from harmful compounds in the blood, but this selectivity also complicates delivery of therapeutic agents to the brain [53, 54]. Some novel approaches have been developed for GBM treatment. These include the use of tumor treating fields (TTFields); where low-intensity electric fields alternating at 200kHz are used to disrupt charge dependent biological processes like cell division [55, 56], and targeted therapies; targeting specific of hurdles in GBM treatment, like MGMT activity in TMZ resistance, vascular endothelial growth factor receptor (VEGFR) role in angiogenesis (Avastin), or central biological pathways like the RTK/PI3K/Akt/mTOR pathway, the PI3K/Akt/mTOR Pathway and the glutamate pathway [57]. Although these therapies have shown some promise, none of these are yet effective enough to be included in standard clinical treatment regime of GBM.

1.3 Cancer stem-cell hypothesis and cellular origin

Much effort has been put into understanding the basis of the fatal nature of cancers, but still the cause of- and relapse of cancers is not yet fully understood. The cellular heterogeneity of tumors, with different sub-populations of cells, has been found important in this regard [58, 59]. One such sub-population of cells are the stem cell-like cells, or cancer stem cells (CSC), initially identified in acute myleiod leukemia (AML) [60]. These cells display three distinct properties: a capacity to initiate tumors and drive proliferation, self-renewal, and ability to give rise to mature non-stem cells [61]. These cells have also shown to be both radio-and chemotherapy resistant [62], subsequently enabling efficient relapse of the tumor (Figure 1.4). Targeting these cells could thus be an interesting approach to GBM treatment.

Glioblastoma stem cells (GSCs) have also been identified and seem to have genetic similarities to neural stem cells (NSCs) [63]. Prominin (CD133) is a marker of healthy NSCs and have also been found expressed on GSCs [64]. Previously, CD133 was believed to be a definite marker of GSCs , which would allow for simple and efficient isolation of GSCs. $CD133^+$ cells showed the capacity to regenerate the tumor upon xenografting, whilst $CD133^-$ cells predominantly did not. $CD133^+$ cells also showed to be resistant to chemotherapy and radiotherapy in GBM, but also in different types of cancers [65, 66, 67, 68, 69, 70]. Later it was understood that CD133 can not be regarded as a definite marker for GSCs, as $CD133^-$ cells also showed some ability to

regenerate tumors [71]. Other intracellular and transmembrane markers have been associated with GSCs, including Nestin, Sox2, LeX/SSEA-1, Bmi1, Ezh2 and Olig2 [72, 73, 74, 75, 76], but no direct isolation methods of GSCs exists today.

NSCs have predominantly been isolated from the brain subventricular zone (SVZ), and subgranular zone (SGZ) in the dentate gyrus (Figure 1.5)[77] . These SVZ astrocyte-like NSCs have also been found to harbour low-level of mutations known to drive GBM tumor growth, like IDH, TERT-promoter, NF1 and PIK3CA gene mutations [78]. The type of cells from which GSCs develop from are still not fully understood; they may develop as a result of oncogenic development in NSCs or progenitor cells, or from differentiated cells that gain stem-cell like abilities by cellular reprogramming or de-differentiation following mutations [79] (Figure 1.6).

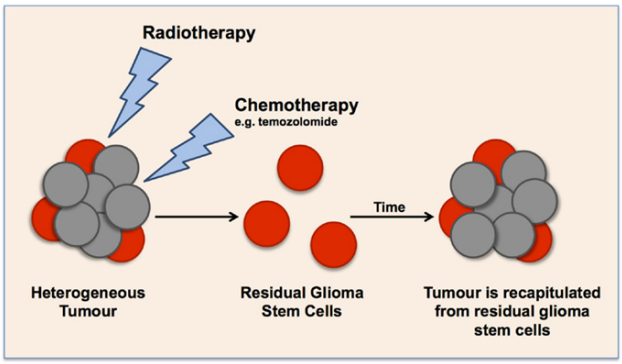

Figure 1.4: The cancer stem cell hypothesis. Cancer stem cells (CSCs) are believed to harbour characteristics enabling radiotherapy- and chemotherapy resistance. These cells will remain after treatment, and are believed to recapitulate the tumor. Source: [62].

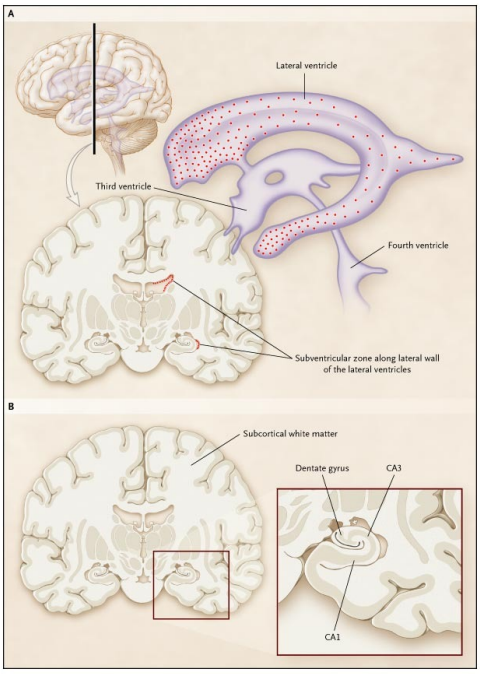

Figure 1.5: Germinal areas of the brain harbouring neural stem cells (NSCs). A) Neural stem cells have been isolated from the subventricular zone (SVZ) and B) subgranular zone (SGZ) of the dentate gyrus in the brain. Source: [80].

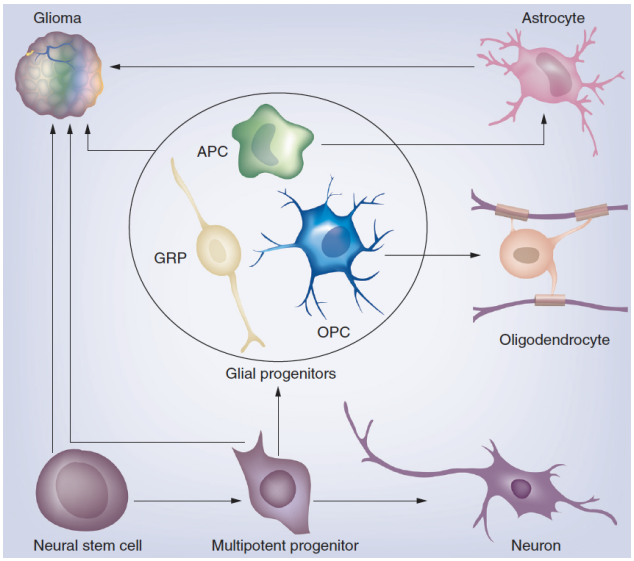

Figure 1.6: Potential cellular origin of GBM cells. The exact cellular origin of GBM cells and GSCs are not yet fully understood, but they could arise from differentiated cells (e.g. astrocytes) that have gained stem-cell like properties through cellular reprogramming, or by de-differentiating following mutations. Mutations and cell differentiation program alterations in neural stem cells or progenitor cells could also potentially serve as a GSCs origin. Source: [81].

1.4 Glioblastoma targeted therapies

Following a deeper understanding of the molecular profiles in GBM, central pathways and pathway components for GBM cell viability have been identified and explored as potential therapeutic targets. Important work on this matter has been conducted through The Cancer Genome Atlas Research Network (TCGA). Some of the identified targets include epidermal growth factor receptor (EGFR), where mutations causing gene deletion (referred to as EGFRvIII) or amplification are the most common genetic alteration in GBM, [82, 83, 84]. EGFR is involved in cancer cell growth, differentiation and viability. Other targets include VEGFR involved in angiogenesis, a central process in tumor growth and metastasis [85, 86]; Hypoxia induced factor 1 (HIF-1), invoked following tumor hypoxia, a result of insufficient oxygenation in rapid cancer cell growth [87, 88]. HIF-1 activate transcription of genes involved in processes like angiogenesis, cell proliferation and metastasis; and PTEN, a tumor suppressor that have shown to be mutated, deleted by LOH or methylated in GBM, resulting in tumor development [89]. Some therapies targeting these components have been through clinical trials, but none have resulted in side-effect-free and complete treatment [90, 91, 92, 93, 94].

1.4.1 Our approach to identify new molecular targets

Targeting GSCs specifically could serve as a potent approach for GBM treatment as these cells seem to have an impact on both relapse and treatment resistance. In an effort to identify key features and potential therapeutic targets in GCSs, our lab (Vilhelm Magnus Laboratory for Neurosurgical Research, Institute for Surgical Research, Oslo University Hospital Rikshospitalet) have compared GSCs to healthy neural stem cells (NSC) from the adult human brain. Although it was found that both cell types shared typical stem cells traits, like the ability to self-renew and differentiate, it was additionally found that GSCs express a selective gene signature that correlate with clinical outcome [95]. In particular, it was found that Wnt-pathway-related genes were dysregulated. In order to functionally validate the identified genes, a CRIPSR/Cas9 based high-throughput loss-of-function screening study was established. Parts of this work was performed during this master thesis; first by validating serum and glucocortocoid-regulated kinase 1 (SGK1) as a positive control target gene in GSCs, and next by exploring the potential role of the Wnt receptor Frizzled-7 (Fzd7) in GSCs.

1.4.2 Serum and glucocorticoid-regulated kinase 1

Serum and glucocorticoid-regulated kinase 1 (Sgk1) has been implicated in central cancer-related biological processes [96, 97]. The gene of SGK1 is located on chromosome 6, which spans over 148 866 nucleotides

divided on 18 exons (NCBI GeneID: 6446), and SGK1 can be expressed in one of five major isomers. SGK1 is transcriptionally regulated by different components and processes, often related to cellular stress, including, as its name suggests, serum and glucocorticoids [98, 99, 100], different hormones and mineralcorticoids [101, 102, 103, 104, 105], cell shrinkage [106], ultra violet and γ-radiation exposure, heat, oxidative stress [107, 108], influenza virus infection [109], and cerebral ischemia and neuronal damage [110]. Sgk1 is part of a larger kinase family, AGC kinases [111] (PK**A**, PK**G** and PK**C** kinase families), that share two highly conserved protein domains; an activation loop in the kinase domain and a hydrophobic motif following the kinase domain [112]. Phosphorylation of these domains leads to activation of the kinase, and in Sgk1 this phosphorylation is done by phosphoinositide dependent protein kinase 1 (Pdk1) and mammalian target of rapamycin 2 (mTORC2) [113, 114, 115, 116, 117]. Pdk1 and mTORC also activates protein kinase B (Akt), another AGC kinase family member, showing great homology to Sgk1 [118, 119]. Downstream processes of Sgk1 includes regulation of immune responses [120], myocardial damage [121, 122], insulin sensitivity [123] and regulation of various ion-channels during cellular stress [124, 125]. Studies in *Caenorhabditis elegans* (*C. elegans*) argues that Sgk1 also plays a part in processes earlier believed to be governed by Akt, particularly in the PI-3-kinase-AKT signaling pathway, further arguing for a resemblance between Akt and Sgk1 [126, 127]. The PI-3-kinase-Akt pathway regulates several cancer-related processes, and downstream effectors include BCL-2 antagonist of cell death (Bad) which regulates apoptosis [112]; and human double minute 2 (Hdm2) involved in p53 degradation [128, 129] (Figure 1.7).

SGK1 is dysregulated in a range of different cancers, including colorectal cancer [130], prostate cancer [131, 132], hepatocarcinoma [133], ovarian cancer [103], breast cancer [134], non-small cell lung cancer [135] and GBM [136], and Sgk1 inhibition in several of these cancers decrease cancer cell viability [137, 138, 139]. In GBM, Sgk1 function have been implicated in GSC function [140, 136], and related to GBM treatment resistance by exhibiting protective functions following oxidative stress and radiotherapy, and inhibition of autophagy [141]. CRISPR/Cas9 knock-down of SGK1 has also shown to result in Sgk1 protein depletion and significantly reduced viability in patient-derived GSCs [140].

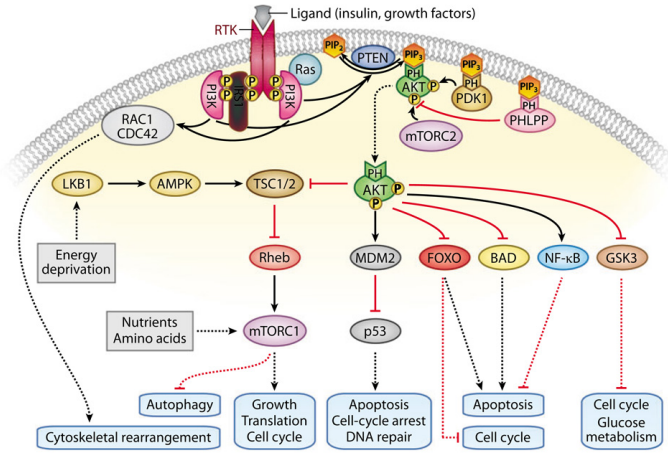

Figure 1.7: PI3-Kinase-Akt signaling pathway, with a selection of downstream processes. Receptor tyrosine kinases (Rtk) is activated upon binding of extracellular ligands, further causing recruitment- and activation of phosphoinositide 3-kinase (Pi3k). Activated Pi3k causes elevated phosphatidylinositol-3,4,5-trisphosphate (Pip3) levels, which allows for recruitment of intracellular proteins, like the serine/theronine kinases Akt, 3-phosphoinositide-dependent kinase (Pdk1), and the phosphatase PH domain and leucine rich repeat protein phosphatase (Phlpp), by binding to PIP3 pleckstrin homology (PH) domains. Akt is activated by phosphorylation by Pdk1 and the rapamycin-insensitive mammalian target of rapamycin (mTOR) complex (mTORC2). Phlpp will dephosphorylate and thus inactivate Sgk1. Several downstream processes of Akt are related to cellular growth, survival, and proliferation. Source: [142]

1.4.3 The Wnt-pathway and Frizzled-7

In the Wnt-pathway, Frizzled-receptors bind secreted Wnt-ligands and initiate downstream processes involved in cell migration, proliferation, embryonic development and cell fate determination [143, 144]. There are 19 Wnt ligands and 10 Frizzled-receptors in humans [145]. The Wnt pathway includes two sub-pathways; the

canonical pathway involving β-catenin and LRP5/6 (Figure 1.8), and the non-canonical pathways not involving β-catenin [144]. The non-canonical pathway includes the planar cell polarity (PCP) pathway and the Wnt/$Ca2^+$ pathway, involved in establishment of cell polarity by cytoskeletal remodelling, and embryonic development and axis determination, respectively. Another alternative Wnt-pathway includes Wnt-FZD/ROR-Gα12/13-Rho-Lats1/2-YAP/TAZ, activating transcriptional coactivator with PDZ-binding motif TAZ (or its homologue YAP) involved in promoting proliferation, cell migration and osteogenesis [146]. In regards to cancer progression, the canonical pathway is the most significant [147].

In the canonical pathway, the absence of Wnt ligand causes intracellular degradation of the transcription regulator β-catenin by the proteasome (Figure 1.8). Thus, β-catenin will not be able to exhort its transcription regulating functions [144]. This is facilitated by β-catenin being retained in a cytoplasmic complex with axis inhibition protein (Axin), adenomatous polyposis coli (Apc), glycogen synthase kinase 3 (Gsk3) and casein kinase 1 (Ck1). Axin functions as a scaffold, whilst Ck1 and Gsk3 phosphorylates β-catenin and marks it for degradation by the proteasome. This degradation is further facilitated by β-Trcp ubiqunination of β-catenin. When the nucleus levels of β-catenin is low, T-cell factor 4 (Tcf4) will bind Groucho (not pictured) and lymphoid enhancer factor 1 (Lef1) (not pictured), and function as a negative transcription regulation of Wnt target genes, like CCND1, ATOH1, CD44, FGF20, JAG1, LGR5 and SNAI1, involved in transcription regulation, cell cycle regulation, proliferation and stem cell maintenance [148]. In the presence of Wnt-ligands, a Wnt-receptor and its co-receptor Lrp5/6 will be phosphorylated on their intracellular domains by Dishvelled (Dsh) and Axin, respectively. This will leave Axin in an unstable unphosphorylated state and β-catenin will be released from the cytoplasmic complex. Binding of Dsh to the Fzd receptor will also allow for inhibition of Ck1 and Gsk3 activity, thus further inhibiting β-catenin degradation. Subsequently, intracellular β-catenin levels rise which allows for β-catenin translocation to the nucleus and binding of β-catenin to Tcf4, resulting in induced transcription of Wnt target genes.

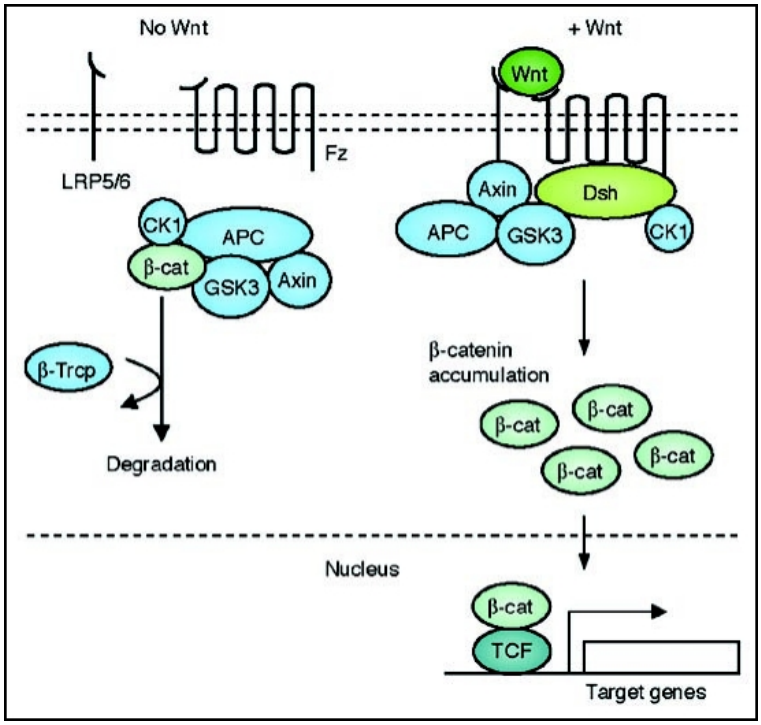

Figure 1.8: The canonical Wnt/β-catenin signaling pathway. In the absence of a Wnt-ligand binding to a Fzd-receptor, β-catenin will be retained- and later degraded in the cytosol and not be able to exhert its transcription regulating functions. In the presence of a Wnt-ligand, its binding to a Fzd-receptor and Lrp5/6 will recruit Dishvelled (Dsh) to the plasma membrane, which further recruits components of the cytoplasmic complex retaining β-catenin to the plasma membrane, thus freeing β-catenin. This will allow for β-catenin accumulation and translocation to the nucleus, where it can function as a transcription regulator. Source: [144]

Therapeutic targeting of the Wnt-pathway in cancer

The Wnt pathway is dysregulated in several cancers, including GBM, making this pathway an attractive therapeutic target [149, 150, 95]. The Wnt-pathway is also involved in cross-talk with other cancer-related pathways, including the Notch, Sonic Hedgehog, JAK/STAT and EGFR pathway [151, 152, 153]. In addition, the Wnt pathway has shown to govern stem cell properties in both embryonic and adult stem cells, in addition to cancer stem cells [154, 155]. Correspondingly, Wnt pathway inhibition has shown to reduce stemness, proliferation and sphere-forming capacities in GSCs [156, 95]. Thus, it is believed that this pathway could contribute to treatment resistance and cancer progression through cancer stem cell processes.

The Wnt pathway can be inhibited by targeting specific components of the pathway [157], like the Wnt receptors, the Dishvelled (Dsh) protein and Tcf/β-catenin. Use of natural inhibitors of the Wnt pathway has also been studied, like dickkopf-related protein (Dkk), Wif and sFRP, where the former bind to and inhibit Lrp5/6, whilst the two latter inhibit Wnt-ligand association with Wnt-receptors [158, 159]. In addition, secondary processes and components related to the Wnt-pathway have been inhibited, like Tankyrase 1 and 2 involved in Axin degradation or Porcupine, a protein ensuring correct post-translational acylation/pamitoylation of secreted Wnt-ligands in the endoplasmatic reticulum (ER) [160, 161]. Also, targeting of closely-connected pathways have been explored, like the Hedgehog and Notch signaling pathways [162]. Three Wnt-targeting drugs have been FDA approved for used in the clinic. These include Sulindac (Merk & Co., Inc.), Pyrvinium (U.S. Pharmacopeia) and Niclosamide (Taj Pharma) [163, 164]. These are all FDA-approved as they were primarily intended and approved for other uses, namely as anti-parasitic and anti-inflammation drugs, but showed to regulate the Wnt-pathway as well. More specific targeting by multiple Fzd-receptors includes OMP-18R5 (Vanticumab, Onco Med Pharmaceuticals) which inhibit half of all Fzd-receptors. Still, its safety is being evaluated [165]. OMP-54 F28 (Ipafricept, Onco Med Pharmaceuticals) inhibits Wnt-signaling by interacting with the extracellular domain of Fzd8 and poses as a highly specific target. But, concerns were raised about side-effects of OMP-54 F28 following Wnt-inhibition in bones, as it seemed to increase the turnover rate of bone cells [166]. Thus, there is need to further explore specific targeting of the Wnt-pathway.

The FZD7 gene encodes a seven-transmembrane Wnt-receptor protein with an extracellular cysteine-rich ligand-binding domain, followed by a transmembrane domain spanning the membrane seven times, and an intracellular domain with a PDZ domain-binding motif (NCBI GeneID: 8324). The gene of FZD7 is located on chromosome 7 and consists of 3850 nucleotides with one exon, resulting in only one transcript variant. FZD7 transcription has been found to be regulated by different factors and processes, including Trp63 and Notch-3 in breast cancer [167, 168], and fibronectin, Wnt3a and β-catenin in colorectal cancer [169]. Fzd7 has been posed as an attractive Wnt-target as it is involved in both the canonical and non-canonical pathway and can associate with several different co-receptors and Fzd proteins [170, 157]. Fzd7 expression also maintains pluripotency of embryonic stem cells, and could conceivably also control stem cell properties of glioblastoma stem cells. In addition, FZD7 is upregulated in GSCs compared to adult healthy neural stem cells [156, 171]. It is believed that the upregulation of Fzd7 causes sustained glioma cell proliferation by upregulating TAZ [171]. TAZ is a downstream effector of the Wnt pathway, with a role in organ size regulation, tissue homeostasis and tumorigenesis. Lastly, expression of FZD7 has been found to negatively affect clinical outcome in GBM patients [156]. All these characteristics of Fzd7 makes it an interesting potential therapeutic target.

1.5 CRISPR/Cas9

Modern techniques for gene-editing have enabled effective and precise alterations of the human genome, by so-called reverse genetics and a "genotype-to-phenotype" approach, compared to the traditional forward genetics and "phenotype-to-genotype" approach [172]. The traditional approach studies the effects of a gene by generating random mutations in the genome, which could be induced by chemicals, radiation, or insertion of gene-disrupting DNA [173, 174]. Following random mutagenesis, genetic screens and selection procedures would be conducted in order to identify mutants with alterations in the desired phenotype. Subsequent analyses to determine what genes are involved in creating these phenotypes would then have to be preformed. This outlines a highly laborious process. The discovery that nucleases combined with DNA-binding proteins could be used to induce targeted and specific mutations in desired genes, followed by study of the phenotypic effect of this specific mutation, demonstrated a "genotype-to-phenotype" approach which allowed for easier, and more effective and specific gene-editing [175]. Earlier methods for study of gene function includes zinc-finger nucleases and transcription activator-like nucleases (TALENs), based on

the engineered use of sequence-specific DNA-binding proteins, joined with a non-specific nuclease, where the sequence-specific proteins can be designed to target any desired genomic sequence [176, 177, 178]. Clustered regularly interspaced short palindromic repeats/CRISPR associated protein 9 (CRISPR/Cas9) is a relatively novel technique for precise gene-editing, and is based on a different principle than zinc-fingers and TALENs, allowing greater modularity, higher specificity and simpler conduction of gene-editing [174].

1.5.1 Bacterial CRISPR-system

The CRISPR/Cas9-system was first discovered in bacteria as part of their inherent adaptive immune system to bacteriophage infection, where bacterial CRISPR loci consisting of DNA from previously encountered viruses, and CRISPR associated genes (cas) genes allows for acquired immunity. Three types of CRISPR immunity have been described, varying in which cas genes are expressed; Type I is mediated by Cas9 nuclease and the Cascade complex, type II by Cas9, and type III by Cas6 [179]. The most commonly described immunity in relations to gene-editing in mammalian cells, and also the first to be adapted to eukaryotic cells, is type II [180].

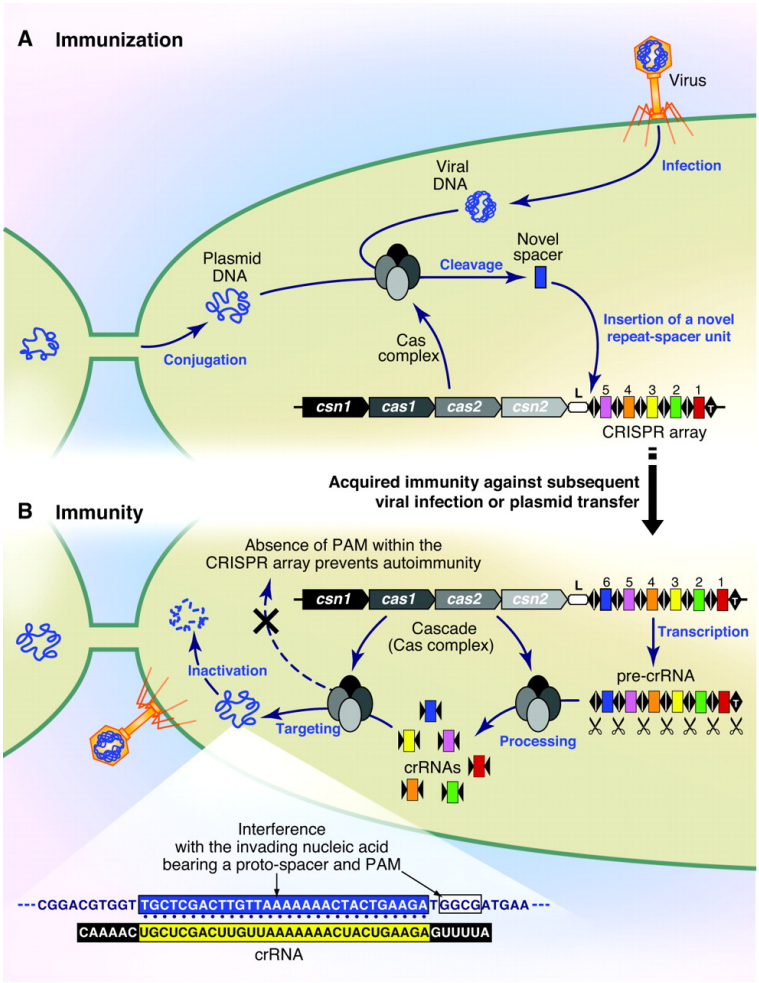

Figure 1.9: Process of CRISPR-mediated adapted immunity in bacteria. A) The first process involves immunization, where the bacteria is infected by a bacteriophage, which injects its viral genome into the bacteria cytoplasm. The viral genome is cleaved by Cas proteins and inserted into the bacterial genome as spacers in-between CRISPR-repeats. B) Subsequent encounters with viruses whose DNA has been inserted as spacers into the bacterial genome, will initiate transcription of the spacer-repeat array (crRNA), which will join with a tracrRNA (not shown) to form a single-guide RNA (sgRNA). The sgRNA will bind to and guide the Cas nuclease to viral DNA complementary to the sgRNA sequence, and the Cas nuclease will cleave viral DNA. This will inhibit further integration and expression of the viral DNA. Source: [181]

Immunization

Bacteriophage infection is initiated by binding to the host cell through interactions with cell surface components such as protein, lipids, glycoproteins, carbohydrates, or other bacterial surface structures like cilia or pili [182]. Binding of the phage to the host cells initiates injection of viral genome into the host cell cytoplasm.

When foreign viral nucleic acids are present in the bacteria cytoplasm, the CRISPR system inserts the DNA, referred to as protospacers, between repeating sequences in the bacterial genome, referred to as CRISPR repeats [183, 184, 185]. The protospacers will serve as a repertoire of viral DNA from previous infections. CRISPR repeats are identical, palindromic DNA sequences of about 20-50 base pairs, separated by the protospacers [181, 185, 184]. The choice of protospacer is believed to be facilitated by a complex of the conserved cas-proteins Cas1-Cas2 [186], and in type II immunity, also by Cas9 [187]. The selection of correct protospacer is pivotal in order to distinguish self- and foreign nucleic acids, as failure to do so would result in cell death. This distinction is believed to be facilitated by a strong preference of non-self DNA in the host cell. For example, in *E.coli* this preference is conferred by over-represented Chi-sites in the genome, which inhibits protospacer acquisition from the self-genome [188]. The protospacer selection occurs by the Cas1-Cas2 complex sampling DNA fragments of the viral DNA [179]. These fragments are believed to be generated from DNA breaks during viral replication. Cas9 also aids in this selection process by favoring protospacers that are flanked by a specific protospacer adjacent motif (PAM) site, used by Cas9 later in the immunity process to locate and damage the correct viral DNA [187]. Next, the protospacer is integrated into the host cell genome by the Cas1-Cas2 complex [189]. This process is facilitated by a free 3' OH end in the protospacer, which allows for a nucleophilic attack on the phoshodiester bonds between the first repeat and spacer sequences [190].

Immunity

Subsequent encounters with infecting viruses whose viral DNA has previously been inserted as a protospacer in the bacterial genome, showcases immunity. When this occurs, the CRISPR repeats and the protospacer arrays are transcribed into so called pre-CRISPR RNAs (pre-crRNAs), probably initiated by a non-coding A/T rich region located immediately upstream of the first repeat, functioning as a promoter [191]. The pre-crRNA is processed into smaller RNA molecules by RNAse III, with a sequence complementary to the protospacer of about 20 nucleotides (nt), and a sequence derived from the repeat region of about 12 nt [181, 192]. The crRNA will be joined with a so-called transactivating crRNA (tracrRNA), transcribed from a nearby site upstream of the CRISPR arrays [193]. The tracrRNA consists of a sequence complementary to the repeats of about 14 nt, called anti-repeats, and two hairpin structures formed by nearby same-strand complementary sequences at the 3' end [194]. The joining of the crRNA and the tracrRNA is facilitated by DNA overhangs in anti-repeat and repeat regions of the tracrRNA and the crRNA, respectively. The DNA overhangs are produced by RNAse III, and the overhangs allows for base-pairing between the tracrRNA and crRNA, forming a so-called single-guide RNA (sgRNA) [193]. When the sgRNA forms it will create distinctive structures enabling correct complex-binding and activity of Cas9 at the target DNA (Figure 1.10).

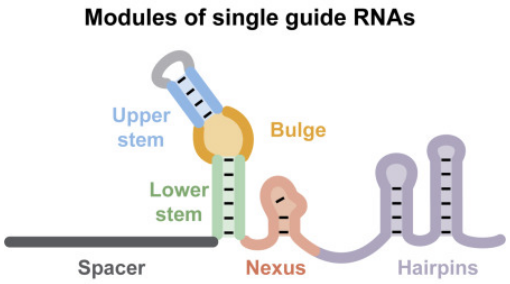

Figure 1.10: Binding of tracrRNA and crRNA to create sgRNAs. The spacer corresponds to the protospacer unit of the crRNA, the stem loop with bulge is created by the crRNA:tracrRNA joining, whilst the nexus and two hairpins are derived from the tracrRNA 3' end. These structures formed in the sgRNA are central for correct DNA binding and function of the Cas9. Source: [194].

Cas9 exists is many homologs amongst prokaryotes and Archea that have been explored for use in gene-editing [195, 196, 197, 198, 199, 200], but the most widely used Cas9 for gene-editing is the Cas9 derived from *Streptococcus pyrogenes* (SpCas9). Cas9 will form a complex with the sgRNA, and the crRNA part of the sgRNA, referred to as the "seed" seqcuence [201], will aid in guiding the complex to the desired cut site through complementary base-pairing [202, 203, 180]. Interactions between the sgRNA and Cas9 relies on the secondary structure of the sgRNA. The tracrRNA portion of the sgRNA creates three stem loop strcuture, and the joining of tracrRNA and crRNA creates another stem loop (Figure 1.10). Studies have shown that of the crRNA:tracrRNA interactions, the stem loop forming form tracrRNA:crRNA joining and the nexus are the most central to ensure the function of Cas9, whilst the 3' more distal structures of the tracrRNA are not pivotal for Cas9 function, but could aid in stabilizing sgRNA binding [203, 204, 205]. The Cas9 will bind 3 basepairs upstream of the desired site if the Cas9 is positioned immediately 5' adjacent to the desired PAM-site [206]. The crystal structure of SpCas9 binding to its desired PAM site (NGG) shows that the NGG site is necessary for correct association with the Cas9:sgRNA complex. Cas9 consists of two lobes; the nuclease (NUC) lobe and the recognition (REC) lobe (Figure 1.11) [207]. The NUC lobe contains the PAM-interacting (PI) domain, and the HNH and RuvC domains which confer the nuclease activity of Cas9, by cutting the strand complementary to the crRNA, and the non-complementary strand, respectively [203]. The PI domain determines the PAM site specificity and ensures binding of the sgRNA/Cas9 complex to the desired site. The REC lobe contains two REC-domains, REC1 and REC2, and a Bridge helix. The REC 1 domain aids in joining the sgRNA/Cas9 complex to the target DNA by binding to the phosphate backbone of the target DNA. The REC2 domain might have a function in occluding the HNH domain when SpCas9 is bound to off-target DNA sequences [208]. The Bridge helix contains a conserved arginine cluster that aids in the recognition of the target DNA by the sgRNA, by allowing binding between the sgRNA/Cas9 complex and the target DNA at the "seed" sequence.

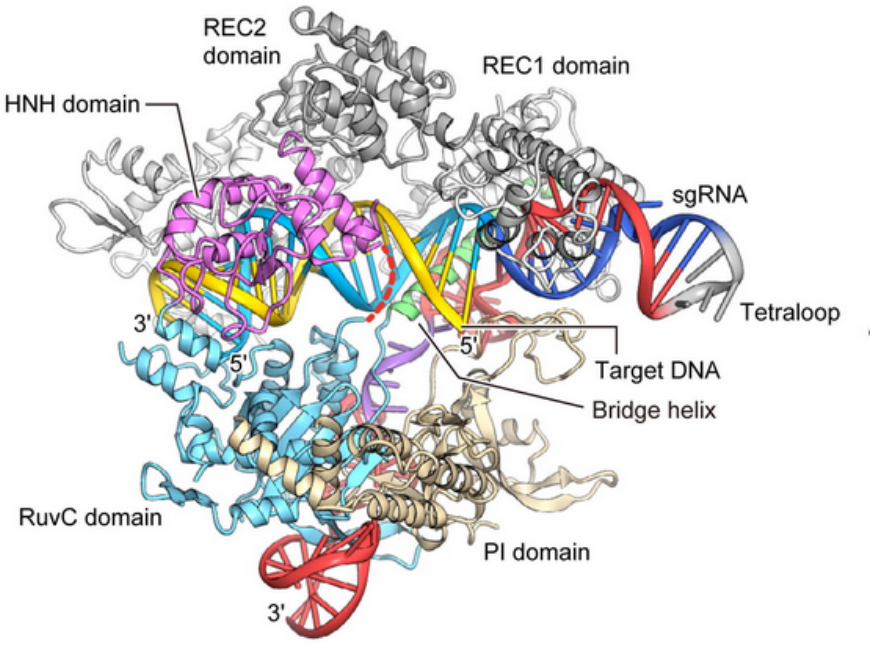

Figure 1.11: Crystal structure of SpCas9 bound to sgRNA and target DNA. SpCas9 consists of two lobes; the nuclease (NUC) lobe and the recognition (REC) lobe. The NUC lobe contains the HNH and RuvC domains which confer the nuclease activity of Cas9, and the PAM-interacting (PI) domain. The REC lobe contains two REC-domains, REC1 and REC2, and a Bridge helix, which aids in sgRNA/Cas9 DNA binding. Source: [207]

1.5.2 Adaption for directed gene-editing in mammalian cells

Transferring the CRISPR/Cas9 system to mammalian cells has allowed for precise and effective gene-editing, and it was successfully adapted to mammalian cells in 2013 [180, 209, 210]. From earlier it was shown that tracrRNA, pre-crRNA, RNase III and Cas9 were needed to generate successful double-stranded breaks in prokaryotes [203, 211, 212, 213]. Later, Cong et. al. demonstrated successful genome-editing in mammalian cells, without RNase III, arguing that the RNAse III functions in pre-crRNA maturation conceivably can be conferred by endogenous RNases in the mammalian cells [180].

Several studies have reported successful generation of synthetic sgRNAs by fusing a sequence complementary to the desired cut site, mimicking the crRNA, to a synthetic tracrRNA via a linker loop [209, 203]. Delivering the RNAs in such a fashion also circumvents the requirement to imitate bacterial transcript maturation machinery in mammalian cells [209]. The specific secondary structure of the native sgRNA and how it aids in full functionality of Cas9 poses some structural requirements on the synthetic sgRNA. Jinek et al [203] showed that the minimal required structures of the sgRNA for Cas9 activity are predominantly the structures forming from the tracrRNA:crRNA joining, whilst the stem loop structures further 3' in the tracrRNA are not as central. Jinek et al. later showed that these minimal secondary structures of the sgRNA promotes Cas9-editing also in human cells [214].

In order for the Cas9 to cut at the desired genomic site, it would need to be adjacent to the PAM site required by the specific Cas9 homolog. The availability of these PAM sites throughout a mammalian genome depends on the choice of Cas9 homolog, but the NGG PAM site of the commonly used SpCas9 can be found at approximately every 30th-40th base in the human genome, making it a highly versatile Cas9 [215]. In order for the bacterial Cas9 to function in mammalian cells, mammalian codon-optimized versions of Cas9 with nuclear localization signals are used, to ensure binding of mammalian tRNA for translation and localization of Cas9 to the nucleus, respectively [209]. The bacterial and mammalian CRISPR-systems are compared in Figure 1.12.

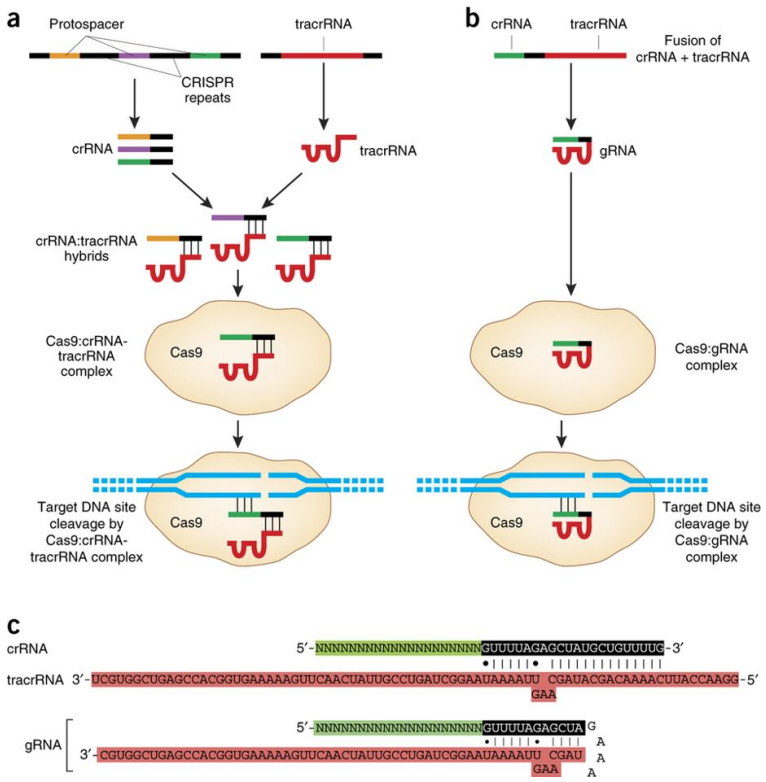

Figure 1.12: Bacterial and mammalian CRISPR-systems. A) CRISPR/Cas9 system as part of bacterial adaptive immune system. B) Adapted CRISPR/Cas9 system for use in targeted gene-editing. C) Example of crRNA:tracrRNA hybrids as found in baterial adaptive immune system (upper). Example of guideRNA (gRNA) used in CRISPR/Cas9 for targeted gene-editing (lower). The gRNA is a fusion of crRNA and tracrRNA by a nucleotide linker. Source: [216].

Repair mechanism following Cas9 activity

Cas9 generates DNA double-stranded breaks, which is followed by activation of two interconnected pathways, namely DNA repair and cell cycle checkpoint, generally referred to as the DNA damage response (DDR) (Figure 1.13). In the cell cycle checkpoint pathway, a complex of Mre1, Rad50 and Nbs1 (MRN) will recruit ataxia–telangiectasia mutated (Atm) to the break site [217]. Atm further activates and recruits several different protein to the break site to aid in repair. Some include H2ax, involved in chromatin-remodelling needed for DSB repair, and replication protein A (Rpa) involved in exposing single-stranded DNA at the break site to allow for repair. DNA-dependent protein kinase (DNA-Pk) and Atm and Rad3 related (Atr) are also recruited to the breaks site. These proteins are involved in activation of Chk2 and Chk1, ensuring cell cycle arrest. This cell cycle checkpoint pathway allows time for the cell to conduct DNA repair.

In the DNA repair pathway, the DSBs can generally be repaired by one of two mechanisms; non-homologous end joining (NHEJ) or homology-directed repair (HDR). HDR requires a homologous template in order to induce repair, and is predominantly functional in S/G2 phase of normal cell cycle, when a sister chromatid and HDR proteins are present, or when it is introduced with a CRISPR/Cas9 system [218]. NHEJ, on the other hand, repairs the DSB by joining the two free ends together and can function in all cell cycle phases. Thus, NHEJ is believed to be the major repair mechanism in mammalian cells. It was earlier believed that NHEJ referred to a single error-prone repair pathway, but later studies have implied that sub-pathways of NHEJ exist, namely classical NHEJ (C-NHEJ) and alternative NHEJ (A-NHEJ) [219, 220]. Whereas the C-NHEJ is indeed able to perfectly regenerate the correct DNA sequence following a double-stranded break, the A-NHEJ is generally more error-prone, but these repair mechanisms are not mutually exclusive. In C-NHEJ, a heterodimer formed from Ku70 and Ku80 bind to the free ends of the DNA, which protects the ends from degradation and aids in preparation of strand ligation [221, 219]. Ku70/Ku80 binding recruits DNA-PKs, which aid in holding the two DNA ends together, and activates downstream repair proteins together with Atm. Next, modification of the ends might be necessary, in order to create ligatable DNA ends. Depending on the nature of the DSB, different enzymes can be used for this process. Finally, the two broken

ends are ligated by DNA ligase IV, which occurs in a complex with X-ray cross complementing protein 4 (Xrcc4), aiding in stabilizing the ligase. The A-NHEJ pathway is not yet fully characterized, but is believed to govern error-prone repair pathways, including microhomology-mediated repair, where homologous regions away from the DSB associate and the 3' overhangs are removed, often causing a gene deletion [222, 223, 224]; or extension of the DNA strand by short microhomology regions and polymerase theta (Polθ), causing insertions close to perfectly matching flanking regions of the DSB [225]. In addition to causing insertion and deletions, these processes have also shown to be able to cause large chromosome translocations [226, 227].

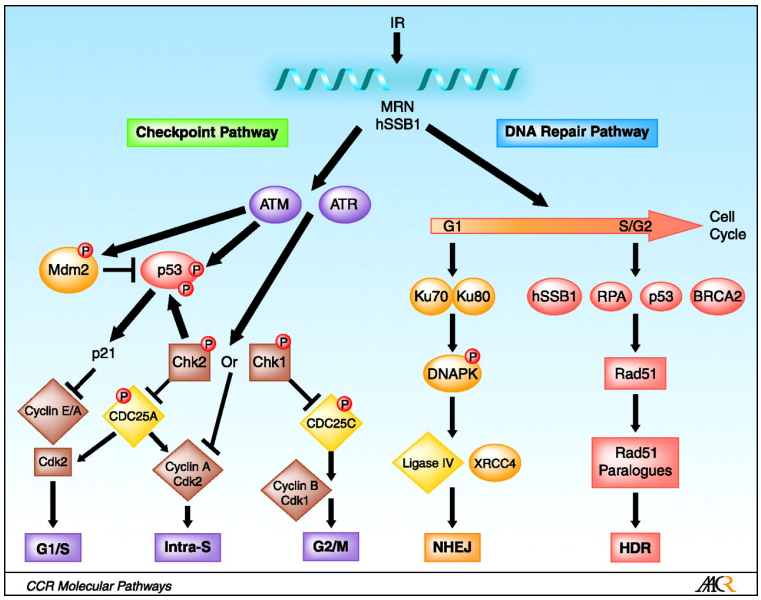

Figure 1.13: Overview of DNA damage response (DDR). Following a DNA DSB the cells will initiate DNA repair and cell cycle checkpoint pathways to ensure repair of the break. Source: [228].

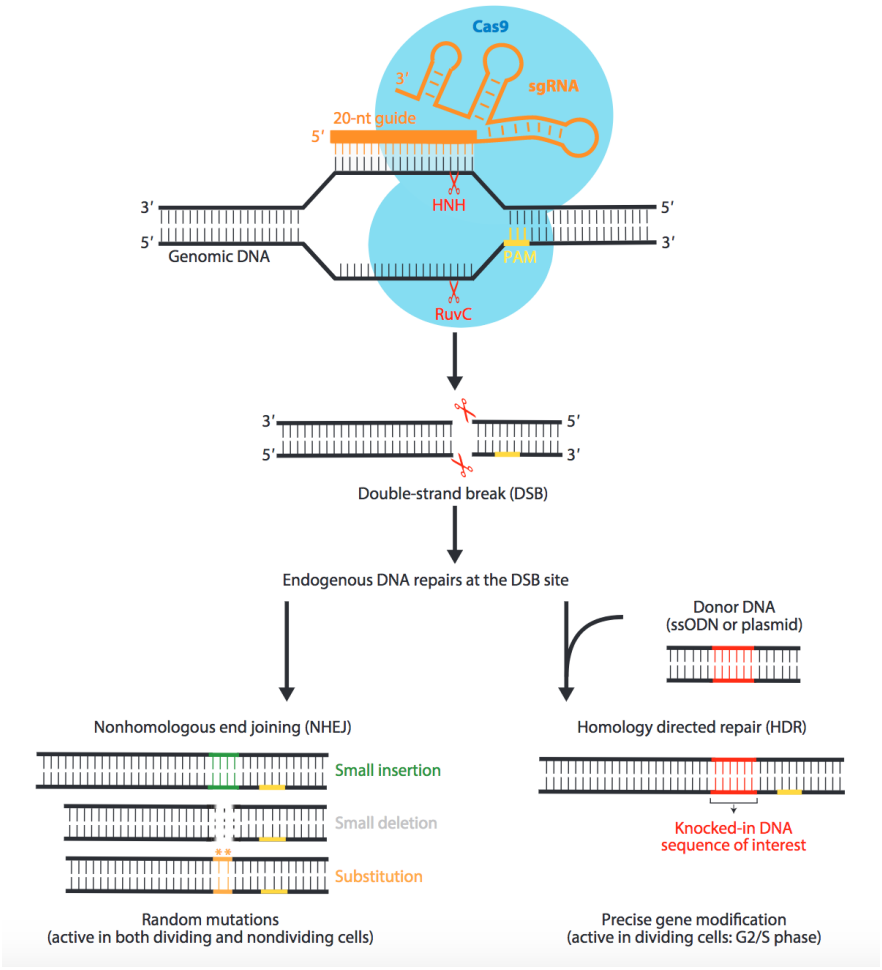

Figure 1.14: DNA double-stranded (DSB) break repair mechanisms. Following DNA DSB from Cas9 activity, the DNA strands can be repaired in one of two ways; by non-homologous end joining (NHEJ) or homology-directed repair (HDR). The first mechanism includes error-prone sub-pathways and can cause small insertions or deletions (indels). The latter mechanism occurs in the presence of a donor template with ends or "arms" homologous to the ends of the DNA cut by Cas9. Source (with modifications): [229].

Consequences of mutated DNA

Following CRISPR-induced DNA damage and error-prone NHEJ repair, different types of mutations can be introduced; non-sense, where the mutation causes translation into premature termination codon (PTC; UAA, UAG, UGA), thus inhibiting further translation; missense, where the mutation causes translation of the DNA triplet into a different amino-acid than in wild-type; and framshift, caused by insertions or deletions that changes the codon reading frame. As all of these mutations have potentially damaging effects on the final protein, quality control processes exist, explained below, to inhibit accumulation of such non-functional mRNAs and proteins.

At mRNA level nonsense mutations are recognized and marked for degradation by nonsense-mediated mRNA decay (NMD). In addition, framshift or missense mutations causing no-stop-codon (NSC), no-go-codon (NGC) or structures causing stalling of the ribosome are degraded by no-stop decay (NSD) and no-go decay (NGD) [230]. These processes are translation-dependent in the manner that the PTC, NGC and NSC is recognized by the ribosome during translation, before the mRNA is degraded. Recognition of PTC is by its location upstream and in proximity to protein complexes binding to exon-exon junctions during mRNA splicing (exon-junction complexes (EJC)). This creates a distinction between native stop codons and PTC, as a native stop codon would be located downstream of EJCs. NGD and NSD is initiated by recognition of stalled ribosome complexes deposited on the mRNA due to absence of start-codon, presence of inhibitory mRNA secondary structures like stem-loops, alteration in miRNA binding sites, or presence of premature poly-A-tails, and ab-

sence of termination codons [231, 232, 233]. Generation of PTC by CRISPR/Cas9 gene-editing is sought after as successful mRNA degradation will inhibit further protein translation and effectively produce a knock-down phenotype. In genomes rich in A and T nucleotides, multiple PTC can be induced by framshift mutations in about every encoded gene. [234]. Thus, if framshift mutations occur, the likelihood of it resulting in PTC is high. Still, NMD decay is complicated by the fact that only about half of PTC are identified and degraded [235, 236, 237]. Missense and frameshift mutations that does not cause changes to stop or start codons, are more difficult to recognize at mRNA level, as cellular repair mechanisms have no understanding of which DNA sequence is correct or incorrect for coding of a particular protein.

If the mutation is not recognized at mRNA level, it can be recognized as damaging at protein level by the alterations it makes to the protein structure. Subsequently, the protein can be degraded by the major protein degradation pathway, governed the ubiquitin-proteasome, [238]. In the ubiquitin-proteasome pathway, proteins that fail to reach their native conformation may be selectively recognized by molecular chaperones (Hsp70 or Hsp90) [239]. These chaperones bind hydrophobic domains, which should normally not be exposed in hydrophilic environments, and unfolded proteins. Chaperons also play an important role in initial protein folding in the endoplasmatic reticulum (ER), by providing an environment facilitating correct folding [240]. Thus, mutated proteins could also be recognized before they reach a potential functional stage. Ubiquitin-activating enzyme (E1) will further activate ubiquitin units in an ATP-dependent manner, and activate a complex of ubiquitin-conjugating enzyme (E2) and ubiquitin ligase (E3), which creates a polyubiquitin-"tail" that marks the protein for further proteasomal degradation. Complexes of E2 and E3 could also be involved in the initial recognition of misfolded proteins. A range of different E2 and E3 ligases exist and their complexing creates a greater number of possible interaction, enabling recognition of a wide range of proteins [241, 242]. Proteins with ubiqutin conjugations are recognized by a large ATP-dependent protease called the 26S proteasome, which will degraded the proteins into small peptides. Despite the presence of these quality control systems, mutated proteins can escape repair and degradation, causing toxic aggregation and accumulation of non-functional proteins, which can have substantial effect on cell viability and function. This have been associated with several diseases, including Alzheimer's disease, Huntington's disease and Parkinson's disease [243], and cancers [244, 245, 246, 247].

1.6 Aims of the study

Due to the aggressive nature of GBM and lack of effective treatment, there is a pressing need for novel therapeutic approaches to treat this type of cancer. Targeting central components or pathways for CSC viability has received much attention, as this approach potentially could eradicate the cells believed to govern cancer characteristics that complicate present day treatment. Gene-editing and gene knock-down by the relatively novel method of CRISPR/Cas9 has showed great promise in recent research, and could function as a tool to investigate new potential therapeutic targets for CSC viability.

The aims of this study was to functionally validate knock-down of the Wnt-pathway receptor Fzd7 using CRISPR/Cas9 technology by,

1. Establishing assay protocol conditions for knock-down and viability assays by targeting a functional control gene (SGK1) in one primary GSC culture. Evaluation of knock-down effect was done at the level of DNA, mRNA and protein.
2. Use the established conditions to explore knock-down of Fzd7 in four primary GSCs cultures.

Materials and methods

2.1 Tumor biopsies and acquisition of primary cell cultures

Gliobastoma primary cells were obtained from four informed and consenting patients undergoing surgery for GBM at Oslo University Hospital. All patients signed an approved consent form from the Norwegian Center for Research Data (NSD), where the patient agreed to allow the biposy to be part of a general biobank. The general biobank is approved by Personvernombudet and the project was approved by the Norwegian Regional Committee for Medical Research (REK 2017/167). All primary cells were derived from patients with confirmed GBM diagnosis following WHO classification.

Following surgical removal, the tumor tissue was placed in a 50 ml tube in cold L-15 media (Leibovitz L-15, without L-Glutamine, LONZA, 12-700F) and transferred to the lab. Blood and blood vessels were removed from the tissue in a petri dish. The tissue was cut into smaller pieces and placed in a tube containing 10 ml L-15, before the tube was centrifuged (Kubota 2420, Kubota Corporation) at 300 x g for 5 minutes. The supernatant was removed and the tissue manually chopped into smaller pieces using a scalpel, for further dissociation. The tissue was then placed in a new tube containing L-15, before being centrifuged at 300 x g for 5 minutes. The supernatant was removed and 1 ml pre-warmed trypsin (37°C, Trypsin 0,05 EDTA, Invitrogen, 25300054) was added, before the tube was left to incubate at 37°C for 5 minutes. The sample was tritruated and 100 ul albumin (200 mg/ml, human serum, Octapharma, 478172) and 10 ml L-15 was added to inhibit the trypsin digestion, before the tube was centrifuged at 300 x g for 5 minutes. The supernatant was removed and the cell pellet tritruated, before the cells were further separated through a cell strainer (40 μm nylon, Corning Inc., 352340) over a 50 ml tube. The cells were seeded in culture flasks (Cell Culture Flasks, Nunc™) at a density of 1,0 x 10^5 media.

2.2 Culture maintenance and cell passage

Cell culture conditions for enrichment of GSCs have previously been described [248]. Sphere-forming GSCs were achieved by incubation in serum-free media, further referred to as full media (Table 2.1). Four different patient-derived sphere-forming GSCs cell cultures were studied, termed T1008, T0965, T1548 and T1547.

	Concentration
DMEM/F12 (Dulbeccos's Modified Eagle Medium (DMEM)/F12 (1:1), with GlutaMAX, GIBCO, 31331-028)	1 X
Pen/Strep (LONZA, 17602E-12, 10000 units/ml each)	100 units/ml each
Hepes buffer (LONZA, BE17-737E)	10 mM
Heparin (LEO® Pharma As, 585661)	2,5 μg/ml
B27 w/o Vit. A (Invitrogen, 12587-010)	1:50
FGF (R&D Systems, 233FB)	10 ng/ml
EGF (R&D Systems, 236-EG)	20 μg/ml

Table 2.1: Composition and component concentration in sphere-forming full media. DMEM/F12 concentration is noted as 1X, as all other components are added to DMEM/F12 at their respective concentrations. Catalog numbers and manufacturers are also given.

For cell passage, cells were collected from culture flasks in a 50 ml tube and the flask was washed with L-15 medium. The cell suspension was centrifuged at 300 x g for 5 minutes, before the supernantant was discarded. 1 ml prewarmed trypsin (37°C) was added to the cell pellet. The cells were incubated in a water bath at 37°C for 5 minutes and triturated briefly, before 100 μl albumin and 10 ml L-15 medium was

added to inhibit the trypsin digestion. The suspension was centrifuged at 300 x g for another 5 minutes. The supernantant was removed before 1-4 ml (depending on the pellet size) full media was added, and the pellet resuspended. 10 μl cell suspension was aliquoted to preform cell counting and 10 μl tryphan blue (Life Technologies, T10282) was added to the aliqout. 10 μl tryphan blue cell solution was applied to a counting chamber (Invitrogen, C10228), and cell counting was performed using an automated cell counter following established protocol (Countess® Automated Cell Counter, Invitrogen, C10227). The cells were seeded in new culture flasks to a density of 1,0 x 10^5 per ml full media. The cells were incubated in an incubator (Thermo Electron Corporation, HeraCell 240, 37°C, 5% CO2) and fed with EGF/FGF two to three times a week. Cells were passaged when sphere size was approximately 100 μm in diameter.

2.3 Optimization studies and establishment of protocol conditions

Certain protocol conditions for viral transductions were established in the lab before this work was conducted. Some of these conditions were re-validated and other protocol conditions specific for this study was optimized in a preliminary round of optimization. Next, a functional control of the CRISPR/Cas9 system was conducted by SGK1 knock-down in order to fully establish CRISPR/Cas9 protocol conditions specific for this study. Established protocol conditions were applied in Fzd7 knock-down studies.

2.4 Gene knock-down by CRISPR/Cas9

2.4.1 Seeding of cells

Lentiviral infection was facilitated by temporary cell well-adhesion, using the cell matrix component laminin. Laminin adherence has earlier showed to greatly increase transduction efficiency in GSCs (Marit Brynjulfsen, Phd Fellow, personal communication), without altering their stem cell properties [249]. Laminin (1-3 mg/ml, BD Biosciences, 354232) was thawed on ice before being added to a concentration of 10 μg/ml full media per well in tissue-culture treated plates (Corning Costar®, 6 Well Cell Culture Cluster, 3516 and Corning Costar®, 96 Well Cell Culture Cluster, 3596). 50 000-60 000 cells/ml full media were seeded to reach desired 60-80% confluency following overnight incubation (37°C, 5% CO2). Lentiviral transduction was preformed the following day.

2.4.2 The Cas9 and sgRNA constructs

Cas9 and sgRNA constructs were provided by Dharmacon™(GE Healthcare, Edit-R™). Three sgRNAs targeting each gene were provided and termed 74, 75 and 79 for targeting SGK1, and 94, 96 and 100 for targeting FZD7. Each sgRNA targeted different genomic sites within the gene exons (Table 2.2, Figure 2.2). sgRNA target sequences were chosen based on an optimized algorithm adopted by the manufacturer. In addition, a non-targeting control (NT) sgRNA was introduced. This sgRNA should not be able to target any site in the human genome. The Cas9 nuclease was derived from *Streptococcus pyogenes*, for function in type II immunity. The Cas9 construct was human codon-optimized and utilized the human cytomegalovirus immediate early promoter (hCMV) to drive gene transcription (Dharmacon, VCAS10124) (Figure 2.1). Choice of hCMV as promoter was based on earlier transduction optimization studies (Marit Brynjulfsen, PhD Fellow, personal communication). Selection of successfully transduced cells was based on antibiotic resistance encoded in the viral constructs; blasticidin resistance in the Cas9 construct, and puromycin resistance in the sgRNA constructs (Figure 2.1 and 2.2). Additional components of the constructs include 5' long terminal repeat (LTR), psi packaging sequence (ψ) and Rev Response Element (RRE) for successful lentiviral production, and genome integration and packaging; Woodchuck Hepatitis Post-transcriptional Regulatory Element (WHPRE) for enhanced transgene expression, and a 3' self-activating long terminal repeat (SIN LTR) for generation of lentiviral particles witout the ability to replicate. The Cas9 construct also encoded a self-cleaving peptide (T2A) allowing expression of both blasticidin resistance and Cas9 from the same transcript.

Catalog number	Gene target	Genomic location	DNA target sequence
VSGH10142-246491709	SGK1 (74)	hg38‖-chr6:134173090-134173112	GTGAAGCACCCTTTCCTGGT
VSGH10142-246491710	SGK1 (75)	hg38‖+chr6:134172246-134172268	TGCAGAGTCCGAAGTCAGTA
VSGH10142-246491714	SGK1 (79)	hg38‖-chr6:134174731-134174753	GGCATGGTGGCAATTCTCAT
VSGH10143-246564094	FZD7 (94)	hg38‖-chr2:202034969-202034991	GTGTGCACCGTGCTCGATCA
VSGH10143-246564096	FZD7 (96)	hg38‖-chr2:202035568-202035590	TCTAGAGGACCGCGCCGTGT
VSGH10143-246564100	FZD7 (100)	hg38‖+chr2:202036247-202036269	TACCTGATGACCATGATCGT
VSGC10216	NT	-	GTAACGCGAACTACGCGGGT
VSGH10231	PPIB	-	GTGTATTTTGACCTACGAAT

Table 2.2: Genomic location and DNA target sequence of the sgRNAs used. Catalog number is also given.

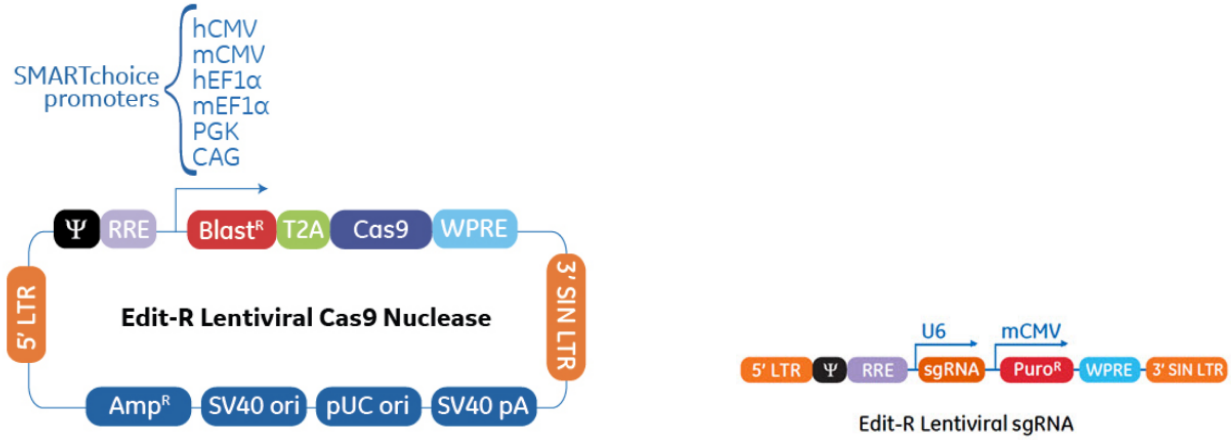

Figure 2.2: Lentiviral constructs for Cas9 (left) and sgRNA (right). 5' LTR: 5' Long Terminal Repeat, ψ: Psi packaging sequence, RRE: Rev Response Element, WPRE: Woodchuck Hepatitis Post-transcriptional Regulatory Element, 3' SIN LTR: 3' Self-inactivating Long Terminal Repeat, T2A: self-cleaving peptide, Blast^R: Blasticidin resistance, Puro^R: Puromycin resistance Source: `https://dharmacon.horizondiscovery.com/gene-editing/crispr-cas9/crispr-guide-rna/lentiviral-sgrna/edit-r-predesigned-lentiviral-sgrna/?sourceId=EntrezGene/6446` (10.10.2018)

2.4.3 Transduction

Lentiviral transduction was chosen as method of introducing the CRISPR/Cas9 system due to its proven efficiency in primary cells and GSCs [250]. Lentiviruses also have the advantage of being taken up in both dividing and non-dividing cells, and generating stable viral DNA intergration into the host cell genome. Lentiviruses belong to the retrovirus family and introduces viral RNA by binding to the host cell membrane and injecting it into the host cytoplasm [251]. All retroviruses synthesizes three important proteins for genome integration and further production of viruses; Group-specific antigen (*gag*) which encodes structural proteins of viruses; Polymerase (*pol*) which encodes reverse transcriptase, protease and integrase; and Envelope (*env*) which encodes transmembrane proteins important for viral fusion and genome introduction. Once viral RNA enters the host cytoplasm, reverse transcriptase transcribes the viral RNA into double-stranded cDNA, and integrase integrates the cDNA into the host genome, allowing viral protein production by the host transcription and translation machniery.

The sgRNA and Cas9 was introduced in two separate steps, as recommended by the manufacturer. Cells were first transduced with Cas9 nuclease constructs and Cas9 positive cells were selected for by blasticidin selection. Next, Cas9 positive cells were transduced with sgRNA constructs, and sgRNA positive cells were selected for by puromycin selection (Figure 2.3). Specific health, environment and safety measures were taken whilst handling viral particles, including conducting the work in a bio safety hood used exclusively for viral work, and by wearing double gloves and protective gowns.

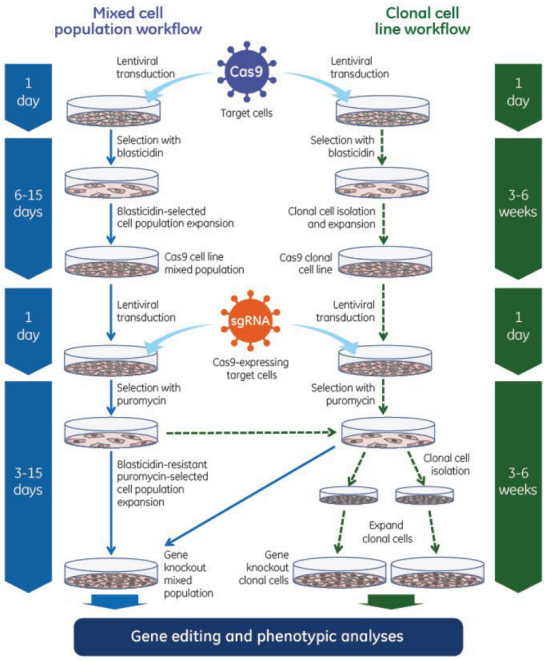

Figure 2.3: Workflow representation illustrating separate introduction of sgRNA and Cas9 to create the fully functional CRISPR/Cas9 system. Our study followed the mixed cell line workflow. Source: `https://dharmacon.horizondiscovery.com/gene-editing/crispr-cas9/crispr-guide-rna/lentiviral-sgrna/edit-r-predesigned-lentiviral-sgrna/?sourceId=EntrezGene/6446` (20.10.2018)

Following cell seeding on laminin-coated wells and overnight incubation, full media in the wells was replaced with full media without Pen/Strep, as the presence of Pen/Strep has shown to affect transduction efficiency (Marit Brynjulfsen, PhD Fellow, personal communication). The amount of virus needed per cell, or multiplicity of infection (MOI), was calculated from the virus batch titer, and added in a polybrene (Sigma, 107689-10G) and DMEM solution (10 μl/ml) to a final volume of 50 μl/well in 96-well plates and 500 μl/well in 6-well plates. Polybrene improves lentiviral delivery across the cell membrane [252]. The manufacturer noted optimal MOI of 1 for human embryonic kidney (HEK293) cells, but earlier virus titering for optimal transduction in GSCs using a non-target lentiviral green fluorescent protein (GFP) shRNA and FACS analysis, found that GSCs required a five times higher MOI than what was suggested by the manufacturer in HEK293 cells (Marit Brynjulfsen, PhD Fellow, personal communication). This was adjusted for in the MOI calculations by accounting for a five times lower concentration of transducing units (TU). The polybrene/virus mix was incubated at room temperature for 20 minutes to allow the components to complex, before the viruses were added to the cells. The cells were let to incubate overnight (37°C, 5% CO2). The next day, full media with Pen/Strep was added to the cells to ensure no bacterial infections, before antibiotic selection was started after 48 hours. Antibiotic selection was done by addition of blasticidin (1μg/ml) for 5 days and puromycin (1μg/ml) for 3 days, for Cas9 and sgRNAs, respectively. These selection conditions were previously established (Marit Brujulfsen, PhD Fellow, personal communication). Blasticidin (2 mg/ml) and puromycin (1 mg/ml,) solutions were prepared from powders by addition of H2O to desired concentrations (Blasticidin, ThermoFischer Scientific, R21001; Puromycin, Sigma, P9620). Cells for DNA, RNA and protein isolation were expanded until they reached a sufficient cell number, before being harvested and snap-frozen as cell pellet for further analyses. About one million cells were collected for DNA and RNA analyses each, whilst three million cells were collected for protein analysis. The experiments were replicated five times.

2.5 Evaluation of genomic alterations

To evaluate CRISPR/Cas9 activity at the specific sgRNA target DNA sites, T7 endonuclease mismatch assay was performed. Genomic DNA was isolated from transduced cells and the sgRNA target regions PCR-amplified with target-specific primers. Next, the amplified fragments were exposed to T7 endonuclease, which cleaves DNA at sites of indels, and the products separated by gel electrophoresis. This would allow for determination of sgRNA-specific indel induction in our cells.

2.5.1 Isolation of genomic DNA

Isolation of genomic DNA was performed using the GeneElute™Mammalian Genomic DNA Miniprep Kit (Sigma-Aldrich, G1N70-1KT), following protocol provided by the manufacturer with alternations optimized for 1 million GSCs. These alterations included an extra step of centrifugation before eluting the DNA in order to remove residues of Wash Buffer, and eluting the DNA in a smaller volume (50 μl) than noted in the protocol in order to increase the DNA concentration. Purity and concentration of the extracted DNA was determined using NanoDrop Spectrophotometer (Saveen & Werner) and its software (ND-1000 V.3.8.1). Purity evaluation of the DNA was determined by the 260/280 and 260/230 absorbance ratio, indicating protein and buffer contamination, respectively. A 260/280 ratio of 1,8 and a 260/230 ratio above 1,8 was considered sufficient for further analyses.

2.5.2 PCR amplification

Primer design

The online tool Primer-BLAST (`https://www.ncbi.nlm.nih.gov/tools/primer-blast/`) provided by the National Center for Biotechnology Information (NCBI, NHI), was used to design PCR primers for amplification of the sgRNA target sequences. A region of about 500 bases centered around the sgRNA target sequence was used as input for the PCR template, and the search mode was set to "User guided". The desired PCR product size was varied in order to identify primers with few or no off-target products, and to find primers that would give easily distinguishable PCR products when separated by gel electrophoresis in the T7 assay. Otherwise, standard settings were used. Primers amplifying the sgRNA target regions of SGK1 and FZD7, termed 4, 7, 10, 3, 6 and 1, and were provided by Eurogentec, whilst the primer for the positive control (PPIB) was provided by Dharmacon (PPIB, U-007001-05). The primer sequences are given in Table 2.3.

Target: Primer number	**Primer sequences**
SGK1 (74): 4	Forward: TGCTTGATGGGGCTGGCATT Reverse: GCGTTCCCTCTGGAGATGGTAGA
SGK1 (75): 7	Forward: CAAGACAGCGCCTACCTCCG Reverse: CTGGAACCACGGGCTCGTTT
SGK1 (79): 10	Forward: CATACGCCGAGCCGGTCTT Reverse: CAGAAGAAGTCTTCGCCTTCCCG
FZD7 (94): 3	Forward: CTCTCCCAACCGCCTCGTC Reverse: AGCCGTCCGACGTGTTCT
FZD7 (96): 6	Forward: GCCAACGGCCTGATGTACTTT Reverse: GCCAGGAACCAAGTGAGAGA
FZD7 (100): 1	Forward: CTTCCGTATCCGCACCATCA Reverse: AAGTCTGTGGTAGAAGCGGC
PPIB (positive control)	Forward: GAACTTAGGCTCCGCTCTT Reverse: CTCTGCAGGTCAGTTTGCTG

Table 2.3: Primer sequences for specific sgRNA target PCR-amplification. Both forward and reverse primer sequence are given.

Polymerase chain reaction

Polymerase chain reaction (PCR)-amplification was conducted following the CRISPR/Cas9 positive control protocol provided by Dharmacon (`https://dharmacon.horizondiscovery.com/uploadedFiles/Resources/sgrna-positive-controls-protocol.pdf`. (30.03.2019)). PCR Mastermix was prepared for each sample and the PCR cycling conditions were set as dictated by the protocol, with minor alterations. These alterations included addition of a higher volume forward and reverse primer (1 μl), kept at concentration as in the protocol, in order to ensure higher accuracy in pipetting, and an additional re-anneling PCR program following the final extension at 72 °C to allow for better DNA re-anneling (Table 2.4). Complete PCR-program is given in the CRISPR/Cas9 positive control protocol provided by Dharamcon.

Cycle step	Temperature	Time	Cycles
Denature	95 °C	5 min	-
Reannealing	95°C - 85°C: -2°C/sec 85°C - 25°C: -0,1°C/sec	10 min	- -
Hold	4°C	∞	-

Table 2.4: Additional re-anneling step in PCR program. This step is follwed by a final extension step at 72°C. The full PCR-program is given in the CRISPR/Cas9 positive control protocol provided by Dharamcon.

2.5.3 T7 endonuclease mismatch detection

Following PCR-amplification, DNA was exposed to T7 endonuclease. The T7 endonuclease cleaves mismatched DNA, or heteroduplexes, which can form during PCR-amplification of DNA with indels following induction of DSBs. T7 endonuclease (New England Biolabs, MO302L) was used according to protocol for CRISPR/Cas9 positive controls from Dharmacon. Following T7 endonuclease exposure, loading dye was added (New England Biolabs, 37024S), and the full reaction volume was run on a 1% agarose gel in borax buffer (5 mM) in an electrophoresis chamber (BioRad) for 1 hour (100 V, 40 mAmp, 100 W). A ladder was also applied in a separate well to estimate band sizes (New England Biolabs, N0550S). Gel bands were visualized using ChemiDoc™ Touch Imaging System (BioRad) and images were studies using the software Image Lab (Image Lab Software 5.2.1., BioRad). The gel was prepared by addition of 1 % powder-agarose (Invitrogen, 16500-500) to borax buffer. GelRed nucleic acid gel stain (Biotium, 41003) was added to the agarose solution before the gel was let to set in a electrophoresis mold.

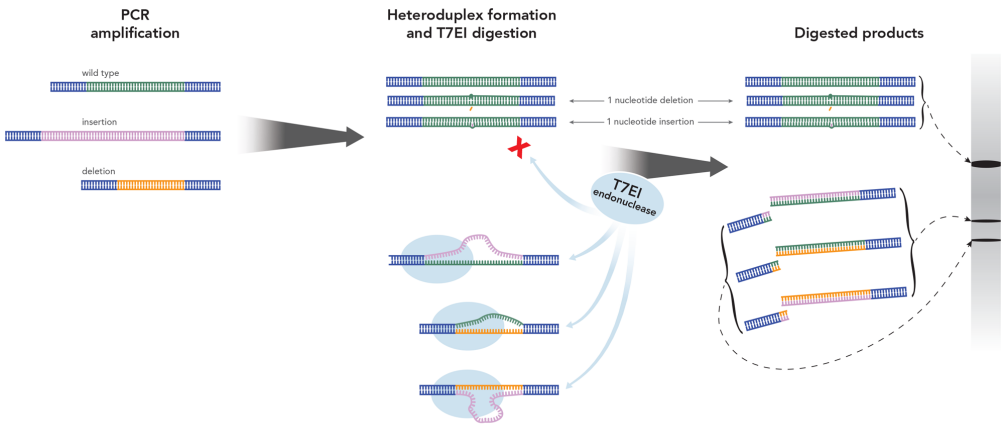

Figure 2.4: Mechanism of T7 endonuclease mismatch detection assay. Amplification of DNA fragments containing indels can results in reannealing of single-strands with indels with wild-type DNA strands. This will cause formation of heteroduplexes, which is recognized and cleaved by T7 endonuclease. The products of the reaction is then separated by gel electrophoresis, and presence of multiple DNA bands will indicate T7 activity and presence of indels. Source: `https://www.idtdna.com/pages/education/decoded/article/a-simple-method-to-detect-on-target-editing-or-measure-genome-editing-efficiency-in-\crispr-experiments` (10.12.2018).

2.6 Evaluation of gene expression

To evaluate CRISPR/Cas9-mediated mRNA degradation, RT qPCR was performed. Total RNA was isolated from transduced cells and reversed transcribed to cDNA. The cDNA was then amplified using gene-specific primers and assay probes.

2.6.1 Isolation of RNA and cDNA conversion

RNA was isolated using the RNeasy Mini Kit (Qiagen, 74104). RNA concentration was determined using the NanoDrop Spectrophotometer (Saveen & Werner) and its software ND-1000 (V.3.8.1). Desired 260/280 and 260/230 ratios were the same as for DNA purity evaluation. Total RNA integrity was determined using

Agilent RNA 6000 Nano Kit (Agilent, 5067-1511) following manufacturers instructions, in order to ensure intact RNA molecules before conducting RT qPCR. The kit and its software (Agilent 2100 Expert) allows for computation of RNA integrity number (RIN) based on microcapillary gel electrophoresis of ribosomal RNA (rRNA). A RIN of 10,0 is considered perfectly intact rRNA molecules, and a RIN of about 8,0 or above was considered sufficient for further analyses in this study. Isolated RNA was exposed to reverse transcriptase according to manufacturers protocol in order to yield cDNA (HighCapacity cDNA Reverse Transcription Kit, Applied BioSystems, 4368814).

2.6.2 Quantitative reverse transcriptase PCR

Quantitative reverse transcriptase polymerase chain reaction (RT qPCR) enables quantification of RNA molecules via cDNA synthesis and quantitative amplification [253]. RT qPCR amplification was done following the TaqMan assay (Applied Biosystems, Figure 2.5). In this assay, two cDNA strands are separated by temperature increase, followed by a lowering of the temperature to allow gene specific probe and primer binding. The primers specifically amplify mRNA derived cDNA from the gene of interest, and contains a 3' nonfluorecent quencher (NFQ) and a 5' fluorescent dye. The NFQ will inhibit signal detection from the fluorescent dye when it is in close vicinity to the dye. The TaqMan polymerase will initiate new strand synthesis, and when the polymerase reaches the probe it causes release of the 5' end flouescent dye, thus enabling detection of the fluorescent signal. The strenght of the signal will be proportional to the amount of cDNA template, and can thus be used as an indirect measure for gene transcript quantification.

The RT qPC conditions were as dictated by the TaqMan protocol (Applied BioSystems, `http://tools.thermofisher.com/content/sfs/manuals/cms_041280.pdf`, (11.07.2019)). Assay probes amplifying SGK1 (Hs00178612_m1) and FZD7 (Hs00275833_s1) were provided by ThermoFischer. Probes amplifying ACTB was also introduced as a control in all samples (ThermoFischer Scientific, Hs99999903_m1). Gene transcript quantification was done using the standard curve method with $R^2 > 0{,}99$. Transcript variants of SGK1 and FZD7 are given in Appendix (A.2), with TaqMan assay probe binding sites mapped (A.3).

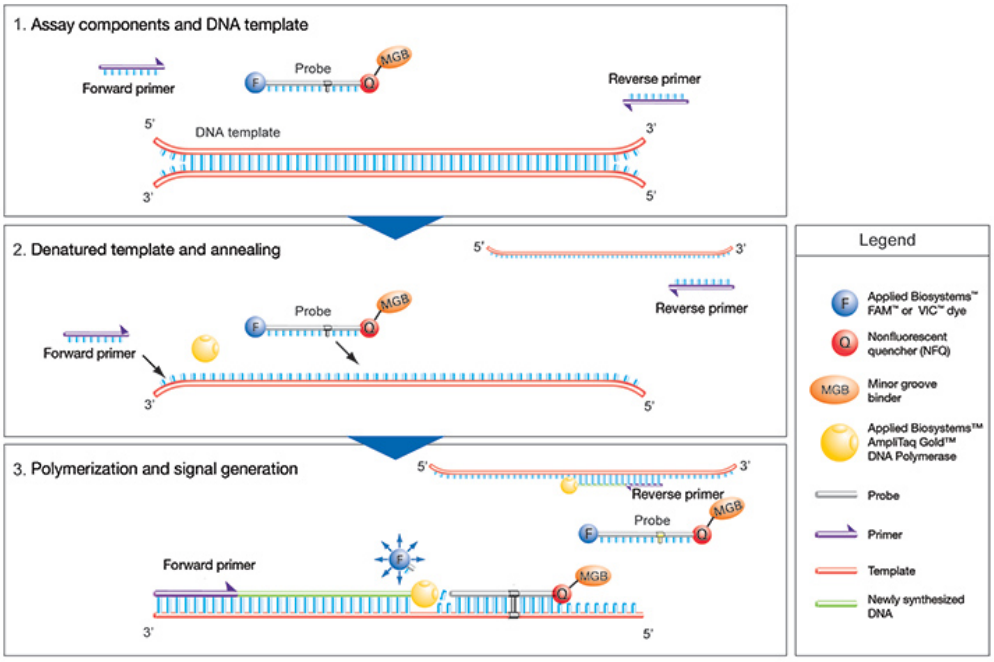

Figure 2.5: TaqMan Assay. Temperature variations allows for separation of the DNA double strands, followed by primer and probe binding. The probe contains a 3' nonfluoresecnt quencher (NFQ) and a 5' fluorescent dye, where the NFQ inhibits detection of fluoresecent signal from the 5' dye when in close vicinity to each other. When TaqMan polymerase conducts new strand synthesis and reaches the 5' end of the probe, the fluorescent dye will be released, allowing for detection of the fluorescent signal. The signal will be an indirect measure of gene expression. Source: `https://www.thermofisher.com/no/en/home/life-science/pcr/real-time-pcr/real-time-pcr-learning-center/real-time-pcr-basics/how-taqman-assays-work.html` (10.01.2019)

2.7 Evaluation of protein expression

To evaluate CRISPR/Cas9-mediated knock-down effect at protein level, Western blot analysis was performed. Proteins were isolated from transduced cells, and Western blot analysis performed with gene-specific antibodies.

2.7.1 Isolation of proteins

Proteins were isolated using Mammalian Cell & Tissue Extraction Kit (BioVision, K269-500). The cell pellet was resuspended in 100 μl Extraction Buffer Mix and phosphatase buffer (1:100), and incubated on ice for 10-20 minutes depending on cell pellet size, before being vortexed for 5 seconds and centrifuged at 14 000 rpm at 4 °C for 10 minutes. The supernantant was transferred to a QiaShredder column (Qiagen, 79656), before the column was centrifuged at 13 000 rpm for 1 minute to yield the protein lysate. Protein lysate concentration was determined using Pierce BCA protein Assay KIT (Thermo Scientific, 23227) following manufactures instructions. This assay enables spectrophotometric determination of protein concentration by light absorbance. Absorbance was measured using spectrophotometer (VICTOR, 560 nm, 0.1 sec) with the software WorkOut 2.5.

2.7.2 Western blot

Western blot allows for identification of proteins, and is performed by electrophoresis separation of cell proteins, followed by transferal of the separated proteins to a protein binding membrane. Next, the membrane is incubated with a primary antibody specific for a desired protein. Then, incubation with a secondary antibody is performed, binding the primary antibody and facilitating visualization of the bound protein. Lastly, the protein bands are visualized by chemiluminisence [254]. This would determine the presence of the CRISPR/Cas9 target protein.

Electrophoresis

A mix for gel-application was made by mixing 30 μg protein lysate to 70% volume in MilliQ(mq) H_2O, 25% loading buffer (ClearPAGE, FB31010) and 5% mercaptophenol (Sigma, M3148), to a total volume of 30 μl. The protein samples were denaturated at 100°C for 5 minutes, before they were applied to the gel (Precast gel, VWR, FK41212). The gel was placed in a electrophoresis chamber (XCell SureLock Minicell, Invitrogen) in running buffer (1x SDS solution, pH: 8,2-8,3: preparation is given in Appendix (A.5)). 10 μl protein standard (BioRad, 161-0373) was loaded in one well, and the full volume of each 30 μl protein sample was loaded in separate wells. The gel was run at 65V for 30 minutes, followed by 125V for 2 hours (100mA limit).

Blotting

Blotting procedure was performed using a transfer apparatus (Trans Blot-Cell, BioRad, 170-3930). Filter papers (Whatman filter papers, 1001 917) and sponges (provided in BioRad tramsfer apparatus kit) were wetted in transfer buffer (1X, pH: 8,2-8,6, preparation is given in Appendix (A.5)), and PVDF membranes (Amersham™ Hybond™, 10600023) were washed and activated in methanol for 20 seconds, and later rinsed in mqH20. The gel was incubated 15 minutes in cold transfer buffer. A transfer sandwich was made by layering sponge, 3-4 filter papers, the gel, 3-4 filter papers and sponge (Figure 2.6). The transfer sandwich was placed in the transfer apparatus and submerged in transfer buffer. The blotting was done on ice at 100 A for 1 hour.

The transfer efficiency was checked by rinsing of the PVDF membrane in mqH_2O with addition of 0,2% Ponceau solution (0,2% w/v 3% acetic acid), before it was incubated at room temperature for 30 minutes. The membrane was washed with mqH_2O and checked for proper visible bands.

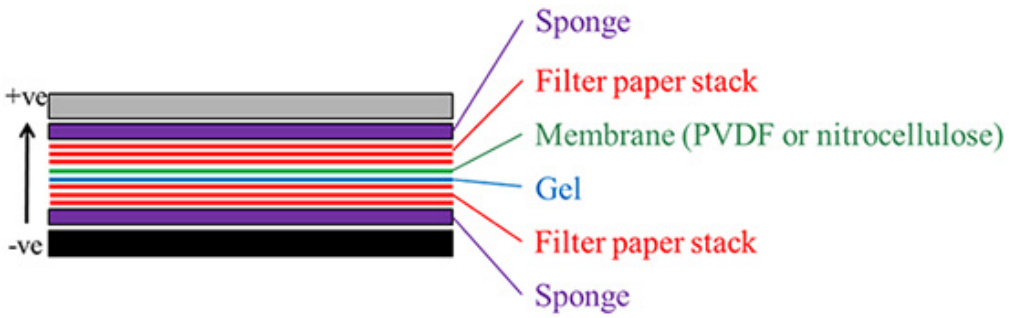

Figure 2.6: Transfer sandwich assembly for Western blotting. Transfer cassettes containing gel and PVDF transfer membrane, covered by filter papers and sponges, were submerged into transfer buffer an placed in a transfer apparatus. Source: `https://www.sigmaaldrich.com/technical-documents/articles/biology/western-blotting.html` (12.07.2019)

Blocking and antibody incubation

If the filters were frozen (-20°C) before proceeding to blocking and antibody incubation, they were reactivated in methanol for 20 seconds, before being rinsed in mqH_2O for 2-3 minutes. The filters were then blocked with TBST (pH: 7,4. 1x Tris buffered saline (TBS): preparation is given in Appendix (A.5), 0,1% Tween (Sigma, P2287)), with 5% Dry Milk (BioRad, 170-6404) for 3,5 hours with shaking at room temperature. Next, incubation with primary antibody in TBST with 5% dry milk or bovine serum albumin (BSA, Sigma, A9085-5G), was conducted according to the antibody protocol (Table 2.5). Incubation was done over night at 4°C with shaking. The membrane was washed in TBST for 10 minutes, followed by 2 x 5 minutes, before secondary antibody incubation was conducted. The membrane was incubated in TBST with 5% dry milk or BSA and secondary antibody following protocol antibody concentration at room temperature for 1 hour with shaking. The membrane was then washed in TBST for 10 minutes, followed by 2 x 5 minutes, and lastly washed with mqH_2O to remove all TBST residues. Antibody binding sites are mapped in the protein sequence of Sgk1 and Fzd7 in Appendix (A.4).

Antibody	**BSA/dry milk**	**Primary dilution**	**Secondary dilution**
Primary antibody Sgk1 (rabbit, Cell Signaling, 12103S)	BSA	1:1000	-
Primary antibody Fzd7 (mouse, Santa Cruz, sc-293261)	dry milk	1:100	-
Primary antibody Cas9 (mouse, Sigma-Aldrich, SAB4200701)	dry milk	1:1000	-
Primary antibody β-actin (mouse, CellSignaling, 8H10D10)	dry milk	1:1000	-
Secondary antibody (Anti-mouse IgG HRP-linked antibody, Cell Signaling, 7076S)	-	-	1:2000
Secondary antibody (Anti-rabbit IgG HRP-linked antibody, Cell Signaling, 7074S)	-	-	1:2000
Secondary antibody (ECL™ peroxidase labelled anti-mouse antibody, NA931VS)	-	-	1:5000
Secondary antibody (ECL™ peroxidase labelled anti-rabbit antibody, NA934VS)	-	-	1:5000

Table 2.5: Primary and secondary antibody dilution. Manufacturer and catalog numbers are also given.

Detection

Detection of proteins was done by submerging the membrane in detection solution (LumiGLO Reserve Chemiluminescent Substrate Kit, VWR, 54-71-00, 1 part solution A + 2 parts solution B) for 1 minute at room temperature. The membrane was then placed between two overhead-foilers (OHP Transparency Film, Nobo) and placed in the detection equipment (ChemiDoc™ Touch Imaging System, BioRad). The ladder was marked

using paint detectable by chemiluminescence (Glowing in the Dark Paint, Panduro). Detection was done for 1-3 minutes, and the blots were studied using the software Image Lab (Image Lab Software 5.2.1., BioRad).

2.8 Evaluation of viability

To evaluate CRISPR/Cas9 knock-down effect on cell viability, XTT viability was performed.

2.8.1 XTT-assay

Metabolically active cells will be able to cleave the yellow tetrazodium salt XTT to the orange formazan dye, by the activity of mitochondrial dehydrogenase [255]. The formazan dye is soluble in aqueous solutions and can be readily quantified using a spectrophotometer. Thus, this assay can be used as an indirect measure of metabolizing or proliferating cells (Figure 2.7 and 2.8).

Cas9 positive cells were temporarily well-adhered by laminin in 96-well plates, as described in the preceding tranductions. The cells were transduced with the three targeting sgRNAs and the non-targeting (NT), in addition to viral particles containing shRNAs introducing green fluorescent protein (GFP) (GIPZ Non-targeting control, Dharmacon, RHS4348). Introduction of the GFP-labelled shRNA would demonstrate the transducability of the cells or how well they take up viral particles. Wells with full media was also included as blank controls. The wells surrounding the controls and construct-transduced cells were filled with DPBS (Dulbecco's Phosphate Buffered Saline, LONZA, 17-512F) in order to avoid bias caused by evaporation. Two days following transduction, the media was added puromycin (1 μg/ml) to initiate antibiotic selection, and six days post-tranduction the XTT reagents were added. In order to approximatly evaluate how many cells were transduced compared to not transduced, cell nucleus were stained with the cell permeable nucleic stain Hoechst stain (Invitrogen, 3258). Hoescht stain was added to shRNA transduced cells to a concentration of 5μg/ml, and let to incubate at 37 °C for 5 hours. The presence of GFP and Hoechst was inspected using fluorescent microscopy (AXIO Observer.Z1, Zeiss), and processing of the images was done using the micorscope software (ZEN 2012 (blue edition), Zeiss).

Cell Proliferation Kit II (XTT) (Roche, 11465015001) was used according to protocol provided by the manufacturer. 5 ml aliquots XTT Labelling Reagent and 100 μl aliquots phenazine methosulfate (PMS) Electron Coupling Reagent were thawed in a water bath at 37 °C. The aliquots were mixed, and 50 μl of the mixture was added to each well, (to a final concentration of 0,3 mg/ml) before the plate was let to incubate at 37 °C. Absorbance was measured by spectrophotometer (VICTOR, 450 nm, 1 second) 24 hours following addition of the XTT-reagents.

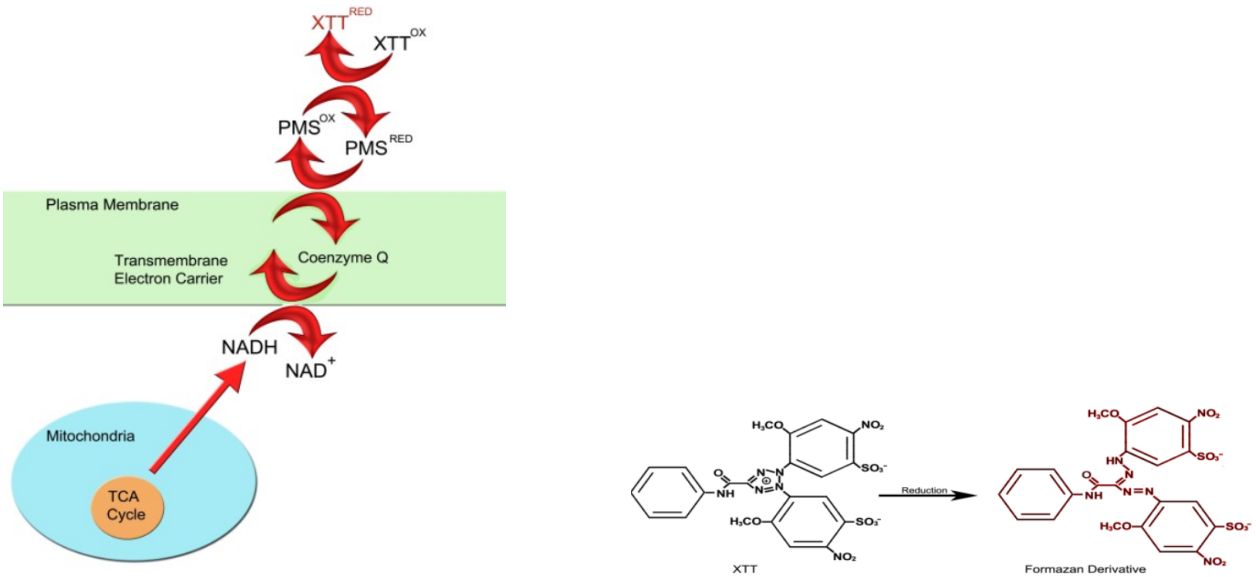

Figure 2.8: Chemical reaction occurring during reduction of XTT assay components in metabolizing cells. Source: `https://www.atcc.org/~/media/56374CEEC36C47159D2040410828B969.ashx`, (24.10.2018)

2.9 Statistical analysis

Choice of correct statistical analysis is critical in order to conduct proper statistical testing. A central consideration in this regard is the data distribution. The most typical assumption to make is that the data are normally distributed, especially if the sample size is large enough (above 30). But, if the sample size is small or the data could not be non-random, the normality assumption can not be reached. The latter is a reasonable assumption to make when working with biological systems [256]. When the data shows non-normal distribution, hypothesis-testing without assuming an underlying distribution can be done, by conducting so-called non-parametric tests [257]. These tests can be used to determine the difference between one or more groups of independent or paired data. Some non-parametric tests include the Wilcoxon signed ranked test, Mann-Whitney U test, Kruskal-Wallis test and the Friedmann's test.

The Kruskal-Wallis test, usually referred to as a non-parametric one-way analysis of variance (ANOVA) test, can be used to determine the statistical difference between multiple different groups that are given different treatments [258]. This test is based on ranking of the observed data from the different groups according to size, before statistical testing by a test statistic is performed. If one group has a mean of ranks that is much smaller or much larger than the other, it might indicate that the two groups are significantly different.

The null-hypothesis states that the samples are from identical distributions, given that the test assumptions hold. The underlying assumptions for the Kruskal-Wallis test are:

1. The data should be unpaired and independent.
2. The data should be obtained from a non-normal distribution.
3. The data distributions from the different groups being compared should be of the same shape.

When conducting multiple comparisons there is a higher risk of achieving significant differences just by chance (type 1 error), which can bias the results. Thus, corrections for multiple comparisons are often applied, like the Dunn's correction.

Results

3.1 Preliminary optimization

Certain conditions for viral transductions were established in the lab before this work was conducted, including choice of hCMV promoter for optimal Cas9 construct expression, laminin-adherence and absence of Pen/strep during viral infections to increase transduction efficiencies, addition of polybrene to facilitate viral infections, optimal antibiotic selection conditions for transduced cells, study of functional viral titer in GSCs, and validation of Cas9 expression and functionality in cell culture T1547. In order to optimize other protocol aspects specific for this study, in addition to re-validating Cas9 expression in our cells, a preliminary round of optimization was performed. These optimizations regarded optimal multiplicity of infection for transductions, optimal seeding density and time point for spectrophotometer reads in the viability assay, validation of correct and specific PCR primer binding, and validation of Cas9 protein expression.

3.1.1 Optimal multiplicity of infection for transductions

Optimal multiplicity of infection (MOI) for transductions was determined in order to correct for insufficient or toxic amounts of virus, which could impede efficient transductions. As earlier determination of functional viral titer in GSCs showed that these cells required a five times higher MOI than what was suggested by the manufacturer in HEK293 cells, this was accounted for in the MOI calculations by assuming a five times lower concentration of transducing units (TU). Optimal MOI was determined by transducing T1547 cells with NT sgRNA using adjusted MOI 1, MOI 5 and MOI 10, and study viability by XTT assay. It was found that MOI 10 resulted in a lower viability compared to MOI 1 and MOI 5, indicating a potential toxic cellular effect, whilst the difference between MOI 5 and MOI 1 was less prominent (Figure 3.1 A). By also taking into account economical considerations regarding cost of lentiviruses, MOI 1 was chosen for further transductions.

3.1.2 Optimal seeding cell density for proliferation assay

In order to facilitate cell exponential growth phase during transductions, optimal cell density per well for the proliferation assay was established. This would ensure proliferation free from potential biases resulting from too high or too low cell density. 3500, 5000 and 7500 cells per well were chosen based on previous experience in the lab (Cecilie Sandberg, postdoctoral fellow, personal communication). Cells of the chosen density were temporarily adhered to the well-bottom as described in Materials and Methods, in order to determine confluency, were 60-80% confluency was used as an indicator if optimal cell density for exponential growth. It was found that a density of 5000 cells per well resulted in the desired confluency following overnight incubation on laminin. Thus, this density was used in the later experiments.

3.1.3 Time point for spectrophotometer read in proliferation assay

Following addition of the XTT proliferation assay reagents, optimal time point for spectrophotometer read was determined by studying absorbance at 4, 24 and 48 hours following reagent addition. These time points were chosen based on previous experience in the lab (Cecilie Sandberg, postdoctoral fellow, personal communication). Absorbance after optimal time would indicate that assay components would have had time to detect proliferation, but not yet induce toxicity and cell death. A plot showing absorbance as a function of time, would indicate this time point by the time the absorbance curve begin to reach a plateau. Absorbance after 24 hours fulfilled these requirements, and this time point was used in later experiments (Figure 3.1 B).

(a) (b)

Figure 3.1: Optimal multiplicity of infection (MOI) and time point for spectrophotometer read in XTT proliferation assay. A) Cell viability measured by XTT assay absorbance following NT sgRNA transductions at GSCs adjusted MOI 1, MOI 5 and MOI 10 (n= 3). B) Absorbance plotted as a function of time following addition of XTT reagents (4, 24 and 48 hours) for 5000 cells per well in a 96-well plate (n = 5). Standard deviations and averages are calculated in Excel 2010 and graphs are generated using GraphPad Prism (5.2.1).

3.1.4 Validation of specific and correct PCR primer-binding

PCR primers used for amplification of the sgRNA target sequences were designed and tested for correct and specific binding in T1547 cells transduced with the NT sgRNA. This would ensure proper detection of CRISPR/Cas9-mediated DNA double-stranded breaks. The PCR program was as described in Materials and Methods for the T7 endonuclease mismatch assay. It was found that primers termed 4, 7, 10, 3, 6, and 1, for sgRNA 74 (SGK1), 75 (SGK1), 79 (SGK1), 94 (FZD7), 96 (FZD7), and 100 (FZD7), respectively, gave bands of predicted sizes, indicating correct and specific primer binding with successful amplification of the target sequences (Figure 3.2). Predicted size of the amplified regions is given in Table 3.1.

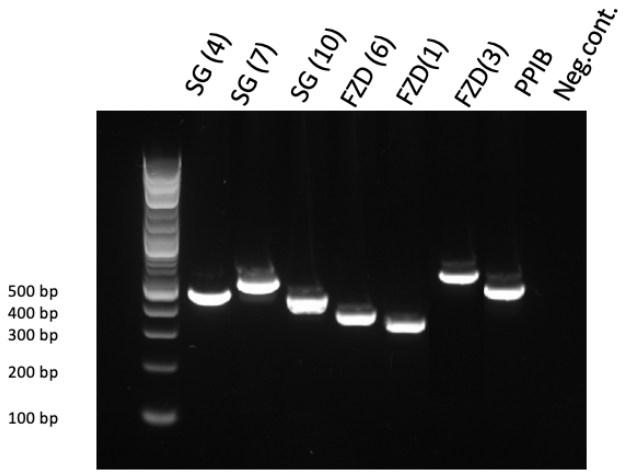

Figure 3.2: Primer binding validation. Primers 4, 7 and 10 targets SGK1 at sites 74, 75 and 79, respectively. Primers 6, 1 and 3 targets FZD7 at sites 94, 96 and 100, respectively. Primer validation was done in T1547 NT cells. A negative control (Neg.cont.) containing no PCR polymerase, and primer for the positive control (PPIB) is also included. Results indicated succsessful and specific amplification of all sgRNA target regions.

Target site	Primer number	Predicted band size (bp)
SGK1 74	4	516
SGK1 75	7	564
SGK1 79	10	454
FZD7 94	3	566
FZD7 96	6	377
FZD7 100	1	347
PPIB		504

Table 3.1: Predicted size of PCR-amplified DNA fragments, using SGK1, FZD7 and PPIB sgRNA target specific primers. Bandsizes are approximated based on sgRNA target specific primer binding sites mapped in Appendix (A.1). bp = basepairs.

3.1.5 Cas9 introduction

Preceding introduction of the different sgRNAs, Ca9 was inserted in T1547 and validated before this work was conducted (data not shown, Marit Brynjulfsen, PhD Fellow, personal communication). Cas9 was introduced into the remaining four different tumors (T0965, T1548, T1008) by lentiviral transduction. Validation of Cas9 protein presence in all tumors was an important premise to establish before continuing with introduction of the sgRNA, to ensure that Cas9 was present to conduct gene-editing when the sgRNAs were introduced. Figure 3.3 shows Cas9 protein expression in all tumors. The Cas9 protein was present in all cells, but protein expression varied between the different tumors. Cas9 function in T1547 was validated despite low protein expression before this work was conducted. Thus, the functional control of the CRISPR/Cas9 system was conducted in this cell culture.

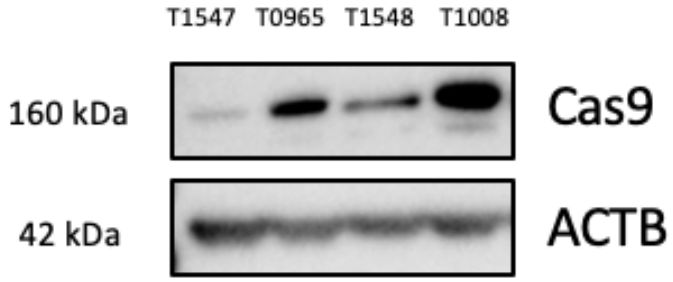

Figure 3.3: Cas9 protein expression in T1547, T0965, T1548 and T1008. β-actin (ACTB) loading control is also showed.

3.2 SGK1 knock-down and protocol optimization

Following preliminary protocol optimization, CRISPR/Cas9-mediated SGK1 knock-down was performed as a functional control of the CRISPR/Cas9 system. SGK1 has previously been identified as a potential target in GSCs, as CRISPR/Cas9-mediated SGK1 knock-down showed significant reduction in viability in patient-derived GSCs [140]. The study was done in T1547 cells, and three different sgRNAs were introduced (74, 75 and 79) targeting the gene of SGK1. This would allow for testing and further optimization of the protocol before knock-down of Fzd7 was attempted.

3.2.1 SGK1 knock-down and at DNA level by T7 endonuclease mismatch detection assay

To evaluate CRISPR/Cas9 activity and induction of DNA indels at the three different sgRNA target sites in SGK1, T7 assay was preformed with sgRNA target specific PCR-primers. The T7 endonuclease would recognize and cleave the DNA where indels had been introduced. Electrophoresis separation of the resulting DNA fragments would allow for detection of indel induction. It was found that all SGK1 targeting sgRNA transduced cells showed induction of DNA indels at the desired sites, resulting in DNA bands of predicted sizes (Figure 3.4). Predicted band sizes following CRISPR/Cas9 activity are given in Table 3.3. The effectiveness

of DNA indel induction by the CRISPR/Cas9 system was observed to be sub-optimal, as results indicated high presence of the uncut, parental strand.

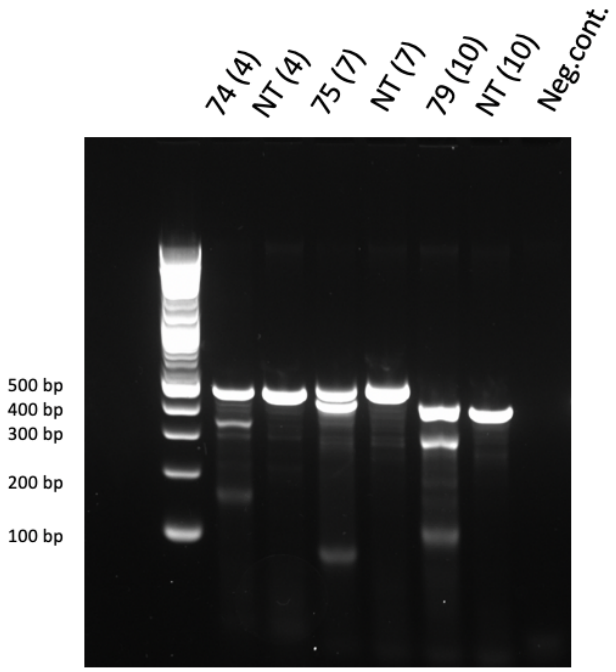

Figure 3.4: Evaluation of CRISPR/Cas9 activity and induction of DSBs at the sgRNA specific sites in SGK1. All targeting sgRNAs (74, 75 and 79) showed to induce DSB at expected genomic sites, resulting in DNA fragments of predicted size. Predicted band sizes are given in Table 3.3. Numbers given in parenthesis indicate primer number used for PCR-amplification (see Table 3.1). A negative control (Neg.cont.) without addition of PCR-polymerase is also shown. bp = basepairs.

Target gene	**sgRNA**	**Predicted band sizes (bp)**
SGK1	74	516 (348 + 168)
	75	564 (493 + 71)
	79	454 (328 + 126)

Table 3.2: Predicted bandsizes resulting from CRISPR/Cas9 activity at the different sgRNA target sites in the gene of SGK1. Bandsizes are approximated by sgRNA target sites and specific target site primer binding sites mapped in Appendix (A.1). bp = basepairs.

3.2.2 SGK1 knock-down at mRNA level by RT qPCR

To evaluate CRISPR/Cas9-mediated SGK1 mRNA degradation, mRNA expression in all sgRNA transduced cells were studied by RT qPCR. RNA integrity was also determined by RNA integrity number (RIN). RIN was in the range of 9,40-9,80 for all sgRNA transduced cells, indicating high RNA integrity (Appendix, A.7). It was found that SGK1 expression was increased in all targeting sgRNA transduced cells, compared to NT transduced cells. The Kruskal-Wallis test with Dunn's correction was conducted for all cells to test for statistical significant difference in SGK1 expression between cells transduced with the three different targeting sgRNAs (74, 75, 79) and the NT sgRNA at alpha level 0,05. None of the sgRNA resulted in a statistical significant increase in SGK1 expression, but number of replicates (n) was smaller than intended due to low number of cells (74 (n=2): $p > 0{,}9999$, 75 (n=3): $p = 0{,}9743$, 79 (n=3): $p = 0{,}1467$.) (Figure 3.5).

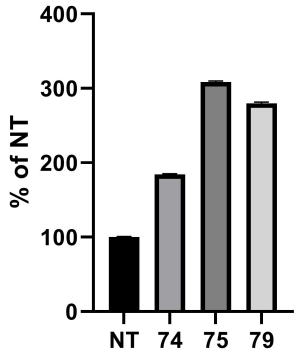

Figure 3.5: Percentage SGK1 gene expression in cells transduced with the three different targeting sgRNAs (74, 75 and 79), relative to cells transduced with the NT sgRNA. Quantities are normalized to β-actin (ACTB) expression.

3.2.3 SGK1 knock-down at protein level by Western blot

To evaluate Sgk1 protein expression following CRISPR/Cas9 activity, proteins were isolated from all sgRNA transduced cells and Western blot was preformed with Sgk1 specific antibody. It was found that sgRNA 79 and 74 transduced cells showed a knock-out effect of SGK1, whilst sgRNA 75 did not (Figure 3.6). The blot indicated disperancy between the protein sizes of Sgk1 from our cells and the positive control derived from rate adrenal gland (PC-12), likely due to different protein isomer expression in different tissues. In order to further investigate which isomer forms were dominate in GSCs, Western blot analysis studying Sgk1 isomer variants in ten different patient-derived GSCs was performed (Figure 3.7). It was found that Sgk1 protein isomer expression varied between tumors, with isomer variants of both 50 and 60 kDa represented.

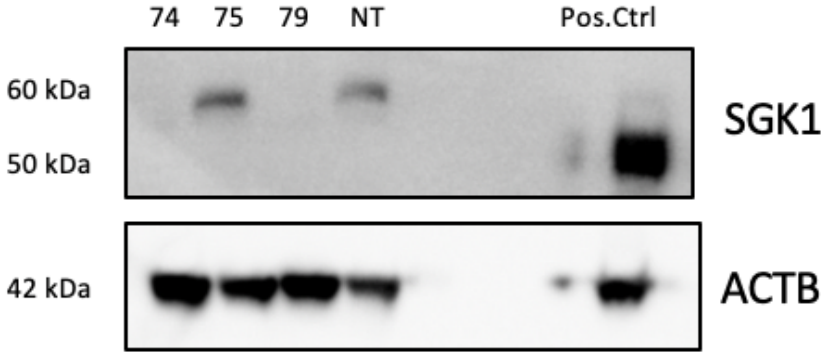

Figure 3.6: SGK1 protein expression in T1547 cells transduced with the three different targeting sgRNAs (74, 76, 79) and the NT sgRNA. The blot indicates knock-out effect of SGK1 in 74 and 79 transduced cells, but not in 75. A commercially available positive control was also applied, derived from cell lysate of PC-12 cell line derived from transplantable rat pheochromocytoma shown at 50 kDa. Loading control showing β-actin (ACTB) protein expression is also shown.

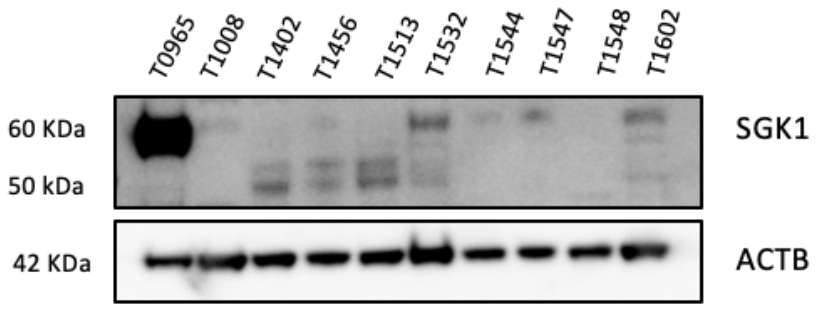

Figure 3.7: Sgk1 protein isomer expression in ten different patient-derived GSCs. The blot indicated varied Sgk1 protein isomer expression between the different cells, but isomers at both 50- and 60 kDa were represented. β-actin (ACTB) loading control is also showed.

3.2.4 SGK1 knock-down at viability by XTT-assay

To evaluate effect of CRISPR/Cas9-mediated SGK1 knock-down on cell viability, XTT assay was performed. Viability assessment was done by measuring absorbance following addition of XTT reagents causing color change in the media if metabolizing cells are present. The Kruskal-Wallis test with Dunn's correction was conducted for all cells to test for statistical significant difference in viability between cells transduced with the three different targeting sgRNAs (74, 75, 79) and the NT sgRNA at alpha level 0,05. It was found that sgRNA 74 gave a significant reduction in viability compared to NT, whilst 75 and 79 gave a smaller, non-significant reduction (74 (n=8): 0,0167, 75 (n= 8): $>$ 0,999, 79 (n=8): 0,7890.) (Figure 3.8). Thus, SGK1 knock-down in T1547 showcased a small but significant decrease in viability by the sgRNA 74. Surprisingly, sgRNA 79 showed successful protein knock-out, but this did not have any impact on viability.

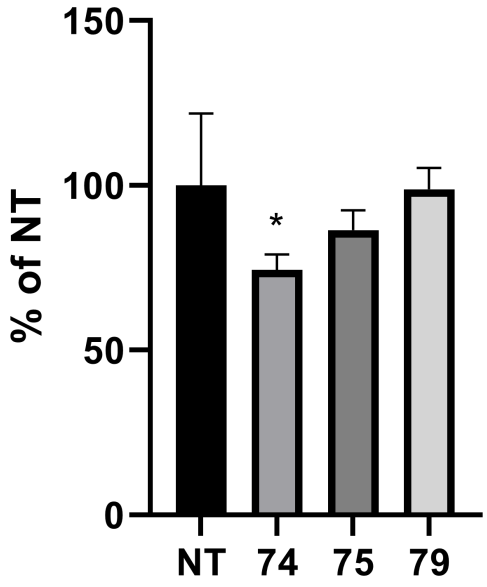

Figure 3.8: Percentage absorbance in T1547 cells transduced with the three different SGK1 specific sgRNAs (74, 75 and 79) relative to cells transduced with the NT sgRNA. Significance level is given by asteriks; *: P $>$ 0,05.

3.2.5 Protocol optimization

The preceding functional control study of the CRISPR/Cas9 system identified aspects in the protocol which could be altered or optimized, before work with FZD7 knock-down was conducted. This would allow for full establishment of CRISPR/Cas9-mediated knock-down protocol conditions.

Time point for harvest of cells

In the studies of SGK1 knock-down, transduced cells for DNA, mRNA and protein analyses, were allowed to grow until they reached sufficient cell number to harvest for further analyses, about 2-4 weeks following transduction. Ideally, five million cells would be harvested from each sgRNA variant (one million cells for DNA and RNA, and three million for protein isolation). Cells transduced with different sgRNAs showed different proliferative abilities, and thus cells transduced with different sgRNAs were harvested at different times following transduction. Following these studies, we considered the potential for off-target effects in cells constitutively expressing sgRNA and Cas9 over time. This consideration has previously been noted by Dow et al. [259]. In order to avoid off-target effects and ensuring better basis for comparison between effects of the different sgRNAs in the different anaylses, it was determined that all cells should be harvested at the same time following transduction. Yuen et al. argued that CRISPR/Cas9 efficiencies and specificity were optimal 5-15 days following transduction [260]. Based on this, all cells for FZD7 knock-down studies were harvested 13 days following sgRNA transduction.

Introduction of a commercial positive control (PPIB) in each experiments

To further ensure CRIPSR/Cas9 functionality and activity in each experiment replicate, a commercial technical control was introduced. This positive control constituted a manufacturer-optimized sgRNA targeting the gene of peptidylprolyl isomerase B (PPIB), recommended for indicating succsessful CRISPR/Cas9 activity. Thus, in addition to the three different targeting sgRNAs and the NT sgRNA, cells were also transduced with sgRNA targeting PPIB in the FZD7 knock-down studies.

Study of wild-type FZD7 protein expression

In order to get a deeper understanding of alterations in Fzd7 protein expression following CRISPR/Cas9 activity, wild-type Fzd7 protein expression was studied in eleven patient-derived GSC by Western blot analysis. These eleven patient cultures included the cells studied in this project (T1547, T0965, T1548 and T1008).

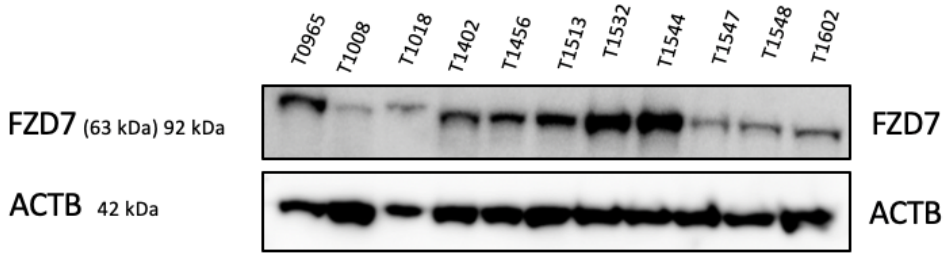

Figure 3.9: FZD7 wild-type protein expression in eleven different patient-derived GSCs established in the lab. There was loaded less than 30 ug of T1018 as the protein concentration available from this tumor was small. This is indicated by the lower ACTB protein expression for this tumor.

Puromycin selection in XTT viability assay

In study of effect on viability following knock-down of SGK1, puromycin selection was not initiated following transduction as it was believed that the effect of the sgRNAs was prominent enough without selection. It was though discovered that the effect of the SGK1 knock-downs was not as prominent as hoped and demonstrated by Cochran et al. [140] (Figure 3.8), where the two sgRNAs used gave about 75% and 90% reduction in viability. Thus, in order to potentially show a stronger knock-down effect by removing cells that were not puromycin resistant, and to fully mimic the conditions of the cells harvested for DNA, RNA and protein analysis, puromycin selection was initiated in FZD7 knock-down studies on cell viability, two days following transduction.

3.3 FZD7 knock-down

Following established protocol conditions for CRISPR/Cas9-mediated gene knock-down and validation of CRIPSR/Cas9 system functionality, FZD7 knock-down was attempted in four patient-derived GSC cultures. This would allow for functional validation of Wnt-receptor Fzd7 knock-down, and exploration of FZD7 knock-down effects in GSCs, potentially validating it as a potent therapeutic target in GBM treatment. In addition, in order to follow transduction efficiencies at all transductions performed, a transduction efficiency assay was performed for each replicate in all experiments. This would illustrate potential differences in transduction efficiencies and subsequent CRISPR/Cas9 activity in the different experiment replicates.

3.3.1 Transduction efficiencies

Transducability of the cells, or how well they take up lentiviral particles, was followed for each experiment replicate in all cell cultures used in the FZD7 knock-down studies (T1547, T0965, T1548 and T1008). This was done by transduction with lentiviral particles introducing GFP by shRNA at MOI 1. Inspection of GFP positive cells by fluorecent microscopy would give an approximate indication of transduction abilities. It was found that all cell cultures showed ability to be transduced and express introduced material, though in varying degree (Figure 3.10). T0965 and T1547 showed greater ability to adhere as single-cells to the well-bottom after laminin coating, whilst T1008 and T1548 formed adherent cell clusters or sphere-like structures. The adherence abilities was found to affect transduction efficencies in earlier optimization studies in the lab, but all cells showed ability to take up viral particles. The effect of puromycin selection in removing cells that have not been tranduced and allowing more growth resources for the transduced cells, had been evaluated earlier, but was also showed by a less powerful visual interpretation in this assay. Puromycin selection caused higher percentage of GFP positive cells by visual inspection.

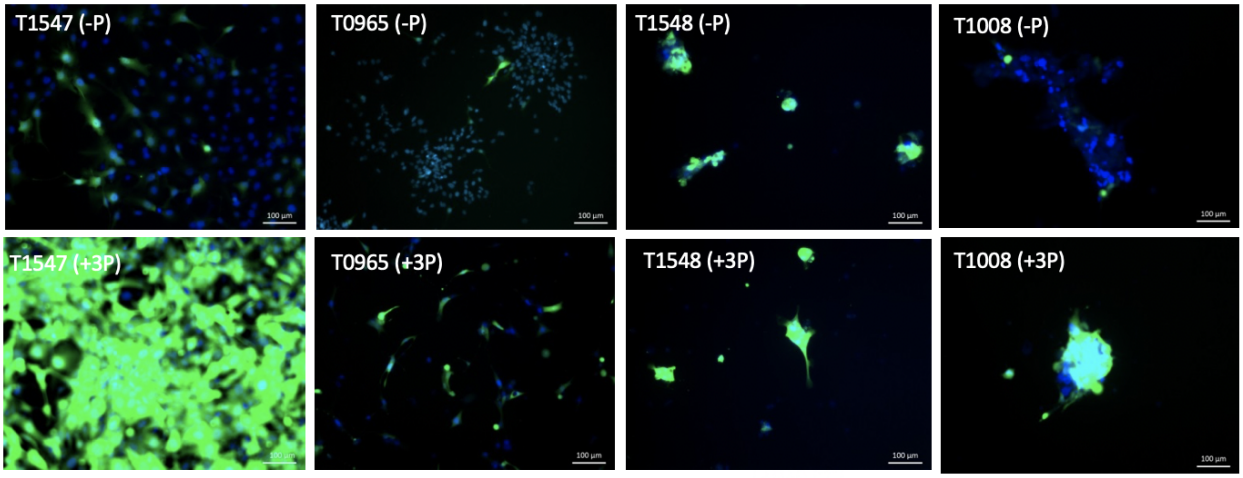

Figure 3.10: Transducability in the four cell types used in FZD7 knock-down study (T1547, T0965, T1548 and T1008). GFP expression (green) one day before (-P) and 3 days following (+3P) initiation of puromycin selection. Cell nucleus is stained with Hoechst stain (blue).

3.3.2 FZD7 knock-down at DNA level by T7 endonuclease mismatch detection assay

To evaluate CRISPR/Cas9 activity and induction of DNA indels at the three different sgRNA target sites of FZD7, the T7 assay was preformed with sgRNA target specific PCR-primers. It was found that all cells transduced with targeting sgRNAs showed induction of DNA double-stranded breaks, indicating successful CRISPR/Cas9 activity (Figure 3.11). The resulting DNA bands corresponded to predicted band sizes, indicating specific CRISPR/Cas9-activity at the desired genomic sites. The efficency was though sub-optimal as noted by the high presence of uncut parental strands. The 70 bp DNA band resulting from T7 activity in sgRNA 100 transduced cells are not visable without picture transformation, but is present in all cells.

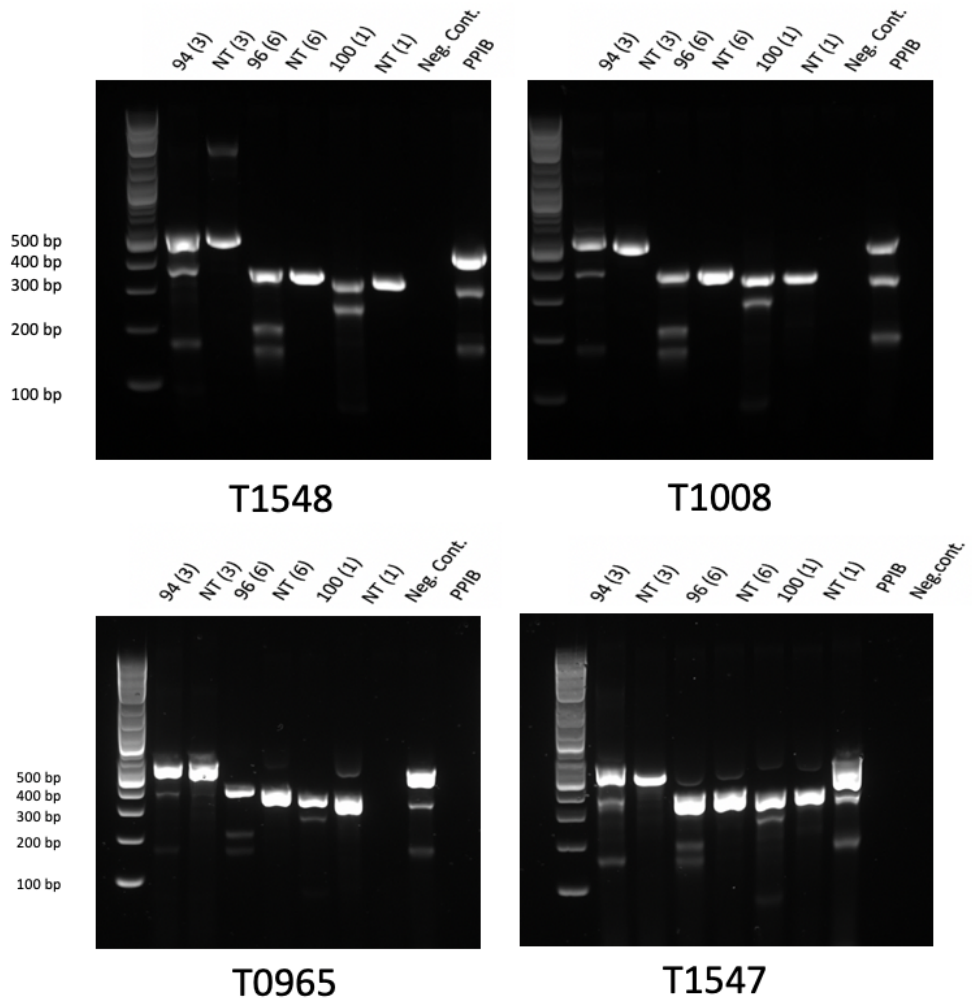

Figure 3.11: Evaluation of CRISPR/Cas9 activity and induction of DSBs at the sgRNA specific sites in FZD7. All targeting sgRNAs (94, 96 and 100) showed to induce DSB at expected genomic sites, resulting in DNA fragments of predicted size. Predicted band sizes are given in Table 3.3. Numbers given in parenthesis indicate primer number used for PCR-amplification (see Table 3.1). A negative control without addition of PCR-polymerase and a positive control with PPIB knock-down is also shown. bp = basepairs.

Target gene	sgRNA	Predicted band sizes (bp)
FZD7	94	566 (401 + 165)
	96	377 (229 + 148)
	100	347 (277 + 70)
PPIB		504 (330 + 174)

Table 3.3: Predicted bandsizes resulting from CRISPR/Cas9 activity at the different sgRNA target sites in the genes of FZD7 and PPIB. Bandsizes are approximated by sgRNA target sites and specific target site primer binding sites mapped in Appendix (A.1). bp = basepairs.

3.3.3 FZD7 knock-down at mRNA level by RT qPCR

To evaluate potential FZD7 mRNA degradation following CRISPR/Cas9-activity, FZD7 mRNA levels in all sgRNA transduced cells were measured by RT qPCR. RNA integrity was also determined for all cells, and RIN values were in the range of 7,7-9,6. RIN was not determined for T1008 NT (Appendix (A.7)). The Kruskal-Wallis test with Dunn's correction was conducted for all cells to test for statistical significant difference between cells transduced with the three different targeting sgRNAs (94, 96, 100) and the NT sgRNA at alpha level 0,05. Cells transduced with targeting sgRNA showed generally lower FZD7 gene expression

than in NT-transduced cells in T1547, T0965 and T1008 (Figure 3.12). The reductions were non-significant. In T1548, there was a general increase in FZD7 gene expression compared to NT-transduced cells. This increase was significant in sgRNA 100 transduced cells. Calculated p-values are given in Table 3.4.

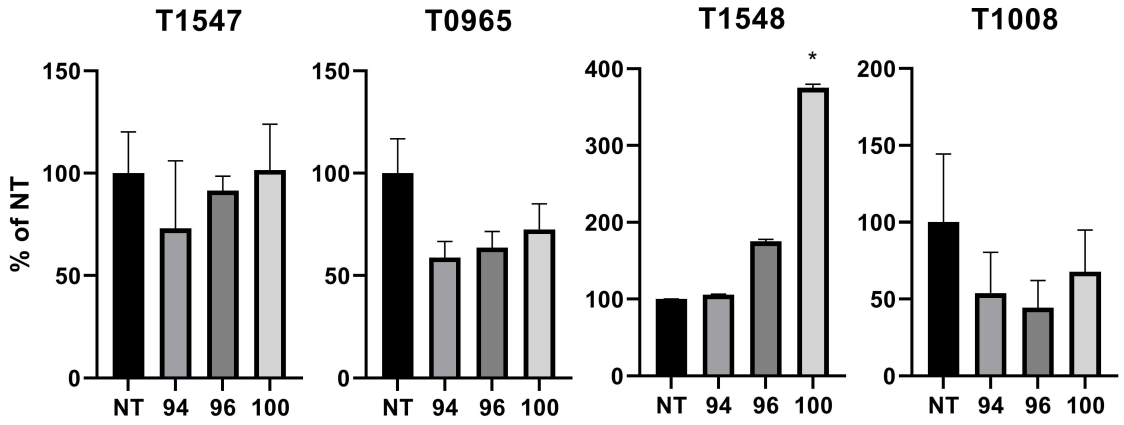

Figure 3.12: Percentage FZD7 gene expression in cells transduced with the three different targeting sgRNAs (94, 96 and 100), relative to cells transduced with the NT sgRNA. Quantities are normalized to β-actin (ACTB) expression. Asteriks marks significance level, *: $p < 0{,}05$. Calculated p-values are given in Table 3.4

Cell type	sgRNA	Adjusted p-value	Significant?
T1547	94	$> 0{,}9999$	ns
	96	$> 0{,}9999$	ns
	100	$> 0{,}9999$	ns
T0965	94	$> 0{,}9999$	ns
	96	$> 0{,}9999$	ns
	100	$> 0{,}9999$	ns
T1548	94	$> 0{,}9999$	ns
	96	0,2683	ns
	100	0,0276	*
T1008	94	0,6388	ns
	96	0,4231	ns
	100	$> 0{,}9999$	ns

Table 3.4: P-values generated from the Kruskal-Wallis test with Dunn's correction at alpha-level 0,05 to test for statistical significant difference in FZD7 gene expression between cells transduced with the three different targeting sgRNAs and the NT sgRNA. Asteriks marks significance level, *: $p < 0{,}05$. n = 3 for all sgRNAs. ns = non-significant.

3.3.4 FZD7 knock-down at protein level by Western blot

To evaluate Fzd7 protein expression following CRISPR/Cas9 activity, proteins were isolated from all sgRNA transduced cells and Western blot was preformed with Fzd7 specific antibody. In T1547, it was found that sgRNA 94 caused a increase in Fzd7 protein expression compared to NT, whilst 100 caused a minor reduction. 96 showed only slight increased FZD7 protein expression compared to NT. Comparison of the different sgRNA transduced cells is complicated by the weakness of the protein bands. In T0965, 94 caused a reduction in Fzd7 protein expression, whilst 96 and 100 displayed increased Fzd7 expression. In T1548, all targeting sgRNAs caused a reduction in Fzd7 protein expression, compared to NT. 94 caused the strongest reduction, whilst 100 showed the lowest reduction. In T1008 all targeting sgRNAs caused a reduction in Fzd7 protein expression, with strongest reduction in 100 and lowest reduction in 96. Degree of reduction or increase was determined by analysis in Image Lab (5.2.1).

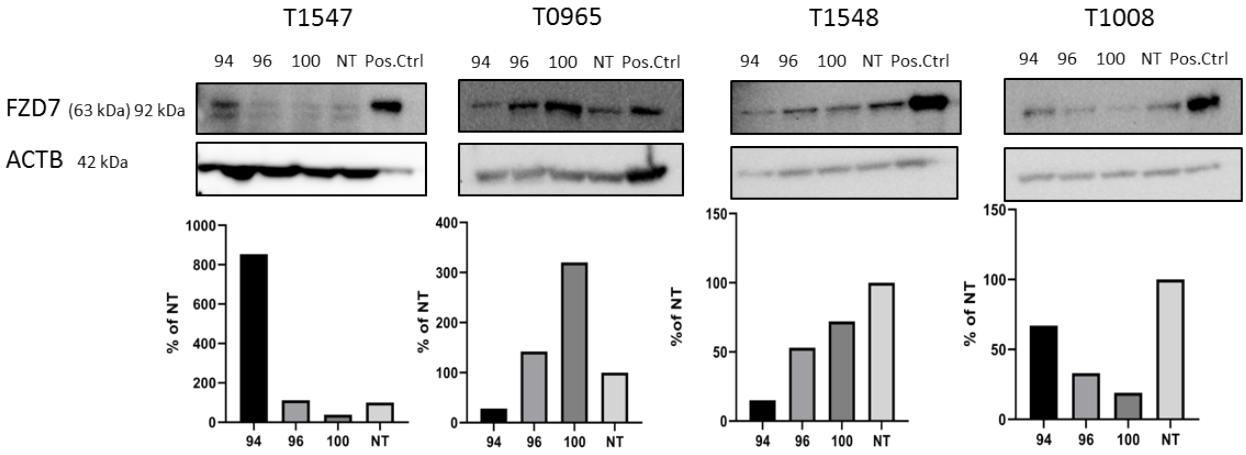

Figure 3.13: FZD7 protein expression in T1547, T0965, T1548 and T1008 tranduced with the three different targeting sgRNA (94, 94, 100) and the NT sgRNA. In T1547 and T0965 the targeting sgRNA generally resulted in an increased Fzd7 protein expression, whilst in T1548 and T1008 all targeting sgRNAs resulted in a lower Fzd7 protein expression. Positive control for T0965 was T1456 (15 ug), T1544 (15 ug) for T1548, and a mix of T1532 and T1402 for T1008 (15 ug). These cell types indicated high Fzd7 expression in the study on FZzd wild-type protein expression (Figure 3.9). For T1547 60 ug protein were applied due to absence of protein bands when applying 18 ug and 30 ug protein. T0965 30 ug protein were loaded in each well, whilst for T1548 and T1008, only 18 ug were loaded in each well. This was due to low cell number and thus lower protein concentration in the two latter cell types. Percentage band strength of the different targeting sgRNAs compared to NT is also given. Percentage band strengths were calculated in Image Lab (5.2.1). Protein size of Fzd7 is noted as 63 kDa in literature and databases, but it recognized as a band of 94 kDa by the antibody used. This is explained by the manufacturer in the data sheet accompanying the antibody (Santa Cruz, sc-293261).

3.3.5 FZD7 knock-down at viability by XTT-assay

To evaluate effect of CRISPR/Cas9-mediated FZD7 knock-down on cell viability, XTT proliferation assay was performed. The Kruskal-Wallis test with Dunn's correction was conducted for all cells to test for statistical significant difference in proliferation between cells transduced with the three different targeting sgRNAs (94, 96, 100) and the NT sgRNA at alpha level 0,05. It was found that all sgRNAs in T1547 and T1548 caused increased proliferation, but only sgRNA 94 and 96 gave a significant increase in proliferation (Figure 3.14). In T0965, all sgRNAs caused no to very little difference in proliferation, compared to NT. For T1008, all sgRNAs caused an increased proliferation, compared to NT, with 100 giving the greatest increase. Calculated p-values are given in Table 3.5.

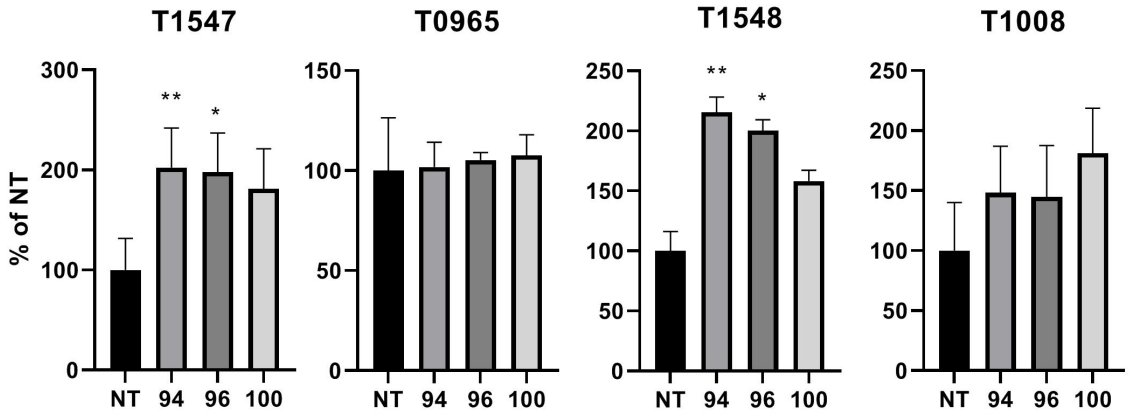

Figure 3.14: Percentage absorbance in T1547, T0965, T1548 and T1008 cells tranduced with the three different FZD7 specific sgRNAs (94, 96, 100), relative to cells transduced with the NT sgRNA. Significance level is given by asteriks; *: $p < 0{,}05$, **: $p < 0{,}01$. Calculated p-vales are given in Table 3.5

Cell type	**sgRNA**	**Adjusted p-value**	**Significant?**
T1547	94	0,0069	**
	96	0,0163	*
	100	0,0852	ns
T0965	94	$> 0{,}9999$	ns
	96	$> 0{,}9999$	ns
	100	$> 0{,}9999$	ns
T1548	94	0,0099	**
	96	0,0192	*
	100	0,8551	ns
T1008	94	0,1630	ns
	96	0,4469	ns
	100	0,4469	ns

Table 3.5: P-values generated from the Kruskal-Wallis test with Dunn's correction at alpha-level 0,05 to test for statistical significant difference in proliferation between cells transduced with the three different targeting sgRNAs (94, 96, 100) and the NT sgRNA. Significance level is given by asteriks; *: $p < 0{,}05$, **: $p < 0{,}01$. $n = 5$ for all sgRNAs. ns = non-significant.

3.4 Validation of statistical assumptions

In order to validate that the assumptions for conducting the Kruskal-Wallis test were met, analysis of the obtained data was performed. The choice of Kruskal-Wallis test was based on the expected small sample size (n=5) and the non-normal assumptions. The latter assumption would be resonable when working with biological systems [256]. It would be desirable to have five or more biological replicates of both RT qPCR and viability data, but due to low cell number harvested for each biological replicate and a set time limit for the project, this was not possible. For RT qPCR n=3, whilst for viability assay n=5. The Kruskal-Wallis test can though still be used as an approximation when $n < 5$ [258].

The assumptions for the Kruskal-Wallis test are as stated,

1. The data should be unpaired and independent.
2. The data should be obtained from a non-normal distribution.
3. The data from the different groups being compared should be of the same distribution.

The data are unpaired and independent as there would be no functional relationship between cells transduced with the different sgRNAs. The data are based on cells of the same patient being given different treatments, but the response from cells transduced with one sgRNA is not dependent on the response from cells transduced with another sgRNA. The data are also assumed to be from a non-normal distribution, as the sample size is not large enough to assume normality. This assumption can be tested by generating histograms or frequency distributions of the data. This will only be done for the viability data, as n=3 for the RT qPCR data would be too small to get a meaningful understanding of the distribution. Histograms of the data is given in Appendix (A.6). These distributions indicate non-normal distributions in all samples, arguably in lower degree for T0965 96, which show some tendency to normal distribution. The next assumption is that the samples compared come from the same distribution, and has proven to be a highly important aspect of the Kruskal-Wallis test [258]. If this assumption is not met, the test can still be conducted but the results only indicate a potential dominance of one group over the other, and cannot say much about statistical significant differences in group mean or medians [261]. The sample distributions are most easily determined by data histograms described above (Appendix (A.6)). By visual inspection it is difficult to exactly determine the distribution similarity of dissimilarity, but some assumptions can be made. Data from T1008 and T1547 SGK1 seems to indicate left-skewness in all samples, thus indicating similar distributions. All other tumors show data distribution skewness and variability within the different sgRNA transduced cells. Thus, it could be argued that conclusions regarding viability results for Fzd7 knock-down in T1547, T0965 and T1548 showcases a dominance , but no clear assumptions can be made based on differences in median or mean.

Discussion

In the past years, accumulating studies have demonstrated that Fzd7 inhibition might be a potential approach in cancer therapy. The results from our studies targeting Fzd7 in GSCs were contrary to this. Although complex to interpret, it was surprisingly found that partial knockdown of Fzd7 induced viability. Validation of the CRISPR/Cas9 system functionality by SGK1 knock-down indicated successful knock-down effects of SGK1 by decreased viability and protein knock-outs, but also indicated low efficiency in indel induction and unexpected increased SGK1 gene expression.

4.1 Increased viability following FZD7 knock-down

All three sgRNAs displayed the ability to decrease Fzd7 protein expression, although varying between the different patient cultures, followed by an increased viability (Figure 3.13 and 3.14). These results could indicate that there may exist a redundant relationship between Fzd7 and other proteins. As there exists several Fzd receptors that share homologous and conserved regions, the function of one Fzd receptor could be rescued by another Fzd receptor if knocked-down. Fzd7 share about 75% sequence identity with Fzd2 and Fzd1, which could salvage Fzd7 functions [262, 263, 264]. Voloshanenko et al. argued that knock-down effect in Wnt-signalling would be especially hard to observe due to potential redundancy effects between the 10 different Fzd receptors [262]. Further, they argued that in order to observe a knock-down effect, a CRISPR/Cas9 system targeting homologous regions shared by highly similar Fzd receptors should be applied. They successfully targeted highly conserved regions in the cystein rich extracellular domain and in the seventh transmembrane region of Fzd7, 1 and 2 in HEK293T cells, using a single sgRNA, and observed significantly decreased Wnt-signaling following CRISPR/Cas9 activity. Kolben et al. argued for a functional redundancy effect between Fzd7 and Fzd5, where ectopic expression of Fzd7 or Fzd5 rescued knock-down of the other [265]. Zhang et al., also argued that the end-product of the canonical Wnt-pathway, β-catenin, is not upregulated in gliomas with high Wnt-pathway activity, arguing that Wnt signaling may promote glioma development through alternative or non-canonical pathways [266]. In addition, Tan et al., argued for a redundancy effect in ovarian cancer between Fzd7 and TWIST-1, a transcription activator involved in epithelial-mesenchymal transition (EMT) during tumorigenesis [267]. They showed that TWIST-1 overexpression partially salvaged the functional phenotype of FZD7. TWIST-1 has also been found to be overexpressed and have a central functional role in gliomas and GBM development [268, 269, 270].

Interestingly, Liu et al. found that glioma stem cells frequently self-inflict DNA double-strand breaks, which unexpectedly sustained tumerogenicity, stemness and proliferation in patient-derived glioma stem cells [271]. The authors argued that glioma stem cells exhibit higher mitochondira permability, causing leakage of cytochrome c into the cell cytoplasm. This further causes induction of caspase-dependent DNase (Cad) and endonuclease G (EndoG), known to induce DNA DSBs. Following DSBs, Atm, a central component of the DNA damage response (DDR), would be activated by phosphorylation and kept in a phosphorylated state persistently due to the high presence of DSBs. Atm activity further activate transcription factors $N_F\kappa B$ and Stat3, both known to be involved in maintaining tumerogenicity and stemness of cancer cells, in addition to drive cell growth. Thus, induction of DSBs by CRISPR/Cas9 activity could conceivably also activate ATM in a similar manner, causing greater growth in cells transduced with the targeting sgRNAs and where DSBs have occured, than in cells transduced with the NT sgRNA where DSB have not occurred. Bao et al. also showed that glioma stem cells very readily activates the DNA damage response and Atm following DNA damage from therapeutic radiation [272]. Similar results were not observed when conducting SGK1 knock-down, which may argue that Sgk1 plays a more central role in viability compared to Fzd7, so that its knock-down effect is large enough to not be masked by a DSB induced increased viability.

The different tumors also showcased heterogeneity in responses to Fzd7 knock-down. Increased viability was observed in three of four tumors, but one indicated no change in viability. The different sgRNAs also

showed different ability to increase viability between the different tumors. This showcases patient response heterogeneity, and may make an argument for patient-specific cancer treatment. Heterogeneity in knock-down responses was also observed at mRNA and protein level, and T1008 was the only GSC culture showcasing knock-down effect at both mRNA and protein level, which is desired following CRISPR/Cas9 activity. A similar correlation was not observed in the other GSC cultures. This heterogeneity in responses at mRNA and protein level may not just be due to tumor or patient heterogeneity, as it is unlikely to observe correlation between mRNA and protein levels in cells [273]. This may be due to post-transcriptional and translational effects, protein half-life, error in RNA and DNA analyses, and rates and modulation of translation, and protein synthesis, and transport of the protein, to mention a few [273, 274, 275, 276].

4.2 Heterogeneity in SGK1 knock-outs

Following knock-down, an unexpected increased SGK1 gene expression was observed (Figure 3.5). SGK1 gene expression has been found to be increased following DNA damage and cellular stress [107, 108, 277, 136]. Thus, in cells were the DSB has been effectively repaired, the mutation is in-frame, or where the indels does not cause alteration to the probe binding site, functional or partly functional transcripts could still be produced and its expression increased just as a consequence of DSBs. This may be reasonable to assume as CRISPR/Cas9 efficency was lower than expected in several assays. In cells were CRISPR/Cas9 have, on the other hand, effectively induced mutations that caused mRNA degradation or otherwise substantially damaged the gene transcript, an increased gene expression would not be observed. [278, 279].

During study of Sgk1 protein expression, it was observed that the positive control protein lysate gave a band of about 50 kDa, whilst Sgk1 protein in T1547 gave a band of about 60 kDa (Figure 3.6). Thus, the different isomers of Sgk1 was further studied. Different Sgk1 isomer have also shown to have different subcellular loaction, function and transcription regulation [280, 281], making determination of the protein isomer variant interesting. It was found that both the 50- and 60 kDa isomer was expressed in our GSCs, but that only the 60 kDa isomer was expressed in T1547 (Figure 3.7). Other studies have also identified both the 50 and 60 kDa isomer present in brain tissue [280, 282, 283, 284]. The 60 kDa isomer differs from the 50 kDa isomer in that it is missing a N-terminal protein sequence (GMVAIL) facilitating polyubiquination of the protein, which allows for efficient 26S proteasome degradation [278, 279], and thus the protein isomer exhibits higher stability than the 50 kDa isomer. Interestingly, the DNA target sequence of sgRNA 79 translates into this exact protein sequence required for proteosomal degradation, and the sgRNA 79 target DNA sequence is not present in the 60 kDa isomer (Appendix (A.4)). Thus, it would not be expected to observe a Sgk1 protein knock-out effect in sgRNA 79 transdcued cells. This was contrary to our results. Possible explanations for the observed knock-out effect from sgRNA 79 was explored, including large genome alterations caused by sgRNA 79 extending into the exons of the 60 kDa isomer, post-translational modifications of Sgk1 which could give the impression of a higher molecular weight, off-targets effects of sgRNA 79, but none of these gave explanation coherent with other results. The function of the CRIPSR/Cas9 system is to induce DNA DSBs at specific desired DNA locations, which would desirably be followed by NHEJ and creation of indels. This ability was clearly demonstrated in the T7 assay, where the CRISPR/Cas9 system showed to cause indel induction at the specific desired target sites for all sgRNAs used. Further knock-down effects at mRNA, protein and viability is in a higher degree dependent on cell regulation and responses to the sgRNA specific DBS, as illustrated above, which could complicate understanding of these results. Still, in order to fully understand these observations, further studies would need to be done.

4.3 CRISPR/Cas9 knock-down efficiency

As the T7 assay indicated sub-optimal CRISPR/Cas9 induced indels, and not full knock-down was observed in all analyses, considerations regarding the CRISPR/Cas9 efficiency was further explored.

4.3.1 T7 assay insensitivity to small indels and CRISPR/Cas9 system efficiency in disrupting both gene alleles

Evaluation of DNA indel induction was done by the T7 endonuclease assay. Results indicated successful and specific DNA DSB induction, but also showed high presence of the uncut parental DNA strands in both SGK1 and FZD7 knock-down, indicating not full CRISPR/Cas9 efficiencies. This could be due to insensitivity of the

T7 assay, particularly for small indels. Single- and small nucleotide indels have shown to be poorly recognized by this assay [285, 286, 287], conceivably due to the small structural change this would cause in heteroduplex formation. In an application note from the CRISPR/Cas9 system manufacturer (Dharmacon, `https://dharmacon.horizondiscovery.com/uploadedFiles/Resources/edit-r-experimental-workflow-appnote.pdf`), the effectiveness of their system was showcased by attempting introduction of CRISPR/Cas9-mediated DSB in PPIB in 42 clonal HEK293T cell lines. It was found that in 4 of the 42 clonal cell lines, the T7 assay identifies no editing, but Sanger sequencing identified small and medium indels (1, 2, 3 and 35 nucleotides) in these cells. Most indels occurring following CRISPR/Cas9 activity are indeed reported to be no longer than 20-45 bps, whereas a majority are less than 10 bp [288, 289, 290, 291], even though larger indels in the kilo- and megabase range also have been observed [292, 293]. These observations could underestimate the effectiveness observed from the CRIPSR/Cas9 activity, which may be likely as a full knock-out effect is observed in sgRNA transduced 74 and 79, but no difference is observed in T7 assay efficiencies between sgRNA 74, 75 and 79.

Another factor that could lower the CRISPR/Cas9 efficiencies are if not both alleles are cut with same efficiency by the Cas9. In the application note from the manufacturer they showed that their system edited the gene of PPIB in 60% of the 42 clonal cell lines of HEK293T cells. 72% of these cell lines that were successfully edited, and 43% of the total amount of clonal cell lines used in the study, got a knock-out of both alleles, as is desired following CRISPR/Cas9 activity, depending on the gene being inherited in a recessive or dominant manner. But, the remaining 57% of the cell lines used in the study would be wild-type (40%) or only contain mutation in one allele (17%). This majority of non-double allele-editing could conceivably contribute to lowering the CRISPR/Cas9 efficiency observed by the T7 assay, but could also argue that full CRIPSR/Cas9 efficiency is not expected using the CRIPSR/Cas9 constructs delivered by Dharmacon. In addition, full CRIPSR/Cas9 efficency could not be expected when working with non-clonal cells, as the observed effect would be the sum of effects in a bulk of cells.

4.3.2 Potential strand preference and general Cas9/sgRNA considerations

Differences in knock-down effects were observed across the different sgRNA used, in both SGK1 and FZD7 knock-down. Wang et al. noted that sgRNAs targeting the transcribed strand were slightly less effective than those targeting the non-transcribed strand [294]. Similar results were observed in this study were sgRNA 74 and 79, targeting the non-transcribed strand, showed higher knock-down effect than sgRNA 75, targeting the transcribed strand (Table 2.2). This effect was observed at mRNA and protein level, and partly at viability (Figure 3.5, 3.6 and 3.8). For Fzd7, a higher knock-down effect was observed from sgRNA 94 and 96, compared to 100, where 94 and 96 were located to the non-transcribed strand, whilst sgRNA target 100 was located to the transcribed strand. This trend was observed for all tumors at mRNA level, and partly at protein level (Figure 3.12 and 3.13). The reasons for this potential strand preference remains unclear, and later studies have shown no significant difference in strand preference [295], but since the trend was observed across all sgRNAs, it makes an interesting observation.

General considerations regarding CRISPR/Cas9 efficiencies in this study have been noted and could be due to several factors. First, low transduction efficiencies would cause lower presence of CRISPR/Cas9 system in the cells, and thus a lower observed DSB induction As described in the results, transduction abilities were lower than earlier demonstrated, potentially due to sub-optimal cell adherence to the well-bottom. Second, the CRISPR/Cas9 system can be delivered in a dual- or single matter, introducing the Cas9 and sgRNA in the same construct or in seperate ones, respectively. Sanjana et al. argued that a single-vector system introducing both Cas9 and the sgRNA in the same vector, would be most suitable for use *in vivo* or in primary cell lines, even though a dual-system has advantages, like the possibility of generating stable Cas9-expressing cells lines for use with different sgRNAs [296]. In addition, primary cells have been showed to be harder to CRISPR/Cas9 modify, but the reasons for this still remains unclear. It could be due to differences in transdcution efficencies, DNA repair mechanisms, activity in construct promoters or exonuclease activity [297].The latter study argued that the effectiveness of the CRISPR/Cas9 in primary cells could be significantly improved by chemically modifying the three nucleotides at the 3' and 5' ends of the sgRNA, with 2'-O-methyl-3'thioPACE (MSP) or also 2'-O-methyl-3'phosphorothioate (MS) to increase sgRNA stability and reduce immune responses following introducton of foregin oligonucleotides. This argues that highly efficient CRISPR/Cas9 activity in primary cells may not be expected. Third, the physical availability of the sgRNA target sequence can lower the observed CRISPR/Cas9 efficency. Studies on this topic are inconsistent, some showing a great effect of DNA target availability and other showing no or little effect.

Cas9 has shown to be significantly less efficient, but not unable, to search for the sgRNA target sequence through heterochromatin [298]. CpG methylations could also infer some structural restrain on Cas9 DNA binding. Wu et al., argued that CpG methylations strongly predict Cas9 binding in mouse embryonic stem cells [299], whilst Hsu et al. showed that Cas9 cleavage is independent on DNA methylations [300]. DNA target sequence availability could arguably vary between tumors and in different cell states, which may explain observed differences in sgRNA efficiency.

Interestingly, Cas9 protein expression varied between the different tumors, with a low expression in T1547. Still, the CRISPR/Cas9 system showed to be active and functional in T1547 as it induced DSBs in the SGK1 study and in the positive control targeting PPIB in the Fzd7 knock-down studies. In fact, Yuen et al. argues that CRIPSR/Cas9 efficiency is not dependent on Cas9 expression, but rather on sgRNA identity and efficiency [260].

Future studies

As results from viability assay in Fzd7 knock-down were inconsistent with previous work, further studies of these observations would be of interest. As this study is done in bulk, non-clonal cells, the observed effects will necessarily be the sum of many different mutations occurring in different cells. Thus, a similar study, potentially also including DNA sequencing, can be conducted in a clonal cell population to get a better understanding of the FZD7 function and the CRISPR/Cas9 mutations induced. Relating to this, it would also be of interest to study whether the Wnt canonical pathway is indeed being affected in our cells. This can be done by studying gene and/or protein expression of the canonical Wnt-pathway effector, β-catenin in our cells.

DNA sequencing could also be relevant in order to study the exact genomic CRISPR/Cas9 effects in sgRNA 79 transduced T1547 cells. Further study into Sgk1 regulation and function in our cells, would also be interesting in this regard. This could give deeper insight into the observed effects in Sgk1 knock-down. Further understanding of CRISPR/Cas9 system functionality and optimized design would also be appropriate, in order to increase knock-down efficiencies. Especially, greater care into choice of CRISPR/Cas9 platform, gene target sequences and design of the sgRNA could be of great importance.

Conclusion

The aim of this study was to functionally validate knock-down of the Wnt-pathway receptor, Fzd7, using CRISPR/Cas9 technology, by first establishing protocol conditions for knock-down and viability assays targeting a functional control gene (SGK1), and second, to use the established protocol conditions to explore knock-down of Fzd7 in four patient-derived primary GSC cultures.

Functional control of the CRISPR/Cas9 system by SGK1 knock-down partly validated the functionality of the system by indicating successful and specific indel induction and decreased viability, though showcasing sub-optimal indel inductions and a potential uncertainty regarding protein knock-out from one of the sgRNAs. Further CRISPR/Cas9-mediated knock-down of FZD7 in four patient-derived GSC cultures unexpectedly showed increased viability in all cell cultures. This could be due to redundancy effects between Fzd7 and other proteins, or unaccounted for DNA damage responses. Knock-down of Fzd7 also showcased sub-optimal DNA indel inductions and variations in Fzd7 gene and protein expression between the different tumors. Only one of four GSC cultures showcased both decreased mRNA and protein levels, as is desired following CRISPR/Cas9 activity. Responses on mRNA and protein level highlighted difficulties in predicting effects of cell regulation, and tumor heterogeneity in responses to CRISPR/Cas9-mediated Fzd7 knock-down. Further understanding of the Wnt-pathway and other central pathways for cancer stem cell viability, and exploration of specific molecular targets should be done in order to identify and validate functional targets for GBM treatment. Additionally, further understanding of CRIPSR/Cas9 effects in GSCs and optimization of CRISPR/Cas9 protocols and designs, should also be done in order to increase CRISPR/Cas9-mediated knock-down effects.

Bibliography

[1] Erlend Skaga et al. "Intertumoral heterogeneity in patient-specific drug sensitivities in treatment-naïve glioblastoma". In: *BMC Cancer* 19.1 (June 2019), p. 628. ISSN: 1471-2407. DOI: 10.1186/s12885-019-5861-4. URL: https://doi.org/10.1186/s12885-019-5861-4.

[2] Percival Bailey and Harvey Williams Cushing. *A Classification of the Tumors of the Glioma Group on a Histo-genetic Basis, with a Correlated Study of Prognosis... With 108 Illustrations*. JB Lippincott Company, 1926.

[3] David N. Louis et al. "The 2016 World Health Organization Classification of Tumors of the Central Nervous System: a summary". In: *Acta Neuropathologica* 131.6 (June 2016), pp. 803–820. ISSN: 1432-0533. DOI: 10.1007/s00401-016-1545-1. URL: https://doi.org/10.1007/s00401-016-1545-1.

[4] J Brat Daniel. "Genetic modulation of hypoxia induced gene expression and angiogenesis: relevance to brain tumors". In: *Frontiers in Bioscience* 8 (Jan. 2003), p. d100. DOI: 10.2741/942.

[5] David N Louis et al. "The 2016 World Health Organization classification of tumors of the central nervous system: a summary". In: *Acta neuropathologica* 131.6 (2016), pp. 803–820.

[6] Christian Frezza, Daniel A. Tennant, and Eyal Gottlieb. "IDH1 Mutations in Gliomas: When an Enzyme Loses Its Grip". In: *Cancer Cell* 17.1 (2010), pp. 7–9. ISSN: 1535-6108. DOI: https://doi.org/10.1016/j.ccr.2009.12.031. URL: http://www.sciencedirect.com/science/article/pii/S1535610809004358.

[7] W. K. Cavenee et al. "Expression of recessive alleles by chromosomal mechanisms in retinoblastoma". In: *Nature* 305.5937 (1983), pp. 779–784. ISSN: 1476-4687. DOI: 10.1038/305779a0. URL: https://doi.org/10.1038/305779a0.

[8] Robert B. Jenkins et al. "A t(1;19)(q10;p10) Mediates the Combined Deletions of 1p and 19q and Predicts a Better Prognosis of Patients with Oligodendroglioma". In: *Cancer Research* 66.20 (2006), pp. 9852–9861. ISSN: 0008-5472. DOI: 10.1158/0008-5472.CAN-06-1796. eprint: http://cancerres.aacrjournals.org/content/66/20/9852.full.pdf. URL: http://cancerres.aacrjournals.org/content/66/20/9852.

[9] Constance A. Griffin et al. "Identification of der(1;19)(q10;p10) in Five Oligodendrogliomas Suggests Mechanism of Concurrent 1p and 19q Loss". In: *Journal of Neuropathology Experimental Neurology* 65.10 (Oct. 2006), pp. 988–994. ISSN: 0022-3069. DOI: 10.1097/01.jnen.0000235122.98052.8f. eprint: http://oup.prod.sis.lan/jnen/article-pdf/65/10/988/9556692/65-10-988.pdf. URL: https://doi.org/10.1097/01.jnen.0000235122.98052.8f.

[10] Justin S. Smith et al. "Mapping of the chromosome 19 q-arm glioma tumor suppressor gene using fluorescence in situ hybridization and novel microsatellite markers". In: *Genes, Chromosomes and Cancer* 29.1 (2000), pp. 16–25. DOI: 10.1002/1098-2264(2000)9999:9999<::AID-GCC1007>3.0.CO;2-I. eprint: https://onlinelibrary.wiley.com/doi/pdf/10.1002/1098-2264$\%$282000$\%$299999$\%$3A9999$\%$3C$\%$3A$\%$3AAID-GCC1007$\%$3E3.0.CO$\%$3B2-I. URL: https://onlinelibrary.wiley.com/doi/abs/10.1002/1098-2264282000$%5C%$299999$%5C%$3A9999$%5C%$3C$%5C%$3A$%5C%$3AAID-GCC100$%5C%$3E3.0.CO$%5C%$3B2-I.

[11] Jeanette E. Eckel-Passow et al. "Glioma Groups Based on 1p/19q, IDH, and TERT Promoter Mutations in Tumors". In: *New England Journal of Medicine* 372.26 (2015). PMID: 26061753, pp. 2499–2508. DOI: 10.1056/NEJMoa1407279. eprint: https://doi.org/10.1056/NEJMoa1407279. URL: https://doi.org/10.1056/NEJMoa1407279.

[12] Benedikt Wiestler et al. "ATRX loss refines the classification of anaplastic gliomas and identifies a subgroup of IDH mutant astrocytic tumors with better prognosis". In: *Acta Neuropathologica* 126.3 (Sept. 2013), pp. 443–451. ISSN: 1432-0533. DOI: 10.1007/s00401-013-1156-z. URL: https://doi.org/10.1007/s00401-013-1156-z.

[13] P. D. Delgado-LΓ*opezAndE.M.Corrales − Garc*ia. "Survival in glioblastoma: a review on the impact of treatment modalities". In: *Clinical and Translational Oncology* 18.11 (Nov. 2016), pp. 1062–1071. ISSN: 1699-3055. DOI: 10.1007/s12094-016-1497-x. URL: https://doi.org/10.1007/s12094-016-1497-x.

[14] Jigisha P. Thakkar et al. "Epidemiologic and Molecular Prognostic Review of Glioblastoma". In: *Cancer Epidemiol Biomarkers Prev* 23.10 (Oct. 2014). 25053711[pmid], pp. 1985–1996. ISSN: 1055-9965. DOI: 10.1158/1055-9965.EPI-14-0275. URL: http://www.ncbi.nlm.nih.gov/pmc/articles/PMC4185005/.

[15] Quinn T. Ostrom et al. "CBTRUS Statistical Report: Primary Brain and Central Nervous System Tumors Diagnosed in the United States in 2006-2010". In: *Neuro Oncol* 15.Suppl 2 (Nov. 2013). 24137015[pmid], pp. ii1–ii56. ISSN: 1522-8517. DOI: 10.1093/neuonc/not151. URL: http://www.ncbi.nlm.nih.gov/pmc/articles/PMC3798196/.

[16] Quinn T. Ostrom et al. "The epidemiology of glioma in adults: a "state of the science" review". In: *Neuro-Oncology* 16.7 (May 2014), pp. 896–913. ISSN: 1522-8517. DOI: 10.1093/neuonc/nou087. eprint: http://oup.prod.sis.lan/neuro-oncology/article-pdf/16/7/896/16665942/nou087.pdf. URL: https://dx.doi.org/10.1093/neuonc/nou087.

[17] Jigisha P. Thakkar et al. "Epidemiologic and Molecular Prognostic Review of Glioblastoma". In: *Cancer Epidemiology and Prevention Biomarkers* 23.10 (2014), pp. 1985–1996. ISSN: 1055-9965. DOI: 10.1158/1055-9965.EPI-14-0275. eprint: http://cebp.aacrjournals.org/content/23/10/1985.full.pdf. URL: http://cebp.aacrjournals.org/content/23/10/1985.

[18] Ahmad Tamimi and Malik Juweid. "Epidemiology and Outcome of Glioblastoma". In: Sept. 2017, pp. 143–153. ISBN: 9780994438126. DOI: 10.15586/codon.glioblastoma.2017.ch8.

[19] Linda C. Hodges et al. "Prevalence of Glioblastoma Multiforme in Subjects with Prior Therapeutic Radiation". In: 24 (May 1992), pp. 79–83.

[20] Janet M. Bruner et al. "-Radiation Sensitivity and Risk of Glioma". In: *JNCI: Journal of the National Cancer Institute* 93.20 (Oct. 2001), pp. 1553–1557. ISSN: 0027-8874. DOI: 10.1093/jnci/93.20.1553. eprint: http://oup.prod.sis.lan/jnci/article-pdf/93/20/1553/9849052/1553.pdf. URL: https://dx.doi.org/10.1093/jnci/93.20.1553.

[21] Margaret Wrensch et al. "Variants in the CDKN2B and RTEL1 regions are associated with high grade glioma susceptibility". In: *Nat Genet* 41.8 (Aug. 2009). 19578366[pmid], pp. 905–908. ISSN: 1061-4036. DOI: 10.1038/ng.408. URL: http://www.ncbi.nlm.nih.gov/pmc/articles/PMC2923561/.

[22] Mohamed Ali Mosrati et al. "TERT promoter mutations and polymorphisms as prognostic factors in primary glioblastoma". In: *Oncotarget* 6.18 (June 2015). 4389[PII], pp. 16663–16673. ISSN: 1949-2553. URL: https://www.ncbi.nlm.nih.gov/pubmed/26143636.

[23] Marc Sanson et al. "Chromosome 7p11.2 (EGFR) variation influences glioma risk". In: *Human Molecular Genetics* 20.14 (Apr. 2011), pp. 2897–2904. ISSN: 0964-6906. DOI: 10.1093/hmg/ddr192. eprint: http://oup.prod.sis.lan/hmg/article-pdf/20/14/2897/17252316/ddr192.pdf. URL: https://dx.doi.org/10.1093/hmg/ddr192.

[24] Sanjay Shete et al. "Genome-wide association study identifies five susceptibility loci for glioma". In: *Nature Genetics* 41 (July 2009), 899 EP -. URL: https://doi.org/10.1038/ng.407.

[25] Margaret Wrensch et al. "Variants in the CDKN2B and RTEL1 regions are associated with high-grade glioma susceptibility". In: *Nature Genetics* 41 (July 2009), 905 EP -. URL: https://doi.org/10.1038/ng.408.

[26] V. Enciso-Mora et al. "Low penetrance susceptibility to glioma is caused by the TP53 variant rs78378222". In: *British Journal Of Cancer* 108 (Apr. 2013). Genetics and Genomics, 2178 EP -. URL: https://doi.org/10.1038/bjc.2013.155.

[27] Kyle M. Walsh et al. "Variants near TERT and TERC influencing telomere length are associated with high-grade glioma risk". In: *Nature Genetics* 46 (June 2014), 731 EP -. URL: https://doi.org/10.1038/ng.3004.

[28] Judith A. Schwartzbaum et al. "Epidemiology and molecular pathology of glioma". In: *Nature Clinical Practice Neurology* 2 (Sept. 2006). Review Article, 494 EP -. URL: https://doi.org/10.1038/ncpneuro0289.

[29] Judith Schwartzbaum et al. “Association between prediagnostic IgE levels and risk of glioma”. In: *J Natl Cancer Inst* 104.16 (Aug. 2012). djs315[PII], pp. 1251–1259. ISSN: 1460-2105. DOI: 10.1093/jnci/djs315. URL: https://www.ncbi.nlm.nih.gov/pubmed/22855780.

[30] Alina V. Brenner et al. “History of allergies and autoimmune diseases and risk of brain tumors in adults”. In: *International Journal of Cancer* 99.2 (), pp. 252–259. DOI: 10.1002/ijc.10320. eprint: https://onlinelibrary.wiley.com/doi/pdf/10.1002/ijc.10320. URL: https://onlinelibrary.wiley.com/doi/abs/10.1002/ijc.10320.

[31] Brigitte Schlehofer et al. “Role of medical history in brain tumour development. Results from the international adult brain tumour study”. In: *International Journal of Cancer* 82.2 (), pp. 155–160. DOI: 10.1002/(SICI)1097-0215(19990719)82:2<155::AID-IJC1>3.0.CO;2-P. eprint: https://onlinelibrary.wiley.com/doi/pdf/10.1002/$\%$28SICI$\%$291097-0215$\%$2819990719$\%$2982$\%$3A2$\%$3C155$\%$3A$\%$3AAID-IJC1$\%$3E3.0.CO$\%$3B2-P. URL: https://onlinelibrary.wiley.com/doi/abs/10.1002/$%5C%$28SICI$%5C%$291097-0215$%5C%$2819990719$%5C%$2982$%5C%$3A2$%5C%$3C155$%5C%$3A$%5C%$3AAID-IJC1$%5C%$3E3.0.CO$%5C%$3B2-P.

[32] Michael E. Scheurer et al. “Effects of antihistamine and anti-inflammatory medication use on risk of specific glioma histologies”. In: *Int J Cancer* 129.9 (Nov. 2011). 21190193[pmid], pp. 2290–2296. ISSN: 0020-7136. DOI: 10.1002/ijc.25883. URL: http://www.ncbi.nlm.nih.gov/pmc/articles/PMC3125483/.

[33] Roger Stupp et al. “Effects of radiotherapy with concomitant and adjuvant temozolomide versus radiotherapy alone on survival in glioblastoma in a randomised phase III study: 5-year analysis of the EORTC-NCIC trial”. In: *The Lancet Oncology* 10.5 (2009), pp. 459–466. ISSN: 1470-2045. DOI: https://doi.org/10.1016/S1470-2045(09)70025-7. URL: http://www.sciencedirect.com/science/article/pii/S1470204509700257.

[34] Cory Adamson et al. “Glioblastoma multiforme: a review of where we have been and where we are going”. In: *Expert Opinion on Investigational Drugs* 18.8 (2009). PMID: 19555299, pp. 1061–1083. DOI: 10.1517/13543780903052764. eprint: https://doi.org/10.1517/13543780903052764. URL: https://doi.org/10.1517/13543780903052764.

[35] Rajamanickam Baskar et al. “Cancer and radiation therapy: current advances and future directions”. In: *International journal of medical sciences* 9.3 (2012). ijmsv09p0193[PII], pp. 193–199. ISSN: 1449-1907. DOI: 10.7150/ijms.3635. URL: https://www.ncbi.nlm.nih.gov/pubmed/22408567.

[36] P.A. Riley. “Free Radicals in Biology: Oxidative Stress and the Effects of Ionizing Radiation”. In: *International Journal of Radiation Biology* 65.1 (1994). PMID: 7905906, pp. 27–33. DOI: 10.1080/09553009414550041. eprint: https://doi.org/10.1080/09553009414550041. URL: https://doi.org/10.1080/09553009414550041.

[37] W. Roa et al. “Abbreviated Course of Radiation Therapy in Older Patients With Glioblastoma Multiforme: A Prospective Randomized Clinical Trial”. In: *Journal of Clinical Oncology* 22.9 (2004). PMID: 15051755, pp. 1583–1588. DOI: 10.1200/JCO.2004.06.082. eprint: https://doi.org/10.1200/JCO.2004.06.082. URL: https://doi.org/10.1200/JCO.2004.06.082.

[38] Malcolm F.G. Stevens and Tracey D. Bradshaw. “Temozolomide: Mechanisms of Action, Repair and Resistance”. In: *Current Molecular Pharmacology* 5.1 (2012), pp. 102–114. ISSN: 1874-4672/1874-4702. DOI: 10.2174/1874467211205010102. URL: http://www.eurekaselect.com/node/94882/article.

[39] Sang Y. Lee. “Temozolomide resistance in glioblastoma multiforme”. In: *Genes Diseases* 3.3 (2016), pp. 198–210. ISSN: 2352-3042. DOI: https://doi.org/10.1016/j.gendis.2016.04.007. URL: http://www.sciencedirect.com/science/article/pii/S2352304216300162.

[40] Manel Esteller et al. “Inactivation of the DNA-Repair Gene MGMT and the Clinical Response of Gliomas to Alkylating Agents”. In: *New England Journal of Medicine* 343.19 (2000). PMID: 11070098, pp. 1350–1354. DOI: 10.1056/NEJM200011093431901. eprint: https://doi.org/10.1056/NEJM200011093431901. URL: https://doi.org/10.1056/NEJM200011093431901.

[41] Monika E Hegi et al. “Clinical Trial Substantiates the Predictive Value of O-6-Methylguanine-DNA Methyltransferase Promoter Methylation in Glioblastoma Patients Treated with Temozolomide”. In: *Clinical cancer research : an official journal of the American Association for Cancer Research* 10 (Apr. 2004), pp. 1871–4. DOI: 10.1158/1078-0432.CCR-03-0384.

[42] Roger Stupp et al. "Effects of radiotherapy with concomitant and adjuvant temozolomide versus radiotherapy alone on survival in glioblastoma in a randomised phase III study: 5-year analysis of the EORTC-NCIC trial". In: *The Lancet Oncology* 10.5 (2009), pp. 459–466. ISSN: 1470-2045. DOI: https://doi.org/10.1016/S1470-2045(09)70025-7. URL: http://www.sciencedirect.com/science/article/pii/S1470204509700257.

[43] Nicholas J. Szerlip et al. "Intratumoral heterogeneity of receptor tyrosine kinases EGFR and PDGFRA amplification in glioblastoma defines subpopulations with distinct growth factor response". In: *Proceedings of the National Academy of Sciences* 109.8 (2012), pp. 3041–3046. ISSN: 0027-8424. DOI: 10.1073/pnas.1114033109. eprint: https://www.pnas.org/content/109/8/3041.full.pdf. URL: https://www.pnas.org/content/109/8/3041.

[44] Frank B. Furnari et al. "Heterogeneity of epidermal growth factor receptor signalling networks in glioblastoma". In: *Nature Reviews Cancer* 15 (Apr. 2015). Perspective, 302 EP -. URL: https://doi.org/10.1038/nrc3918.

[45] Andrea Sottoriva et al. "Intratumor heterogeneity in human glioblastoma reflects cancer evolutionary dynamics". In: *Proceedings of the National Academy of Sciences* 110.10 (2013), pp. 4009–4014. ISSN: 0027-8424. DOI: 10.1073/pnas.1219747110. eprint: https://www.pnas.org/content/110/10/4009.full.pdf. URL: https://www.pnas.org/content/110/10/4009.

[46] Roel G.W. Verhaak et al. "Integrated Genomic Analysis Identifies Clinically Relevant Subtypes of Glioblastoma Characterized by Abnormalities in PDGFRA, IDH1, EGFR, and NF1". In: *Cancer Cell* 17.1 (2010), pp. 98–110. ISSN: 1535-6108. DOI: https://doi.org/10.1016/j.ccr.2009.12.020. URL: http://www.sciencedirect.com/science/article/pii/S1535610809004322.

[47] David N. Louis et al. "The 2007 WHO Classification of Tumours of the Central Nervous System". In: *Acta Neuropathologica* 114.2 (Aug. 2007), pp. 97–109. ISSN: 1432-0533. DOI: 10.1007/s00401-007-0243-4. URL: https://doi.org/10.1007/s00401-007-0243-4.

[48] P. Korkolopoulou et al. "Prognostic implications of microvessel morphometry in diffuse astrocytic neoplasms". In: *Neuropathology and Applied Neurobiology* 28.1 (2002), pp. 57–66. DOI: 10.1046/j.1365-2990.2002.00367.x. eprint: https://onlinelibrary.wiley.com/doi/pdf/10.1046/j.1365-2990.2002.00367.x. URL: https://onlinelibrary.wiley.com/doi/abs/10.1046/j.1365-2990.2002.00367.x.

[49] Robert G. Bristow and Richard P. Hill. "Hypoxia, DNA repair and genetic instability". In: *Nature Reviews Cancer* 8 (Mar. 2008). Review Article, 180 EP -. URL: https://doi.org/10.1038/nrc2344.

[50] Gelareh Zadeh et al. "GBM's multifaceted landscape: highlighting regional and microenvironmental heterogeneity". In: *Neuro-Oncology* 16.9 (Mar. 2014), pp. 1167–1175. ISSN: 1522-8517. DOI: 10.1093/neuonc/nou035. eprint: http://oup.prod.sis.lan/neuro-oncology/article-pdf/16/9/1167/7639651/nou035.pdf. URL: https://dx.doi.org/10.1093/neuonc/nou035.

[51] Vishnu Anand Cuddapah et al. "A neurocentric perspective on glioma invasion". In: *Nature Reviews Neuroscience* 15 (June 2014). Review Article, 455 EP -. URL: https://doi.org/10.1038/nrn3765.

[52] Tim Demuth and Michael E. Berens. "Molecular Mechanisms of Glioma Cell Migration and Invasion". In: *Journal of Neuro-Oncology* 70.2 (Nov. 2004), pp. 217–228. ISSN: 1573-7373. DOI: 10.1007/s11060-004-2751-6. URL: https://doi.org/10.1007/s11060-004-2751-6.

[53] Graeme F. Woodworth et al. "Emerging Insights into Barriers to Effective Brain Tumor Therapeutics". In: *Frontiers in Oncology* 4 (2014), p. 126. ISSN: 2234-943X. DOI: 10.3389/fonc.2014.00126. URL: https://www.frontiersin.org/article/10.3389/fonc.2014.00126.

[54] Sang-Soo Kim et al. "Effective treatment of glioblastoma requires crossing the blood–brain barrier and targeting tumors including cancer stem cells: The promise of nanomedicine". In: *Biochemical and Biophysical Research Communications* 468.3 (2015). Nanomedicine, pp. 485–489. ISSN: 0006-291X. DOI: https://doi.org/10.1016/j.bbrc.2015.06.137. URL: http://www.sciencedirect.com/science/article/pii/S0006291X15301893.

[55] Andreas F. Hottinger, Patricia Pacheco, and Roger Stupp. "Tumor treating fields: a novel treatment modality and its use in brain tumors". In: *Neuro Oncol* 18.10 (Oct. 2016). now182[PII], pp. 1338–1349. ISSN: 1523-5866. DOI: 10.1093/neuonc/now182. URL: https://www.ncbi.nlm.nih.gov/pubmed/27664860.

[56] Qi Chen et al. "Treatment of Human Glioblastoma with a Live Attenuated Zika Virus Vaccine Candidate". In: *mBio* 9.5 (2018). Ed. by W. Ian Lipkin. DOI: 10.1128/mBio.01683-18. eprint: https://mbio.asm.org/content/9/5/e01683-18.full.pdf. URL: https://mbio.asm.org/content/9/5/e01683-18.

[57] Fumiharu Ohka, Atsushi Natsume, and Toshihiko Wakabayashi. "Current Trends in Targeted Therapies for Glioblastoma Multiforme". In: *Neurology research international* 2012 (Mar. 2012), p. 878425. DOI: 10.1155/2012/878425.

[58] R. Fisher, L. Pusztai, and C. Swanton. "Cancer heterogeneity: implications for targeted therapeutics". In: *British journal of cancer* 108.3 (Feb. 2013). bjc2012581[PII], pp. 479–485. ISSN: 1532-1827. DOI: 10.1038/bjc.2012.581. URL: https://www.ncbi.nlm.nih.gov/pubmed/23299535.

[59] Ke Chen, Ying-hui Huang, and Ji-long Chen. "Understanding and targeting cancer stem cells: therapeutic implications and challenges". In: *Acta Pharmacologica Sinica* 34 (May 2013). Review, 732 EP -. URL: https://doi.org/10.1038/aps.2013.27.

[60] Tsvee Lapidot et al. "A cell initiating human acute myeloid leukaemia after transplantation into SCID mice". In: *Nature* 367.6464 (1994), pp. 645–648. ISSN: 1476-4687. DOI: 10.1038/367645a0. URL: https://doi.org/10.1038/367645a0.

[61] Tannishtha Reya et al. "Stem cells, cancer, and cancer stem cells". In: *Nature* 414.6859 (2001), pp. 105–111. ISSN: 1476-4687. DOI: 10.1038/35102167. URL: https://doi.org/10.1038/35102167.

[62] Tracy Seymour, Anna Nowak, and Foteini Kakulas. "Targeting Aggressive Cancer Stem Cells in Glioblastoma". In: *Frontiers in Oncology* 5 (2015), p. 159. ISSN: 2234-943X. DOI: 10.3389/fonc.2015.00159. URL: https://www.frontiersin.org/article/10.3389/fonc.2015.00159.

[63] Sheila Alcantara Llaguno et al. "Malignant Astrocytomas Originate from Neural Stem/Progenitor Cells in a Somatic Tumor Suppressor Mouse Model". In: *Cancer Cell* 15.1 (2009), pp. 45–56. ISSN: 1535-6108. DOI: https://doi.org/10.1016/j.ccr.2008.12.006. URL: http://www.sciencedirect.com/science/article/pii/S1535610808004091.

[64] Sheila K. Singh et al. "Identification of human brain tumour initiating cells". In: *Nature* 432 (Nov. 2004), 396 EP -. URL: https://doi.org/10.1038/nature03128.

[65] Qunzhou Zhang et al. "A subpopulation of CD133+ cancer stem-like cells characterized in human oral squamous cell carcinoma confer resistance to chemotherapy". In: *Cancer Letters* 289.2 (2010), pp. 151–160. ISSN: 0304-3835. DOI: https://doi.org/10.1016/j.canlet.2009.08.010. URL: http://www.sciencedirect.com/science/article/pii/S0304383509005266.

[66] Zangiacomi Vincent et al. "CD133-positive cancer stem cells from Colo205 human colon adenocarcinoma cell line show resistance to chemotherapy and display a specific metabolomic profile". In: *Genes Cancer* 5.7-8 (July 2014). 23[PII], pp. 250–260. ISSN: 1947-6019. URL: https://www.ncbi.nlm.nih.gov/pubmed/25221643.

[67] Abdelouahid El-Khattouti et al. "Identification and analysis of CD133+ melanoma stem-like cells conferring resistance to taxol: An insight into the mechanisms of their resistance and response". In: *Cancer Letters* 343.1 (2014), pp. 123–133. ISSN: 0304-3835. URL: http://www.sciencedirect.com/science/article/pii/S0304383513006939.

[68] Mollie H. Wright et al. "Brca1 breast tumors contain distinct CD44 and CD133 with cancer stem cell characteristics". In: *Breast Cancer Research* 10.1 (Feb. 2008), R10. ISSN: 1465-542X. DOI: 10.1186/bcr1855. URL: https://doi.org/10.1186/bcr1855.

[69] Joo Mi Yi et al. "Abnormal DNA Methylation of CD133 in Colorectal and Glioblastoma Tumors". In: *Cancer Research* 68.19 (2008), pp. 8094–8103. ISSN: 0008-5472. DOI: 10.1158/0008-5472.CAN-07-6208. eprint: http://cancerres.aacrjournals.org/content/68/19/8094.full.pdf. URL: http://cancerres.aacrjournals.org/content/68/19/8094.

[70] S. Maeda et al. "CD133 expression is correlated with lymph node metastasis and vascular endothelial growth factor-C expression in pancreatic cancer". In: *British Journal Of Cancer* 98 (Mar. 2008). Molecular Diagnostics, 1389 EP -. URL: https://doi.org/10.1038/sj.bjc.6604307.

[71] Jian Wang et al. "CD133 negative glioma cells form tumors in nude rats and give rise to CD133 positive cells". In: *International Journal of Cancer* 122.4 (2008), pp. 761–768. DOI: 10.1002/ijc.23130. eprint: https://www.onlinelibrary.wiley.com/doi/pdf/10.1002/ijc.23130. URL: https://www.onlinelibrary.wiley.com/doi/abs/10.1002/ijc.23130.

[72] Sheila K. Singh et al. “Identification of a Cancer Stem Cell in Human Brain Tumors”. In: *Cancer Research* 63.18 (2003), pp. 5821–5828. ISSN: 0008-5472. eprint: http://cancerres.aacrjournals.org/content/63/18/5821.full.pdf. URL: http://cancerres.aacrjournals.org/content/63/18/5821.

[73] Houman D. Hemmati et al. “Cancerous stem cells can arise from pediatric brain tumors”. In: *Proceedings of the National Academy of Sciences* 100.25 (2003), pp. 15178–15183. ISSN: 0027-8424. DOI: 10.1073/pnas.2036535100. eprint: https://www.pnas.org/content/100/25/15178.full.pdf. URL: https://www.pnas.org/content/100/25/15178.

[74] Urban Lendahl, Lyle B. Zimmerman, and Ronald D.G. McKay. “CNS stem cells express a new class of intermediate filament protein”. In: *Cell* 60.4 (1990), pp. 585–595. ISSN: 0092-8674. DOI: https://doi.org/10.1016/0092-8674(90)90662-X. URL: http://www.sciencedirect.com/science/article/pii/009286749090662X.

[75] Myung Jin Son et al. “SSEA-1 Is an Enrichment Marker for Tumor-Initiating Cells in Human Glioblastoma”. In: *Cell Stem Cell* 4.5 (2009), pp. 440–452. ISSN: 1934-5909. DOI: https://doi.org/10.1016/j.stem.2009.03.003. URL: http://www.sciencedirect.com/science/article/pii/S1934590909001040.

[76] Alexandra Capela and Sally Temple. “LeX/ssea-1 Is Expressed by Adult Mouse CNS Stem Cells, Identifying Them as Nonependymal”. In: *Neuron* 35.5 (2002), pp. 865–875. ISSN: 0896-6273. DOI: https://doi.org/10.1016/S0896-6273(02)00835-8. URL: http://www.sciencedirect.com/science/article/pii/S0896627302008358.

[77] Arnold Kriegstein and Arturo Alvarez-Buylla. “The glial nature of embryonic and adult neural stem cells”. In: *Annu Rev Neurosci* 32 (2009). PMC3086722[pmcid], pp. 149–184. ISSN: 1545-4126. DOI: 10.1146/annurev.neuro.051508.135600. URL: https://www.ncbi.nlm.nih.gov/pubmed/19555289.

[78] Joo Ho Lee et al. “Human glioblastoma arises from subventricular zone cells with low-level driver mutations”. In: *Nature* 560.7717 (2018), pp. 243–247. ISSN: 1476-4687. DOI: 10.1038/s41586-018-0389-3. URL: https://doi.org/10.1038/s41586-018-0389-3.

[79] Toru Kondo and Martin Raff. “Oligodendrocyte Precursor Cells Reprogrammed to Become Multipotential CNS Stem Cells”. In: *Science* 289.5485 (2000), pp. 1754–1757. ISSN: 0036-8075. DOI: 10.1126/science.289.5485.1754. eprint: http://science.sciencemag.org/content/289/5485/1754.full.pdf. URL: http://science.sciencemag.org/content/289/5485/1754.

[80] Nader Sanai, Arturo Alvarez-Buylla, and Mitchel S. Berger. “Neural Stem Cells and the Origin of Gliomas”. In: *New England Journal of Medicine* 353.8 (2005). PMID: 16120861, pp. 811–822. DOI: 10.1056/NEJMra043666. eprint: https://doi.org/10.1056/NEJMra043666. URL: https://doi.org/10.1056/NEJMra043666.

[81] Hui Zong, Roel GW Verhaak, and Peter Canoll. “The cellular origin for malignant glioma and prospects for clinical advancements”. In: *Expert Review of Molecular Diagnostics* 12.4 (2012). PMID: 22616703, pp. 383–394. DOI: 10.1586/erm.12.30. eprint: https://doi.org/10.1586/erm.12.30. URL: https://doi.org/10.1586/erm.12.30.

[82] Brian Thiessen et al. “A phase I/II trial of GW572016 (lapatinib) in recurrent glioblastoma multiforme: clinical outcomes, pharmacokinetics and molecular correlation”. In: *Cancer Chemotherapy and Pharmacology* 65.2 (Jan. 2010), pp. 353–361. ISSN: 1432-0843. DOI: 10.1007/s00280-009-1041-6. URL: https://doi.org/10.1007/s00280-009-1041-6.

[83] Udo Bode et al. “Nimotuzumab treatment of malignant gliomas”. In: *Expert Opinion on Biological Therapy* 12.12 (2012). PMID: 23043252, pp. 1649–1659. DOI: 10.1517/14712598.2012.733367. eprint: https://doi.org/10.1517/14712598.2012.733367. URL: https://doi.org/10.1517/14712598.2012.733367.

[84] John H. Sampson et al. “Tumor-specific immunotherapy targeting the EGFRvIII mutation in patients with malignant glioma”. In: *Seminars in Immunology* 20.5 (2008). Tumor-Specific Immune Responses, pp. 267–275. ISSN: 1044-5323. DOI: https://doi.org/10.1016/j.smim.2008.04.001. URL: http://www.sciencedirect.com/science/article/pii/S1044532308000444.

[85] Michael J Cross and Lena Claesson-Welsh. “FGF and VEGF function in angiogenesis: signalling pathways, biological responses and therapeutic inhibition”. In: *Trends in Pharmacological Sciences* 22.4 (2001), pp. 201–207. ISSN: 0165-6147. DOI: https://doi.org/10.1016/S0165-6147(00)01676-X. URL: http://www.sciencedirect.com/science/article/pii/S016561470001676X.

[86] Napoleone Ferrara. "VEGF and the quest for tumour angiogenesis factors". In: *Nature Reviews Cancer* 2 (Oct. 2002). Perspective, 795 EP -. URL: https://doi.org/10.1038/nrc909.

[87] Gregg L. Semenza. "Targeting HIF-1 for cancer therapy". In: *Nature Reviews Cancer* 3 (Oct. 2003). Review Article, 721 EP -. URL: https://doi.org/10.1038/nrc1187.

[88] L. Qiang et al. "HIF-1a is critical for hypoxia-mediated maintenance of glioblastoma stem cells by activating Notch signaling pathway". In: *Cell Death And Differentiation* 19 (Aug. 2011). Original Paper, 284 EP -. URL: https://doi.org/10.1038/cdd.2011.95.

[89] Tim F Cloughesy et al. "Antitumor Activity of Rapamycin in a Phase I Trial for Patients with Recurrent PTEN-Deficient Glioblastoma". In: *PLOS Medicine* 5.1 (Jan. 2008), pp. 1–13. DOI: 10.1371/journal.pmed.0050008. URL: https://doi.org/10.1371/journal.pmed.0050008.

[90] Jeffrey A Engelman and Jeffrey Settleman. "Acquired resistance to tyrosine kinase inhibitors during cancer therapy". In: *Current Opinion in Genetics Development* 18.1 (2008). Genetic and cellular mechanisms of oncogenesis, pp. 73–79. ISSN: 0959-437X. DOI: https://doi.org/10.1016/j.gde.2008.01.004. URL: http://www.sciencedirect.com/science/article/pii/S0959437X08000087.

[91] Jill Wykosky et al. "Escape from targeted inhibition: The dark side of kinase inhibitor therapy". In: *Cell Cycle* 9.9 (2010). PMID: 20404502, pp. 1661–1662. DOI: 10.4161/cc.9.9.11592. eprint: https://doi.org/10.4161/cc.9.9.11592. URL: https://doi.org/10.4161/cc.9.9.11592.

[92] Jeffrey A. Engelman and Pasi A. Jänne. "Mechanisms of Acquired Resistance to Epidermal Growth Factor Receptor Tyrosine Kinase Inhibitors in Non–Small Cell Lung Cancer". In: *Clinical Cancer Research* 14.10 (2008), pp. 2895–2899. ISSN: 1078-0432. DOI: 10.1158/1078-0432.CCR-07-2248. eprint: http://clincancerres.aacrjournals.org/content/14/10/2895.full.pdf. URL: http://clincancerres.aacrjournals.org/content/14/10/2895.

[93] Olivier Keunen et al. "Anti-VEGF treatment reduces blood supply and increases tumor cell invasion in glioblastoma". In: *Proceedings of the National Academy of Sciences* 108.9 (2011), pp. 3749–3754. ISSN: 0027-8424. DOI: 10.1073/pnas.1014480108. eprint: https://www.pnas.org/content/108/9/3749.full.pdf. URL: https://www.pnas.org/content/108/9/3749.

[94] Susan M. Chang et al. "Phase II study of CCI-779 in patients with recurrent glioblastoma multiforme". In: *Investigational New Drugs* 23.4 (Aug. 2005), pp. 357–361. ISSN: 1573-0646. DOI: 10.1007/s10637-005-1444-0. URL: https://doi.org/10.1007/s10637-005-1444-0.

[95] Cecilie Jonsgar Sandberg et al. "Comparison of glioma stem cells to neural stem cells from the adult human brain identifies dysregulated Wnt- signaling and a fingerprint associated with clinical outcome". In: *Experimental Cell Research* 319.14 (2013), pp. 2230–2243. ISSN: 0014-4827. DOI: https://doi.org/10.1016/j.yexcr.2013.06.004. URL: http://www.sciencedirect.com/science/article/pii/S0014482713002553.

[96] L. DΓ*AntonaEtal*.. "SI113, a Specific Inhibitor of the Sgk1 Kinase Activity that Counteracts Cancer Cell Proliferation". In: *Cellular Physiology and Biochemistry* 35.5 (2015), pp. 2006–2018. ISSN: 1015-8987. DOI: 10.1159/000374008. URL: https://www.karger.com/DOI/10.1159/000374008.

[97] Florian Lang, Nicola Perrotti, and Christos Stournaras. "Colorectal carcinoma cells,ÄîRegulation of survival and growth by SGK1". In: *The International Journal of Biochemistry Cell Biology* 42.10 (2010), pp. 1571–1575. ISSN: 1357-2725. DOI: https://doi.org/10.1016/j.biocel.2010.05.016. URL: http://www.sciencedirect.com/science/article/pii/S1357272510001974.

[98] Gary L Firestone, Jennifer R Giampaolo, and Bridget A O'Keeffe. "Stimulus-Dependent Regulation of Serum and Glucocorticoid Inducible Protein Kinase (SGK) Transcription, Subcellular Localization and Enzymatic Activity". In: *Cellular physiology and biochemistry : international journal of experimental cellular physiology, biochemistry, and pharmacology* 13 (Feb. 2003), pp. 1–12. DOI: 10.1159/000070244.

[99] M K Webster, L Goya, and G L Firestone. "Immediate-early transcriptional regulation and rapid mRNA turnover of a putative serine/threonine protein kinase." In: *Journal of Biological Chemistry* 268.16 (1993), pp. 11482–11485. eprint: http://www.jbc.org/content/268/16/11482.full.pdf+html. URL: http://www.jbc.org/content/268/16/11482.abstract.

[100] M. K. Webster et al. "Characterization of sgk, a novel member of the serine/threonine protein kinase gene family which is transcriptionally induced by glucocorticoids and serum". In: *Mol Cell Biol* 13.4 (Apr. 1993). PMC359524[pmcid], pp. 2031–2040. ISSN: 0270-7306. URL: https://www.ncbi.nlm.nih.gov/pubmed/8455596.

[101] John W. Funder et al. "The Serum- and Glucocorticoid-Induced Kinase Is a Physiological Mediator of Aldosterone Action*". In: *Endocrinology* 142.4 (Apr. 2001), pp. 1587–1594. ISSN: 0013-7227. DOI: 10.1210/endo.142.4.8095. eprint: http://oup.prod.sis.lan/endo/article-pdf/142/4/1587/10364685/endo1587.pdf. URL: https://doi.org/10.1210/endo.142.4.8095.

[102] Johannes Loffing et al. "Aldosterone induces rapid apical translocation of ENaC in early portion of renal collecting system: possible role of SGK". In: *American Journal of Physiology-Renal Physiology* 280.4 (2001). PMID: 11249859, F675–F682. DOI: 10.1152/ajprenal.2001.280.4.F675. eprint: https://doi.org/10.1152/ajprenal.2001.280.4.F675. URL: https://doi.org/10.1152/ajprenal.2001.280.4.F675.

[103] D.L. Healy et al. "FSH-regulated gene expression profiles in ovarian tumours and normal ovaries". In: *MHR: Basic science of reproductive medicine* 8.5 (May 2002), pp. 426–433. ISSN: 1360-9947. DOI: 10.1093/molehr/8.5.426. eprint: http://oup.prod.sis.lan/molehr/article-pdf/8/5/426/9894677/080426.pdf. URL: https://dx.doi.org/10.1093/molehr/8.5.426.

[104] JoAnne S. Richards. "New Signaling Pathways for Hormones and Cyclic Adenosine 3,5-Monophosphate Action in Endocrine Cells". In: *Molecular Endocrinology* 15.2 (Feb. 2001), pp. 209–218. ISSN: 0888-8809. DOI: 10.1210/mend.15.2.0606. eprint: http://oup.prod.sis.lan/mend/article-pdf/15/2/209/8948821/mend0209.pdf. URL: https://doi.org/10.1210/mend.15.2.0606.

[105] JEFFREY W. CLEMENS et al. "Ovarian Cell Differentiation: A Cascade of Multiple Hormones, Cellular Signals, and Regulated Genes". In: *Proceedings of the 1993 Laurentian Hormone Conference*. Ed. by C. WAYNE BARDIN. Vol. 50. Recent Progress in Hormone Research. Boston: Academic Press, 1995, pp. 223–254. ISBN: 978-0-12-571150-0. DOI: https://doi.org/10.1016/B978-0-12-571150-0.50014-7. URL: http://www.sciencedirect.com/science/article/pii/B9780125711500500147.

[106] Siegfried Waldegger et al. "Cloning and characterization of a putative human serine/threonine protein kinase transcriptionally modified during anisotonic and isotonic alterations of cell volume". In: *Proceedings of the National Academy of Sciences* 94.9 (1997), pp. 4440–4445. ISSN: 0027-8424. DOI: 10.1073/pnas.94.9.4440. eprint: https://www.pnas.org/content/94/9/4440.full.pdf. URL: https://www.pnas.org/content/94/9/4440.

[107] Meredith L. L. Leong et al. "Expression of the Serum- and Glucocorticoid-inducible Protein Kinase, Sgk, Is a Cell Survival Response to Multiple Types of Environmental Stress Stimuli in Mammary Epithelial Cells". In: *Journal of Biological Chemistry* 278.8 (2003), pp. 5871–5882. DOI: 10.1074/jbc.M211649200. eprint: http://www.jbc.org/content/278/8/5871.full.pdf+html. URL: http://www.jbc.org/content/278/8/5871.abstract.

[108] Zhiyuan Tang et al. "Serum and glucocorticoid-regulated kinase 1 (SGK1) is a predictor of poor prognosis in non-small cell lung cancer, and its dynamic pattern following treatment with SGK1 inhibitor and -ray irradiation was elucidated". English. In: *Oncology reports* 39.3 (2018). Copyright - Copyright Spandidos Publications UK Ltd. 2018; Last updated - 2018-02-07, p. 1505. URL: https://search.proquest.com/docview/1994734538?accountid=39517.

[109] Judith G. Alamares-Sapuay et al. "Serum- and glucocorticoid-regulated kinase 1 is required for nuclear export of the ribonucleoprotein of influenza A virus". In: *Journal of virology* 87.10 (May 2013). JVI.01258-12[PII], pp. 6020–6026. ISSN: 1098-5514. DOI: 10.1128/JVI.01258-12. URL: https://www.ncbi.nlm.nih.gov/pubmed/23487453.

[110] Yayoi Nishida et al. "Alteration of serum/glucocorticoid regulated kinase-1 (sgk-1) gene expression in rat hippocampus after transient global ischemia". In: *Molecular Brain Research* 123.1 (2004), pp. 121–125. ISSN: 0169-328X. DOI: https://doi.org/10.1016/j.molbrainres.2004.01.008. URL: http://www.sciencedirect.com/science/article/pii/S0169328X04000385.

[111] José M. Arencibia et al. "AGC protein kinases: From structural mechanism of regulation to allosteric drug development for the treatment of human diseases". In: *Biochimica et Biophysica Acta (BBA) - Proteins and Proteomics* 1834.7 (2013). Inhibitors of Protein Kinases, pp. 1302–1321. ISSN: 1570-9639. DOI: https://doi.org/10.1016/j.bbapap.2013.03.010. URL: http://www.sciencedirect.com/science/article/pii/S1570963913001234.

[112] Laura R. Pearce, David Komander, and Dario R. Alessi. "The nuts and bolts of AGC protein kinases". In: *Nature Reviews Molecular Cell Biology* 11 (Jan. 2010). Review Article, 9 EP -. URL: https://doi.org/10.1038/nrm2822.

[113] Juan M. Garcıa-Martınez and Dario R. Alessi. “mTOR complex 2 (mTORC2) controls hydrophobic motif phosphorylation and activation of serum- and glucocorticoid-induced protein kinase 1 (SGK1)”. In: *Biochemical Journal* 416.3 (2008), pp. 375–385. ISSN: 0264-6021. DOI: 10.1042/BJ20081668. eprint: http://www.biochemj.org/content/416/3/375.full.pdf. URL: http://www.biochemj.org/content/416/3/375.

[114] T. Kobayashi and P. Cohen. “Activation of serum- and glucocorticoid-regulated protein kinase by agonists that activate phosphatidylinositide 3-kinase is mediated by 3-phosphoinositide-dependent protein kinase-1 (PDK1) and PDK2”. In: *Biochem J* 339 (Pt 2).Pt 2 (Apr. 1999). PMC1220160[pmcid], pp. 319–328. ISSN: 0264-6021. URL: https://www.ncbi.nlm.nih.gov/pubmed/10191262.

[115] Jongsun Park et al. “Serum and glucocorticoid-inducible kinase (SGK) is a target of the PI 3-kinase-stimulated signaling pathway”. In: *The EMBO Journal* 18.11 (1999), pp. 3024–3033. ISSN: 0261-4189. DOI: 10.1093/emboj/18.11.3024. eprint: http://emboj.embopress.org/content/18/11/3024.full.pdf. URL: http://emboj.embopress.org/content/18/11/3024.

[116] Ming Lu et al. “mTOR Complex-2 Activates ENaC by Phosphorylating SGK1”. In: *Journal of the American Society of Nephrology* 21.5 (2010), pp. 811–818. ISSN: 1046-6673. DOI: 10.1681/ASN.2009111168. eprint: https://jasn.asnjournals.org/content/21/5/811.full.pdf. URL: https://jasn.asnjournals.org/content/21/5/811.

[117] Florian Lang et al. “Significance of SGK1 in the regulation of neuronal function”. In: *The Journal of Physiology* 588.18 (2010), pp. 3349–3354. DOI: 10.1113/jphysiol.2010.190926. eprint: https://physoc.onlinelibrary.wiley.com/doi/pdf/10.1113/jphysiol.2010.190926. URL: https://physoc.onlinelibrary.wiley.com/doi/abs/10.1113/jphysiol.2010.190926.

[118] Antonio Di Cristofano. “Chapter Two - SGK1: The Dark Side of PI3K Signaling”. In: *Protein Kinases in Development and Disease*. Ed. by Andreas Jenny. Vol. 123. Current Topics in Developmental Biology. Academic Press, 2017, pp. 49–71. DOI: https://doi.org/10.1016/bs.ctdb.2016.11.006. URL: http://www.sciencedirect.com/science/article/pii/S0070215316301922.

[119] Antonio Di Cristofano. “Chapter Two - SGK1: The Dark Side of PI3K Signaling”. In: *Protein Kinases in Development and Disease*. Ed. by Andreas Jenny. Vol. 123. Current Topics in Developmental Biology. Academic Press, 2017, pp. 49–71. DOI: https://doi.org/10.1016/bs.ctdb.2016.11.006. URL: http://www.sciencedirect.com/science/article/pii/S0070215316301922.

[120] Emily B. Heikamp et al. “The AGC kinase SGK1 regulates TH1 and TH2 differentiation downstream of the mTORC2 complex”. In: *Nature Immunology* 15 (Apr. 2014). Article, 457 EP -. URL: https://doi.org/10.1038/ni.2867.

[121] Elham Zarrinpashneh et al. “Ablation of SGK1 Impairs Endothelial Cell Migration and Tube Formation Leading to Decreased Neo-Angiogenesis Following Myocardial Infarction”. In: *PLOS ONE* 8.11 (Nov. 2013). DOI: 10.1371/journal.pone.0080268. URL: https://doi.org/10.1371/journal.pone.0080268.

[122] Eva Andres-Mateos et al. “Activation of serum/glucocorticoid-induced kinase 1 (SGK1) is important to maintain skeletal muscle homeostasis and prevent atrophy”. In: *EMBO Molecular Medicine* 5.1 (2013), pp. 80–91. ISSN: 1757-4676. DOI: 10.1002/emmm.201201443. eprint: http://embomolmed.embopress.org/content/5/1/80.full.pdf. URL: http://embomolmed.embopress.org/content/5/1/80.

[123] Hao Liu et al. “Hepatic serum- and glucocorticoid-regulated protein kinase 1 (SGK1) regulates insulin sensitivity in mice via extracellular-signal-regulated kinase 1/2 (ERK1/2)”. In: *Biochemical Journal* 464.2 (2014), pp. 281–289. ISSN: 0264-6021. DOI: 10.1042/BJ20141005. eprint: http://www.biochemj.org/content/464/2/281.full.pdf. URL: http://www.biochemj.org/content/464/2/281.

[124] Florian Grahammer et al. “Intestinal function of gene-targeted mice lacking serum- and glucocorticoid-inducible kinase 1”. In: *American Journal of Physiology-Gastrointestinal and Liver Physiology* 290.6 (2006). PMID: 16410368, G1114–G1123. DOI: 10.1152/ajpgi.00231.2005.

[125] Christine G Schnackenberg et al. “Compensatory role for Sgk2 mediated sodium reabsorption during salt deprivation in Sgk1 knockout mice”. In: *The FASEB Journal* 21.5 (2007), A508–A508. DOI: 10.1096/fasebj.21.5.A508-a. eprint: https://www.fasebj.org/doi/pdf/10.1096/fasebj.21.5.A508-a. URL: https://www.fasebj.org/doi/abs/10.1096/fasebj.21.5.A508-a.

[126] Kevin T Jones et al. "Rictor/TORC2 Regulates Caenorhabditis elegans Fat Storage, Body Size, and Development through sgk-1". In: *PLOS Biology* 7.3 (Mar. 2009), pp. 1–12. DOI: 10.1371/journal.pbio.1000060. URL: https://doi.org/10.1371/journal.pbio.1000060.

[127] Alexander A. Soukas et al. "Rictor/TORC2 regulates fat metabolism, feeding, growth, and life span in Caenorhabditis elegans". In: *Genes Development* 23.4 (2009), pp. 496–511. DOI: 10.1101/gad.1775409. eprint: http://genesdev.cshlp.org/content/23/4/496.full.pdf+html. URL: http://genesdev.cshlp.org/content/23/4/496.abstract.

[128] David W. Meek and Uwe Knippschild. "Posttranslational Modification of MDM2". In: *Molecular Cancer Research* 1.14 (2003), pp. 1017–1026. ISSN: 1541-7786. eprint: http://mcr.aacrjournals.org/content/1/14/1017.full.pdf. URL: http://mcr.aacrjournals.org/content/1/14/1017.

[129] Rosario Amato et al. "Sgk1 activates MDM2-dependent p53 degradation and affects cell proliferation, survival, and differentiation". In: *Journal of Molecular Medicine* 87.12 (Sept. 2009), p. 1221. ISSN: 1432-1440. DOI: 10.1007/s00109-009-0525-5. URL: https://doi.org/10.1007/s00109-009-0525-5.

[130] Yasuyoshi Naishiro et al. "Morphological and transcriptional responses of untransformed intestinal epithelial cells to an oncogenic b-catenin protein". In: *Oncogene* 24 (Feb. 2005). Original Paper, 3141 EP -. URL: https://doi.org/10.1038/sj.onc.1208517.

[131] Hanna E. Rauhala et al. "Dual-specificity phosphatase 1 and serum/glucocorticoid-regulated kinase are downregulated in prostate cancer". In: *International Journal of Cancer* 117.5 (2005), pp. 738–745. DOI: 10.1002/ijc.21270. eprint: https://onlinelibrary.wiley.com/doi/pdf/10.1002/ijc.21270. URL: https://onlinelibrary.wiley.com/doi/abs/10.1002/ijc.21270.

[132] Russell Z. Szmulewitz et al. "Serum/glucocorticoid-regulated kinase 1 expression in primary human prostate cancers". In: *The Prostate* 72.2 (2012), pp. 157–164. DOI: 10.1002/pros.21416. eprint: https://onlinelibrary.wiley.com/doi/pdf/10.1002/pros.21416. URL: https://onlinelibrary.wiley.com/doi/abs/10.1002/pros.21416.

[133] Eun Jung Chung et al. "Gene expression profile analysis in human hepatocellular carcinoma by cDNA microarray". In: *Molecules and cells* 14 (Jan. 2003), pp. 382–7.

[134] Eeva M. Sommer et al. "Elevated SGK1 predicts resistance of breast cancer cells to Akt inhibitors". In: *Biochemical Journal* 452.3 (2013), pp. 499–508. ISSN: 0264-6021. DOI: 10.1042/BJ20130342. eprint: http://www.biochemj.org/content/452/3/499.full.pdf. URL: http://www.biochemj.org/content/452/3/499.

[135] Claudia Abbruzzese et al. "Determination of SGK1 mRNA in non-small cell lung cancer samples underlines high expression in squamous cell carcinomas". In: *Journal of Experimental & Clinical Cancer Research* 31.1 (Jan. 2012), p. 4. ISSN: 1756-9966. DOI: 10.1186/1756-9966-31-4. URL: https://doi.org/10.1186/1756-9966-31-4.

[136] Cristina Talarico et al. "SI113, a SGK1 inhibitor, potentiates the effects of radiotherapy, modulates the response to oxidative stress and induces cytotoxic autophagy in human glioblastoma multiforme cells". In: *Oncotarget* 7.13 (Feb. 2016). 7520[PII], pp. 15868–15884. ISSN: 1949-2553. URL: https://www.ncbi.nlm.nih.gov/pubmed/26908461.

[137] Domenico Conza et al. "The SGK1 inhibitor SI113 induces autophagy, apoptosis, and endoplasmic reticulum stress in endometrial cancer cells". In: *Journal of Cellular Physiology* 232.12 (2017), pp. 3735–3743. DOI: 10.1002/jcp.25850. eprint: https://onlinelibrary.wiley.com/doi/pdf/10.1002/jcp.25850. URL: https://onlinelibrary.wiley.com/doi/abs/10.1002/jcp.25850.

[138] Nicola Perrotti et al. "SI113, a Specific Inhibitor of the Sgk1 Kinase Activity that Counteracts Cancer Cell Proliferation". In: *Cellular Physiology and Biochemistry* 35 (Mar. 2015), pp. 2006–2018. DOI: 10.1159/000374008.

[139] Guilai Liu et al. "Inhibition of SGK1 enhances mAR-induced apoptosis in MCF-7 breast cancer cells". In: *Cancer Biol Ther* 16.1 (Nov. 2014). PMC4622018[pmcid], pp. 52–59. ISSN: 1555-8576. DOI: 10.4161/15384047.2014.986982. URL: https://www.ncbi.nlm.nih.gov/pubmed/25427201.

[140] Shreya Kulkarni et al. "A Large-scale RNAi Screen Identifies SGK1 as a Key Survival Kinase for GBM Stem Cells". In: *Molecular Cancer Research* (2017). ISSN: 1541-7786. DOI: 10.1158/1541-7786.MCR-17-0146. eprint: http://mcr.aacrjournals.org/content/early/2017/10/07/1541-7786.MCR-17-0146.full.pdf. URL: http://mcr.aacrjournals.org/content/early/2017/10/07/1541-7786.MCR-17-0146.

[141] Bodo Schoenebeck et al. "Sgk1, a cell survival response in neurodegenerative diseases". In: *Molecular and Cellular Neuroscience* 30.2 (2005), pp. 249–264. ISSN: 1044-7431. DOI: https://doi.org/10.1016/j.mcn.2005.07.017. URL: http://www.sciencedirect.com/science/article/pii/S1044743105001727.

[142] Nader Chalhoub and Suzanne J. Baker. "PTEN and the PI3-Kinase Pathway in Cancer". In: *Annual Review of Pathology: Mechanisms of Disease* 4.1 (2009). PMID: 18767981, pp. 127–150. DOI: 10.1146/annurev.pathol.4.110807.092311. eprint: https://doi.org/10.1146/annurev.pathol.4.110807.092311. URL: https://doi.org/10.1146/annurev.pathol.4.110807.092311.

[143] Jamie N. Anastas and Randall T. Moon. "WNT signalling pathways as therapeutic targets in cancer". In: *Nature Reviews Cancer* 13 (Dec. 2012). Review Article, 11 EP -. URL: https://doi.org/10.1038/nrc3419.

[144] Yuko Komiya and Raymond Habas. "Wnt signal transduction pathways". In: *Organogenesis* 4.2 (2008). PMC2634250[pmcid], pp. 68–75. ISSN: 1547-6278. URL: https://www.ncbi.nlm.nih.gov/pubmed/19279717.

[145] Karl Willert and Roel Nusse. "Wnt Proteins". In: *Cold Spring Harbor Perspectives in Biology* 4.9 (2012). DOI: 10.1101/cshperspect.a007864. eprint: http://cshperspectives.cshlp.org/content/4/9/a007864.full.pdf+html. URL: http://cshperspectives.cshlp.org/content/4/9/a007864.abstract.

[146] Hyun Woo Park et al. "Alternative Wnt Signaling Activates YAP/TAZ". In: *Cell* 162.4 (2015), pp. 780–794. ISSN: 0092-8674. DOI: https://doi.org/10.1016/j.cell.2015.07.013. URL: http://www.sciencedirect.com/science/article/pii/S0092867415008508.

[147] Tannishtha Reya and Hans Clevers. "Wnt signalling in stem cells and cancer". In: *Nature* 434.7035 (2005), pp. 843–850. ISSN: 1476-4687. DOI: 10.1038/nature03319. URL: https://doi.org/10.1038/nature03319.

[148] Masaru Katoh. "Canonical and non-canonical WNT signaling in cancer stem cells and their niches: Cellular heterogeneity, omics reprogramming, targeted therapy and tumor plasticity (Review)". In: *International journal of oncology* 51.5 (Sept. 2017). PMC5642388[pmcid], pp. 1357–1369. ISSN: 1791-2423. DOI: 10.3892/ijo.2017.4129. URL: https://www.ncbi.nlm.nih.gov/pubmed/29048660.

[149] Paul Polakis. "Wnt signaling and cancer". In: *Genes Development* 14.15 (2000), pp. 1837–1851. DOI: 10.1101/gad.14.15.1837. eprint: http://genesdev.cshlp.org/content/14/15/1837.full.pdf+html. URL: http://genesdev.cshlp.org/content/14/15/1837.short.

[150] Nick Barker and Hans Clevers. "Mining the Wnt pathway for cancer therapeutics". In: *Nature Reviews Drug Discovery* 5 (Dec. 2006). Review Article, 997 EP -. URL: https://doi.org/10.1038/nrd2154.

[151] Tilman Borggrefe et al. "The Notch intracellular domain integrates signals from Wnt, Hedgehog, TGF/BMP and hypoxia pathways". In: *Biochimica et Biophysica Acta (BBA) - Molecular Cell Research* 1863.2 (2016), pp. 303–313. ISSN: 0167-4889. DOI: https://doi.org/10.1016/j.bbamcr.2015.11.020. URL: http://www.sciencedirect.com/science/article/pii/S0167488915004048.

[152] Giovanna M. Collu, Ana Hidalgo-Sastre, and Keith Brennan. "Wnt-Notch signalling crosstalk in development and disease". In: *Cellular and Molecular Life Sciences* 71.18 (Sept. 2014), pp. 3553–3567. ISSN: 1420-9071. DOI: 10.1007/s00018-014-1644-x. URL: https://doi.org/10.1007/s00018-014-1644-x.

[153] Indranil Paul et al. "Current Understanding on EGFR and Wnt/-Catenin Signaling in Glioma and Their Possible Crosstalk". In: *Genes & Cancer* 4.11-12 (2013). PMID: 24386505, pp. 427–446. DOI: 10.1177/1947601913503341. eprint: https://doi.org/10.1177/1947601913503341. URL: https://doi.org/10.1177/1947601913503341.

[154] Jane D Holland et al. "Wnt signaling in stem and cancer stem cells". In: *Current Opinion in Cell Biology* 25.2 (2013). Cell regulation, pp. 254–264. ISSN: 0955-0674. DOI: https://doi.org/10.1016/j.ceb.2013.01.004. URL: http://www.sciencedirect.com/science/article/pii/S0955067413000057.

[155] Jin-A Kim et al. "Identification of a Stroma-Mediated Wnt/-Catenin Signal Promoting Self-Renewal of Hematopoietic Stem Cells in the Stem Cell Niche". In: *STEM CELLS* 27.6 (2009), pp. 1318–1329. DOI: 10.1002/stem.52. eprint: https://stemcellsjournals.onlinelibrary.wiley.com/doi/pdf/10.1002/stem.52. URL: https://stemcellsjournals.onlinelibrary.wiley.com/doi/abs/10.1002/stem.52.

[156] Kirsten Strømme Kierulf-Vieira et al. "Wnt inhibition is dysregulated in gliomas and its re-establishment inhibits proliferation and tumor sphere formation". In: *Experimental Cell Research* 340.1 (2016), pp. 53–61. ISSN: 0014-4827. DOI: https://doi.org/10.1016/j.yexcr.2015.12.010. URL: http://www.sciencedirect.com/science/article/pii/S0014482715301786.

[157] Toby Phesse, Dustin Flanagan, and Elizabeth Vincan. "Frizzled7: A Promising Achilles' Heel for Targeting the Wnt Receptor Complex to Treat Cancer". In: *Cancers* 8.5 (May 2016). PMC4880867[pmcid], p. 50. ISSN: 2072-6694. DOI: 10.3390/cancers8050050. URL: https://www.ncbi.nlm.nih.gov/pubmed/27196929.

[158] Steve E. Jones and Catherine Jomary. "Secreted Frizzled-related proteins: searching for relationships and patterns". In: *BioEssays* 24.9 (2002), pp. 811–820. DOI: 10.1002/bies.10136. eprint: https://onlinelibrary.wiley.com/doi/pdf/10.1002/bies.10136. URL: https://onlinelibrary.wiley.com/doi/abs/10.1002/bies.10136.

[159] Jen-Chih Hsieh et al. "A new secreted protein that binds to Wnt proteins and inhibits their activites". In: *Nature* 398.6726 (1999), pp. 431–436. ISSN: 1476-4687. DOI: 10.1038/18899. URL: https://doi.org/10.1038/18899.

[160] Shih-Min A. Huang et al. "Tankyrase inhibition stabilizes axin and antagonizes Wnt signalling". In: *Nature* 461 (Sept. 2009). Article, 614 EP -. URL: https://doi.org/10.1038/nature08356.

[161] Jun Liu et al. "Targeting Wnt-driven cancer through the inhibition of Porcupine by LGK974". In: *Proceedings of the National Academy of Sciences* 110.50 (2013), pp. 20224–20229. ISSN: 0027-8424. DOI: 10.1073/pnas.1314239110. eprint: https://www.pnas.org/content/110/50/20224.full.pdf. URL: https://www.pnas.org/content/110/50/20224.

[162] Naoko Takebe et al. "Targeting Notch, Hedgehog, and Wnt pathways in cancer stem cells: clinical update". In: *Nature Reviews Clinical Oncology* 12 (Apr. 2015). Review Article, 445 EP -. URL: https://doi.org/10.1038/nrclinonc.2015.61.

[163] Kamal Ahmed et al. "A Second WNT for Old Drugs: Drug Repositioning against WNT-Dependent Cancers". In: *Cancers* 8.7 (July 2016). PMC4963808[pmcid], p. 66. ISSN: 2072-6694. DOI: 10.3390/cancers8070066. URL: https://www.ncbi.nlm.nih.gov/pubmed/27429001.

[164] Phuong N. Le, Jessica D. McDermott, and Antonio Jimeno. "Targeting the Wnt pathway in human cancers: therapeutic targeting with a focus on OMP-54F28". In: *Pharmacology & therapeutics* 146 (Feb. 2015). S0163-7258(14)00162-4[PII], pp. 1–11. ISSN: 1879-016X. DOI: 10.1016/j.pharmthera.2014.08.005. URL: https://www.ncbi.nlm.nih.gov/pubmed/25172549.

[165] David C. Smith et al. "First-in-human evaluation of the human monoclonal antibody vantictumab (OMP-18R5; anti-Frizzled) targeting the WNT pathway in a phase I study for patients with advanced solid tumors." In: *Journal of Clinical Oncology* 31.15_suppl (2013), pp. 2540–2540. DOI: 10.1200/jco.2013.31.15$_$suppl.2540. eprint: https://ascopubs.org/doi/pdf/10.1200/jco.2013.31.15_suppl.2540. URL: https://ascopubs.org/doi/abs/10.1200/jco.2013.31.15_suppl.2540.

[166] Steven R. Goldring and Mary B. Goldring. "Eating bone or adding it: the Wnt pathway decides". In: *Nature Medicine* 13.2 (2007), pp. 133–134. ISSN: 1546-170X. DOI: 10.1038/nm0207-133. URL: https://doi.org/10.1038/nm0207-133.

[167] Rumela Chakrabarti et al. "DNp63 promotes stem cell activity in mammary gland development and basal-like breast cancer by enhancing Fzd7 expression and Wnt signalling". In: *Nature cell biology* 16.10 (Oct. 2014). ncb3040[PII], pp. 1004–13. ISSN: 1476-4679. DOI: 10.1038/ncb3040. URL: https://www.ncbi.nlm.nih.gov/pubmed/25241036.

[168] Vasudeva Bhat et al. "Notch-Induced Expression of FZD7 Requires Noncanonical NOTCH3 Signaling in Human Breast Epithelial Cells". In: *Stem Cells and Development* 25.7 (2016). PMID: 26847503, pp. 522–529. DOI: 10.1089/scd.2015.0315. eprint: https://doi.org/10.1089/scd.2015.0315. URL: https://doi.org/10.1089/scd.2015.0315.

[169] Elizabeth Vincan et al. "Variable FZD7 expression in colorectal cancers indicates regulation by the tumour microenvironment". In: *Developmental Dynamics* 239.1 (2010), pp. 311–317. DOI: 10.1002/dvdy.22045. eprint: https://onlinelibrary.wiley.com/doi/pdf/10.1002/dvdy.22045. URL: https://onlinelibrary.wiley.com/doi/abs/10.1002/dvdy.22045.

[170] Araceli Medina, Wolfgang Reintsch, and Herbert Steinbeisser. "Xenopus frizzled 7 can act in canonical and non-canonical Wnt signaling pathways: implications on early patterning and morphogenesis". In: *Mechanisms of Development* 92.2 (2000), pp. 227–237. ISSN: 0925-4773. DOI: https://doi.org/10.1016/S0925-4773(00)00240-9. URL: http://www.sciencedirect.com/science/article/pii/S0925477300002409.

[171] Xia Qiu et al. "Overexpression of FZD7 promotes glioma cell proliferation by upregulating TAZ". In: *Oncotarget* 7.52 (Dec. 2016). 13292[PII], pp. 85987–85999. ISSN: 1949-2553. URL: https://www.ncbi.nlm.nih.gov/pubmed/27852064.

[172] Ophir Shalem, Neville E. Sanjana, and Feng Zhang. "High-throughput functional genomics using CRISPR-Cas9". In: *Nature Reviews Genetics* 16 (Apr. 2015). Review Article, 299 EP -. URL: https://doi.org/10.1038/nrg3899.

[173] Bruce. Alberts et al. *Molecular Biology of the Cell. Sixth Edition*. Garland Science, 2008, p. 1094.

[174] Francisco J. M. Mojica and Lluis Montoliu. "On the Origin of CRISPR-Cas Technology: From Prokaryotes to Mammals". In: *Trends in Microbiology* 24.10 (Oct. 2016), pp. 811–820. ISSN: 0966-842X. DOI: 10.1016/j.tim.2016.06.005. URL: https://doi.org/10.1016/j.tim.2016.06.005.

[175] Fatima Smih et al. "Double-strand breaks at the target locus stimulate gene targeting in embryonic stem cells". In: *Nucleic Acids Research* 23.24 (Jan. 1995), pp. 5012–5019. ISSN: 0305-1048. DOI: 10.1093/nar/23.24.5012. eprint: http://oup.prod.sis.lan/nar/article-pdf/23/24/5012/7123418/23-24-5012.pdf. URL: https://dx.doi.org/10.1093/nar/23.24.5012.

[176] Thomas Gaj, Charles A. Gersbach, and Carlos F. Barbas. "ZFN, TALEN, and CRISPR/Cas-based methods for genome engineering". In: *Trends in Biotechnology* 31.7 (2013), pp. 397–405. ISSN: 0167-7799. DOI: https://doi.org/10.1016/j.tibtech.2013.04.004. URL: http://www.sciencedirect.com/science/article/pii/S0167779913000875.

[177] J. Keith Joung and Jeffry D. Sander. "TALENs: a widely applicable technology for targeted genome editing". In: *Nature Reviews Molecular Cell Biology* 14 (Nov. 2012). Perspective, 49 EP -. URL: https://doi.org/10.1038/nrm3486.

[178] Fyodor D. Urnov et al. "Genome editing with engineered zinc finger nucleases". In: *Nature Reviews Genetics* 11 (Sept. 2010). Review Article, 636 EP -. URL: https://doi.org/10.1038/nrg2842.

[179] Luciano A. Marraffini. "CRISPR-Cas immunity in prokaryotes". In: *Nature* 526 (Oct. 2015). Review Article, 55 EP -. URL: https://doi.org/10.1038/nature15386.

[180] Le Cong et al. "Multiplex Genome Engineering Using CRISPR/Cas Systems". In: *Science* 339.6121 (2013), pp. 819–823. ISSN: 0036-8075. DOI: 10.1126/science.1231143. eprint: http://science.sciencemag.org/content/339/6121/819.full.pdf. URL: http://science.sciencemag.org/content/339/6121/819.

[181] Philippe Horvath and Rodolphe Barrangou. "CRISPR/Cas, the Immune System of Bacteria and Archaea". In: *Science* 327.5962 (2010), pp. 167–170. ISSN: 0036-8075. DOI: 10.1126/science.1179555. eprint: http://science.sciencemag.org/content/327/5962/167.full.pdf. URL: http://science.sciencemag.org/content/327/5962/167.

[182] Bo Hu et al. "Structural remodeling of bacteriophage T4 and host membranes during infection initiation". In: *Proceedings of the National Academy of Sciences* 112.35 (2015), E4919–E4928. ISSN: 0027-8424. DOI: 10.1073/pnas.1501064112. eprint: https://www.pnas.org/content/112/35/E4919.full.pdf. URL: https://www.pnas.org/content/112/35/E4919.

[183] Francisco J. M. Mojica et al. "Intervening Sequences of Regularly Spaced Prokaryotic Repeats Derive from Foreign Genetic Elements". In: *Journal of Molecular Evolution* 60.2 (2005), pp. 174–182. ISSN: 1432-1432. DOI: 10.1007/s00239-004-0046-3. URL: https://doi.org/10.1007/s00239-004-0046-3.

[184] Francisco J. M. Mojica et al. "Biological significance of a family of regularly spaced repeats in the genomes of Archaea, Bacteria and mitochondria". In: *Molecular Microbiology* 36.1 (2000), pp. 244–246. DOI: 10.1046/j.1365-2958.2000.01838.x. eprint: https://onlinelibrary.wiley.com/doi/pdf/10.1046/j.1365-2958.2000.01838.x. URL: https://onlinelibrary.wiley.com/doi/abs/10.1046/j.1365-2958.2000.01838.x.

[185] Ruud. Jansen et al. "Identification of genes that are associated with DNA repeats in prokaryotes". In: *Molecular Microbiology* 43.6 (2002), pp. 1565–1575. DOI: 10.1046/j.1365-2958.2002.02839.x. eprint: https://onlinelibrary.wiley.com/doi/pdf/10.1046/j.1365-2958.2002.02839.x. URL: https://onlinelibrary.wiley.com/doi/abs/10.1046/j.1365-2958.2002.02839.x.

[186] James K. Nuñez et al. "Cas1-Cas2 complex formation mediates spacer acquisition during CRISPR-Cas adaptive immunity". In: *Nature Structural &Amp; Molecular Biology* 21 (May 2014). Article, 528 EP -. URL: https://doi.org/10.1038/nsmb.2820.

[187] Robert Heler et al. "Cas9 specifies functional viral targets during CRISPR-Cas adaptation". In: *Nature* 519 (Feb. 2015). Article, 199 EP -. URL: https://doi.org/10.1038/nature14245.

[188] Asaf Levy et al. "CRISPR adaptation biases explain preference for acquisition of foreign DNA". In: *Nature* 520 (Apr. 2015). Article, 505 EP -. URL: https://doi.org/10.1038/nature14302.

[189] Zihni Arslan et al. "Detection and characterization of spacer integration intermediates in type I-E CRISPR–Cas system". In: *Nucleic Acids Research* 42.12 (June 2014), pp. 7884–7893. ISSN: 0305-1048. DOI: 10.1093/nar/gku510. eprint: http://oup.prod.sis.lan/nar/article-pdf/42/12/7884/3907028/gku510.pdf. URL: https://dx.doi.org/10.1093/nar/gku510.

[190] James K. Nuñez et al. "Integrase-mediated spacer acquisition during CRISPR-Cas adaptive immunity". In: *Nature* 519 (Feb. 2015). Article, 193 EP -. URL: https://doi.org/10.1038/nature14237.

[191] Reidun K. Lillestøl et al. "CRISPR families of the crenarchaeal genus Sulfolobus: bidirectional transcription and dynamic properties". In: *Molecular Microbiology* 72.1 (2009), pp. 259–272. DOI: 10.1111/j.1365-2958.2009.06641.x. eprint: https://onlinelibrary.wiley.com/doi/pdf/10.1111/j.1365-2958.2009.06641.x. URL: https://onlinelibrary.wiley.com/doi/abs/10.1111/j.1365-2958.2009.06641.x.

[192] Gang Liang et al. "Selection of highly efficient sgRNAs for CRISPR/Cas9-based plant genome editing". In: *Scientific Reports* 6 (Feb. 2016). Article, 21451 EP -. URL: https://doi.org/10.1038/srep21451.

[193] Elitza Deltcheva et al. "CRISPR RNA maturation by trans-encoded small RNA and host factor RNase III". In: *Nature* 471 (Mar. 2011). Article, 602 EP -. URL: https://doi.org/10.1038/nature09886.

[194] "Guide RNA Functional Modules Direct Cas9 Activity and Orthogonality". In: *Molecular Cell* 56.2 (2014), pp. 333–339. ISSN: 1097-2765. DOI: https://doi.org/10.1016/j.molcel.2014.09.019. URL: http://www.sciencedirect.com/science/article/pii/S1097276514007515.

[195] Hisato Hirano et al. "Structure and Engineering of Francisella novicida Cas9". In: *Cell* 164.5 (2016), pp. 950–961. ISSN: 0092-8674. DOI: https://doi.org/10.1016/j.cell.2016.01.039. URL: http://www.sciencedirect.com/science/article/pii/S0092867416300538.

[196] F. Ann Ran et al. "In vivo genome editing using Staphylococcus aureus Cas9". In: *Nature* 520 (Apr. 2015). Article, 186 EP -. URL: https://doi.org/10.1038/nature14299.

[197] Rimantas Sapranauskas et al. "The Streptococcus thermophilus CRISPR/Cas system provides immunity in Escherichia coli". In: *Nucleic Acids Research* 39.21 (Aug. 2011), pp. 9275–9282. ISSN: 0305-1048. DOI: 10.1093/nar/gkr606. eprint: http://oup.prod.sis.lan/nar/article-pdf/39/21/9275/16778730/gkr606.pdf. URL: https://doi.org/10.1093/nar/gkr606.

[198] Zhonggang Hou et al. "Efficient genome engineering in human pluripotent stem cells using Cas9 from Neisseria meningitidis". In: *Proceedings of the National Academy of Sciences* 110.39 (2013), pp. 15644–15649. ISSN: 0027-8424. DOI: 10.1073/pnas.1313587110. eprint: https://www.pnas.org/content/110/39/15644.full.pdf. URL: https://www.pnas.org/content/110/39/15644.

[199] Kevin M. Esvelt et al. "Orthogonal Cas9 proteins for RNA-guided gene regulation and editing". In: *Nature Methods* 10 (Sept. 2013). Article, 1116 EP -. URL: https://doi.org/10.1038/nmeth.2681.

[200] Guocai Zhong et al. "Cpf1 proteins excise CRISPR RNAs from mRNA transcripts in mammalian cells". In: *Nature Chemical Biology* 13 (June 2017), 839 EP -. URL: https://doi.org/10.1038/nchembio.2410.

[201] Ekaterina Semenova et al. "Interference by clustered regularly interspaced short palindromic repeat (CRISPR) RNA is governed by a seed sequence". In: *Proceedings of the National Academy of Sciences* 108.25 (2011), pp. 10098–10103. ISSN: 0027-8424. DOI: 10.1073/pnas.1104144108. eprint: https://www.pnas.org/content/108/25/10098.full.pdf. URL: https://www.pnas.org/content/108/25/10098.

[202] Caryn R. Hale et al. "RNA-guided RNA cleavage by a CRISPR RNA-Cas protein complex". In: *Cell* 139.5 (Nov. 2009). S0092-8674(09)00977-5[PII], pp. 945–956. ISSN: 1097-4172. DOI: 10.1016/j.cell.2009.07.040. URL: https://www.ncbi.nlm.nih.gov/pubmed/19945378.

[203] Martin Jinek et al. "A Programmable Dual-RNA–Guided DNA Endonuclease in Adaptive Bacterial Immunity". In: *Science* 337.6096 (2012), pp. 816–821. ISSN: 0036-8075. DOI: 10.1126/science.1225829. eprint: http://science.sciencemag.org/content/337/6096/816.full.pdf. URL: http://science.sciencemag.org/content/337/6096/816.

[204] Addison V. Wright et al. "Rational design of a split-Cas9 enzyme complex". In: *Proc Natl Acad Sci U S A* 112.10 (Mar. 2015). 1501698112[PII], pp. 2984–2989. ISSN: 1091-6490. DOI: 10.1073/pnas.1501698112. URL: https://www.ncbi.nlm.nih.gov/pubmed/25713377.

[205] Vladimir Mekler et al. "Kinetics of the CRISPR-Cas9 effector complex assembly and the role of 3'-terminal segment of guide RNA". In: *Nucleic Acids Res* 44.6 (Apr. 2016). gkw138[PII], pp. 2837–2845. ISSN: 1362-4962. DOI: 10.1093/nar/gkw138. URL: https://www.ncbi.nlm.nih.gov/pubmed/26945042.

[206] Carolin Anders et al. "Structural basis of PAM-dependent target DNA recognition by the Cas9 endonuclease". In: *Nature* 513 (July 2014), 569 EP -. URL: https://doi.org/10.1038/nature13579.

[207] Hiroshi Nishimasu et al. "Crystal structure of Cas9 in complex with guide RNA and target DNA". In: *Cell* 156.5 (Feb. 2014). S0092-8674(14)00156-1[PII], pp. 935–949. ISSN: 1097-4172. DOI: 10.1016/j.cell.2014.02.001. URL: https://www.ncbi.nlm.nih.gov/pubmed/24529477.

[208] Janice S. Chen et al. "Enhanced proofreading governs CRISPR-Cas9 targeting accuracy". In: *Nature* 550 (Sept. 2017), 407 EP -. URL: https://doi.org/10.1038/nature24268.

[209] Prashant Mali et al. "RNA-Guided Human Genome Engineering via Cas9". In: *Science* 339.6121 (2013), pp. 823–826. ISSN: 0036-8075. DOI: 10.1126/science.1232033. eprint: http://science.sciencemag.org/content/339/6121/823.full.pdf. URL: http://science.sciencemag.org/content/339/6121/823.

[210] Woong Y. Hwang et al. "Efficient genome editing in zebrafish using a CRISPR-Cas system". In: *Nature Biotechnology* 31 (Jan. 2013), 227 EP -. URL: https://doi.org/10.1038/nbt.2501.

[211] Giedrius Gasiunas et al. "Cas9–crRNA ribonucleoprotein complex mediates specific DNA cleavage for adaptive immunity in bacteria". In: *Proceedings of the National Academy of Sciences* 109.39 (2012), E2579–E2586. ISSN: 0027-8424. DOI: 10.1073/pnas.1208507109. eprint: https://www.pnas.org/content/109/39/E2579.full.pdf. URL: https://www.pnas.org/content/109/39/E2579.

[212] Rimantas Sapranauskas et al. "The Streptococcus thermophilus CRISPR/Cas system provides immunity in Escherichia coli". In: *Nucleic Acids Research* 39.21 (Aug. 2011), pp. 9275–9282. ISSN: 0305-1048. DOI: 10.1093/nar/gkr606. eprint: http://oup.prod.sis.lan/nar/article-pdf/39/21/9275/16778730/gkr606.pdf. URL: https://dx.doi.org/10.1093/nar/gkr606.

[213] Alfonso H. Magadán et al. "Cleavage of Phage DNA by the Streptococcus thermophilus CRISPR3-Cas System". In: *PLOS ONE* 7.7 (July 2012), pp. 1–8. DOI: 10.1371/journal.pone.0040913. URL: https://doi.org/10.1371/journal.pone.0040913.

[214] Martin Jinek et al. "RNA-programmed genome editing in human cells". In: *eLife* 2 (Jan. 2013). Ed. by Detlef Weigel, e00471. ISSN: 2050-084X. DOI: 10.7554/eLife.00471. URL: https://doi.org/10.7554/eLife.00471.

[215] Vinod Ranganathan et al. "Expansion of the CRISPR-Cas9 genome targeting space through the use of H1 promoter-expressed guide RNAs". In: *Nature communications* 5 (Aug. 2014). ncomms5516[PII], pp. 4516–4516. ISSN: 2041-1723. DOI: 10.1038/ncomms5516. URL: https://www.ncbi.nlm.nih.gov/pubmed/25105359.

[216] Jeffry D. Sander and J. Keith Joung. "CRISPR-Cas systems for editing, regulating and targeting genomes". In: *Nature Biotechnology* 32 (Mar. 2014), 347 EP -. URL: https://doi.org/10.1038/nbt.2842.

[217] Tin Tin Su. "Cellular Responses to DNA Damage: One Signal, Multiple Choices". In: *Annual Review of Genetics* 40.1 (2006). PMID: 16805666, pp. 187–208. DOI: 10.1146/annurev.genet.40.110405.090428. eprint: https://doi.org/10.1146/annurev.genet.40.110405.090428. URL: https://doi.org/10.1146/annurev.genet.40.110405.090428.

[218] Sandeep Burma, Benjamin P.C. Chen, and David J. Chen. "Role of non-homologous end joining (NHEJ) in maintaining genomic integrity". In: *DNA Repair* 5.9 (2006). Mechanisms of chromosomal translocation, pp. 1042–1048. ISSN: 1568-7864. DOI: https://doi.org/10.1016/j.dnarep.2006.05.026. URL: http://www.sciencedirect.com/science/article/pii/S1568786406001650.

[219] Howard H. Y. Chang et al. "Non-homologous DNA end joining and alternative pathways to double-strand break repair". In: *Nature Reviews Molecular Cell Biology* 18 (May 2017). Review Article, 495 EP -. URL: https://doi.org/10.1038/nrm.2017.48.

[220] Rositsa Dueva and George Iliakis. "Alternative pathways of non-homologous end joining (NHEJ) in genomic instability and cancer". In: *Translational Cancer Research* 2.3 (2013). ISSN: 2219-6803. URL: http://tcr.amegroups.com/article/view/1152.

[221] Anthony J. Davis and David J. Chen. "DNA double strand break repair via non-homologous end-joining". In: *Transl Cancer Res* 2.3 (June 2013). PMC3758668[pmcid], pp. 130–143. ISSN: 2218-676X. DOI: 10.3978/j.issn.2218-676X.2013.04.02. URL: https://www.ncbi.nlm.nih.gov/pubmed/24000320.

[222] Nianhan Ma et al. "Yeast Mre11 and Rad1 proteins define a Ku-independent mechanism to repair double-strand breaks lacking overlapping end sequences." In: *Molecular and Cellular Biology* 23 (Jan. 2003), pp. 8820–8828. DOI: 10.1128/MCB.23.23.8820828.2003.

[223] Mitch McVey and Sang Eun Lee. "MMEJ repair of double-strand breaks (director,Äôs cut): deleted sequences and alternative endings". In: *Trends in Genetics* 24.11 (2008), pp. 529–538. ISSN: 0168-9525. DOI: https://doi.org/10.1016/j.tig.2008.08.007. URL: http://www.sciencedirect.com/science/article/pii/S0168952508002291.

[224] Anabelle Decottignies. "Alternative end-joining mechanisms: a historical perspective". In: *Frontiers in Genetics* 4 (2013), p. 48. ISSN: 1664-8021. DOI: 10.3389/fgene.2013.00048. URL: https://www.frontiersin.org/article/10.3389/fgene.2013.00048.

[225] Amy Marie Yu and Mitch McVey. "Synthesis-dependent microhomology-mediated end joining accounts for multiple types of repair junctions". In: *Nucleic Acids Res* 38.17 (Sept. 2010). gkq379[PII], pp. 5706–5717. ISSN: 1362-4962. DOI: 10.1093/nar/gkq379. URL: https://www.ncbi.nlm.nih.gov/pubmed/20460465.

[226] Chengming Zhu et al. "Unrepaired DNA Breaks in p53-Deficient Cells Lead to Oncogenic Gene Amplification Subsequent to Translocations". In: *Cell* 109.7 (2002), pp. 811–821. ISSN: 0092-8674. DOI: https://doi.org/10.1016/S0092-8674(02)00770-5. URL: http://www.sciencedirect.com/science/article/pii/S0092867402007705.

[227] Deniz Simsek and Maria Jasin. "Alternative end-joining is suppressed by the canonical NHEJ component Xrcc4-ligase IV during chromosomal translocation formation". In: *Nat Struct Mol Biol* 17.4 (Apr. 2010). nsmb.1773[PII], pp. 410–416. ISSN: 1545-9985. DOI: 10.1038/nsmb.1773. URL: https://www.ncbi.nlm.nih.gov/pubmed/20208544.

[228] Emma Bolderson et al. "Recent Advances in Cancer Therapy Targeting Proteins Involved in DNA Double-Strand Break Repair". In: *Clinical cancer research : an official journal of the American Association for Cancer Research* 15 (Oct. 2009), pp. 6314–20. DOI: 10.1158/1078-0432.CCR-09-0096.

[229] Fuguo Jiang and Jennifer A Doudna. "CRISPR-Cas9 Structures and Mechanisms". In: *Annual review of biophysics* 46 (Mar. 2017). DOI: 10.1146/annurev-biophys-062215-010822.

[230] Andrey L. Karamyshev and Zemfira N. Karamysheva. "Lost in Translation: Ribosome-Associated mRNA and Protein Quality Controls". In: *Frontiers in Genetics* 9 (2018), p. 431. ISSN: 1664-8021. DOI: 10.3389/fgene.2018.00431. URL: https://www.frontiersin.org/article/10.3389/fgene.2018.00431.

[231] Christopher J. Shoemaker and Rachel Green. "Translation drives mRNA quality control". In: *Nature Structural &Amp; Molecular Biology* 19 (June 2012). Perspective, 594 EP -. URL: https://doi.org/10.1038/nsmb.2301.

[232] Marco Antonio Valencia-Sanchez et al. "Control of translation and mRNA degradation by miRNAs and siRNAs". In: *Genes Development* 20.5 (2006), pp. 515–524. DOI: 10.1101/gad.1399806. eprint: http://genesdev.cshlp.org/content/20/5/515.full.pdf+html. URL: http://genesdev.cshlp.org/content/20/5/515.abstract.

[233] Almog Bregman et al. "Promoter Elements Regulate Cytoplasmic mRNA Decay". In: *Cell* 147.7 (2011), pp. 1473–1483. ISSN: 0092-8674. DOI: https://doi.org/10.1016/j.cell.2011.12.005. URL: http://www.sciencedirect.com/science/article/pii/S0092867411015030.

[234] Michael R. Culbertson. "RNA surveillance: unforeseen consequences for gene expression, inherited genetic disorders and cancer". In: *Trends in Genetics* 15.2 (1999), pp. 74–80. ISSN: 0168-9525. DOI: https://doi.org/10.1016/S0168-9525(98)01658-8. URL: http://www.sciencedirect.com/science/article/pii/S0168952598016588.

[235] Yumi Yamaguchi-Kabata et al. "Distribution and Effects of Nonsense Polymorphisms in Human Genes". In: *PLOS ONE* 3.10 (Oct. 2008), pp. 1–8. DOI: 10.1371/journal.pone.0003393. URL: https://doi.org/10.1371/journal.pone.0003393.

[236] Areum Han, Woo-Yeon Kim, and Seong-Min Park. "SNP2NMD: A database of human single nucleotide polymorphisms causing nonsense-mediated mRNA decay". In: *Bioinformatics* 23.3 (Nov. 2006), pp. 397–399. ISSN: 1367-4803. DOI: 10.1093/bioinformatics/btl593. eprint: http://oup.prod.sis.lan/bioinformatics/article-pdf/23/3/397/644073/btl593.pdf. URL: https://doi.org/10.1093/bioinformatics/btl593.

[237] Sevtap Savas, Sukru Tuzmen, and Hilmi Ozcelik. "Human SNPs resulting in premature stop codons and protein truncation". In: *Human Genomics* 2.5 (Mar. 2006), p. 274. DOI: 10.1186/1479-7364-2-5-274. URL: https://doi.org/10.1186/1479-7364-2-5-274.

[238] Lene Clausen et al. "Chapter Two - Protein stability and degradation in health and disease". In: *Molecular Chaperones in Human Disorders*. Ed. by Rossen Donev. Vol. 114. Advances in Protein Chemistry and Structural Biology. Academic Press, 2019, pp. 61–83. DOI: https://doi.org/10.1016/bs.apcsb.2018.09.002. URL: http://www.sciencedirect.com/science/article/pii/S1876162318300580.

[239] Alfred L. Goldberg. "Protein degradation and protection against misfolded or damaged proteins". In: *Nature* 426.6968 (2003), pp. 895–899. ISSN: 1476-4687. DOI: 10.1038/nature02263. URL: https://doi.org/10.1038/nature02263.

[240] Bernd Bukau, Jonathan Weissman, and Arthur Horwich. "Molecular Chaperones and Protein Quality Control". In: *Cell* 125.3 (May 2006), pp. 443–451. ISSN: 0092-8674. DOI: 10.1016/j.cell.2006.04.014. URL: https://doi.org/10.1016/j.cell.2006.04.014.

[241] Gozde Kar et al. "Human proteome-scale structural modeling of E2-E3 interactions exploiting interface motifs". In: *Journal of proteome research* 11.2 (Feb. 2012). PMC3285560[pmcid], pp. 1196–1207. ISSN: 1535-3907. DOI: 10.1021/pr2009143. URL: https://www.ncbi.nlm.nih.gov/pubmed/22149024.

[242] Viduth K. Chaugule and Helen Walden. "Specificity and disease in the ubiquitin system". In: *Biochemical Society transactions* 44.1 (Feb. 2016). BST20150209[PII], pp. 212–227. ISSN: 1470-8752. DOI: 10.1042/BST20150209. URL: https://www.ncbi.nlm.nih.gov/pubmed/26862208.

[243] Christopher A. Ross and Michelle A. Poirier. "Protein aggregation and neurodegenerative disease". In: *Nature Medicine* 10 (July 2004), S10 EP -. URL: https://doi.org/10.1038/nm1066.

[244] Guilherme A. P. de Oliveira et al. "Misfolding, Aggregation, and Disordered Segments in c-Abl and p53 in Human Cancer". In: *Frontiers in Oncology* 5 (2015), p. 97. ISSN: 2234-943X. DOI: 10.3389/fonc.2015.00097. URL: https://www.frontiersin.org/article/10.3389/fonc.2015.00097.

[245] Jerson L. Silva et al. "Expanding the prion concept to cancer biology: dominant-negative effect of aggregates of mutant p53 tumour suppressor". In: *Bioscience Reports* 33.4 (2013). ISSN: 0144-8463. DOI: 10.1042/BSR20130065. eprint: http://www.bioscirep.org/content/33/4/e00054.full.pdf. URL: http://www.bioscirep.org/content/33/4/e00054.

[246] Ana P. D. Ano Bom et al. "Mutant p53 Aggregates into Prion-like Amyloid Oligomers and Fibrils: IMPLICATIONS FOR CANCER". In: *Journal of Biological Chemistry* 287.33 (2012), pp. 28152–28162. DOI: 10.1074/jbc.M112.340638. eprint: http://www.jbc.org/content/287/33/28152.full.pdf+html. URL: http://www.jbc.org/content/287/33/28152.abstract.

[247] Y. Yang-Hartwich et al. "p53 protein aggregation promotes platinum resistance in ovarian cancer". In: *Oncogene* 34 (Sept. 2014). Original Article, 3605 EP -. URL: https://doi.org/10.1038/onc.2014.296.

[248] Einar Vik-Mo et al. "Brain tumor stem cells maintain overall phenotype and tumorigenicity after in vitro culturing in serum-free conditions [J]". In: *Neuro-oncology* 12 (Dec. 2010), pp. 1220–30. DOI: 10.1093/neuonc/noq102.

[249] Steven M. Pollard et al. “Glioma Stem Cell Lines Expanded in Adherent Culture Have Tumor-Specific Phenotypes and Are Suitable for Chemical and Genetic Screens”. In: *Cell Stem Cell* 4.6 (June 2009), pp. 568–580. ISSN: 1934-5909. DOI: 10.1016/j.stem.2009.03.014. URL: https://doi.org/10.1016/j.stem.2009.03.014.

[250] Kiera Walker and Anita Hjelmeland. “Method for Efficient Transduction of Cancer Stem Cells”. In: *J Cancer Stem Cell Res* 2 (2014). e1008[PII], e1008. ISSN: 2329-5872. URL: https://www.ncbi.nlm.nih.gov/pubmed/27547779.

[251] Ashley T. Haase. “Pathogenesis of lentivirus infections”. In: *Nature* 322.6075 (1986), pp. 130–136. ISSN: 1476-4687. DOI: 10.1038/322130a0. URL: https://doi.org/10.1038/322130a0.

[252] Howard E. Davis, Jeffrey R. Morgan, and Martin L. Yarmush. “Polybrene increases retrovirus gene transfer efficiency by enhancing receptor-independent virus adsorption on target cell membranes”. In: *Biophysical Chemistry* 97.2 (2002), pp. 159–172. ISSN: 0301-4622. DOI: https://doi.org/10.1016/S0301-4622(02)00057-1. URL: http://www.sciencedirect.com/science/article/pii/S0301462202000571.

[253] Robert E. Farrell. “Chapter 18 - RT-PCR: A Science and an Art Form”. In: *RNA Methodologies (Fourth Edition)*. Ed. by Robert E. Farrell. Fourth Edition. San Diego: Academic Press, 2010, pp. 385–448. ISBN: 978-0-12-374727-3. DOI: https://doi.org/10.1016/B978-0-12-374727-3.00018-8. URL: http://www.sciencedirect.com/science/article/pii/B9780123747273000188.

[254] Tahrin Mahmood and Ping-Chang Yang. “Western blot: technique, theory, and trouble shooting”. In: *N Am J Med Sci* 4.9 (Sept. 2012). NAJMS-4-429[PII], pp. 429–434. ISSN: 1947-2714. DOI: 10.4103/1947-2714.100998. URL: https://www.ncbi.nlm.nih.gov/pubmed/23050259.

[255] Dominic A. Scudiero et al. “Evaluation of a Soluble Tetrazolium/Formazan Assay for Cell Growth and Drug Sensitivity in Culture Using Human and Other Tumor Cell Lines”. In: *Cancer Research* 48.17 (1988), pp. 4827–4833. ISSN: 0008-5472. eprint: http://cancerres.aacrjournals.org/content/48/17/4827.full.pdf. URL: http://cancerres.aacrjournals.org/content/48/17/4827.

[256] Jessica C. Mar. “The rise of the distributions: why non-normality is important for understanding the transcriptome and beyond”. In: *Biophysical Reviews* 11.1 (Feb. 2019), pp. 89–94. ISSN: 1867-2469. DOI: 10.1007/s12551-018-0494-4. URL: https://doi.org/10.1007/s12551-018-0494-4.

[257] Evie McCrum-Gardner. “Which is the correct statistical test to use?” In: *British Journal of Oral and Maxillofacial Surgery* 46.1 (2008), pp. 38–41. ISSN: 0266-4356. DOI: https://doi.org/10.1016/j.bjoms.2007.09.002. URL: http://www.sciencedirect.com/science/article/pii/S0266435607004378.

[258] Yvonne Chan and Roy P Walmsley. “Learning and Understanding the Kruskal-Wallis One-Way Analysis-of-Variance-by-Ranks Test for Differences Among Three or More Independent Groups”. In: *Physical Therapy* 77.12 (Dec. 1997), pp. 1755–1761. ISSN: 0031-9023. DOI: 10.1093/ptj/77.12.1755. eprint: http://oup.prod.sis.lan/ptj/article-pdf/77/12/1755/10761628/ptj1755.pdf. URL: https://doi.org/10.1093/ptj/77.12.1755.

[259] Lukas E. Dow et al. “Inducible in vivo genome editing with CRISPR-Cas9”. In: *Nature Biotechnology* 33 (Feb. 2015), 390 EP -. URL: https://doi.org/10.1038/nbt.3155.

[260] Garmen Yuen et al. “CRISPR/Cas9-mediated gene knockout is insensitive to target copy number but is dependent on guide RNA potency and Cas9/sgRNA threshold expression level”. In: *Nucleic Acids Research* 45.20 (Sept. 2017), pp. 12039–12053. ISSN: 0305-1048. DOI: 10.1093/nar/gkx843. eprint: http://oup.prod.sis.lan/nar/article-pdf/45/20/12039/21743310/gkx843.pdf. URL: https://doi.org/10.1093/nar/gkx843.

[261] Morten W. Fagerland and Leiv Sandvik. “The Wilcoxon,ÄìMann,ÄìWhitney test under scrutiny”. In: *Statistics in Medicine* 28.10 (2009), pp. 1487–1497. DOI: 10.1002/sim.3561. eprint: https://onlinelibrary.wiley.com/doi/pdf/10.1002/sim.3561. URL: https://onlinelibrary.wiley.com/doi/abs/10.1002/sim.3561.

[262] Oksana Voloshanenko et al. “Mapping of Wnt-Frizzled interactions by multiplex CRISPR targeting of receptor gene families”. In: *The FASEB Journal* 31 (July 2017), fj.201700144R. DOI: 10.1096/fj.201700144R.

[263] Robert Fredriksson et al. "The G-Protein-Coupled Receptors in the Human Genome Form Five Main Families. Phylogenetic Analysis, Paralogon Groups, and Fingerprints". In: *Molecular Pharmacology* 63.6 (2003), pp. 1256–1272. ISSN: 0026-895X. DOI: 10.1124/mol.63.6.1256. eprint: http://molpharm.aspetjournals.org/content/63/6/1256.full.pdf. URL: http://molpharm.aspetjournals.org/content/63/6/1256.

[264] Hui-Chuan Huang and Peter S. Klein. "The Frizzled family: receptors for multiple signal transduction pathways". In: *Genome Biology* 5.7 (June 2004), p. 234. ISSN: 1474-760X. DOI: 10.1186/gb-2004-5-7-234. URL: https://doi.org/10.1186/gb-2004-5-7-234.

[265] Thomas Kolben et al. "Dissecting the impact of Frizzled receptors in Wnt/-catenin signaling of human mesenchymal stem cells". In: *Biological chemistry* 393 (Dec. 2012), pp. 1433–1447. DOI: 10.1515/hsz-2012-0186.

[266] Hao Zhang et al. "Expression profile and clinical significance of Wnt signaling in human gliomas". In: *Oncology Letters* 15 (Nov. 2017). DOI: 10.3892/ol.2017.7315.

[267] Ming Tan et al. "The FZD7-TWIST1 axis is responsible for anoikis resistance and tumorigenesis in ovarian carcinoma". In: *Molecular Oncology* 13 (Dec. 2018). DOI: 10.1002/1878-0261.12425.

[268] Maria C. Elias et al. "TWIST is expressed in human gliomas and promotes invasion". In: *Neoplasia (New York, N.Y.)* 7.9 (Sept. 2005). PMC1501937[pmcid], pp. 824–837. ISSN: 1522-8002. DOI: 10.1593/neo.04352. URL: https://www.ncbi.nlm.nih.gov/pubmed/16229805.

[269] Sebastian Krossa et al. "Down regulation of Akirin-2 increases chemosensitivity in human glioblastomas more efficiently than Twist-1". In: *Oncotarget* 6.25 (Apr. 2015). 3763[PII], pp. 21029–21045. ISSN: 1949-2553. URL: https://www.ncbi.nlm.nih.gov/pubmed/26036627.

[270] Svetlana A. Mikheeva et al. "TWIST1 promotes invasion through mesenchymal change in human glioblastoma". In: *Molecular cancer* 9 (July 2010). 1476-4598-9-194[PII], pp. 194–194. ISSN: 1476-4598. DOI: 10.1186/1476-4598-9-194. URL: https://www.ncbi.nlm.nih.gov/pubmed/20646316.

[271] Xinjian Liu et al. "Self-inflicted DNA double-strand breaks sustain tumorigenicity and stemness of cancer cells". In: *Cell research* 27.6 (June 2017). cr201741[PII], pp. 764–783. ISSN: 1748-7838. DOI: 10.1038/cr.2017.41. URL: https://www.ncbi.nlm.nih.gov/pubmed/28337983.

[272] Shideng Bao et al. "Glioma stem cells promote radioresistance by preferential activation of the DNA damage response". In: *Nature* 444.7120 (2006), pp. 756–760. ISSN: 1476-4687. DOI: 10.1038/nature05236. URL: https://doi.org/10.1038/nature05236.

[273] Tobias Maier, Marc Güell, and Luis Serrano. "Correlation of mRNA and protein in complex biological samples". In: *FEBS Letters* 583.24 (2009), pp. 3966–3973. DOI: 10.1016/j.febslet.2009.10.036. eprint: https://febs.onlinelibrary.wiley.com/doi/pdf/10.1016/j.febslet.2009.10.036. URL: https://febs.onlinelibrary.wiley.com/doi/abs/10.1016/j.febslet.2009.10.036.

[274] Marcus Gry et al. "Correlations between RNA and protein expression profiles in 23 human cell lines". In: *BMC Genomics* 10.1 (Aug. 2009), p. 365. ISSN: 1471-2164. DOI: 10.1186/1471-2164-10-365. URL: https://doi.org/10.1186/1471-2164-10-365.

[275] Fredrik Edfors et al. "Gene-specific correlation of RNA and protein levels in human cells and tissues". In: *Molecular Systems Biology* 12.10 (2016), p. 883. DOI: 10.15252/msb.20167144. eprint: https://www.embopress.org/doi/pdf/10.15252/msb.20167144. URL: https://www.embopress.org/doi/abs/10.15252/msb.20167144.

[276] Dov Greenbaum et al. "Comparing protein abundance and mRNA expression levels on a genomic scale". In: *Genome biology* 4.9 (2003). PMC193646[pmcid], pp. 117–117. ISSN: 1474-760X. DOI: 10.1186/gb-2003-4-9-117. URL: https://www.ncbi.nlm.nih.gov/pubmed/12952525.

[277] Maren Hertweck, Christine Göbel, and Ralf Baumeister. "C. elegans SGK-1 Is the Critical Component in the Akt/PKB Kinase Complex to Control Stress Response and Life Span". In: *Developmental Cell* 6.4 (2004), pp. 577–588. ISSN: 1534-5807. DOI: https://doi.org/10.1016/S1534-5807(04)00095-4. URL: http://www.sciencedirect.com/science/article/pii/S1534580704000954.

[278] Arne Engelsberg, Franziska Kobelt, and Dietmar Kuhl. "The N-terminus of the serum- and glucocorticoid-inducible kinase Sgk1 specifies mitochondrial localization and rapid turnover". In: *Biochemical Journal* 399.1 (2006), pp. 69–76. ISSN: 0264-6021. DOI: 10.1042/BJ20060386. eprint: http://www.biochemj.org/content/399/1/69.full.pdf. URL: http://www.biochemj.org/content/399/1/69.

[279] Deanna R. Brickley et al. "Ubiquitin Modification of Serum and Glucocorticoid-induced Protein Kinase-1 (SGK-1)". In: *Journal of Biological Chemistry* 277.45 (2002), pp. 43064–43070. DOI: 10.1074/jbc.M207604200. eprint: http://www.jbc.org/content/277/45/43064.full.pdf+html. URL: http://www.jbc.org/content/277/45/43064.abstract.

[280] Maria F. Arteaga et al. "A brain-specific SGK1 splice isoform regulates expression of ASIC1 in neurons". In: *Proceedings of the National Academy of Sciences* 105.11 (2008), pp. 4459–4464. ISSN: 0027-8424. DOI: 10.1073/pnas.0800958105. eprint: https://www.pnas.org/content/105/11/4459.full.pdf. URL: https://www.pnas.org/content/105/11/4459.

[281] Perikles Simon et al. "Differential Regulation of Serum- and Glucocorticoid-Inducible Kinase 1 (SGK1) Splice Variants Based on Alternative Initiation of Transcription". In: *Cellular physiology and biochemistry : international journal of experimental cellular physiology, biochemistry, and pharmacology* 20 (Feb. 2007), pp. 715–28. DOI: 10.1159/000110432.

[282] Liang Wang et al. "Up-regulation of serum- and glucocorticoid-induced protein kinase 1 in the brain tissue of human and experimental epilepsy". In: *Neurochemistry International* 57.8 (2010), pp. 899–905. ISSN: 0197-0186. DOI: https://doi.org/10.1016/j.neuint.2010.09.009. URL: http://www.sciencedirect.com/science/article/pii/S0197018610002998.

[283] P. Sahin et al. "The cell survival kinase SGK1 and its targets FOXO3a and NDRG1 in aged human brain". In: *Neuropathology and Applied Neurobiology* 39.6 (2013), pp. 623–633. DOI: 10.1111/nan.12023. eprint: https://onlinelibrary.wiley.com/doi/pdf/10.1111/nan.12023. URL: https://onlinelibrary.wiley.com/doi/abs/10.1111/nan.12023.

[284] Nandita S. Raikwar, Peter M. Snyder, and Christie P. Thomas. "An evolutionarily conserved N-terminal Sgk1 variant with enhanced stability and improved function". In: *American Journal of Physiology-Renal Physiology* 295.5 (2008). PMID: 18753299, F1440–F1448. DOI: 10.1152/ajprenal.90239.2008. eprint: https://doi.org/10.1152/ajprenal.90239.2008. URL: https://doi.org/10.1152/ajprenal.90239.2008.

[285] Robert D. Mashal, Jason Koontz, and Jeffrey Sklar. "Detection of mutations by cleavage of DNA heteroduplexes with bacteriophage resolvases". In: *Nature Genetics* 9.2 (1995), pp. 177–183. ISSN: 1546-1718. DOI: 10.1038/ng0295-177. URL: https://doi.org/10.1038/ng0295-177.

[286] Léna Vouillot, Aurore Thélie, and Nicolas Pollet. "Comparison of T7E1 and Surveyor Mismatch Cleavage Assays to Detect Mutations Triggered by Engineered Nucleases". In: *G3: Genes, Genomes, Genetics* 5.3 (2015), pp. 407–415. DOI: 10.1534/g3.114.015834. eprint: https://www.g3journal.org/content/5/3/407.full.pdf. URL: https://www.g3journal.org/content/5/3/407.

[287] Takanori Tsuji and Yo Niida. "Development of a simple and highly sensitive mutation screening system by enzyme mismatch cleavage with optimized conditions for standard laboratories". In: *ELECTROPHORESIS* 29.7 (2008), pp. 1473–1483. DOI: 10.1002/elps.200700729. eprint: https://onlinelibrary.wiley.com/doi/pdf/10.1002/elps.200700729. URL: https://onlinelibrary.wiley.com/doi/abs/10.1002/elps.200700729.

[288] E-Pien Tan et al. "Off-target assessment of CRISPR-Cas9 guiding RNAs in human iPS and mouse ES cells". In: *genesis* 53.2 (2015), pp. 225–236. DOI: 10.1002/dvg.22835. eprint: https://onlinelibrary.wiley.com/doi/pdf/10.1002/dvg.22835. URL: https://onlinelibrary.wiley.com/doi/abs/10.1002/dvg.22835.

[289] Hiroko Koike-Yusa et al. "Genome-wide recessive genetic screening in mammalian cells with a lentiviral CRISPR-guide RNA library". In: *Nature Biotechnology* 32 (Dec. 2013), 267 EP -. URL: https://doi.org/10.1038/nbt.2800.

[290] Wei Li et al. "Simultaneous generation and germline transmission of multiple gene mutations in rat using CRISPR-Cas systems". In: *Nature Biotechnology* 31 (Aug. 2013), 684 EP -. URL: https://doi.org/10.1038/nbt.2652.

[291] Monica F. Sentmanat et al. "A Survey of Validation Strategies for CRISPR-Cas9 Editing". In: *Scientific Reports* 8.1 (2018), p. 888. ISSN: 2045-2322. DOI: 10.1038/s41598-018-19441-8. URL: https://doi.org/10.1038/s41598-018-19441-8.

[292] Michael Kosicki, Kärt Tomberg, and Allan Bradley. "Repair of double-strand breaks induced by CRISPR-Cas9 leads to large deletions and complex rearrangements". In: *Nature Biotechnology* 36 (July 2018), 765 EP -. URL: https://doi.org/10.1038/nbt.4192.

[293] Matthew C. Canver et al. "Characterization of Genomic Deletion Efficiency Mediated by Clustered Regularly Interspaced Palindromic Repeats (CRISPR)/Cas9 Nuclease System in Mammalian Cells". In: *Journal of Biological Chemistry* 289.31 (2014), pp. 21312–21324. DOI: 10.1074/jbc.M114.564625. eprint: http://www.jbc.org/content/289/31/21312.full.pdf+html. URL: http://www.jbc.org/content/289/31/21312.abstract.

[294] Tim Wang et al. "Genetic screens in human cells using the CRISPR-Cas9 system". In: *Science (New York, N.Y.)* 343.6166 (Jan. 2014). science.1246981[PII], pp. 80–84. ISSN: 1095-9203. DOI: 10.1126/science.1246981. URL: https://www.ncbi.nlm.nih.gov/pubmed/24336569.

[295] John G. Doench et al. "Rational design of highly active sgRNAs for CRISPR-Cas9-mediated gene inactivation". In: *Nature Biotechnology* 32 (Sept. 2014), 1262 EP -. URL: https://doi.org/10.1038/nbt.3026.

[296] Neville E. Sanjana, Ophir Shalem, and Feng Zhang. "Improved vectors and genome-wide libraries for CRISPR screening". In: *Nature Methods* 11 (July 2014). Correspondence, 783 EP -. URL: https://doi.org/10.1038/nmeth.3047.

[297] Ayal Hendel et al. "Chemically modified guide RNAs enhance CRISPR-Cas genome editing in human primary cells". In: *Nature Biotechnology* 33 (June 2015), 985 EP -. URL: https://doi.org/10.1038/nbt.3290.

[298] Spencer C. Knight et al. "Dynamics of CRISPR-Cas9 genome interrogation in living cells". In: *Science* 350.6262 (2015), pp. 823–826. ISSN: 0036-8075. DOI: 10.1126/science.aac6572. eprint: https://science.sciencemag.org/content/350/6262/823.full.pdf. URL: https://science.sciencemag.org/content/350/6262/823.

[299] Xuebing Wu et al. "Genome-wide binding of the CRISPR endonuclease Cas9 in mammalian cells". In: *Nature Biotechnology* 32 (Apr. 2014), 670 EP -. URL: https://doi.org/10.1038/nbt.2889.

[300] Patrick D. Hsu et al. "DNA targeting specificity of RNA-guided Cas9 nucleases". In: *Nature Biotechnology* 31 (July 2013), 827 EP -. URL: https://doi.org/10.1038/nbt.2647.

Appendices

A.1: PCR-primer binding sites

This chapter shows PCR-primer binding sites mapped relative to the different sgRNA target DNA sequences for both SGK1 and FZD7. The strand identity (reverse complement or complement) of the DNA sequence is also given. Forward and reverse primer is color-marked according to its sgRNA target amplification region, and the sgRNA target sequence is given in gray, positioned between its respective forward and reverse primer. The PAM site and Cas9 cute site is also given.

SGK1 (reverse complement)

4 (74)
7 (75)
10 (79)
sgRNA target
PAM-site
| Cas9 cut site

>NC_000006.12:c134318112-134169246 Homo sapiens chromosome 6, GRCh38.p12 Primary Assembly

.... (last ~700 nucleotides of the full sequence)
ATGACCTGCAGGGTTTTCAGGTGGGACAGCGGGAGAGGAGCAGGCCCCACAGAGGAATCGAGGATGCCCG
GTTCACGCCAGGTCTGCCCCCGGGCAAAGCTACCCCTCCCTTCGCTTGTTACCTCCTCACGTGTTCTTGG
CATGGCAGAGATTAAAAATGCAAGGAAAAAAATTACATGCGGAACGGACAAAATGTTCTCAGAGATTACT
TCAGAAAAAAAAAAGTGAAATGCAGATTGTACTTCTTCCTTTAGTGCAGAGACGACTTTTATTTCCGCCC
CCTCCCCTCCACATTCCTGACCTCTCCCTCCCCCTTTTCCCTCTTTCTTTCCTTCCTTCCTCCTCTTCCA
AGTTCTGGGATTTTTCAGCCTTGCTTGGTTTTGGCCAAAAGCACAAAAAAGGCGTTTTCGGAAGCGACCC
GACCGTGCACAAGGGCCATTTGTTTGTTTTGGGACTCGGGGCAGGAAATCTTGCCCGGCCTGAGTCACGG
CGGCTCCTTCAAGGAAACGTCAGTGCTCGCCGGTCGCTCTCGTCTGCCGCGCGCCCCGCCGCCCGCTGCC
CATGGGGGAGATGCAGGGCGCGCTGGCCAGAGCCCGGCTCGAGTCCCTGCTGCGGCCCCGCCACAAAAAG
AGGGCCGAGGCGCAGAAAAGGAGCGAGTCCTTCCTGCTGAGCGGACTGGGTAAGCGCCGCCGCCGGCCCC
GCTGGGGGCTTGGCTCACTTCCCCAGAGCGGCTTGGAGGCAGGGGCCGGCTTTCGTCGGAGTTCTCGGGG
CCGGGGTCCCGGCGGCGGGAACGGGAGGACCTGGCGGGCGAGGTCGCGCGCGCAGGCCTGCGCCCCAGGG
ATAAACCCCGGAGGGTGGCGCGCACCGCCGGCTCGGGTTGGGGAGGAGGGTGGGAGTCCGGCCGCAGGAC
GGCGCCTGGCCGGGGAGAGGGTATCTGCAGGGACAGTGAGCGAAGCCACCGTGGCCGCCGCGCACCCGCC
GGGAAGCGCTTCGGCGCTGCGAACCCGGCTTTCTCCGGCGGCGGAATAAATGAGAGAGGTGGAAAACTAC
CCCGGGCTCTCCGGCCCTCCCCGCGCCCTCCGCCGGCGCGTTCTCTCTCTCCTGCCCCAGGAGCCGATGG
AGACTGATAACGGCCCTGCGCCAGGCCGTCCCCGGGCGGTCCTCGCGCCCCCGCCCGGGGCTCGCCCTCT
CAATGGGGACAGAACCGCCCGCCGCAGGCAGCGTAGCCGCCAGCAAACCGCGAGGCGGCCGGGGCGGGGC
GAGGGGCGAGGCGAAGGGCGGGGCCACTTCTCACTGTCGCGCAGGCCCCGCCCCCGCGGCGGTGCCTTTT
TTATAAGGCCGAGCGCGCGGCCTGGCGCAGCATACGCCGAGCCGGTCTTTGAGCGCTAACGTCTTTCTGT
CTCCCCGCGGTGGTGATGACGGTGAAAACTGAGGCTGCTAAGGGCACCCTCACTTACTCCAGGATGAGGG
GCATGGTGGCAATTCT|CATCGGTGAGTGCAGGAATCTTGCGGGACTTCTGCTCCAGGAGACGCAAAGTGG
AAATTTTTTGAAAGTCCCGGATCAGATTAGTGTGTGTGGCGCCGGACGTTATGAAGCCGTCTAAACGTTT
CTTTATTTCTCCTCCTTCATCCACAGCTTTCATGAAGCAGAGGAGGATGGGTCTGAACGACTTTATTCAG

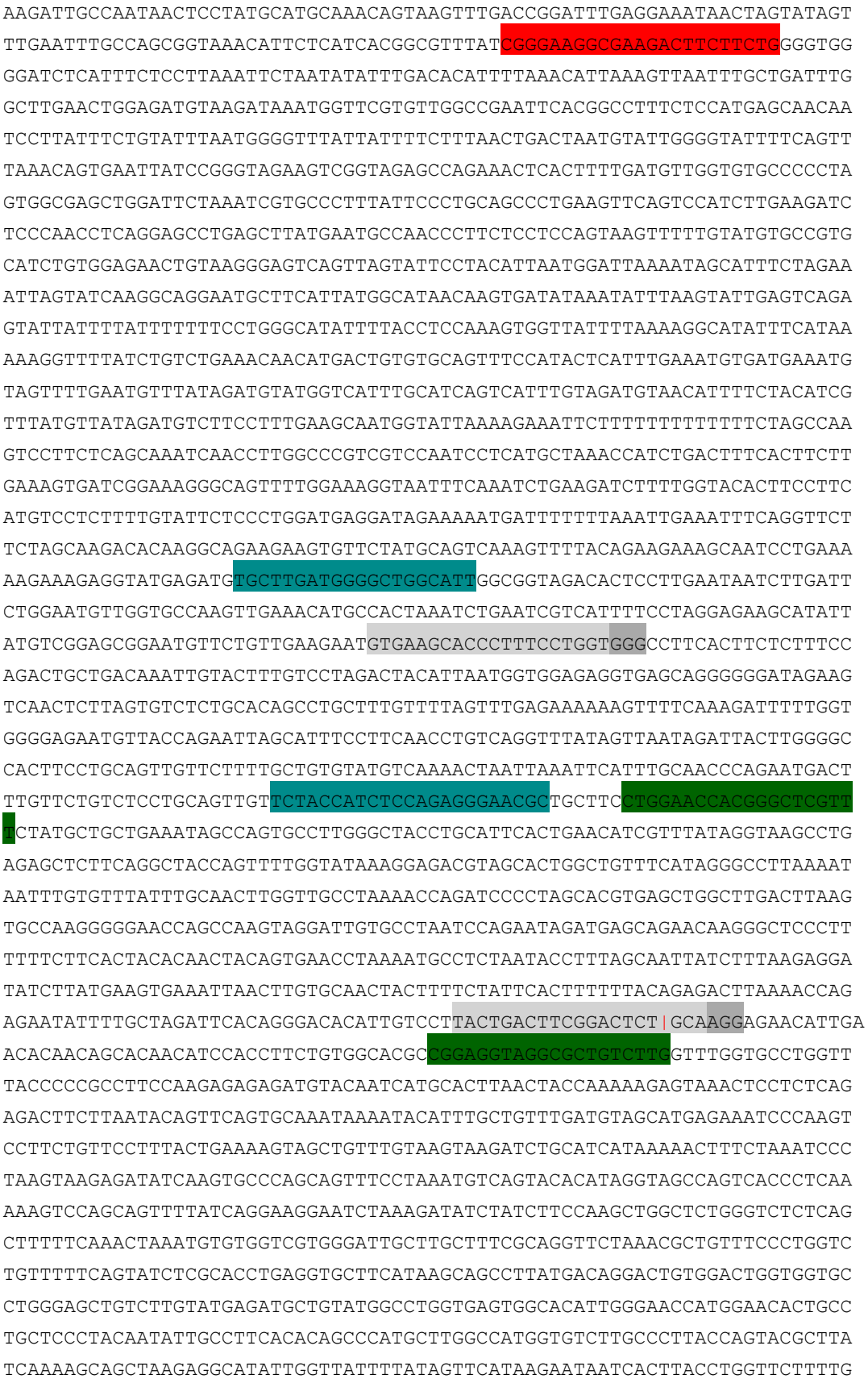
AAGATTGCCAATAACTCCTATGCATGCAAACAGTAAGTTTGACCGGATTTGAGGAAATAACTAGTATAGT
TTGAATTTGCCAGCGGTAAACATTCTCATCACGGCGTTTATCGGGAAGGCGAAGACTTCTTCTGGGGTGG
GGATCTCATTTCTCCTTAAATTCTAATATATTTGACACATTTTAAACATTAAAGTTAATTTGCTGATTTG
GCTTGAACTGGAGATGTAAGATAAATGGTTCGTGTTGGCCGAATTCACGGCCTTTCTCCATGAGCAACAA
TCCTTATTTCTGTATTTAATGGGGTTTATTATTTTCTTTAACTGACTAATGTATTGGGGTATTTTCAGTT
TAAACAGTGAATTATCCGGGTAGAAGTCGGTAGAGCCAGAAACTCACTTTTGATGTTGGTGTGCCCCCTA
GTGGCGAGCTGGATTCTAAATCGTGCCCTTTATTCCCTGCAGCCCTGAAGTTCAGTCCATCTTGAAGATC
TCCCAACCTCAGGAGCCTGAGCTTATGAATGCCAACCCTTCTCCTCCAGTAAGTTTTTGTATGTGCCGTG
CATCTGTGGAGAACTGTAAGGGAGTCAGTTAGTATTCCTACATTAATGGATTAAAATAGCATTTCTAGAA
ATTAGTATCAAGGCAGGAATGCTTCATTATGGCATAACAAGTGATATAAATATTTAAGTATTGAGTCAGA
GTATTATTTTATTTTTTTCCTGGGCATATTTTACCTCCAAAGTGGTTATTTTAAAAGGCATATTTCATAA
AAAGGTTTTATCTGTCTGAAACAACATGACTGTGTGCAGTTTCCATACTCATTTGAAATGTGATGAAATG
TAGTTTTGAATGTTTATAGATGTATGGTCATTTGCATCAGTCATTTGTAGATGTAACATTTTCTACATCG
TTTATGTTATAGATGTCTTCCTTTGAAGCAATGGTATTAAAAGAAATTCTTTTTTTTTTTTTCTAGCCAA
GTCCTTCTCAGCAAATCAACCTTGGCCCGTCGTCCAATCCTCATGCTAAACCATCTGACTTTCACTTCTT
GAAAGTGATCGGAAAGGGCAGTTTTGGAAAGGTAATTTCAAATCTGAAGATCTTTTGGTACACTTCCTTC
ATGTCCTCTTTTGTATTCTCCCTGGATGAGGATAGAAAAATGATTTTTTTAAATTGAAATTTCAGGTTCT
TCTAGCAAGACACAAGGCAGAAGAAGTGTTCTATGCAGTCAAAGTTTTACAGAAGAAAGCAATCCTGAAA
AAGAAAGAGGTATGAGATGTGCTTGATGGGGCTGGCATTGGCGGTAGACACTCCTTGAATAATCTTGATT
CTGGAATGTTGGTGCCAAGTTGAAACATGCCACTAAATCTGAATCGTCATTTTCCTAGGAGAAGCATATT
ATGTCGGAGCGGAATGTTCTGTTGAAGAATGTGAAGCACCCTTTCCTGGTGGGCCTTCACTTCTCTTTCC
AGACTGCTGACAAATTGTACTTTGTCCTAGACTACATTAATGGTGGAGAGGTGAGCAGGGGGGATAGAAG
TCAACTCTTAGTGTCTCTGCACAGCCTGCTTTGTTTTAGTTTGAGAAAAAAGTTTTCAAAGATTTTTGGT
GGGGAGAATGTTACCAGAATTAGCATTTCCTTCAACCTGTCAGGTTTATAGTTAATAGATTACTTGGGGC
CACTTCCTGCAGTTGTTCTTTTGCTGTGTATGTCAAAACTAATTAAATTCATTTGCAACCCAGAATGACT
TTGTTCTGTCTCCTGCAGTTGTTCTACCATCTCCAGAGGGAACGCTGCTTCCTGGAACCACGGGCTCGTT
TCTATGCTGCTGAAATAGCCAGTGCCTTGGGCTACCTGCATTCACTGAACATCGTTTATAGGTAAGCCTG
AGAGCTCTTCAGGCTACCAGTTTTGGTATAAAGGAGACGTAGCACTGGCTGTTTCATAGGGCCTTAAAAT
AATTTGTGTTTATTTGCAACTTGGTTGCCTAAAACCAGATCCCCTAGCACGTGAGCTGGCTTGACTTAAG
TGCCAAGGGGGAACCAGCCAAGTAGGATTGTGCCTAATCCAGAATAGATGAGCAGAACAAGGGCTCCCTT
TTTTCTTCACTACACAACTACAGTGAACCTAAAATGCCTCTAATACCTTTAGCAATTATCTTTAAGAGGA
TATCTTATGAAGTGAAATTAACTTGTGCAACTACTTTTCTATTCACTTTTTTACAGAGACTTAAAACCAG
AGAATATTTTGCTAGATTCACAGGGACACATTGTCCTTACTGACTTCGGACTCT|GCAAGGAGAACATTGA
ACACAACAGCACAACATCCACCTTCTGTGGCACGCCGGAGGTAGGCGCTGTCTTCGGTTTGGTGCCTGGTT
TACCCCCGCCTTCCAAGAGAGAGATGTACAATCATGCACTTAACTACCAAAAAGAGTAAACTCCTCTCAG
AGACTTCTTAATACAGTTCAGTGCAAATAAAATACATTTGCTGTTTGATGTAGCATGAGAAATCCCAAGT
CCTTCTGTTCCTTTACTGAAAAGTAGCTGTTTGTAAGTAAGATCTGCATCATAAAAACTTTCTAAATCCC
TAAGTAAGAGATATCAAGTGCCCAGCAGTTTCCTAAATGTCAGTACACATAGGTAGCCAGTCACCCTCAA
AAAGTCCAGCAGTTTTATCAGGAAGGAATCTAAAGATATCTATCTTCCAAGCTGGCTCTGGGTCTCTCAG
CTTTTTCAAACTAAATGTGTGGTCGTGGGATTGCTTGCTTTCGCAGGTTCTAAACGCTGTTTCCCTGGTC
TGTTTTTCAGTATCTCGCACCTGAGGTGCTTCATAAGCAGCCTTATGACAGGACTGTGGACTGGTGGTGC
CTGGGAGCTGTCTTGTATGAGATGCTGTATGGCCTGGTGAGTGGCACATTGGGAACCATGGAACACTGCC
TGCTCCCTACAATATTGCCTTCACACAGCCCATGCTTGGCCATGGTGTCTTGCCCTTACCAGTACGCTTA
TCAAAAGCAGCTAAGAGGCATATTGGTTATTTTATAGTTCATAAGAATAATCACTTACCTGGTTCTTTTG

TGCATTTCACATTTTACTAGATAGGACCACATTGAACCTGTGTGGTGGTGAAAAACTACCACTTATTAAC
ATCTACCCCCTCACCCTCCACACACACACACACAAACACACACACGGGTTGCAAAGTAGACACTTAAATA
GCAAGGGAAAAGAAAGCATTGAGGTGGGGAGAGTTTCTCAAATCGAGCCTAATATTTATTGCCGTTTATA
TCTTTTTCTCTACTGGTAATGTGTGCCATATGAAACTTCCAATTAAGTCTAAAGTAATTTTCCCCTTCTT
TCAGCCGCCTTTTTTATAGCCGAAACACAGCTGAAATGTACGACAACATTCTGAACAAGCCTCTCCAGCTG
AAACCAAATATTACAAATTCCGCAAGACACCTCCTGGAGGGCCTCCTGCAGAAGGACAGGACAAAGCGGC
TCGGGGCCAAGGATGACTTCGTGAGTGATGTTTTCCTGTCCTCCTGGGCCGGCCGGGACGTGCACTAGAC
CTCCCTGCCCTTATTGAATGCACCTGTCTAAATTAATCTTGGGTTTCTTATCAACAGATGGAGATTAAGA
GTCATGTCTTCTTCTCCTTAATTAACTGGGATGATCTCATTAATAAGAAGATTACTCCCCCTTTTAACCC
AAATGTGGTGAGTATCTGTCTCTCTTCTAAGTATAGAGAAGCCCAAAGGGCATTTATTTTAATTCAGAAT
TGTCTGGGGGAGGGTTGGAAGGAATACATTGGCAGATGTTTTCTCCATAAACCTGTTATTTTACCTACAT
AAAAAGCACATTTTTGTGTCCCAACAAGGCTCCCATAATTTTTAGACACATTTATCAATTCGAAGCACCA
AAAGGCAACAAGTGAACATTATTCTTATGTTTAACTGTGTGTAGCCTTTTGAGATTTTGTGCTTGAAGTG
GGTGATTATGGAAGTTGATATAAGACTTAAACTTGGTATTTAAAGCCTGGTCAAGATTTCCCTGTCCTGT
GTCTAGTGTGAGTTCTTGACAAGAGTGTTTTTCCCTTCCCGTCACAGAGTGGGCCCAACGACCTACGGCA
CTTTGACCCCGAGTTTACCGAAGAGCCTGTCCCCAACTCCATTGGCAAGTCCCCTGACAGCGTCCTCGTC
ACAGCCAGCGTCAAGGAAGCTGCCGAGGCTTTCCTAGGCTTTTCCTATGCGCCTCCCACGGACTCTTTCC
TCTGAACCCTGTTAGGGCTTGGTTTTAAAGGATTTTATGTGTGTTTCCGAATGTTTTAGTTAGCCTTTTG
GTGGAGCCGCCAGCTGACAGGACATCTTACAAGAGAATTTGCACATCTCTGGAAGCTTAGCAATCTTATT
GCACACTGTTCGCTGGAAGCTTTTTGAAGAGCACATTCTCCTCAGTGAGCTCATGAGGTTTTCATTTTTA
TTCTTCCTTCCAACGTGGTGCTATCTCTGAAACGAGCGTTAGAGTGCCGCCTTAGACGGAGGCAGGAGTT
TCGTTAGAAAGCGGACGCTGTTCTAAAAAAGGTCTCCTGCAGATCTGTCTGGGCTGTGATGACGAATATT
ATGAAATGTGCCTTTTCTGAAGAGATTGTGTTAGCTCCAAAGCTTTTCCTATCGCAGTGTTTCAGTTCTT
TATTTTCCCTTGTGGATATGCTGTGTGAACCGTCGTGTGAGTGTGGTATGCCTGATCACAGATGGATTTT
GTTATAAGCATCAATGTGACACTTGCAGGACACTACAACGTGGGACATTGTTTGTTTCTTCCATATTTGG
AAGATAAATTTATGTGTAGACTTTTTTGTAAGATACGGTTAATAACTAAAATTTATTGAAATGGTCTTGC
AATGACTCGTATTCAGATGCTTAAAGAAAGCATTGCTGCTACAAATATTTCTATTTTTAGAAAGGGTTTT
TATGGACCAATGCCCCAGTTGTCAGTCAGAGCCGTTGGTGTTTTTCATTGTTTAAAATGTCACCTGTAAA
ATGGGCATTATTTATGTTTTTTTTTTTGCATTCCTGATAATTGTATGTATTGTATAAAGAACGTCTGTAC
ATTGGGTTATAACACTAGTATATTTAAACTTACAGGCTTATTTGTAATGTAAACCACCATTTTAATGTAC
TGTAATTAACATGGTTATAATACGTACAATCCTTCCCTCATCCCATCACACAACTTTTTTTGTGTGTGAT
AAACTGATTTTGGTTTGCAATAAAACCTTGAAAAATATTTACATATA

FZD7 (complement)

3 (94)
6 (96)
1 (100)
sgRNA target
PAM-site
| Cas9 cut site

>NC_000002.12:202034587-202038437 Homo sapiens chromosome 2, GRCh38.p12 Primary Assembly
CTCTCCCAACCGCCTCGTCGCACTCCTCAGGCTGAGAGCACCGCTGCACTCGCGGCCGGCGATGCGGGAC
CCCGGCGCGGCCGCTCCGCTTTCGTCCCTGGGCCTCTGTGCCCTGGTGCTGGCGCTGCTGGGCGCACTGT
CCGCGGGCGCCGGGGCGCAGCCGTACCACGGAGAGAAGGGCATCTCCGTGCCGGACCACGGCTTCTGCCA
GCCCATCTCCATCCCGCTGTGCACGGACATCGCCTACAACCAGACCATCCTGCCCAACCTGCTGGGCCAC
ACGAACCAAGAGGACGCGGGCCTCGAGGTGCACCAGTTCTACCCGCTGGTGAAGGTGCAGTGTTCTCCCG
AACTCCGCTTTTTCTTATGCTCCATGTATGCGCCCGTGTGCACCGTGCTCG|ATCAGGCCATCCCGCCGTG
TCGTTCTCTGTGCGAGCGCGCCCGCCAGGGCTGCGAGGCGCTCATGAACAAGTTCGGCTTCCAGTGGCCC
GAGCGGCTGCGCTGCGAGAACTTCCCGGTGCACGGTGCGGGCGAGATCTGCGTGGGCCAGAACACGTCGG
ACGGCTCCGGGGGCCCAGGCGGCGGCCCCACTGCCTACCCTACCGCGCCCTACCTGCCGGACCTGCCCTT
CACCGCGCTGCCCCCGGGGGCCTCAGATGGCAGGGGGCGTCCCGCCTTCCCCTTCTCATGCCCCCGTCAG
CTCAAGGTGCCCCCGTACCTGGGCTACCGCTTCCTGGGTGAGCGCGATTGTGGCGCCCCGTGCGAACCGG
GCCGTGCCAACGGCCTGATGTACTTTAAGGAGGAGGAGAGGCGCTTCGCCCGCCTCTGGGTGGGCGTGTG
GTCCGTGCTGTGCTGCGCCTCGACGCTCTTTACCGTTCTCACCTACCTGGTGGACATGCGGCGCTTCAGC
TACCCAGAGCGGCCCATCATCTTCCTGTCGGGCTGCTACTTCATGGTGGCCGTGGCGCACGTGGCCGGCT
TCCTTCTAGAGGACCGCGCCGTGT|GCGTGGAGCGCTTCTCGGACGATGGCTACCGCACGGTGGCGCAGGG
CACCAAGAAGGAGGGCTGCACCATCCTCTTCATGGTGCTCTACTTCTTCGGCATGGCCAGCTCCATCTGG
TGGGTCATTCTGTCTCTCACTTGGTTCCTGGCGGCCGGCATGAAGTGGGGCCACGAGGCCATCGAGGCCA
ACTCGCAGTACTTCCACCTGGCCGCGTGGGCCGTGCCCGCCGTCAAGACCATCACTATCCTGGCCATGGG
CCAGGTAGACGGGGACCTGCTGAGCGGGGTGTGCTACGTTGGCCTCTCCAGTGTGGACGCGCTGCGGGGC
TTCGTGCTGGCGCCTCTGTTCGTCTACCTCTTCATAGGCACGTCCTTCTTGCTGGCCGGCTTCGTGTCCC
TCTTCCGTATCCGCACCATCATGAAACACGACGGCACCAAGACCGAGAAGCTGGAGAAGCTCATGGTGCG
CATCGGCGTCTTCAGCGTGCTCTACACAGTGCCCGCCACCATCGTCCTGGCCTGCTACTTCTACGAGCAG
GCCTTCCGCGAGCACTGGGAGCGCACCTGGCTCCTGCAGACGTGCAAGAGCTATGCCGTGCCCTGCCCGC
CCGGCCACTTCCCGCCCATGAGCCCCGACTTCACCGTCTTCATGATCAAGTACCTGATGACCATGAT|CGT
CGGCATCACCACTGGCTTCTGGATCTGGTCGGGCAAGACCCTGCAGTCGTGGCGCCGCTTCTACCACAGA
CTTAGCCACAGCAGCAAGGGGGAGACTGCGGTATGAGCCCCGGCCCCTCCCCACCTTTCCCACCCCAGCC
CTCTTGCAAGAGGAGAGGCACGGTAGGGAAAAGAACTGCTGGGTGGGGGCCTGTTTCTGTAACTTTCTCC
CCCTCTACTGAGAAGTGACCTGGAAGTGAGAAGTTCTTTGCAGATTTGGGGCGAGGGGTGATTTGGAAAA
GAAGACCTGGGTGGAAAGCGGTTTGGATGAAAAGATTTCAGGCAAAGACTTGCAGGAAGATGATGATAAC
GGCGATGTGAATCGTCAAAGGTACGGGCCAGCTTGTGCCTAATAGAAGGTTGAGACCAGCAGAGACTGCT
GTGAGTTTCTCCCGGCTCCGAGGCTGAACGGGGACTGTGAGCGATCCCCCTGCTGCAGGGCGAGTGGCCT
GTCCAGACCCCTGTGAGGCCCCGGGAAAGGTACAGCCCTGTCTGCGGTGGCTGCTTTGTTGGAAAGAGGG
AGGGCCTCCTGCGGTGTGCTTGTCAAGCAGTGGTCAAACCATAATCTCTTTTCACTGGGGCCAAACTGGA
GCCCAGATGGGTTAATTTCCAGGGTCAGACATTACGGTCTCTCCTCCCCTGCCCCCTCCCGCCTGTTTTT

CCTCCCGTACTGCTTTCAGGTCTTGTAAAATAAGCATTTGGAAGTCTTGGGAGGCCTGCCTGCTAGAATC
CTAATGTGAGGATGCAAAAGAAATGATGATAACATTTTGAGATAAGGCCAAGGAGACGTGGAGTAGGTAT
TTTTGCTACTTTTTCATTTTCTGGGGAAGGCAGGAGGCAGAAAGACGGGTGTTTTATTTGGTCTAATACC
CTGAAAAGAAGTGATGACTTGTTGCTTTTCAAAACAGGAATGCATTTTTCCCCTTGTCTTTGTTGTAAGA
GACAAAAGAGGAAACAAAAGTGTCTCCCTGTGGAAAGGCATAACTGTGACGAAAGCAACTTTTATAGGCA
AAGCAGCGCAAATCTGAGGTTTCCCGTTGGTTGTTAATTTGGTTGAGATAAACATTCCTTTTTAAGGAAA
AGTGAAGAGCAGTGTGCTGTCACACACCGTTAAGCCAGAGGTTCTGACTTCGCTAAAGGAAATGTAAGAG
GTTTTGTTGTCTGTTTTAAATAAATTTAATTCGGAACACATGATCCAACAGACTATGTTAAAATATTCAG
GGAAATCTCTCCCTTCATTTACTTTTTCTTGCTATAAGCCTATATTTAGGTTTCTTTTCTATTTTTTTCT
CCCATTTGGATCCTTTGAGGTAAAAAAACATAATGTCTTCAGCCTCATAATAAAGGAAAGTTAATTAAAA
AAAAAAAGCAAAGAGCCATTTTGTCCTGTTTTCTTGGTTCCATCAATCTGTTTATTAAACATCATCCATA
TGCTGACCCTGTCTCTGTGTGGTTGGGTTGGGAGGCGATCAGCAGATACCATAGTGAACGAAGAGGAAGG
TTTGAACCATGGGCCCCATCTTTAAAGAAAGTCATTAAAAGAAGGTAAACTTCAAAGTGATTCTGGAGTT
CTTTGAAATGTGCTGGAAGACTTAAATTTATTAATCTTAAATCATGTACTTTTTTTCTGTAATAGAACTC
GGATTCTTTTGCATGATGGGGTAAAGCTTAGCAGAGAATCATGGGAGCTAACCTTTATCCCACCTTTGAC
ACTACCCTCCAATCTTGCAACACTATCCTGTTTCTCAGAACAGTTTTTAAATGCCAATCATAGAGGGTAC
TGTAAAGTGTACAAGTTACTTTATATATGTAATGTTCACTTGAGTGGAACTGCTTTTTACATTAAAGTTA
AAATCGATCTTGTGTTTCTTCAACCTTCAAAACTATCTCATCTGTCAGATTTTTAAAACTCCAACACAGG
TTTTGGCATCTTTTGTGCTGTATCTTTTAAGTGCATGTGAAATTTGTAAAATAGAGATAAGTACAGTATG
TATATTTTGTAAATCTCCCATTTTTGTAAGAAAATATATATTGTATTTATACATTTTTACTTTGGATTTT
TGTTTTGTTGGCTTTAAAGGTCTACCCCACTTTATCACATGTACAGATCACAAATAAATTTTTTTAAATA
C

A.2: Transcript variants

This chapter gives insight into the transcript variants of SGK1 and FZD7. The protein size of the given transcript variant is also given.

SGK1

RefSeq mRNA sequence	RefSeq protein sequence	Protein size	Description of transcript variant
NM_005627.3	NP_005618.2	50 kDa	This variant (1) represents the predominant transcript and encodes the shortest isoform (1).
NM_001143676.1	NP_001137148.1	59 kDa	This variant (2) contains additional in-frame exons at the 5' end compared to transcript variant 1, resulting in an isoform (2) with a longer and an unique N-terminus compared to isoform 1. Isoform 2 is reported to have an increased protein half-life, and is preferentially targeted to the plasma membrane.
NM_001143677.1	NP_001137149.1	52 kDa	This variant (3) contains an alternative in-frame, 5' terminal exon compared to transcript variant 1, resulting in an isoform (3) with a longer and an unique N-terminus compared to isoform 1.
NM_001143678.1	NP_001137150.1	51 kDa	This variant (4) contains an alternative in-frame, 5' terminal exon compared to transcript variant 1, resulting in an isoform (4) with a longer and an unique N-terminus compared to isoform 1.
NM_001291995.1	NP_001278924.1	49 kDa	This variant (5) lacks an alternate in-frame exon compared to variant 1. The resulting isoform (5) has the same N- and C-termini but is shorter compared to isoform 1.

Table A.2.1: Transcript variants of SGK1. Data regarding RefSeq mRNA sequence, RefSeq protein sequence and description of transcript variant is obtained directly from NCBI https://www.ncbi.nlm.nih.gov/gene/6446 (05.07.2019). Data regarding protein size is obtained from https://www.uniprot.org/uniprot/O00141 (05.07.2019).

FZD7

RefSeq mRNA sequence	RefSeq protein sequence	Protein size	Description of transcript variant
NM_003507.1	NP_003498.1	63 kDa	This is the only transcript variant described.

Table A.2.2: FZD7 transcript variant. . Data regarding RefSeq mRNA sequence, RefSeq protein sequence and description of transcript variant is obtained directly from NCBI https://www.ncbi.nlm.nih.gov/gene/8324 (05.07.2019). Data regarding protein size is obtained from https://www.uniprot.org/uniprot/O75084 (05.07.2019).

A.3: TaqMan probe binding sites

This chapter shows TaqMan probe binding sites in the different transcript variants of SGK1 and in the transcript of FZD7. The probe binding site is also mapped according to the sgRNA target sequences. TaqMan probe binding sites in the different SGK1 transcript variants is given in Table A.3.1. Mapping of these binding sites according to SGK1 specific sgRNA target sequences is given below the Table A.3.1. TaqMan probe binding sites in the FZD7 transcript is given in Table A.3.2. Mapping of this binding site according to FZD7 specific sgRNA target sequences is given below the Table A.3.2.

Interrogated Sequence		**Translated Protein**	**Exon Boundary**	**Assay Location**	**Amplicon Length**
RefSeq	**NM_001143676.1**	**NP_001137148.1**	10-11	1672	81
	NM_001143677.1	**NP_001137149.1**	8-9	923	81
	NM_001143678.1	**NP_001137150.1**	8-9	1102	81
	NM_001291995.1	**NP_001278924.1**	7-8	746	81
	NM_005627.3	**NP_005618.2**	8-9	878	81

Table A.3.1: SGK1 TaqMan probe binding sites in the different transcript variants of SGK1. Data obtained directly from: https://www.thermofisher.com/taqman-gene-expression/product/Hs00178612_m1?CID=&ICID=&subtype= (05.07.2019).

sgRNA 74 target: red

sgRNA 75 target: green

sgRNA 79 target: yellow

TaqMan probe binding site: purple

DNA origin of transcript variant 1 (**NM_005627.3**)

```
  1 gcagcatacg ccgagccggt ctttgagcgc taacgtcttt ctgtctcccc gcggtggtga
 61 tgacggtgaa aactgaggct gctaagggca ccctcactta ctccaggatg agggggcatgg
121 tggcaattct catcgctttc atgaagcaga ggaggatggg tctgaacgac tttattcaga
181 agattgccaa taactcctat gcatgcaaac accctgaagt tcagtccatc ttgaagatct
```

```
 241 cccaacctca ggagcctgag cttatgaatg ccaacccttc tcctccacca agtccttctc
 301 agcaaatcaa ccttggcccg tcgtccaatc ctcatgctaa accatctgac tttcacttct
 361 tgaaagtgat cggaaagggc agttttggaa aggttcttct agcaagacac aaggcagaag
 421 aagtgttcta tgcagtcaaa gttttacaga agaaagcaat cctgaaaaag aaagaggaga
 481 agcatattat gtcggagcgg aatgttctgt tgaagaatgt gaagcaccct ttcctggtgg
 541 gccttcactt ctctttccag actgctgaca aattgtactt tgtcctagac tacattaatg
 601 gtggagagtt gttctaccat ctccagaggg aacgctgctt cctggaacca cgggctcgtt
 661 tctatgctgc tgaaatagcc agtgccttgg gctacctgca ttcactgaac atcgtttata
 721 gagacttaaa accagagaat attttgctag attcacaggg acacattgtc cttactgact
 781 tcggactctg caaggagaac attgaacaca acagcacaac atccaccttc tgtggcacgc
 841 cggagtatct cgcacctgag gtgcttcata agcagcctta tgacaggact gtggactggt
 901 ggtgcctggg agctgtcttg tatgagatgc tgtatggcct gccgcctttt tatagccgaa
 961 acacagctga aatgtacgac aacattctga acaagcctct ccagctgaaa ccaaatatta
1021 caaattccgc aagacacctc ctggagggcc tcctgcagaa ggacaggaca aagcggctcg
1081 gggccaagga tgacttcatg gagattaaga gtcatgtctt cttctcctta attaactggg
1141 atgatctcat taataagaag attactcccc cttttaaccc aaatgtgagt gggcccaacg
1201 acctacggca ctttgacccc gagtttaccg aagagcctgt ccccaactcc attggcaagt
1261 cccctgacag cgtcctcgtc acagccagcg tcaaggaagc tgccgaggct ttcctaggct
1321 tttcctatgc gcctcccacg gactctttcc tctgaaccct gttagggctt ggttttaaag
1381 gattttatgt gtgtttccga atgttttagt tagccttttg gtggagccgc cagctgacag
1441 gacatcttac aagagaattt gcacatctct ggaagcttag caatcttatt gcacactgtt
1501 cgctggaagc tttttgaaga gcacattctc ctcagtgagc tcatgaggtt ttcattttta
1561 ttcttccttc caacgtggtg ctatctctga aacgagcgtt agagtgccgc cttagacgga
1621 ggcaggagtt tcgttagaaa gcggacgctg ttctaaaaaa ggtctcctgc agatctgtct
1681 gggctgtgat gacgaatatt atgaaatgtg ccttttctga agagattgtg ttagctccaa
1741 agcttttcct atcgcagtgt ttcagttctt tattttccct tgtggatatg ctgtgtgaac
1801 cgtcgtgtga gtgtggtatg cctgatcaca gatggatttt gttataagca tcaatgtgac
1861 acttgcagga cactacaacg tgggacattg tttgtttctt ccatatttgg aagataaatt
1921 tatgtgtaga ctttttttgta agatacggtt aataactaaa atttattgaa atggtcttgc
1981 aatgactcgt attcagatgc ttaaagaaag cattgctgct acaaatattt ctatttttag
2041 aaagggtttt tatggaccaa tgccccagtt gtcagtcaga gccgttggtg tttttcattg
2101 tttaaaatgt cacctgtaaa atgggcatta tttatgtttt ttttttgca ttcctgataa
2161 ttgtatgtat tgtataaaga acgtctgtac attgggttat aacactagta tatttaaact
2221 tacaggctta tttgtaatgt aaaccaccat tttaatgtac tgtaattaac atggttataa
2281 tacgtacaat ccttccctca tcccatcaca caacttttt tgtgtgtgat aaactgattt
2341 tggtttgcaa taaaaccttg aaaaata
```

DNA origin of transcript variant 2 (**NM_001143676.1)**

```
1 agatattcat gaaccgttgc ttcttccagc ctcgccttct cgctccctct gcctttctgg
       61 cgctgttctc cctccctccc tctggcttct gctctttctt actccttctc tcagctgctt
      121 aactacagct cccactggaa cttgcacaat caaaaacaac tctcctctct caagccgcct
      181 ccaggagcgc atcacctgga gaagagcgac tcgctccccg cgccggccgc ggaagagcag
      241 ccaggtagct gggggcgggg aggcgtaccc ttctcccgct cggtaagagc cacagcatct
      301 ccccggagat tggccgtatc ccaccgtccg gcccccaggg tcctgcagcg gtgatgcata
      361 tgtttcggag caatgatgga aggagaaaag ccgctgtcgg tggcaactga aagtggggag
      421 aggttgctgc agtagctggt gctgcagaat gcgcgagtga agaactgagc cccgctagat
      481 tctccatccc gctcagtctt cattaactgt ctgcaggagg taaaccgggg aaacagatat
      541 gcactaacca ggcgggtgcc aacctggatc tataactgtg aattccccac ggtggaaaat
      601 ggtaaacaaa gacatgaatg gattcccagt caagaaatgc tcagccttcc aatttttaa
      661 gaagcgggta cgaaggtgga tcaagagccc aatggtcagt gtggacaagc atcagagtcc
      721 cagcctgaag tacaccggct cctccatggt gcacatccct ccaggggagc cagacttcga
      781 gtcttccttg tgtcaaacat gcctgggtga acatgctttc caaagagggg ttctccctca
      841 ggagaacgag tcatgttcat gggaaactca atctgggtgt gaagtgagag agccatgtaa
      901 tcatgccaac atcctgacca agcccgatcc aagaaccttc tggactaatg atgatccagc
      961 tttcatgaag cagaggagga tgggtctgaa cgactttatt cagaagattg ccaataactc
     1021 ctatgcatgc aaacaccctg aagttcagtc catcttgaag atctcccaac ctcaggagcc
     1081 tgagcttatg aatgccaacc cttctcctcc accaagtcct tctcagcaaa tcaaccttgg
     1141 cccgtcgtcc aatcctcatg ctaaaccatc tgactttcac ttcttgaaag tgatcggaaa
     1201 gggcagtttt ggaaaggttc ttctagcaag acacaaggca gaagaagtgt tctatgcagt
     1261 caaagtttta cagaagaaag caatcctgaa aaagaaagag gagaagcata ttatgtcgga
     1321 gcggaatgtt ctgttgaaga atgtgaagca ccctttcctg gtgggccttc acttctcttt
     1381 ccagactgct gacaaattgt actttgtcct agactacatt aatggtggag agttgttcta
     1441 ccatctccag agggaacgct gcttcctgga accacgggct cgtttctatg ctgctgaaat
     1501 agccagtgcc ttgggctacc tgcattcact gaacatcgtt tatagagact taaaaccaga
     1561 gaatattttg ctagattcac agggacacat tgtcttact gacttcggac tctgcaagga
     1621 gaacattgaa cacaacagca caacatccac cttctgtggc acgccggagt atctcgcacc
     1681 tgaggtgctt cataagcagc cttatgacag gactgtggac tggtggtgcc tgggagctgt
     1741 cttgtatgag atgctgtatg gcctgccgcc tttttatagc cgaaacacag ctgaaatgta
     1801 cgacaacatt ctgaacaagc ctctccagct gaaaccaaat attacaaatt ccgcaagaca
     1861 cctcctggag ggcctcctgc agaaggacag gacaaagcgg ctcggggcca aggatgactt
     1921 catggagatt aagagtcatg tcttcttctc cttaattaac tgggatgatc tcattaataa
     1981 gaagattact ccccctttta acccaaatgt gagtgggccc aacgacctac ggcactttga
     2041 ccccgagttt accgaagagc ctgtccccaa ctccattggc aagtcccctg acagcgtcct
     2101 cgtcacagcc agcgtcaagg aagctgccga ggctttccta ggcttttcct atgcgcctcc
     2161 cacggactct ttcctctgaa ccctgttagg gcttggtttt aaaggatttt atgtgtgttt
     2221 ccgaatgttt tagttagcct tttggtggag ccgccagctg acaggacatc ttacaagaga
     2281 atttgcacat ctctggaagc ttagcaatct tattgcacac tgttcgctgg aagcttttg
     2341 aagagcacat tctcctcagt gagctcatga ggttttcatt tttattcttc cttccaacgt
     2401 ggtgctatct ctgaaacgag cgttagagtg ccgccttaga cggaggcagg agtttcgtta
```

```
2461 gaaagcggac gctgttctaa aaaaggtctc ctgcagatct gtctgggctg tgatgacgaa
2521 tattatgaaa tgtgcctttt ctgaagagat tgtgttagct ccaaagcttt tcctatcgca
2581 gtgtttcagt tctttatttt cccttgtgga tatgctgtgt gaaccgtcgt gtgagtgtgg
2641 tatgcctgat cacagatgga ttttgttata agcatcaatg tgacacttgc aggacactac
2701 aacgtgggac attgtttgtt tcttccatat ttggaagata aatttatgtg tagacttttt
2761 tgtaagatac ggttaataac taaaatttat tgaaatggtc ttgcaatgac tcgtattcag
2821 atgcttaaag aaagcattgc tgctacaaat atttctattt ttagaaaggg tttttatgga
2881 ccaatgcccc agttgtcagt cagagccgtt ggtgtttttc attgtttaaa atgtcacctg
2941 taaaatgggc attatttatg ttttttttt tgcattcctg ataattgtat gtattgtata
3001 aagaacgtct gtacattggg ttataacact agtatattta aacttacagg cttatttgta
3061 atgtaaacca ccattttaat gtactgtaat taacatggtt ataatacgta caatccttcc
3121 ctcatcccat cacacaactt tttttgtgtg tgataaactg attttggttt gcaataaaac
3181 cttgaaaaat atttacatat aaaaaaaa
```

DNA origin of transcript variant 3 (**NM_001143677.1**)

```
1 ataacagaac agggatagcc gtctctggct cgtgctctca tgtcatctca gagttccagc
  61 ttatcagagg catgtagcag ggaggcttat tccagccata actgggctct acctccagcc
 121 tccagaagta atccccaacc tgcatatcct tgggcaaccc gaagaatgaa agaagaagct
 181 ataaaacccc ctttgaaagc tttcatgaag cagaggagga tgggtctgaa cgactttatt
 241 cagaagattg ccaataactc ctatgcatgc aaacaccctg aagttcagtc catcttgaag
 301 atctcccaac ctcaggagcc tgagcttatg aatgccaacc cttctcctcc accaagtcct
 361 tctcagcaaa tcaaccttgg cccgtcgtcc aatcctcatg ctaaaccatc tgactttcac
 421 ttcttgaaag tgatcggaaa gggcagtttt ggaaaggttc ttctagcaag acacaaggca
 481 gaagaagtgt tctatgcagt caaagtttta cagaagaaag caatcctgaa aaagaaagag
 541 gagaagcata ttatgtcgga gcggaatgtt ctgttgaaga atgtgaagca ccctttcctg
 601 gtgggccttc acttctcttt ccagactgct gacaaattgt actttgtcct agactacatt
 661 aatggtggag agttgttcta ccatctccag agggaacgct gcttcctgga accacgggct
 721 cgtttctatg ctgctgaaat agccagtgcc ttgggctacc tgcattcact gaacatcgtt
 781 tatagagact taaaaccaga gaatattttg ctagattcac agggacacat tgtcctcact
 841 gacttcggac tctgcaagga gaacattgaa cacaacagca caacatccac cttctgtggc
 901 acgccggagt atctcgcacc tgaggtgctt cataagcagc cttatgacag gactgtggac
 961 tggtggtgcc tgggagctgt cttgtatgag atgctgtatg gcctgccgcc tttttatagc
1021 cgaaacacag ctgaaatgta cgacaacatt ctgaacaagc ctctccagct gaaaccaaat
1081 attacaaatt ccgcaagaca cctcctggag ggcctcctgc agaaggacag gacaaagcgg
1141 ctcggggcca aggatgactt catggagatt aagagtcatg tcttcttctc cttaattaac
1201 tgggatgatc tcattaataa gaagattact ccccctttta acccaaatgt gagtgggccc
1261 aacgacctac ggcactttga ccccgagttt accgaagagc ctgtccccaa ctccattggc
1321 aagtcccctg acagcgtcct cgtcacagcc agcgtcaagg aagctgccga ggctttccta
1381 ggcttttcct atgcgcctcc cacggactct ttcctctgaa ccctgttagg gcttggtttt
1441 aaaggatttt atgtgtgttt ccgaatgttt tagttagcct tttggtggag ccgccagctg
1501 acaggacatc ttacaagaga atttgcacat ctctggaagc ttagcaatct tattgcacac
1561 tgttcgctgg aagctttttg aagagcacat tctcctcagt gagctcatga ggttttcatt
1621 tttattcttc cttccaacgt ggtgctatct ctgaaacgag cgttagagtg ccgccttaga
```

```
1681 cggaggcagg agtttcgtta gaaagcggac gctgttctaa aaaaggtctc ctgcagatct
1741 gtctgggctg tgatgacgaa tattatgaaa tgtgcctttt ctgaagagat tgtgttagct
1801 ccaaagcttt tcctatcgca gtgtttcagt tctttatttt cccttgtgga tatgctgtgt
1861 gaaccgtcgt gtgagtgtgg tatgcctgat cacagatgga ttttgttata agcatcaatg
1921 tgacacttgc aggacactac aacgtgggac attgtttgtt tcttccatat ttggaagata
1981 aatttatgtg tagacttttt tgtaagatac ggttaataac taaaatttat tgaaatggtc
2041 ttgcaatgac tcgtattcag atgcttaaag aaagcattgc tgctacaaat atttctattt
2101 ttagaaaggg tttttatgga ccaatgcccc agttgtcagt cagagccgtt ggtgtttttc
2161 attgtttaaa atgtcacctg taaaatgggc attatttatg ttttttttt tgcattcctg
2221 ataattgtat gtattgtata aagaacgtct gtacattggg ttataacact agtatattta
2281 aacttacagg cttatttgta atgtaaacca ccattttaat gtactgtaat taacatggtt
2341 ataatacgta caatccttcc ctcatcccat cacacaactt tttttgtgtg tgataaactg
2401 attttggttt gcaataaaac cttgaaaaat a
```

DNA origin of transcript 4 (**NM_001143678.1)**

```
1 gtcagtgctc gccggtcgct ctcgtctgcc gcgcgccccg ccgcccgctg cccatggggg
       61 agatgcaggg cgcgctggcc agagcccggc tcgagtccct gctgcggccc cgccacaaaa
      121 agagggccga ggcgcagaaa aggagcgagt ccttcctgct gagcggactg gctttcatga
      181 agcagaggag gatgggtctg aacgacttta ttcagaagat tgccaataac tcctatgcat
      241 gcaaacaccc tgaagttcag tccatcttga agatctccca acctcaggag cctgagctta
      301 tgaatgccaa cccttctcct ccaccaagtc cttctcagca aatcaacctt ggcccgtcgt
      361 ccaatcctca tgctaaacca tctgactttc acttcttgaa agtgatcgga aagggcagtt
      421 ttggaaaggt tcttctagca agacacaagg cagaagaagt gttctatgca gtcaaagttt
      481 tacagaagaa agcaatcctg aaaaagaaag aggagaagca tattatgtcg gagcggaatg
      541 ttctgttgaa gaatgtgaag caccctttcc tggtgggcct tcacttctct ttccagactg
      601 ctgacaaatt gtactttgtc ctagactaca ttaatggtgg agagttgttc taccatctcc
      661 agagggaacg ctgcttcctg gaaccacggg ctcgtttcta tgctgctgaa atagccagtg
      721 ccttgggcta cctgcattca ctgaacatcg tttatagaga cttaaaacca gagaatattt
      781 tgctagattc acagggacac attgtcctta ctgacttcgg actctgcaag gagaacattg
      841 aacacaacag cacaacatcc accttctgtg gcacgccgga gtatctcgca cctgaggtgc
      901 ttcataagca gccttatgac aggactgtgg actggtggtg cctgggagct gtcttgtatg
      961 agatgctgta tggcctgccg ccttttttata gccgaaacac agctgaaatg tacgacaaca
     1021 ttctgaacaa gcctctccag ctgaaaccaa atattacaaa ttccgcaaga cacctcctgg
     1081 agggcctcct gcagaaggac aggacaaagc ggctcggggc caaggatgac ttcatggaga
     1141 ttaagagtca tgtcttcttc tccttaatta actgggatga tctcattaat aagaagatta
     1201 ctccccctttt taacccaaat gtgagtgggc ccaacgacct acggcacttt gaccccgagt
     1261 ttaccgaaga gcctgtcccc aactccattg gcaagtcccc tgacagcgtc ctcgtcacag
     1321 ccagcgtcaa ggaagctgcc gaggctttcc taggcttttc ctatgcgcct cccacggact
     1381 ctttcctctg aaccctgtta gggcttggtt ttaaaggatt ttatgtgtgt ttccgaatgt
     1441 tttagttagc cttttggtgg agccgccagc tgacaggaca tcttacaaga gaatttgcac
     1501 atctctggaa gcttagcaat cttattgcac actgttcgct ggaagctttt tgaagagcac
     1561 attctcctca gtgagctcat gaggttttca tttttattct tccttccaac gtggtgctat
     1621 ctctgaaacg agcgttagag tgccgcctta gacggaggca ggagtttcgt tagaaagcgg
```

```
1681 acgctgttct aaaaaaggtc tcctgcagat ctgtctgggc tgtgatgacg aatattatga
1741 aatgtgcctt ttctgaagag attgtgttag ctccaaagct tttcctatcg cagtgtttca
1801 gttctttatt ttcccttgtg gatatgctgt gtgaaccgtc gtgtgagtgt ggtatgcctg
1861 atcacagatg gattttgtta taagcatcaa tgtgacactt gcaggacact acaacgtggg
1921 acattgtttg tttcttccat atttggaaga taaatttatg tgtagacttt tttgtaagat
1981 acggttaata actaaaattt attgaaatgg tcttgcaatg actcgtattc agatgcttaa
2041 agaaagcatt gctgctacaa atatttctat ttttagaaag ggtttttatg gaccaatgcc
2101 ccagttgtca gtcagagccg ttggtgtttt tcattgttta aaatgtcacc tgtaaaatgg
2161 gcattattta tgtttttttt tttgcattcc tgataattgt atgtattgta taaagaacgt
2221 ctgtacattg ggttataaca ctagtatatt taaacttaca ggcttatttg taatgtaaac
2281 caccatttta atgtactgta attaacatgg ttataatacg tacaatcctt ccctcatccc
2341 atcacacaac tttttttgtg tgtgataaac tgattttggt ttgcaataaa accttgaaaa
2401 ata
```

DNA origin of transcript 5 (**NM_001291995.1**)

```
   1 gcagcatacg ccgagccggt ctttgagcgc taacgtcttt ctgtctcccc gcggtggtga
  61 tgacggtgaa aactgaggct gctaagggca ccctcactta ctccaggatg agggggcatgg
 121 tggcaattct catcgctttc atgaagcaga ggaggatggg tctgaacgac tttattcaga
 181 agattgccaa taactcctat gcatgcaaac accctgaagt tcagtccatc ttgaagatct
 241 cccaacctca ggagcctgag cttatgaatg ccaacccttc tcctccacca agtccttctc
 301 agcaaatcaa ccttggcccg tcgtccaatc ctcatgctaa accatctgac tttcacttct
 361 tgaaagtgat cggaaagggc agttttggaa aggttcttct agcaagacac aaggcagaag
 421 aagtgttcta tgcagtcaaa gttttacaga agaaagcaat cctgaaaaag aaagagttgt
 481 tctaccatct ccagagggaa cgctgcttcc tggaaccacg ggctcgtttc tatgctgctg
 541 aaatagccag tgccttgggc tacctgcatt cactgaacat cgtttataga gacttaaaac
 601 cagagaatat tttgctagat tcacagggac acattgtcct tactgacttc ggactctgca
 661 aggagaacat tgaacacaac agcacaacat ccaccttctg tggcacgccg gagtatctcg
 721 cacctgaggt gcttcataag cagcctatg acaggactgt ggactggtgg tgcctgggag
 781 ctgtcttgta tgagatgctg tatggcctgc cgccttttta tagccgaaac acagctgaaa
 841 tgtacgacaa cattctgaac aagcctctcc agctgaaacc aaatattaca aattccgcaa
 901 gacacctcct ggagggcctc ctgcagaagg acaggacaaa gcggctcggg gccaaggatg
 961 acttcatgga gattaagagt catgtcttct tctccttaat taactgggat gatctcatta
1021 ataagaagat tactcccct tttaacccaa atgtgagtgg gcccaacgac ctacggcact
1081 ttgaccccga gtttaccgaa gagcctgtcc ccaactccat tggcaagtcc cctgacagcg
1141 tcctcgtcac agccagcgtc aaggaagctg ccgaggcttt cctaggcttt tcctatgcgc
1201 ctcccacgga ctctttcctc tgaaccctgt tagggcttgg ttttaaagga ttttatgtgt
1261 gtttccgaat gttttagtta gccttttggt ggagccgcca gctgacagga catcttacaa
1321 gagaatttgc acatctctgg aagcttagca atcttattgc acactgttcg ctggaagctt
1381 tttgaagagc acattctcct cagtgagctc atgaggtttt catttttatt cttccttcca
1441 acgtggtgct atctctgaaa cgagcgttag agtgccgcct tagacggagg caggagtttc
1501 gttagaaagc ggacgctgtt ctaaaaaagg tctcctgcag atctgtctgg gctgtgatga
1561 cgaatattat gaaatgtgcc ttttctgaag agattgtgtt agctccaaag cttttcctat
1621 cgcagtgttt cagttcttta ttttcccttg tggatatgct gtgtgaaccg tcgtgtgagt
```

```
1681 gtggtatgcc tgatcacaga tggattttgt tataagcatc aatgtgacac ttgcaggaca
1741 ctacaacgtg ggacattgtt tgtttcttcc atatttggaa gataaattta tgtgtagact
1801 tttttgtaag atacggttaa taactaaaat ttattgaaat ggtcttgcaa tgactcgtat
1861 tcagatgctt aaagaaagca ttgctgctac aaatatttct atttttagaa agggttttta
1921 tggaccaatg ccccagttgt cagtcagagc cgttggtgtt tttcattgtt taaaatgtca
1981 cctgtaaaat gggcattatt tatgtttttt tttttgcatt cctgataatt gtatgtattg
2041 tataaagaac gtctgtacat tgggttataa cactagtata tttaaactta caggcttatt
2101 tgtaatgtaa accaccattt taatgtactg taattaacat ggttataata cgtacaatcc
2161 ttccctcatc ccatcacaca actttttttg tgtgtgataa actgattttg gtttgcaata
2221 aaaccttgaa aaata
```

Interrogated Sequence		Translated Protein	Exon Boundary	Assay Location	Amplicon Length
RefSeq	**NM_003507.1**	**NP_003498.1**	1-1	2400	70

Table A.3.2: FZD7 TaqMan probe binding site in the FZD7 transcript. Data obtained directly from: https://www.thermofisher.com/taqman-gene-expression/product/Hs00275833_s1?CID=&ICID=&subtype= (05.07.2019).

sgRNA 94 target: Red

sgRNA 96 target: Purple

sgRNA 100 target: Turqiouse

TaqMan probe binding site: yellow

```
   1 ctctcccaac cgcctcgtcg cactcctcag gctgagagca ccgctgcact cgcggccggc
  61 gatgcgggac cccggcgcgg ccgctccgct ttcgtccctg ggcctctgtg ccctggtgct
 121 ggcgctgctg ggcgcactgt ccgcgggcgc cggggcgcag ccgtaccacg gagagaaggg
 181 catctccgtg ccggaccacg gcttctgcca gcccatctcc atcccgctgt gcacggacat
 241 cgcctacaac cagaccatcc tgcccaacct gctgggccac acgaaccaag aggacgcggg
 301 cctcgaggtg caccagttct acccgctggt gaaggtgcag tgttctcccg aactccgctt
 361 tttcttatgc tccatgtatg cgcccgtgtg caccgtgctc gatcaggcca tcccgccgtg
 421 tcgttctctg tgcgagcgcg cccgccaggg ctgcgaggcg ctcatgaaca agttcggctt
 481 ccagtggccc gagcggctgc gctgcgagaa cttcccggtg cacggtgcgg gcgagatctg
 541 cgtgggccag aacacgtcgg acggctccgg gggcccaggc ggcggcccca ctgcctaccc
 601 taccgcgccc tacctgccgg acctgccctt caccgcgctg cccccggggg cctcagatgg
 661 caggggcgt cccgccttcc ccttctcatg cccccgtcag ctcaaggtgc ccccgtacct
 721 gggctaccgc ttcctgggtg agcgcgattg tggcgccccg tgcgaaccgg gccgtgccaa
 781 cggcctgatg tactttaagg aggaggagag gcgcttcgcc cgcctctggg tgggcgtgtg
 841 gtccgtgctg tgctgcgcct cgacgctctt taccgttctc acctacctgg tggacatgcg
 901 gcgcttcagc tacccagagc ggcccatcat cttcctgtcg ggctgctact tcatggtggc
 961 cgtggcgcac gtggccggct tcctctctaga ggaccgcgcc gtgtgcgtgg agcgcttctc
1021 ggacgatggc taccgcacgg tggcgcaggg caccaagaag gagggctgca ccatcctctt
1081 catggtgctc tacttcttcg gcatggccag ctccatctgg tgggtcattc tgtctctcac
1141 ttggttcctg gcggccggca tgaagtgggg ccacgaggcc atcgaggcca actcgcagta
1201 cttccacctg gccgcgtggg ccgtgcccgc cgtcaagacc atcactatcc tggccatggg
```

1261 ccaggtagac ggggacctgc tgagcggggt gtgctacgtt ggcctctcca gtgtggacgc
1321 gctgcggggc ttcgtgctgg cgcctctgtt cgtctacctc ttcataggca cgtccttctt
1381 gctggccggc ttcgtgtccc tcttccgtat ccgcaccatc atgaaacacg acggcaccaa
1441 gaccgagaag ctggagaagc tcatggtgcg catcggcgtc ttcagcgtgc tctacacagt
1501 gcccgccacc atcgtcctgg cctgctactt ctacgagcag gccttccgcg agcactggga
1561 gcgcacctgg ctcctgcaga cgtgcaagag ctatgccgtg ccctgcccgc ccggccactt
1621 cccgcccatg agccccgact tcaccgtctt catgatcaag tacctgatga ccatgatcgt
1681 cggcatcacc actggcttct ggatctggtc gggcaagacc ctgcagtcgt ggcgccgctt
1741 ctaccacaga cttagccaca gcagcaaggg ggagactgcg gtatgagccc cggcccctcc
1801 ccacctttcc caccccagcc ctcttgcaag aggagaggca cggtagggaa aagaactgct
1861 gggtgggggc ctgtttctgt aactttctcc ccctctactg agaagtgacc tggaagtgag
1921 aagttctttg cagatttggg gcgaggggtg atttggaaaa gaagacctgg gtggaaagcg
1981 gtttggatga aaagatttca ggcaaagact tgcaggaaga tgatgataac ggcgatgtga
2041 atcgtcaaag gtacgggcca gcttgtgcct aatagaaggt tgagaccagc agagactgct
2101 gtgagtttct cccggctccg aggctgaacg gggactgtga gcgatccccc tgctgcaggg
2161 cgagtggcct gtccagaccc ctgtgaggcc ccgggaaagg tacagccctg tctgcggtgg
2221 ctgctttgtt ggaaagaggg agggcctcct gcggtgtgct tgtcaagcag tggtcaaacc
2281 ataatctctt ttcactgggg ccaaactgga gcccagatgg gttaatttcc agggtcagac
2341 attacggtct ctcctcccct gccccctccc gcctgttttt cctcccgtac tgctttcagg
2401 tcttgtaaaa taagcatttg gaagtcttgg gaggcctgcc tgctagaatc ctaatgtgag
2461 gatgcaaaag aaatgatgat aacattttga gataaggcca aggagacgtg gagtaggtat
2521 ttttgctact ttttcatttt ctggggaagg caggaggcag aaagacgggt gttttatttg
2581 gtctaatacc ctgaaaagaa gtgatgactt gttgcttttc aaaacaggaa tgcatttttc
2641 cccttgtctt tgttgtaaga gacaaaagag gaaacaaaag tgtctccctg tggaaaggca
2701 taactgtgac gaaagcaact tttataggca aagcagcgca aatctgaggt ttcccgttgg
2761 ttgttaattt ggttgagata aacattcctt tttaaggaaa agtgaagagc agtgtgctgt
2821 cacacaccgt taagccagag gttctgactt cgctaaagga aatgtaagag gttttgttgt
2881 ctgttttaaa taaatttaat tcggaacaca tgatccaaca gactatgtta aaatattcag
2941 ggaaatctct cccttcattt acttttttctt gctataagcc tatatttagg tttcttttct
3001 attttttttct cccatttgga tcctttgagg taaaaaaaca taatgtcttc agcctcataa
3061 taaaggaaag ttaattaaaa aaaaaaagca aagagccatt ttgtcctgtt ttcttggttc
3121 catcaatctg tttattaaac atcatccata tgctgaccct gtctctgtgt ggttgggttg
3181 ggaggcgatc agcagatacc atagtgaacg aagaggaagg tttgaaccat gggccccatc
3241 tttaaagaaa gtcattaaaa gaaggtaaac ttcaaagtga ttctggagtt ctttgaaatg
3301 tgctggaaga cttaaattta ttaatcttaa atcatgtact ttttttctgt aatagaactc
3361 ggattctttt gcatgatggg gtaaagctta gcagagaatc atgggagcta acctttatcc
3421 caccttttgac actaccctcc aatcttgcaa cactatcctg tttctcagaa cagtttttaa
3481 atgccaatca tagagggtac tgtaaagtgt acaagttact ttatatatgt aatgttcact
3541 tgagtggaac tgctttttac attaaagtta aaatcgatct tgtgtttctt caaccttcaa
3601 aactatctca tctgtcagat ttttaaaact ccaacacagg ttttggcatc ttttgtgctg
3661 tatcttttaa gtgcatgtga aatttgtaaa atagagataa gtacagtatg tatattttgt
3721 aaatctccca tttttgtaag aaaatatata ttgtatttat acatttttac tttggatttt
3781 tgttttgttg gctttaaagg tctaccccac tttatcacat gtacagatca caaataaatt
3841 tttttaaata c

A.4: Mapping of protein domains and antibody binding.

This chapter gives insight into domains of Sgk1 (50 and 60 kDa isomers) and Fzd7. Binding sites of Sgk1 and Fzd7 specific antibodies are also given. Figure A.4.1 shows protein sequence of the 50 kDa Sgk1 isomer, Figure A.4.2 shows sequence of the 60 kDa Sgk1 isomer, and Figure A.4.3 shows protein sequence of Fzd7.

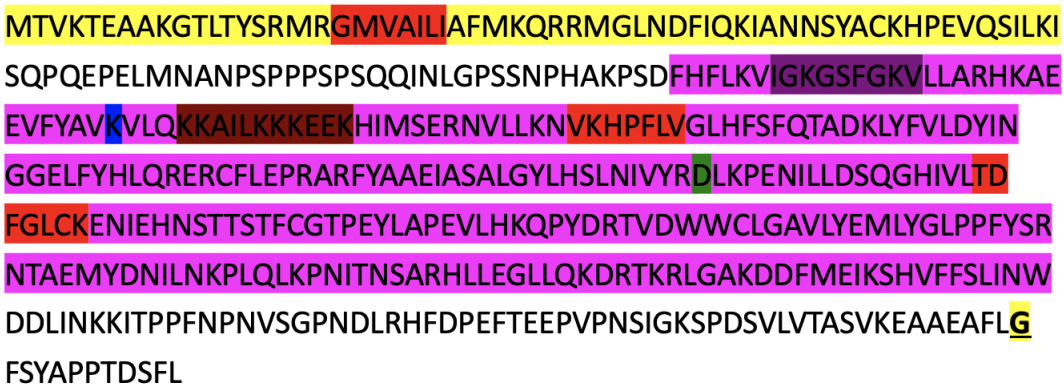

Figure A.4.1: Protein sequence of isoform 1 of SGK1 (50 kDa). The genomic target off the three different sgRNAs was translated to their respective protein sequence, in the six possible reading frame using the translation tool from EMBOSS Transeq (European Bioinformatics Institute (EMBL-EBI)). Dark blue (K): ATP-binding site, green (D): proton acceptor (ATP), purple (I-V): nucleotide binding, pink (F-W): protein kinase, yellow (M-I): signal sequence for localization to mitochondria, brown (K-K): nuclear localization, red: target sequences of the different sgRNAs (74: VKHPFLV, 75: TDFGLCK, 79: GMVAIL). Yellow underline: Sgk1 specific antibody binding site, used in Western blot analyses.

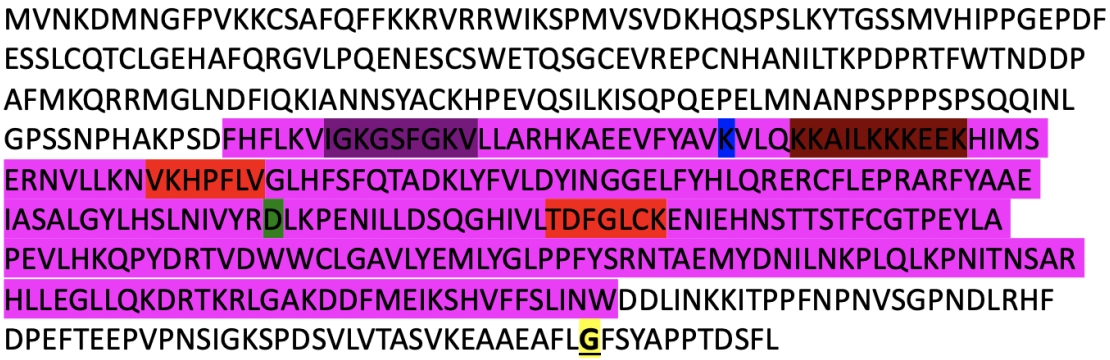

Figure A.4.2: Protein sequence of isoform 2 (60 kDa) of SGK1. The genomic target off the three different sgRNAs was translated to their respective protein sequence, in the six possible reading frame using the translation tool from EMBOSS Transeq (European Bioinformatics Institute (EMBL-EBI)). Dark blue (K): ATP-

binding site, green (D): proton acceptor (ATP), purple (I-V): nucleotide binding, pink (F-W): protein kinase, yellow (M-I): signal sequence for localization to mitochondria, brown (K-K): nuclear localization, red: target sequences of the different sgRNAs (74: VKHPFLV, 75: TDFGLCK). Yellow underline: Sgk1 specific antibody binding site, used in Western blot analyses.

MRDPGAAAPLSSLGLCALVLALLGALSAGAGAQPYHGEKGISVPDHGFCQPISIPLCTDI
AYNQTILPNLLGHTNQEDAGLEVHQFYPLVKVQCSPELRFFLCSMYAPVCTVLDQAIPPC
RSLCERARQGCEALMNKFGFQWPERLRCENFPVHGAGEICVGQNTSDGSGGPGGGPTAY
P TAPYLPDLPFTALPPGASDGRGRPAFPFSCPRQLKVPPYLGYRFLGERDCGAPCEPGRAN
GLMYFKEEERRFARLWVGVWSVLCCASTLFTVLTYLVDMRRFSYPERPIIFLSGCYFMVA
VAHVAGFLLEDRAVCVERFSDDGYRTVAQGTKKEGCTILFMVLYFFGMASSIWWVILSLT
WFLAAGMKWGHEAIEANSQYFHLAAWAVPAVKTITILAMGQVDGDLLSGVCYVGLSSVDA
LRGFVLAPLFVYLFIGTSFLLAGFVSLFRIRTIMKHDGTKTEKLEKLMVRIGVFSVLYTV
PATIVLACYFYEQAFREHWERTWLLQTCKSYAVPCPPGHFPPMSPDFTVFMIKYLMTMIV
GITTGFWIWSGKTLQSWRRFYHRLSHSSKGETAV

Figure A.4.3: Protein sequence of FZD7. The genomic target of the three different sgRNAs was translated to their respective protein sequence, in the six possible reading frame using the translation tool from EMBOSS Transeq (European Bioinformatics Institute (EMBL-EBI)). Later the protein locations of these targets were identified. Pink: extracellular domain, green: helical, transmembrane region, turquoise: cytoplasmic/intracellular region, yellow (M-A): Signal peptide sequence, red: target sequences of the different sgRNAs (94: VCTVLDQ, 96: LEDRAV, 100: YLMTMIV). Yellow underline: Fzd7 specific antibody binding site, used in Western blot analyses.

A.5: Preparation of solution for Western blotting

Running buffer 20X 0,5 L:

0.8M Tricine (Sigma, T5816)

1,2MTrizma base (Sigma, T1503)

2% SDS (Sodium dodecyl sulphate, Sigma, L4509)

mq$H_2$0 to 0,5 L volume

Transfer buffer 10X (1L):

30.3g Trizma base (Sigma, T1503)

144g Glycine (Sigma, G7126)

mq$H_2$0 to 1 L volume

1x Transfer buffer was made to a total volume of 1 liter with 20% methanol (100 ml Transfer buffer 10X, 200 ml methanol, 700 ml mq$H_2$0).

TBS 10X (1L):

60.6 g Trizma Base (Sigma, T1503)

87.7g NaCl (Sigma, 55886)

mqH_2O to 1 L volume

A.6: Viability data distributions

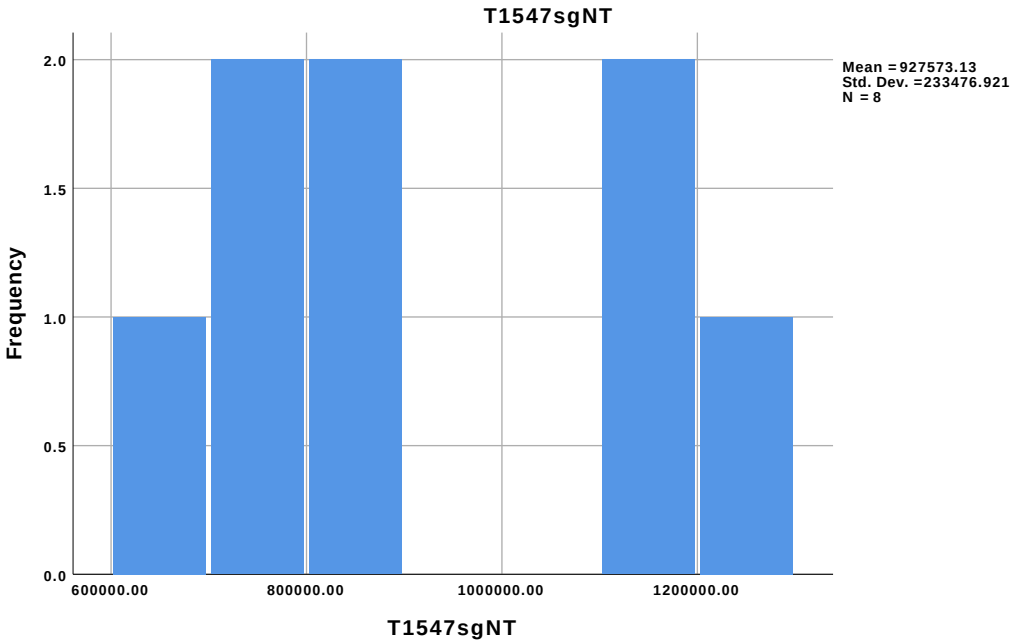
T1547sgNT
Mean = 927573.13
Std. Dev. =233476.921
N = 8
Frequency
2.0
1.5
1.0
0.5
0.0
600000.00
800000.00
1000000.00
1200000.00
T1547sgNT

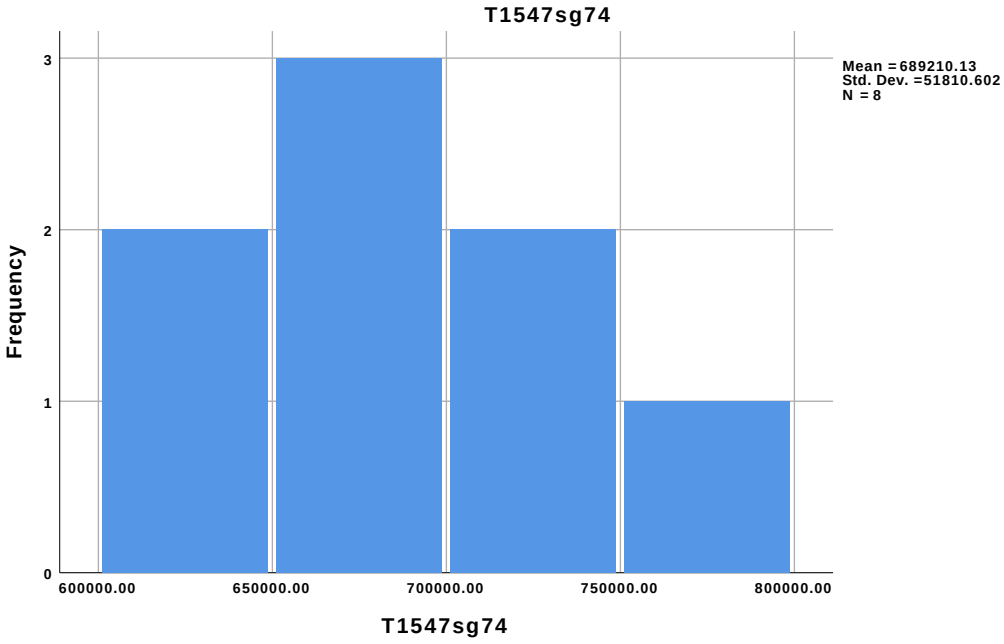
T1547sg74
Mean = 689210.13
Std. Dev. =51810.602
N = 8
Frequency
3
2
1
0
600000.00
650000.00
700000.00
750000.00
800000.00
T1547sg74

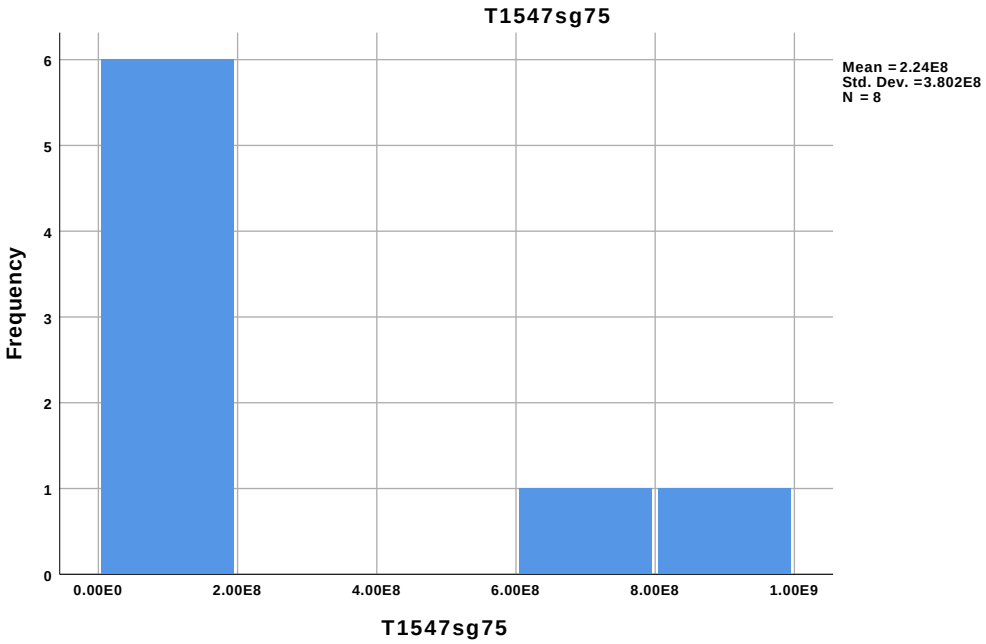
T1547sg75
Mean = 2.24E8
Std. Dev. =3.802E8
N = 8
Frequency
0
1
2
3
4
5
6
0.00E0
2.00E8
4.00E8
6.00E8
8.00E8
1.00E9
T1547sg75

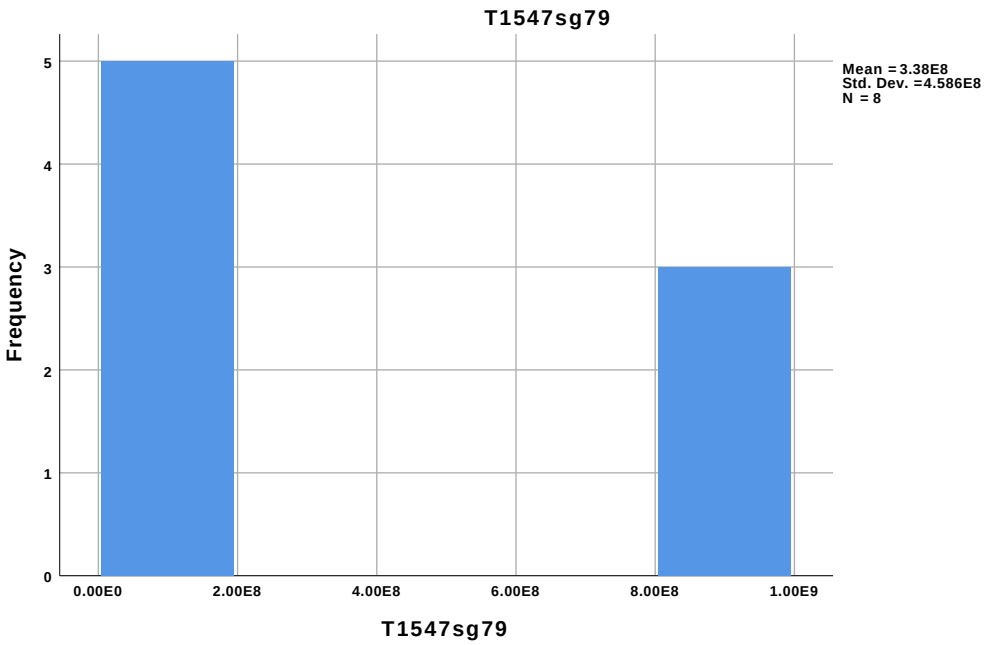
T1547sg79
Mean = 3.38E8
Std. Dev. =4.586E8
N = 8
Frequency
0
1
2
3
4
5
0.00E0
2.00E8
4.00E8
6.00E8
8.00E8
1.00E9
T1547sg79

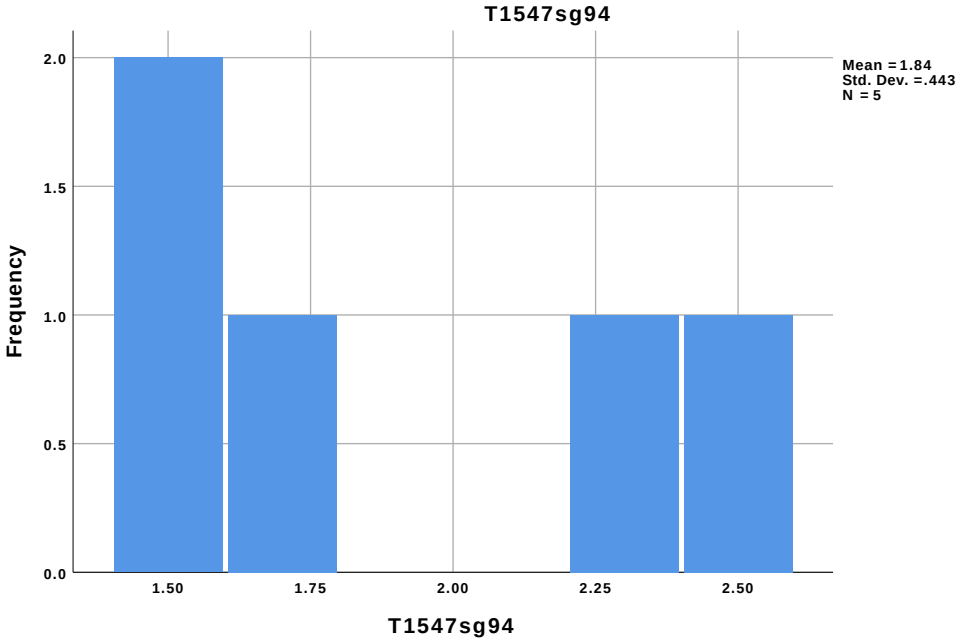
T1547sg94
Mean =1.84
Std. Dev. =.443
N = 5
Frequency
2.0
1.5
1.0
0.5
0.0
1.50
1.75
2.00
2.25
2.50
T1547sg94

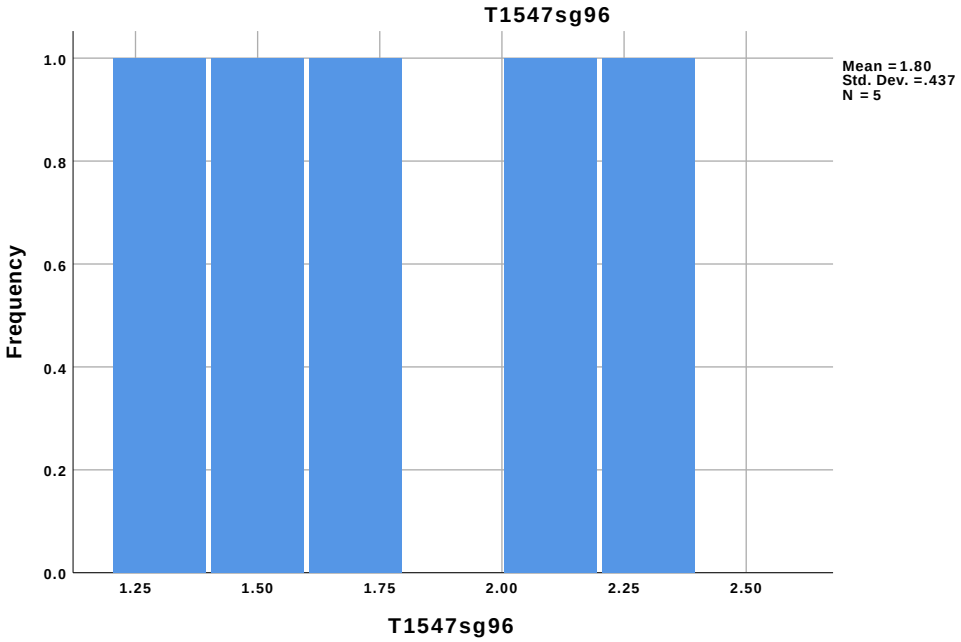
T1547sg96
Mean =1.80
Std. Dev. =.437
N = 5
Frequency
1.0
0.8
0.6
0.4
0.2
0.0
1.25
1.50
1.75
2.00
2.25
2.50
T1547sg96

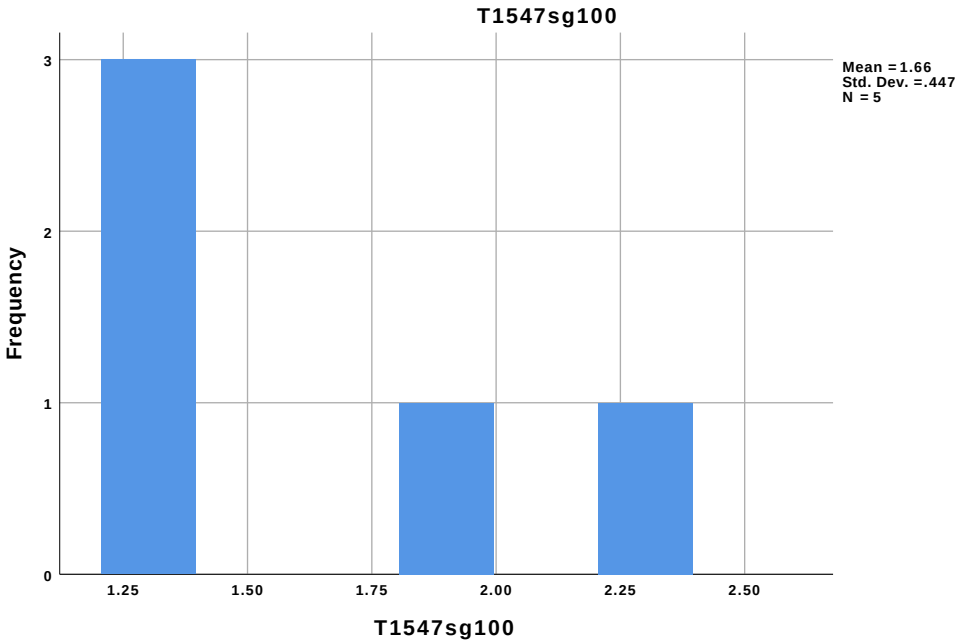
T1547sg100
Mean =1.66
Std. Dev. =.447
N = 5
Frequency
3
2
1
0
1.25
1.50
1.75
2.00
2.25
2.50
T1547sg100

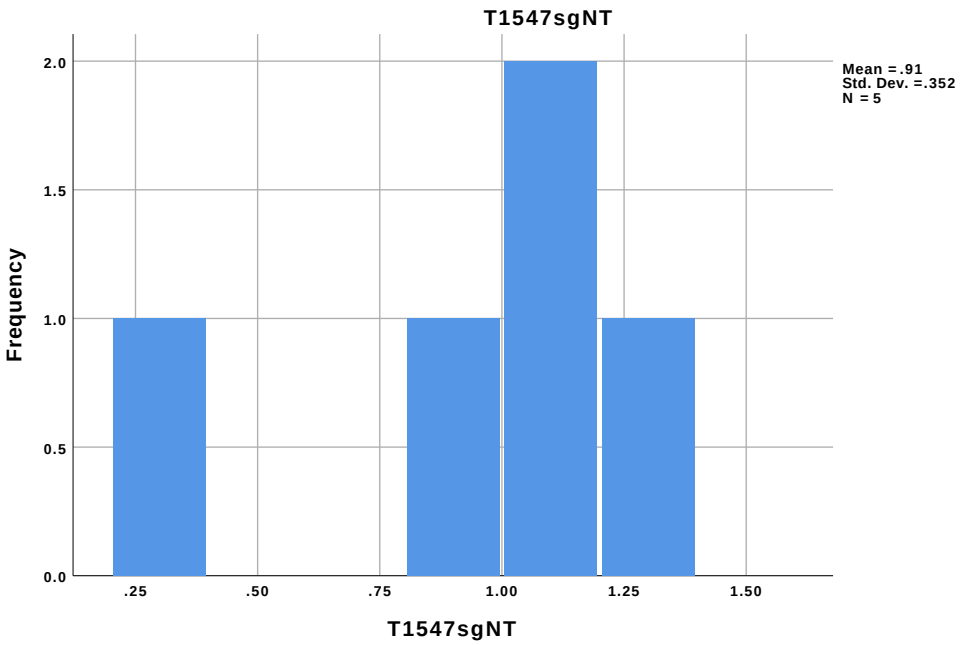
T1547sgNT
Mean =.91
Std. Dev. =.352
N = 5
Frequency
2.0
1.5
1.0
0.5
0.0
.25
.50
.75
1.00
1.25
1.50
T1547sgNT

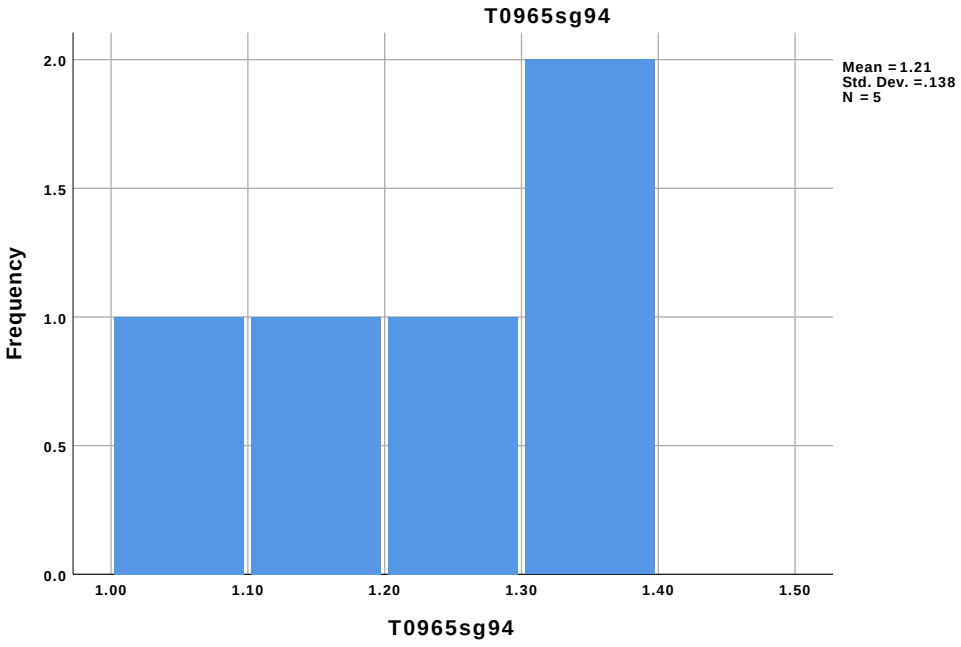
T0965sg94
Mean =1.21
Std. Dev. =.138
N = 5
Frequency
2.0
1.5
1.0
0.5
0.0
1.00
1.10
1.20
1.30
1.40
1.50
T0965sg94

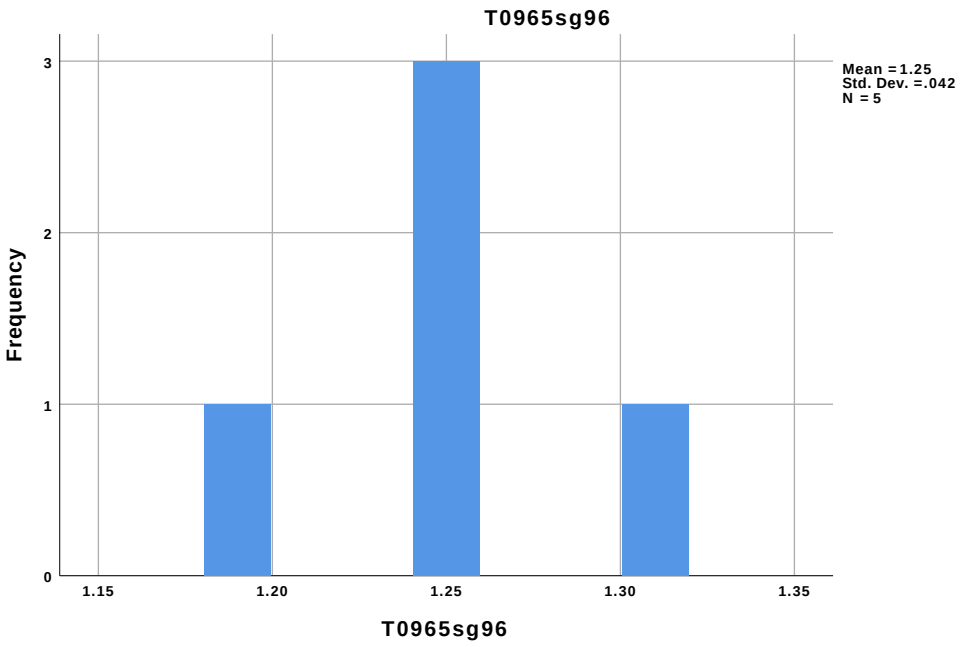
T0965sg96
Mean =1.25
Std. Dev. =.042
N = 5
Frequency
3
2
1
0
1.15
1.20
1.25
1.30
1.35
T0965sg96

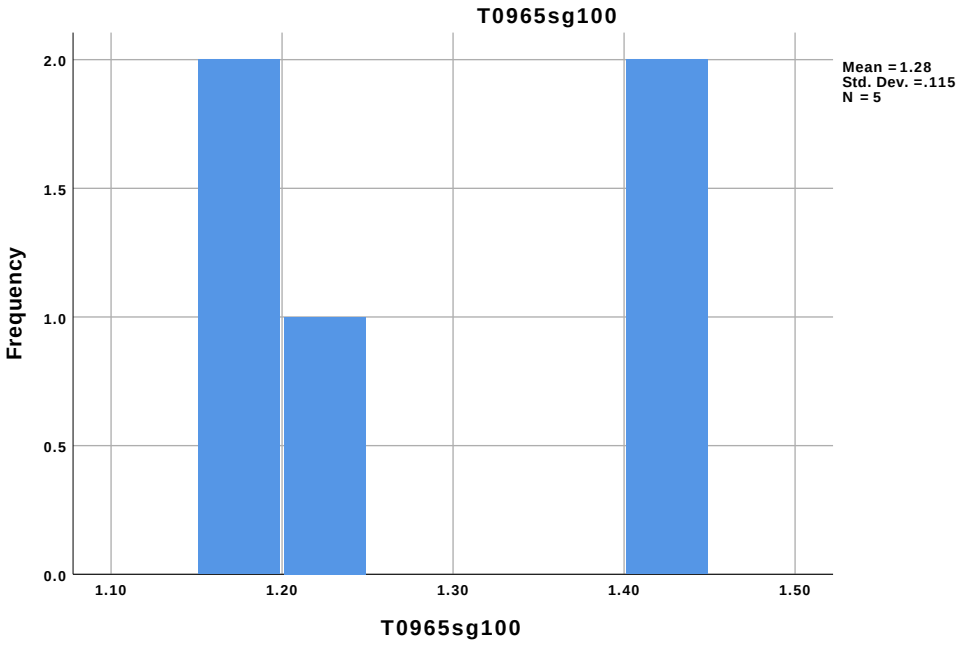
T0965sg100
Mean =1.28
Std. Dev. =.115
N = 5
Frequency
2.0
1.5
1.0
0.5
0.0
1.10
1.20
1.30
1.40
1.50
T0965sg100

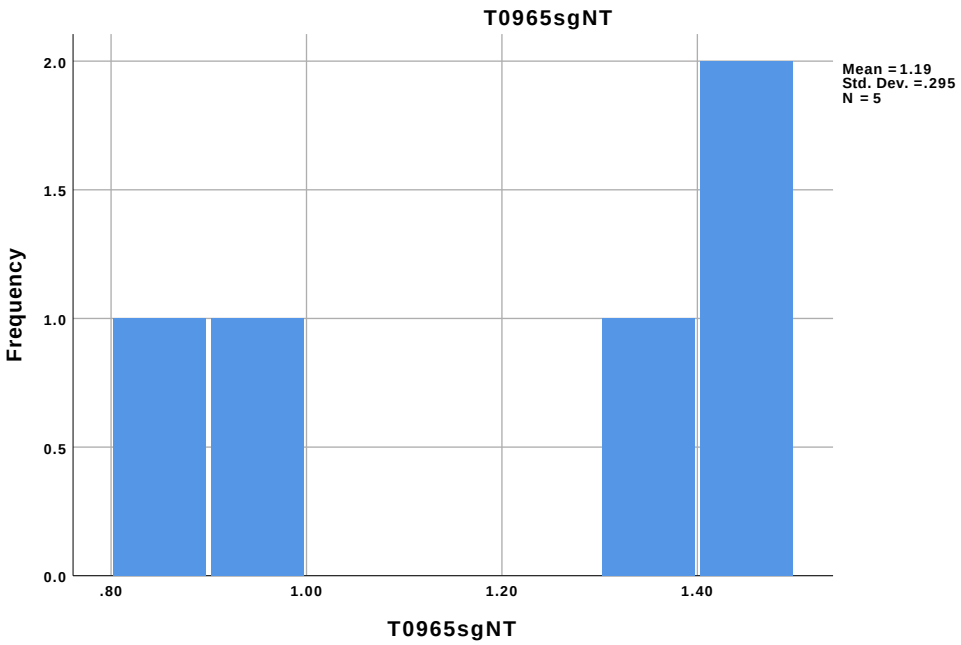
T0965sgNT
Mean =1.19
Std. Dev. =.295
N = 5
Frequency
2.0
1.5
1.0
0.5
0.0
.80
1.00
1.20
1.40
T0965sgNT

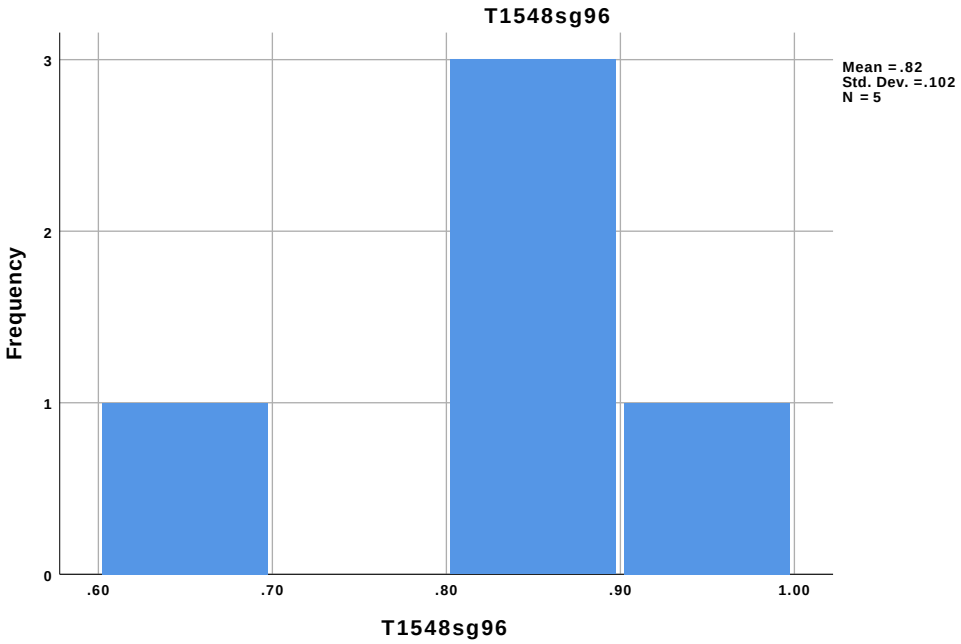
T1548sg96
Mean =.82
Std. Dev. =.102
N = 5
Frequency
3
2
1
0
.60
.70
.80
.90
1.00
T1548sg96

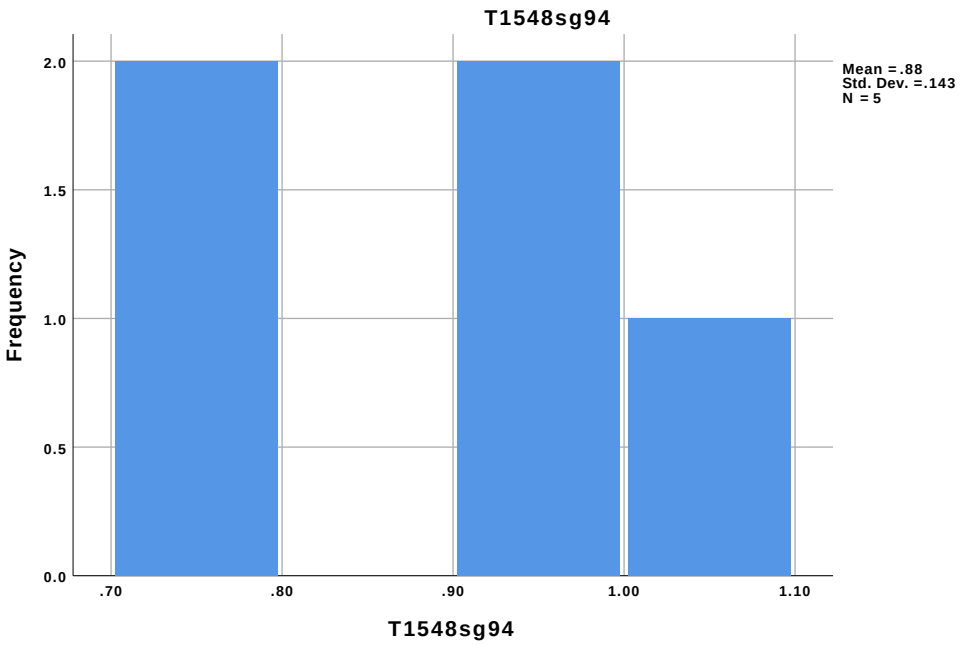
T1548sg94
Mean =.88
Std. Dev. =.143
N = 5
Frequency
2.0
1.5
1.0
0.5
0.0
.70
.80
.90
1.00
1.10
T1548sg94

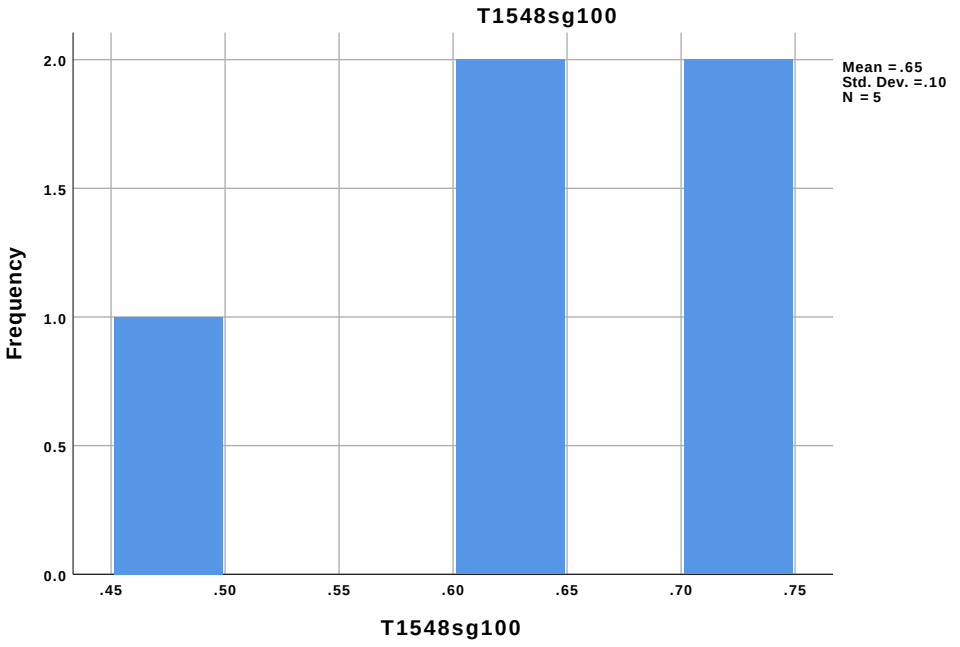
T1548sg100
Mean =.65
Std. Dev. =.10
N = 5
Frequency
2.0
1.5
1.0
0.5
0.0
.45
.50
.55
.60
.65
.70
.75
T1548sg100

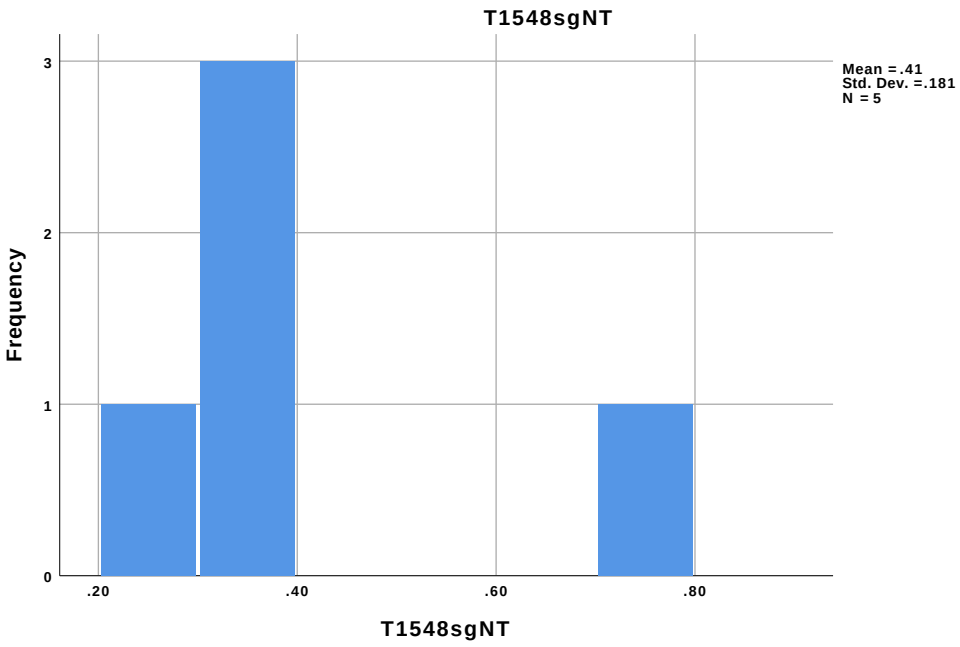
T1548sgNT
Mean =.41
Std. Dev. =.181
N = 5
Frequency
3
2
1
0
.20
.40
.60
.80
T1548sgNT

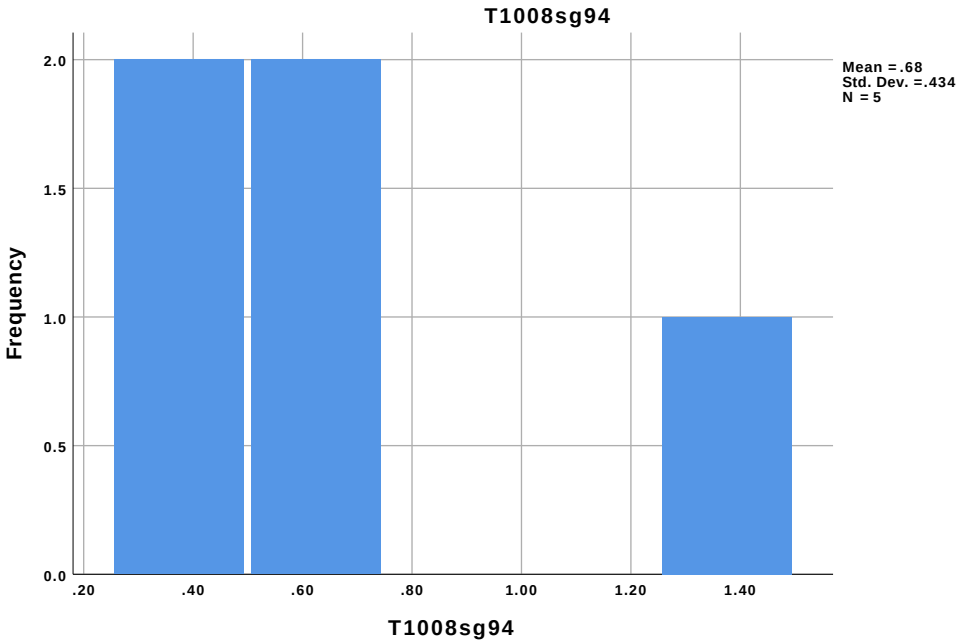
T1008sg94
Mean =.68
Std. Dev. =.434
N = 5
Frequency
2.0
1.5
1.0
0.5
0.0
.20
.40
.60
.80
1.00
1.20
1.40
T1008sg94

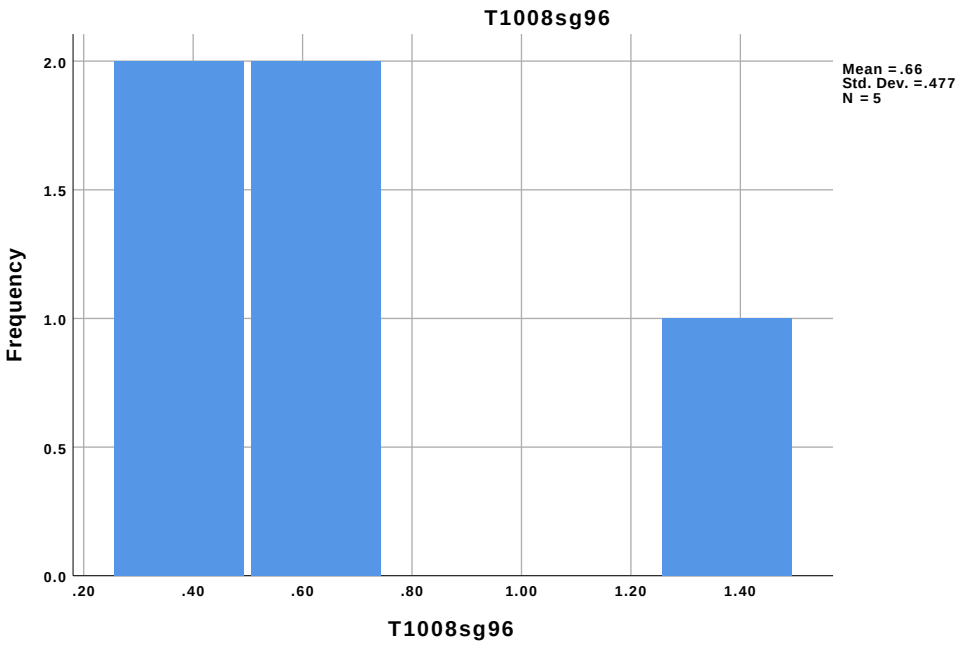
T1008sg96
Mean =.66
Std. Dev. =.477
N = 5
Frequency
2.0
1.5
1.0
0.5
0.0
.20
.40
.60
.80
1.00
1.20
1.40
T1008sg96

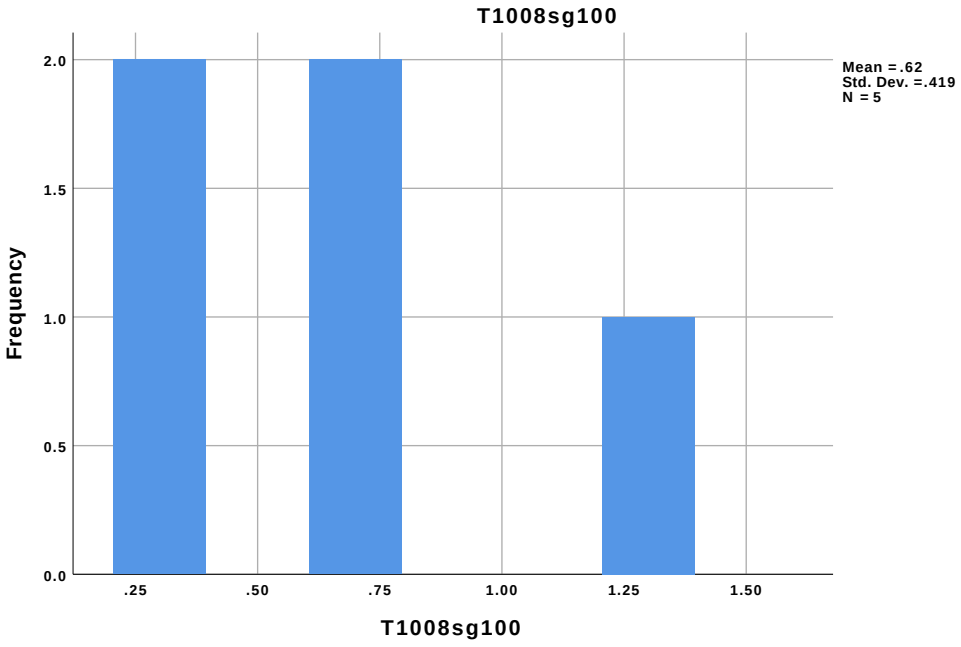
T1008sg100
Mean =.62
Std. Dev. =.419
N = 5
Frequency
2.0
1.5
1.0
0.5
0.0
.25
.50
.75
1.00
1.25
1.50
T1008sg100

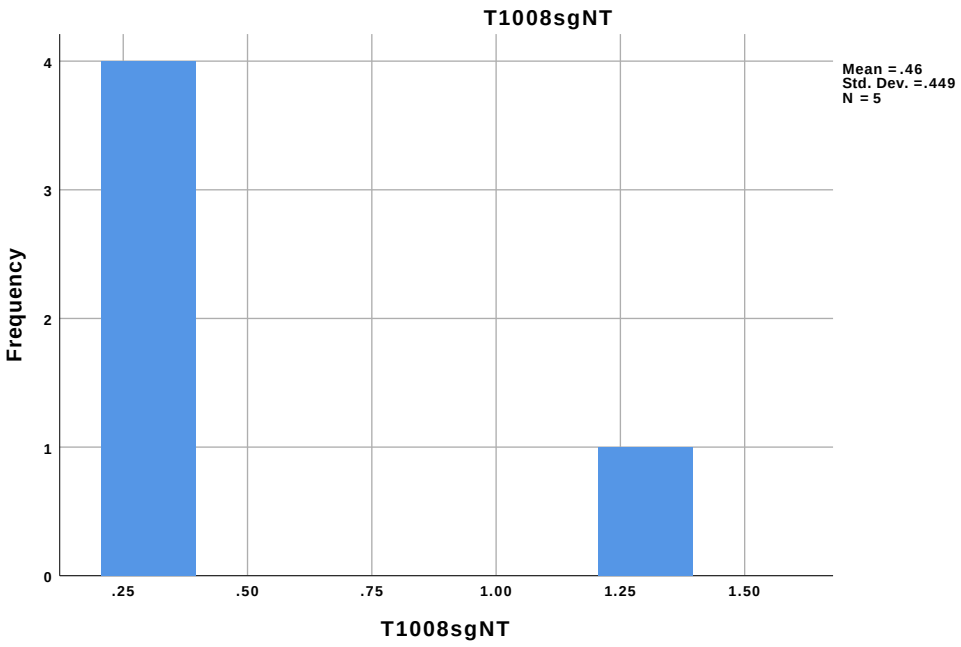
T1008sgNT
Mean =.46
Std. Dev. =.449
N = 5
Frequency
4
3
2
1
0
.25
.50
.75
1.00
1.25
1.50
T1008sgNT

A.7: RNA integrity data

First read (16.04.2019):

Sample 1: T1547 (SGK1) 74

Sample 2: T1547 (SGK1) 75

Sample 3: T1547 (SGK1) 79

Sample 4: T1547 (SGK1) NT

Sample 5: T1547 (FZD7) 94

Sample 6: T1547 (FZD7) 96

Sample 7: T1547 (FZD7) 100

Sample 8: T1547 (FZD7) NT

Sample 9: T1547 (FZD7) PPIB (not included in the study)

Sample 10: T0965 total RNA isolated earlier, with known RIN (added as a control).

Sample 11: RNAse-free water

Sample 12: RNAse-free water

Second read (20.06.2019):

Sample 1: T0965 (FZD7) 94

Sample 2: T0965 (FZD7) 96

Sample 3: T0965 (FZD7) 100

Sample 4: T0965 (FZD7) NT

Sample 5: T1548 (FZD7) 94

Sample 6: T1548 (FZD7) 96

Sample 7: T1548 (FZD7) 100

Sample 8: T1548 (FZD7) NT

Sample 9: T1008 (FZD7) 94

Sample 10: T1008 (FZD7) 96

Sample 11: T1008 (FZD7) 100

Sample 12: T1008 (FZD7) NT

Assay Class: Eukaryote Total RNA Nano
Data Path: E:\Eukaryote Total RNA Nano_2019-04-16_11-01-09.xad

Created: 4/16/2019 11:01:08 AM
Modified: 4/16/2019 11:46:31 AM

Electrophoresis File Run Summary

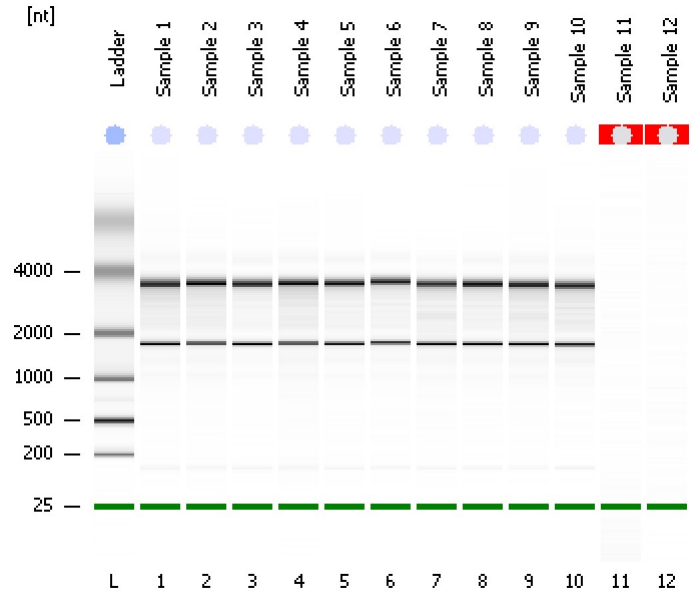

Instrument Information:

Instrument Name: DE54704709 Firmware: C.01.069
Serial#: DE54704709 Type: G2938C

Assay Information:

Assay Origin Path: C:\Program Files\Agilent\2100 bioanalyzer\2100 expert\assays\RNA\Eukaryote Total RNA Nano Series II.xsy

Assay Class: Eukaryote Total RNA Nano

Version: 2.6

Assay Comments: Total RNA Analysis ng sensitivity (Eukaryote)

Chip Information:

Chip Lot #:

Reagent Kit Lot #:

Chip Comments:

Sample 1
RIN: 9.60

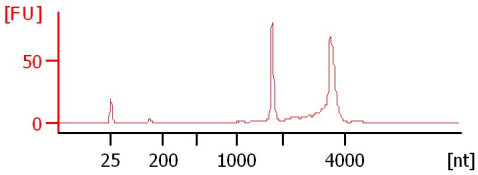

Sample 2
RIN: 9.50

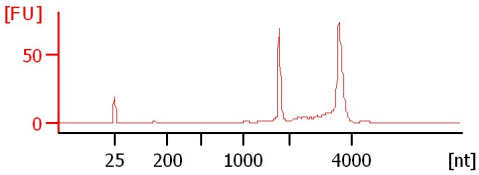

Sample 3
RIN: 9.80

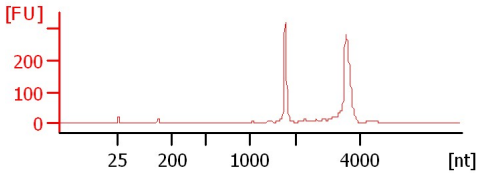

Sample 4
RIN: 9.40

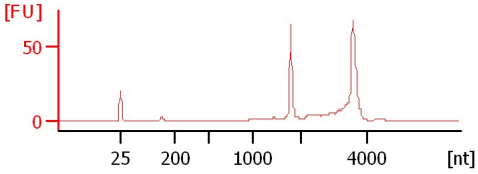

Sample 5
RIN: 9.60

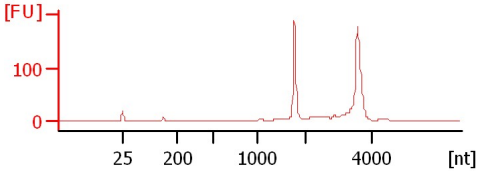

Sample 6
RIN: 9.60

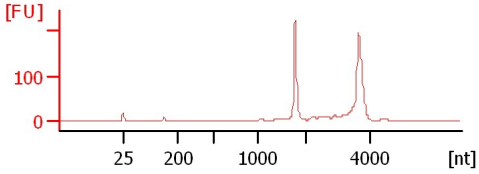

Sample 7
RIN: 9.30

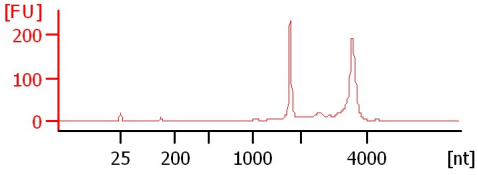

Sample 8
RIN: 9.50

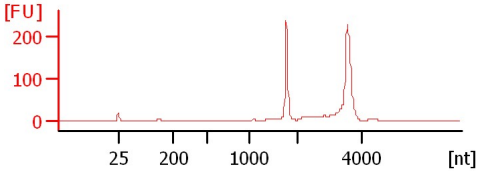

Sample 9
RIN: 9.60

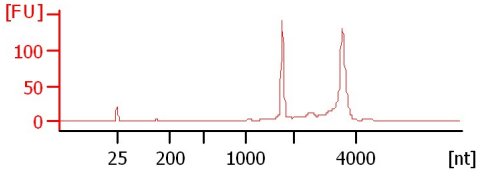

Sample 10
RIN: 9.20

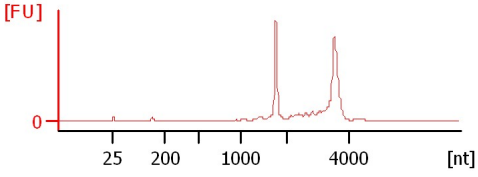

Sample 11
RIN N/A

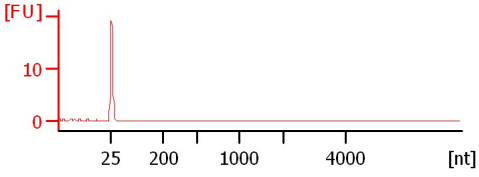

Sample 12
RIN N/A

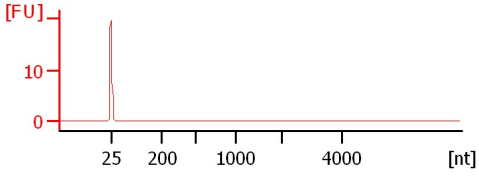

Assay Class: Eukaryote Total RNA Nano
Data Path: E:\Eukaryote Total RNA Nano_2019-04-16_11-01-09.xad

Created: 4/16/2019 11:01:08 AM
Modified: 4/16/2019 11:46:31 AM

Electrophoresis File Run Summary (Chip Summary)

Sample Name	Sample Comment	Status	Result Label	Result Color
Sample 1		✓	RIN: 9.60	
Sample 2		✓	RIN: 9.50	
Sample 3		✓	RIN: 9.80	
Sample 4		✓	RIN: 9.40	
Sample 5		✓	RIN: 9.60	
Sample 6		✓	RIN: 9.60	
Sample 7		✓	RIN: 9.30	
Sample 8		✓	RIN: 9.50	
Sample 9		✓	RIN: 9.60	
Sample 10		✓	RIN: 9.20	
Sample 11		✓	RIN N/A	
Sample 12		✓	RIN N/A	
Ladder		✓	All Other Samples	

Chip Lot #

Reagent Kit Lot #

Chip Comments :

Assay Class: Eukaryote Total RNA Nano
Data Path: E:\Eukaryote Total RNA Nano_2019-04-16_11-01-09.xad

Created: 4/16/2019 11:01:08 AM
Modified: 4/16/2019 11:46:31 AM

Electropherogram Summary

Ladder

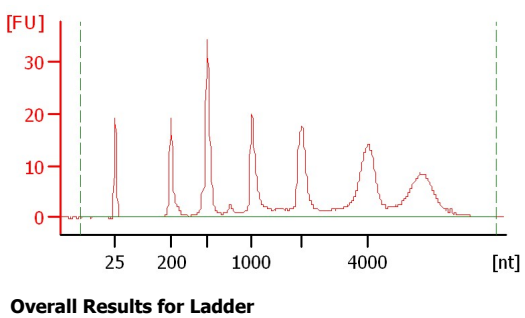

Overall Results for Ladder

RNA Area:	338.4
RNA Concentration:	150 ng/µl
Result Flagging Color:	
Result Flagging Label:	All Other Samples

Sample 1

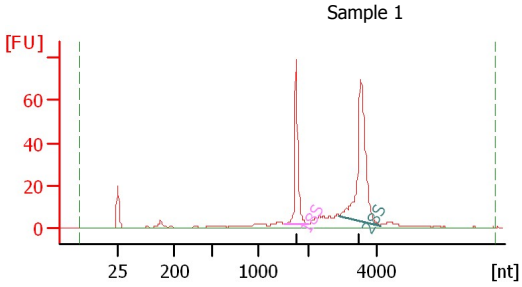

Overall Results for sample 1 : Sample 1

RNA Area:	336.5
RNA Concentration:	149 ng/µl
rRNA Ratio [28s / 18s]:	1.9
RNA Integrity Number (RIN):	9.6 (B.02.08)
Result Flagging Color:	
Result Flagging Label:	RIN: 9.60

Fragment table for sample 1 : Sample 1

Name	Start Size [nt]	End Size [nt]	Area	% of total Area
18S	1,538	1,996	72.8	21.6
28S	2,919	4,104	136.2	40.5

Sample 2

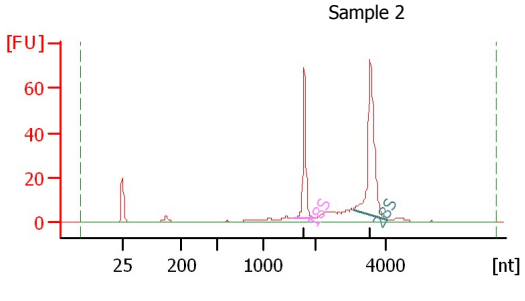

Overall Results for sample 2 : Sample 2

RNA Area:	295.7
RNA Concentration:	131 ng/µl
rRNA Ratio [28s / 18s]:	1.8
RNA Integrity Number (RIN):	9.5 (B.02.08)
Result Flagging Color:	
Result Flagging Label:	RIN: 9.50

Fragment table for sample 2 : Sample 2

Name	Start Size [nt]	End Size [nt]	Area	% of total Area
18S	1,574	1,991	60.0	20.3
28S	3,080	4,076	110.9	37.5

Sample 3

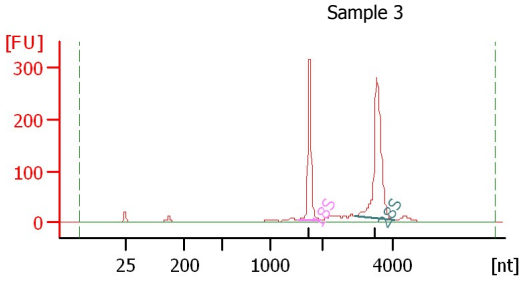

Overall Results for sample 3 : Sample 3

RNA Area:	1,096.7
RNA Concentration:	486 ng/µl
rRNA Ratio [28s / 18s]:	1.8
RNA Integrity Number (RIN):	9.8 (B.02.08)
Result Flagging Color:	
Result Flagging Label:	RIN: 9.80

Fragment table for sample 3 : Sample 3

Name	Start Size [nt]	End Size [nt]	Area	% of total Area
18S	1,538	1,980	283.9	25.9
28S	2,948	4,057	498.0	45.4

Assay Class: Eukaryote Total RNA Nano
Data Path: E:\Eukaryote Total RNA Nano_2019-04-16_11-01-09.xad

Created: 4/16/2019 11:01:08 AM
Modified: 4/16/2019 11:46:31 AM

Electropherogram Summary Continued ...

Sample 4

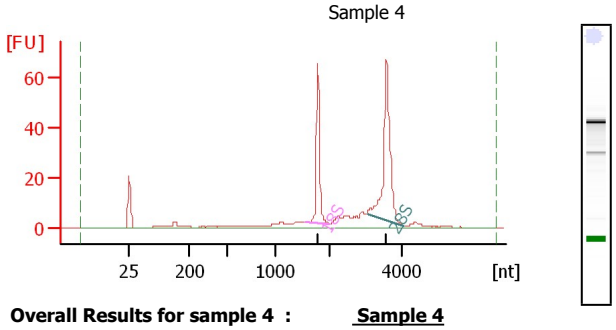

Overall Results for sample 4 : **Sample 4**

RNA Area:	281.2
RNA Concentration:	125 ng/µl
rRNA Ratio [28s / 18s]:	1.9
RNA Integrity Number (RIN):	9.4 (B.02.08)
Result Flagging Color:	
Result Flagging Label:	RIN: 9.40

Fragment table for sample 4 : **Sample 4**

Name	Start Size [nt]	End Size [nt]	Area	% of total Area
18S	1,541	1,992	55.3	19.7
28S	3,044	4,053	103.9	36.9

Sample 5

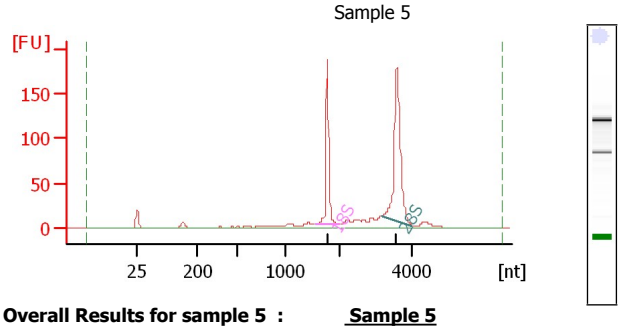

Overall Results for sample 5 : **Sample 5**

RNA Area:	666.0
RNA Concentration:	295 ng/µl
rRNA Ratio [28s / 18s]:	1.6
RNA Integrity Number (RIN):	9.6 (B.02.08)
Result Flagging Color:	
Result Flagging Label:	RIN: 9.60

Fragment table for sample 5 : **Sample 5**

Name	Start Size [nt]	End Size [nt]	Area	% of total Area
18S	1,556	1,994	157.7	23.7
28S	3,153	4,025	258.3	38.8

Sample 6

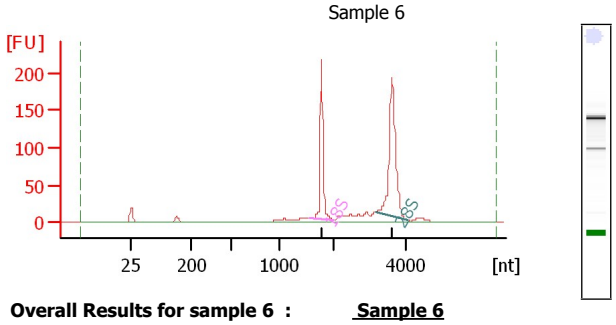

Overall Results for sample 6 : **Sample 6**

RNA Area:	753.0
RNA Concentration:	334 ng/µl
rRNA Ratio [28s / 18s]:	1.6
RNA Integrity Number (RIN):	9.6 (B.02.08)
Result Flagging Color:	
Result Flagging Label:	RIN: 9.60

Fragment table for sample 6 : **Sample 6**

Name	Start Size [nt]	End Size [nt]	Area	% of total Area
18S	1,562	2,026	186.5	24.8
28S	3,190	4,075	294.1	39.1

Sample 7

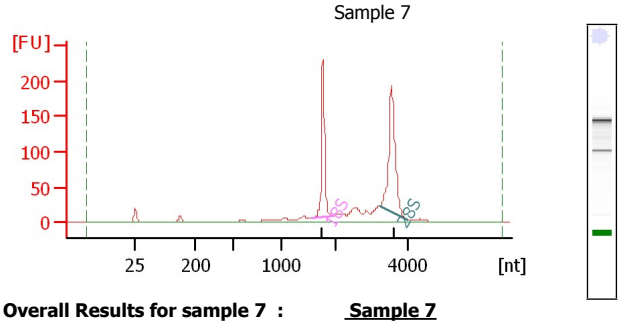

Overall Results for sample 7 : **Sample 7**

RNA Area:	885.1
RNA Concentration:	392 ng/µl
rRNA Ratio [28s / 18s]:	1.4
RNA Integrity Number (RIN):	9.3 (B.02.08)
Result Flagging Color:	
Result Flagging Label:	RIN: 9.30

Fragment table for sample 7 : **Sample 7**

Name	Start Size [nt]	End Size [nt]	Area	% of total Area
18S	1,549	1,976	200.8	22.7
28S	3,243	4,006	284.5	32.1

Assay Class: Eukaryote Total RNA Nano
Data Path: E:\Eukaryote Total RNA Nano_2019-04-16_11-01-09.xad

Created: 4/16/2019 11:01:08 AM
Modified: 4/16/2019 11:46:31 AM

Electropherogram Summary Continued ...

Sample 8

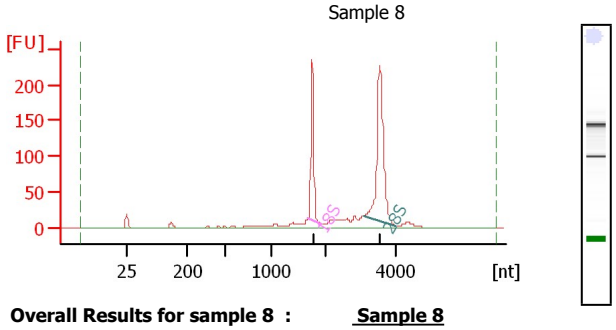

Overall Results for sample 8 : Sample 8

RNA Area:	854.1
RNA Concentration:	379 ng/µl
rRNA Ratio [28s / 18s]:	1.9
RNA Integrity Number (RIN):	9.5 (B.02.08)
Result Flagging Color:	
Result Flagging Label:	RIN: 9.50

Fragment table for sample 8 : Sample 8

Name	Start Size [nt]	End Size [nt]	Area	% of total Area
18S	1,693	1,957	185.0	21.7
28S	3,112	4,038	347.6	40.7

Sample 9

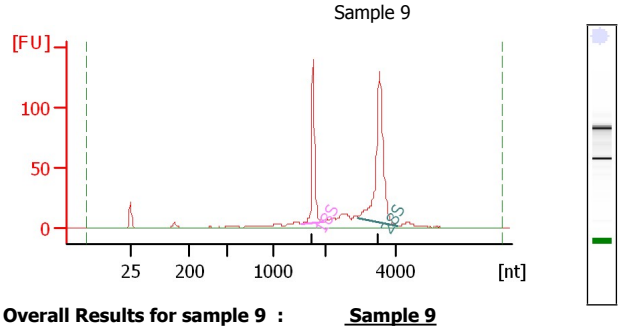

Overall Results for sample 9 : Sample 9

RNA Area:	548.0
RNA Concentration:	243 ng/µl
rRNA Ratio [28s / 18s]:	1.9
RNA Integrity Number (RIN):	9.6 (B.02.08)
Result Flagging Color:	
Result Flagging Label:	RIN: 9.60

Fragment table for sample 9 : Sample 9

Name	Start Size [nt]	End Size [nt]	Area	% of total Area
18S	1,540	1,970	120.2	21.9
28S	2,917	4,034	223.4	40.8

Sample 10

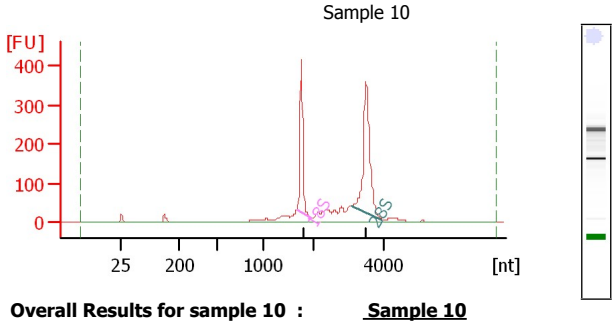

Overall Results for sample 10 : Sample 10

RNA Area:	1,716.8
RNA Concentration:	761 ng/µl
rRNA Ratio [28s / 18s]:	1.6
RNA Integrity Number (RIN):	9.2 (B.02.08)
Result Flagging Color:	
Result Flagging Label:	RIN: 9.20

Fragment table for sample 10 : Sample 10

Name	Start Size [nt]	End Size [nt]	Area	% of total Area
18S	1,678	1,941	348.7	20.3
28S	3,095	3,961	571.1	33.3

Sample 11

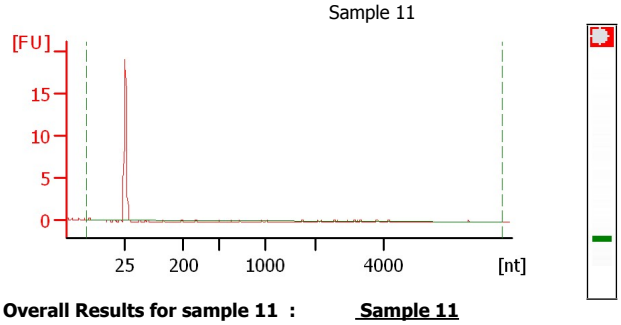

Overall Results for sample 11 : Sample 11

RNA Area:	1.5
RNA Concentration:	1 ng/µl
rRNA Ratio [28s / 18s]:	0.0
RNA Integrity Number (RIN):	N/A (B.02.08)
Result Flagging Color:	
Result Flagging Label:	RIN N/A

Assay Class: Eukaryote Total RNA Nano
Data Path: E:\Eukaryote Total RNA Nano_2019-04-16_11-01-09.xad

Created: 4/16/2019 11:01:08 AM
Modified: 4/16/2019 11:46:31 AM

Electropherogram Summary Continued ...

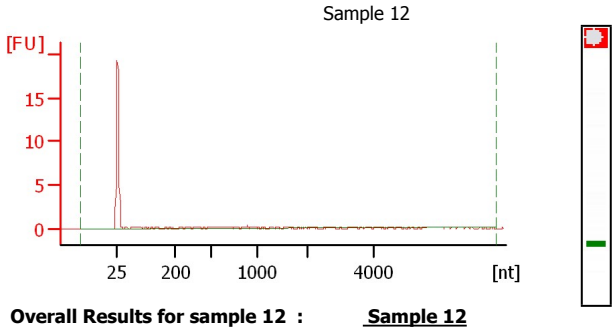

Overall Results for sample 12 : **Sample 12**

RNA Area:	4.9
RNA Concentration:	2 ng/µl
rRNA Ratio [28s / 18s]:	0.0
RNA Integrity Number (RIN):	N/A (B.02.08)
Result Flagging Color:	
Result Flagging Label:	RIN N/A

Assay Class: Eukaryote Total RNA Nano
Data Path: E:\Eukaryote Total RNA Nano_2019-04-16_11-01-09.xad

Created: 4/16/2019 11:01:08 AM
Modified: 4/16/2019 11:46:31 AM

Gel Image

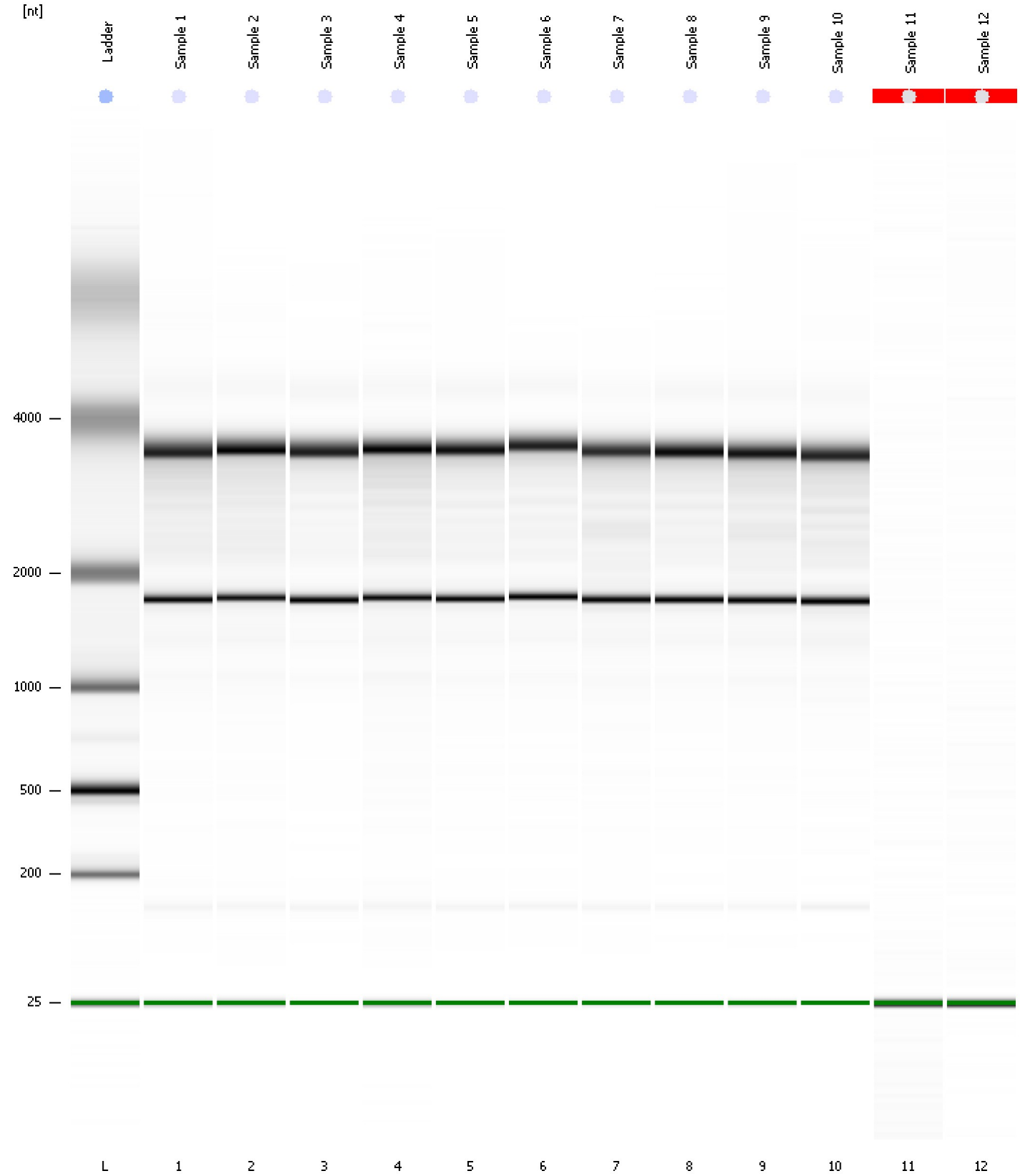

Assay Class: Eukaryote Total RNA Nano
Data Path: E:\Eukaryote Total RNA Nano_2019-04-16_11-01-09.xad

Created: 4/16/2019 11:01:08 AM
Modified: 4/16/2019 11:46:31 AM

Curves

Standard Curve

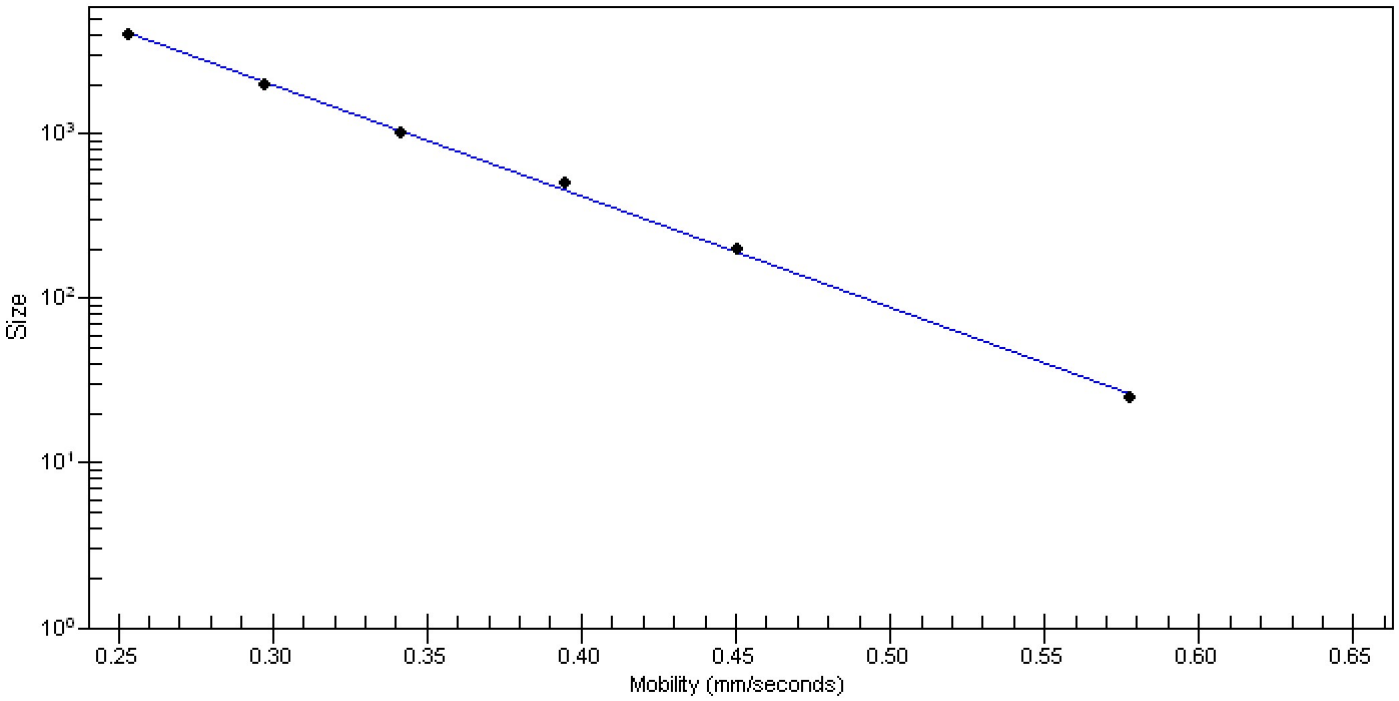

Assay Class: Eukaryote Total RNA Nano
Data Path: C:\...2019-06-20\Eukaryote Total RNA Nano_2019-06-20_10-22-02.xad

Created: 6/20/2019 10:22:01 AM
Modified: 6/20/2019 10:45:58 AM

Electrophoresis File Run Summary

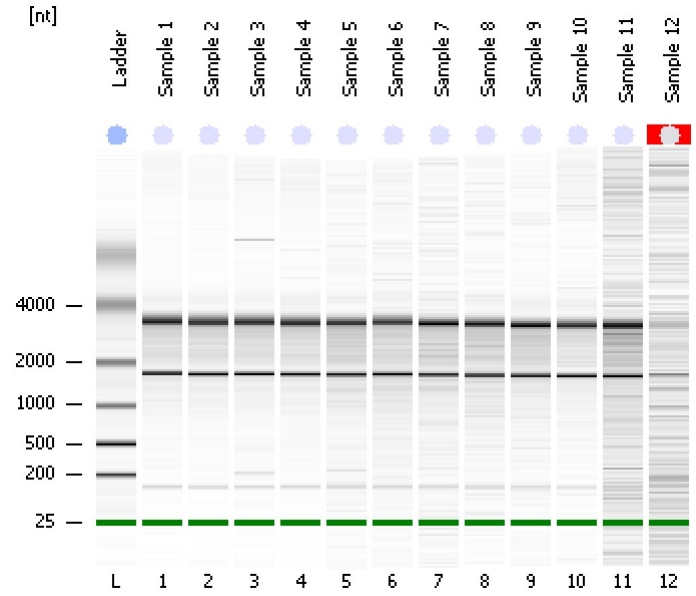

Instrument Information:

Instrument Name: DE54704709 Firmware: C.01.069
Serial#: DE54704709 Type: G2938C

Assay Information:

Assay Origin Path: C:\Program Files\Agilent\2100 bioanalyzer\2100 expert\assays\RNA\Eukaryote Total RNA Nano Series II.xsy
Assay Class: Eukaryote Total RNA Nano
Version: 2.6
Assay Comments: Total RNA Analysis ng sensitivity (Eukaryote)

Chip Information:

Chip Lot #:
Reagent Kit Lot #:
Chip Comments:

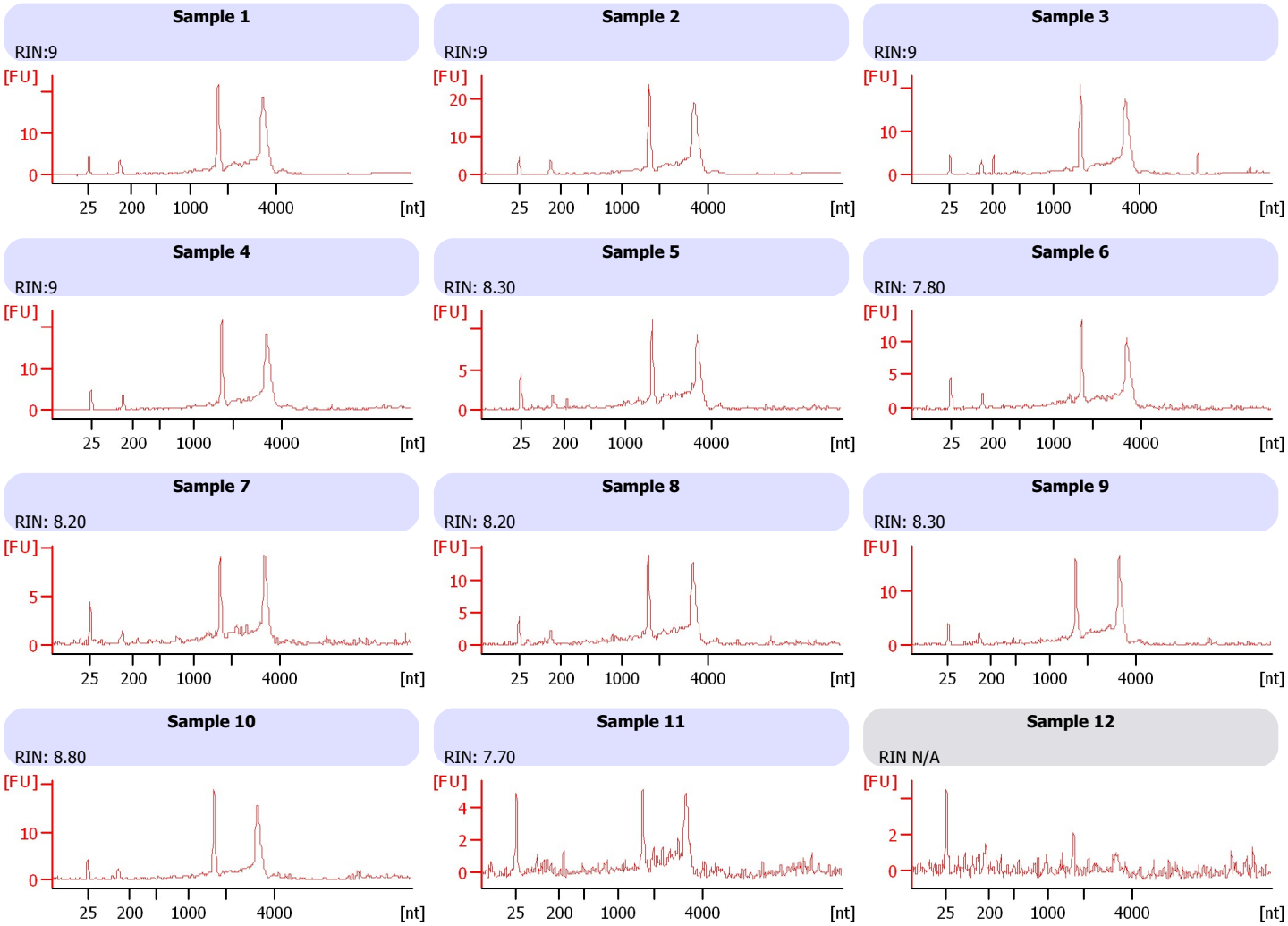

Assay Class: Eukaryote Total RNA Nano
Data Path: C:\...2019-06-20\Eukaryote Total RNA Nano_2019-06-20_10-22-02.xad

Created: 6/20/2019 10:22:01 AM
Modified: 6/20/2019 10:45:58 AM

Electrophoresis File Run Summary (Chip Summary)

Sample Name	Sample Comment	Status	Result Label	Result Color
Sample 1		✔	RIN:9	
Sample 2		✔	RIN:9	
Sample 3		✔	RIN:9	
Sample 4		✔	RIN:9	
Sample 5		✔	RIN: 8.30	
Sample 6		✔	RIN: 7.80	
Sample 7		✔	RIN: 8.20	
Sample 8		✔	RIN: 8.20	
Sample 9		✔	RIN: 8.30	
Sample 10		✔	RIN: 8.80	
Sample 11		✔	RIN: 7.70	
Sample 12		✔	RIN N/A	
Ladder		✔	All Other Samples	

Chip Lot #

Reagent Kit Lot #

Chip Comments :

Assay Class: Eukaryote Total RNA Nano
Data Path: C:\...2019-06-20\Eukaryote Total RNA Nano_2019-06-20_10-22-02.xad

Created: 6/20/2019 10:22:01 AM
Modified: 6/20/2019 10:45:58 AM

Electrophoresis Assay Details

General Analysis Settings

Number of Available Sample and Ladder Wells (Max.) : 13
Minimum Visible Range [s] : 17
Maximum Visible Range [s] : 70
Start Analysis Time Range [s] : 19
End Analysis Time Range [s] : 69
Ladder Concentration [ng/µl] : 150
Lower Marker Concentration [ng/µl] : 0
Upper Marker Concentration [ng/µl] : 0
Used Lower Marker for Quantitation
Standard Curve Fit is Logarithmic
Show Data Aligned to Lower Marker

Integrator Settings

Integration Start Time [s] : 19
Integration End Time [s] : 69
Slope Threshold : 0.6
Height Threshold [FU] : 0.5
Area Threshold : 0.2
Width Threshold [s] : 0.5
Baseline Plateau [s] : 6

Filter Settings

Filter Width [s] : 0.5
Polynomial Order : 4

Ladder

Ladder Peak	Size
1	25
2	200
3	500
4	1000
5	2000
6	4000

Assay Class: Eukaryote Total RNA Nano
Data Path: C:\...2019-06-20\Eukaryote Total RNA Nano_2019-06-20_10-22-02.xad

Created: 6/20/2019 10:22:01 AM
Modified: 6/20/2019 10:45:58 AM

Electropherogram Summary

Ladder

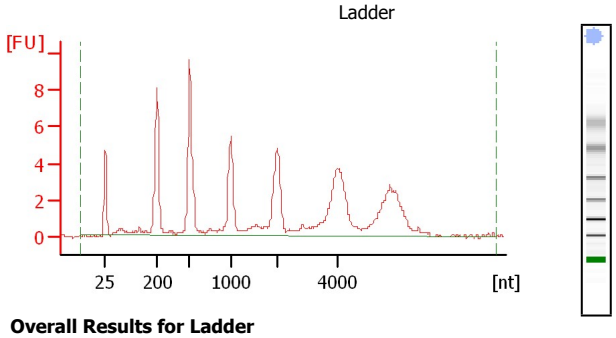

Overall Results for Ladder

RNA Area:	98.7
RNA Concentration:	150 ng/µl
Result Flagging Color:	
Result Flagging Label:	All Other Samples

Sample 1

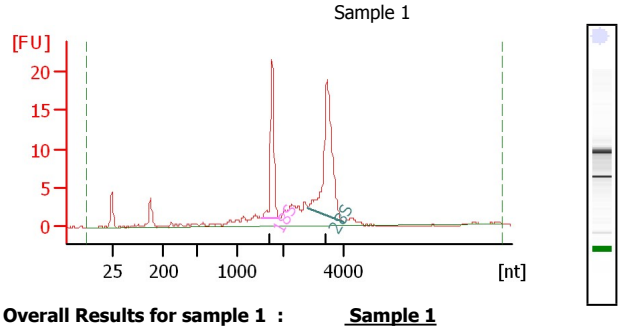

Overall Results for sample 1 : Sample 1

RNA Area:	123.1
RNA Concentration:	187 ng/µl
rRNA Ratio [28s / 18s]:	1.8
RNA Integrity Number (RIN):	9 (B.02.08)
Result Flagging Color:	
Result Flagging Label:	RIN:9

Fragment table for sample 1 : Sample 1

Name	Start Size [nt]	End Size [nt]	Area	% of total Area
18S	1,510	1,882	23.0	18.7
28S	2,788	3,982	42.0	34.1

Sample 2

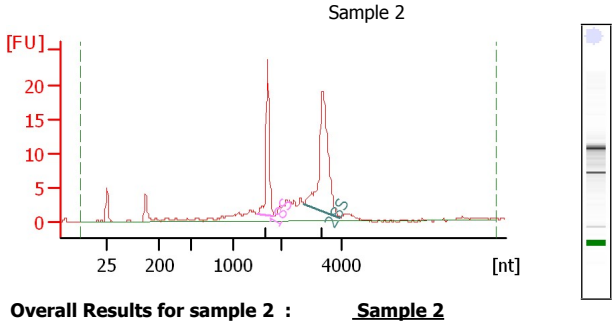

Overall Results for sample 2 : Sample 2

RNA Area:	134.0
RNA Concentration:	204 ng/µl
rRNA Ratio [28s / 18s]:	1.8
RNA Integrity Number (RIN):	9 (B.02.08)
Result Flagging Color:	
Result Flagging Label:	RIN:9

Fragment table for sample 2 : Sample 2

Name	Start Size [nt]	End Size [nt]	Area	% of total Area
18S	1,480	1,850	24.8	18.5
28S	2,772	3,959	45.6	34.0

Sample 3

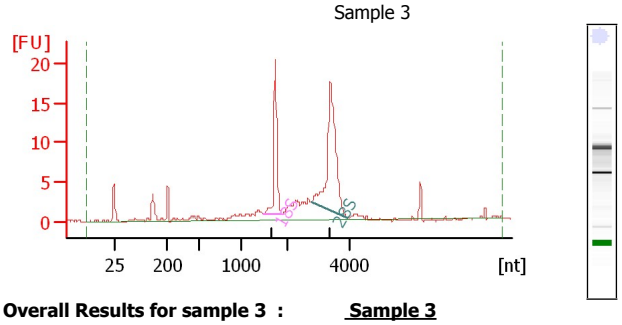

Overall Results for sample 3 : Sample 3

RNA Area:	122.7
RNA Concentration:	187 ng/µl
rRNA Ratio [28s / 18s]:	1.9
RNA Integrity Number (RIN):	9 (B.02.08)
Result Flagging Color:	
Result Flagging Label:	RIN:9

Fragment table for sample 3 : Sample 3

Name	Start Size [nt]	End Size [nt]	Area	% of total Area
18S	1,475	1,861	20.8	16.9
28S	2,757	3,953	39.7	32.3

Assay Class: Eukaryote Total RNA Nano
Data Path: C:\...2019-06-20\Eukaryote Total RNA Nano_2019-06-20_10-22-02.xad

Created: 6/20/2019 10:22:01 AM
Modified: 6/20/2019 10:45:58 AM

Electropherogram Summary Continued ...

Sample 4

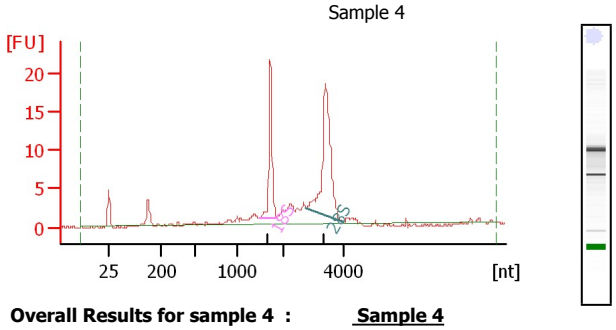

Overall Results for sample 4 : **Sample 4**

RNA Area:	109.1
RNA Concentration:	166 ng/µl
rRNA Ratio [28s / 18s]:	1.9
RNA Integrity Number (RIN):	9 (B.02.08)
Result Flagging Color:	
Result Flagging Label:	RIN:9

Fragment table for sample 4 : **Sample 4**

Name	Start Size [nt]	End Size [nt]	Area	% of total Area
18S	1,470	1,854	21.5	19.7
28S	2,743	3,988	39.8	36.5

Sample 5

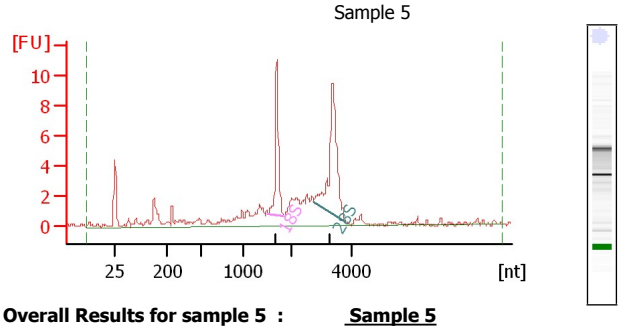

Overall Results for sample 5 : **Sample 5**

RNA Area:	84.8
RNA Concentration:	129 ng/µl
rRNA Ratio [28s / 18s]:	1.7
RNA Integrity Number (RIN):	8.3 (B.02.08)
Result Flagging Color:	
Result Flagging Label:	RIN: 8.30

Fragment table for sample 5 : **Sample 5**

Name	Start Size [nt]	End Size [nt]	Area	% of total Area
18S	1,525	1,855	11.0	12.9
28S	2,770	3,833	18.6	21.9

Sample 6

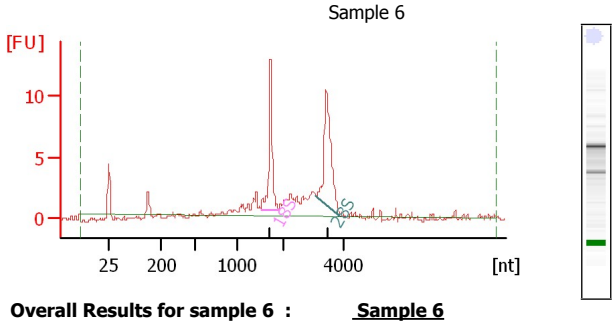

Overall Results for sample 6 : **Sample 6**

RNA Area:	67.4
RNA Concentration:	102 ng/µl
rRNA Ratio [28s / 18s]:	1.3
RNA Integrity Number (RIN):	7.8 (B.02.08)
Result Flagging Color:	
Result Flagging Label:	RIN: 7.80

Fragment table for sample 6 : **Sample 6**

Name	Start Size [nt]	End Size [nt]	Area	% of total Area
18S	1,515	1,890	13.7	20.3
28S	3,061	3,864	18.4	27.3

Sample 7

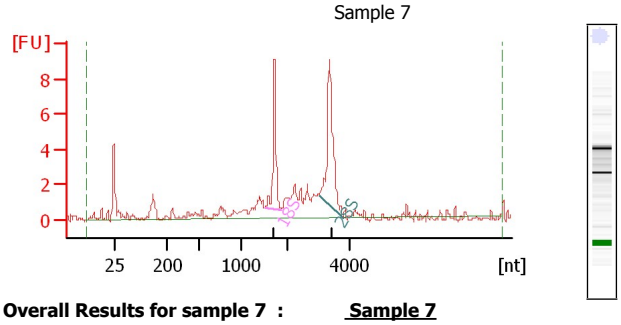

Overall Results for sample 7 : **Sample 7**

RNA Area:	60.8
RNA Concentration:	92 ng/µl
rRNA Ratio [28s / 18s]:	1.6
RNA Integrity Number (RIN):	8.2 (B.02.08)
Result Flagging Color:	
Result Flagging Label:	RIN: 8.20

Fragment table for sample 7 : **Sample 7**

Name	Start Size [nt]	End Size [nt]	Area	% of total Area
18S	1,493	1,852	8.7	14.3
28S	3,049	3,800	13.9	22.9

Assay Class: Eukaryote Total RNA Nano
Data Path: C:\...2019-06-20\Eukaryote Total RNA Nano_2019-06-20_10-22-02.xad

Created: 6/20/2019 10:22:01 AM
Modified: 6/20/2019 10:45:58 AM

Electropherogram Summary Continued ...

Sample 8

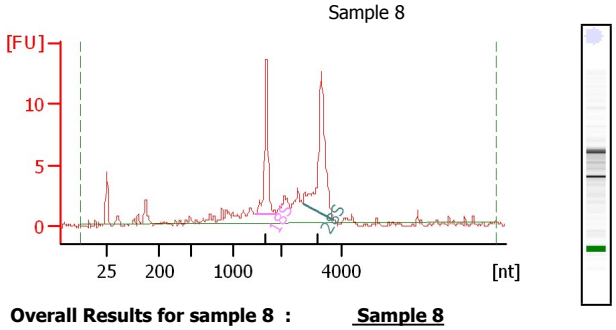

Overall Results for sample 8 : Sample 8

RNA Area:	85.6
RNA Concentration:	130 ng/µl
rRNA Ratio [28s / 18s]:	1.6
RNA Integrity Number (RIN):	8.2 (B.02.08)
Result Flagging Color:	
Result Flagging Label:	RIN: 8.20

Fragment table for sample 8 : Sample 8

Name	Start Size [nt]	End Size [nt]	Area	% of total Area
18S	1,462	1,895	14.6	17.1
28S	2,744	3,763	23.9	27.9

Sample 9

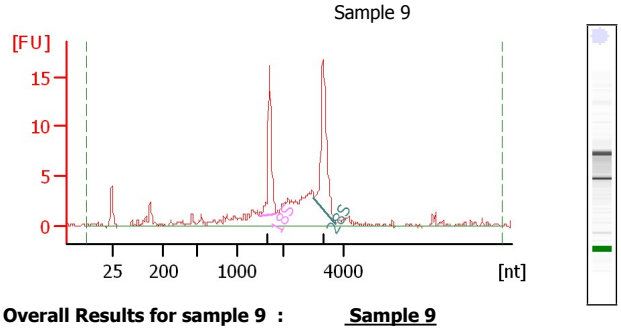

Overall Results for sample 9 : Sample 9

RNA Area:	107.0
RNA Concentration:	163 ng/µl
rRNA Ratio [28s / 18s]:	1.3
RNA Integrity Number (RIN):	8.3 (B.02.08)
Result Flagging Color:	
Result Flagging Label:	RIN: 8.30

Fragment table for sample 9 : Sample 9

Name	Start Size [nt]	End Size [nt]	Area	% of total Area
18S	1,456	1,828	17.6	16.5
28S	2,999	3,743	23.6	22.0

Sample 10

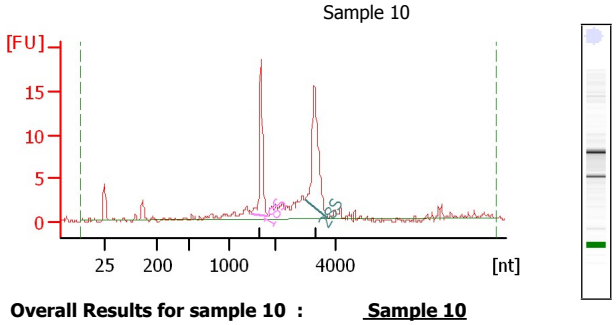

Overall Results for sample 10 : Sample 10

RNA Area:	99.6
RNA Concentration:	151 ng/µl
rRNA Ratio [28s / 18s]:	1.4
RNA Integrity Number (RIN):	8.8 (B.02.08)
Result Flagging Color:	
Result Flagging Label:	RIN: 8.80

Fragment table for sample 10 : Sample 10

Name	Start Size [nt]	End Size [nt]	Area	% of total Area
18S	1,468	1,824	19.4	19.5
28S	2,973	3,765	26.4	26.5

Sample 11

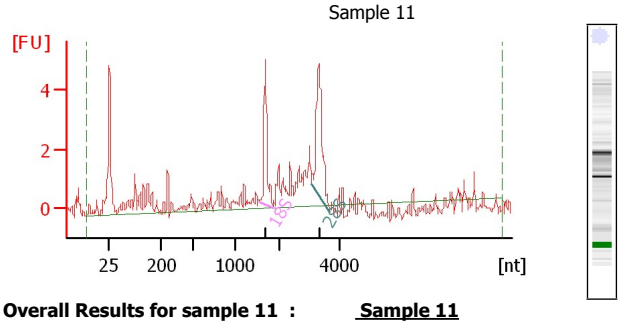

Overall Results for sample 11 : Sample 11

RNA Area:	43.9
RNA Concentration:	67 ng/µl
rRNA Ratio [28s / 18s]:	1.5
RNA Integrity Number (RIN):	7.7 (B.02.08)
Result Flagging Color:	
Result Flagging Label:	RIN: 7.70

Fragment table for sample 11 : Sample 11

Name	Start Size [nt]	End Size [nt]	Area	% of total Area
18S	1,556	1,840	5.2	11.8
28S	3,060	3,657	7.9	18.0

Assay Class: Eukaryote Total RNA Nano
Data Path: C:\...2019-06-20\Eukaryote Total RNA Nano_2019-06-20_10-22-02.xad

Created: 6/20/2019 10:22:01 AM
Modified: 6/20/2019 10:45:58 AM

Electropherogram Summary Continued ...

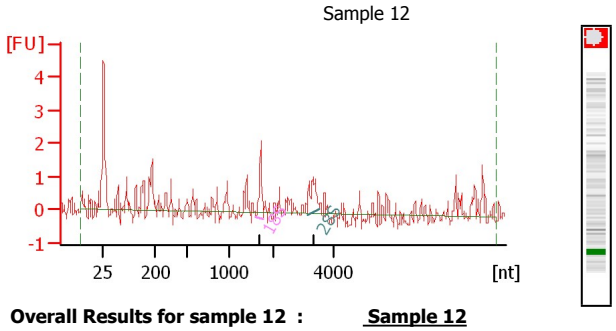

Overall Results for sample 12 : **Sample 12**

RNA Area:	23.9
RNA Concentration:	36 ng/µl
rRNA Ratio [28s / 18s]:	0.9
RNA Integrity Number (RIN):	N/A (B.02.08)
Result Flagging Color:	
Result Flagging Label:	RIN N/A

Fragment table for sample 12 : **Sample 12**

Name	Start Size [nt]	End Size [nt]	Area	% of total Area
18S	1,602	1,758	2.1	8.6
28S	3,131	3,515	1.9	7.8

Assay Class: Eukaryote Total RNA Nano
Data Path: C:\...2019-06-20\Eukaryote Total RNA Nano_2019-06-20_10-22-02.xad

Created: 6/20/2019 10:22:01 AM
Modified: 6/20/2019 10:45:58 AM

Gel Image

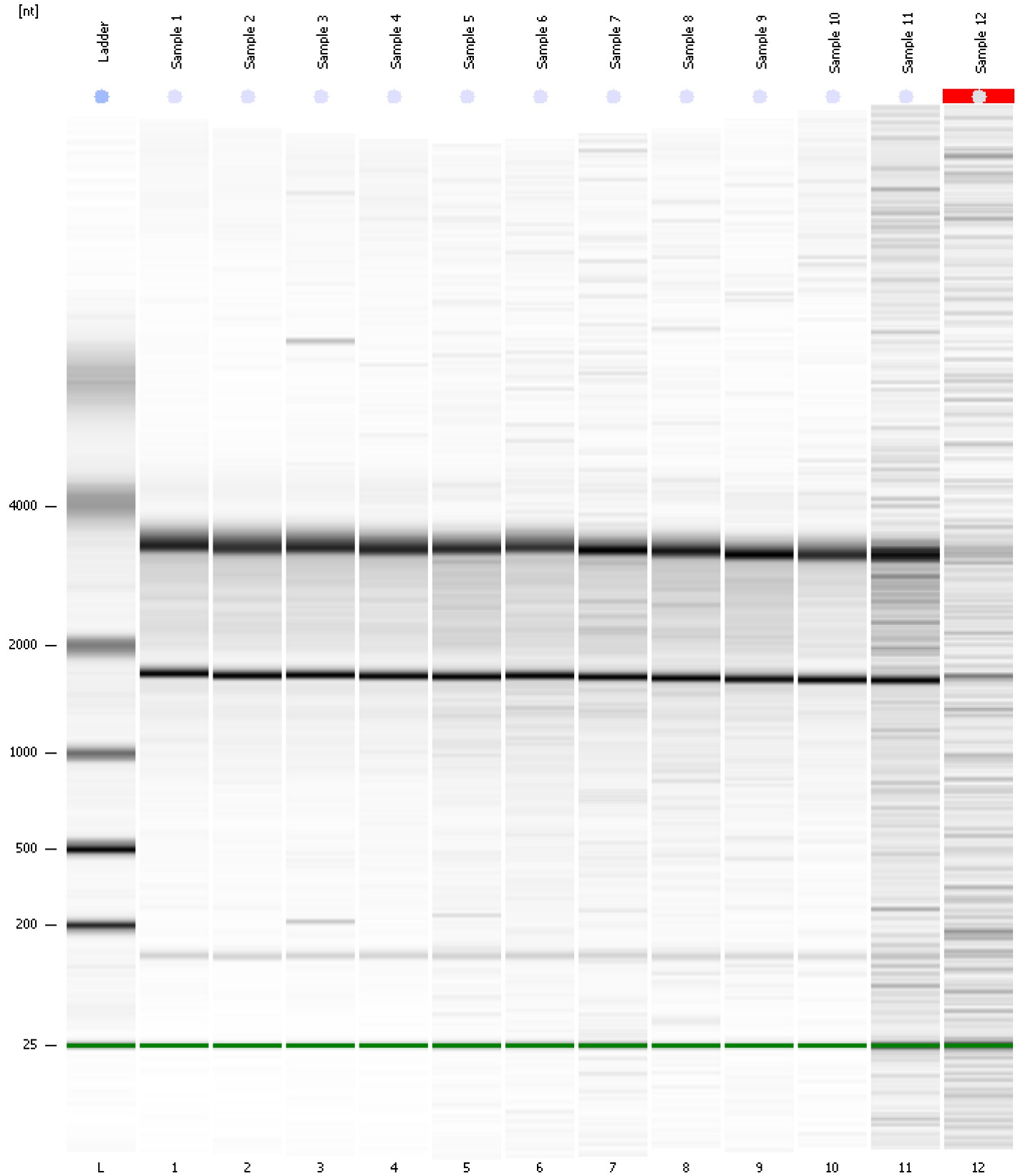

Assay Class: Eukaryote Total RNA Nano
Data Path: C:\...2019-06-20\Eukaryote Total RNA Nano_2019-06-20_10-22-02.xad

Created: 6/20/2019 10:22:01 AM
Modified: 6/20/2019 10:45:58 AM

Curves

Standard Curve